University of Naples Federico II

School of Agricultural Sciences and Veterinary Medicine

Department of Veterinary Medicine and Animal Production

Ph.D. Course in Veterinary Sciences

Coronaviruses and herpesviruses infections: potential antiviral activity of natural and synthetic compounds

Claudia Cerracchio

Coordinator

Prof. Paolo de Girolamo

Advisor

Prof. Filomena Fiorito

XXXVI Cycle 2020-2024

University of Naples Federico II

School of Agricultural Sciences and Veterinary Medicine

Department of Veterinary Medicine and Animal Production

Ph.D. Course in Veterinary Sciences

Coronaviruses and herpesviruses infections: potential antiviral activity of natural and synthetic compounds

Claudia Cerracchio

Coordinator

Prof. Paolo de Girolamo

Supervisor

Prof. Filomena Fiorito

Co-supervisor

Prof. Graciela Andrei

XXXVI Cycle 2020-2024

ABSTRACT

Coronaviruses (CoVs) emerge or remerge and can mutate into new and more dangerous strains, such as SARS CoV-2, causing coronavirus disease 2019 (COVID-19) pandemic and CCoV-HuPn-2018, a novel canine-feline recombinant alphacoronavirus isolated from human patients.

Herpesviruses are another challenge both for humans and animals. Clinical symptoms caused by lesions in the peripheral and central nervous system and upper respiratory tract are provoked by primary infection by herpes simplex virus type 1 (HSV-1). Recurrent ocular shedding leads to corneal scarring which can progress to vision loss. Similar properties to HSV-1 are provoked by Bovine herpesvirus 1 (BoHV-1), which causes health and economic losses to the cattle industry. Both these viruses established latency in sensory neurons of trigeminal ganglia, but immunosuppression leads to a periodic reactivation of the infection, provoking a spread of virus and recurrent disease. And several case of drug resistance have been detected from monotherapy or combination therapy of DNA polymerase inhibitors against HSV-1. In this context, the pharmaceutical industry is constantly looking for new active drugs involving original mechanisms of action.

Based on this evidence, this PhD research project focused on the study of both coronaviruses and herpesviruses infections.

Thus, to explore the mechanism of action of two alphacoronaviruses, CCoV and Feline Coronavirus (FCoV), the aryl hydrocarbon receptor (AhR), a ligand-activated transcription factor involving in several functions, like chemical and microbial defence was investigated. It has been observed that AhR was considerably activated by CCoV and FCoV infections, and that the selective AhR antagonist CH223191 reduces *in vitro* replication of these CoVs, responsible for both enteric and respiratory diseases in dogs and cats, respectively. Interestingly, 3-O-methylfunicone (OMF), penisimplicissin (PS) and vermistatin (VER), which are funicone-like compounds produced by the fungus *Talaromyces pinophilus*, as well as 6-Pentyl-α-Pyrone (6PP), isolated from *Trichoderma atroviride*, have shown antiviral activity against CCoV, potentially inhibiting AhR. In addition, it has been observed the alkalinization of lysosomes in the presence of VER or PS, which may be involved in the observed antiviral activities.

The AhR activation also modulates viral replication of BoHV-1. Hence, during BoHV-1 *in vitro* infection, the potential antiviral activity of some natural compounds, like OMF,

and Taurisolo®, a grape pomace polyphenolic extract obtained from the Aglianico cultivar grape, was investigated. Both these natural substances have shown an excellent defence reaction during BoHV-1 infection involving AhR.

Furthermore, experiments of combination therapy of DNA polymerase inhibitors, like acyclovir (ACV) and foscarnet (PFA), and helicase-primase complex inhibitor, such as amenamevir (AMV), have been carried out against HSV-1 to know if these combination therapies may represent a valid alternative to well-known monotherapy of ACV or PFA, that have shown cases of HSV-1 drug resistance.

Overall, these findings provide evidence on structural knowledge as well as on functional mechanism of new potential antivirals. They may be considered useful starting points for the development of drugs against coronaviruses as well as herpesviruses infections.

TABLE OF CONTENTS

THESIS OUTLINE 10

CHAPTER 1 – STATE OF THE ART 13

Aims 16

References 17

CHAPTER 2 - Mechanism of action of AhR during CCoV and FCoV infection 21

Introduction 23

Materials and Methods 25

Results 30

Discussion and Conclusions 41

References 44

Chapter 3 - *In vitro* evaluation of natural compounds against CCoV infection 52

Introduction 54

Materials and Methods 55

Results 59

Discussion and Conclusions 84

References 88

Chapter 4 - *In vitro* evaluation of natural compounds against BoHV-1 infection 96

Antiviral Property of the Fungal Metabolite 3-O-Methylfunicone in Bovine Herpesvirus 1 Infection

Introduction 98

Materials and Methods 100

Results 103

Discussion and Conclusions 111

References 113

Antiviral activity of Taurisolo® during bovine alphaherpesvirus 1 infection

Introduction 117

Materials and Methods 118

Results 121

Discussion and Conclusions 128

References 131

Chapter 5 - Evaluating the effect of Amenamevir combination therapy on HSV-1 resistance emergence 138

Introduction 139

Materials and Methods 141

Results 143

Discussion 149

References 150

Chapter 6 – FINAL REMARKS 154

THESIS OUTLINE

In Chapter 1, the state of the art addressing the main topics as well as the aims of the work.

In Chapters 2, to explore the mechanism of action of two alphacoronaviruses, CCoV and FCoV, the aryl hydrocarbon receptor (AhR) was investigated using a selective inhibitor (CH223191) of AhR. All the results obtained are discussed.

This work, after identifying of novel target (AhR) involved in CCoV and FCoV infection, is also focused on the identification of potential antivirals towards these animal coronaviruses infection, using both natural and synthetic compounds. Antiviral activity against CCoV by the fungal secondary metabolites 3-O-methylfunicone (OMF), penisimplicissin (PS) and vermistatin (VER), and 6-pentyl-α-pyrone (6PP) have been shown in Chapter 3.
Interestingly, in the presence of VER or PS, the alkalinization of lysosomes in CCoV-infected cells was detected. We suppose that this action may be involved in the observed antiviral activities.

About herpesviruses, during BoHV-1 *in vitro* infection, the potential antiviral properties of natural compounds, such as OMF and Taurisolo®, a grape pomace polyphenolic extract obtained from the Aglianico cultivar grape, were investigated. The promising results of these investigations involving AhR were displayed in Chapter 4.

Finally, in Chapter 5, the synergistic effects of AMV + ACV or AMV + PFA have been evaluated in order to determine if these combination therapies may represent a valid alternative to well-known monotherapy of acyclovir or foscarnet, that have shown cases of HSV-1 drug resistance.

It should be noticed that the achievement of this project, both in chemical and biological points, was guaranteed by expertise of components of different research groups, and by their equipment and facilities involved in the present work. This work was in collaboration with:

Prof. Graciela Andrei, Prof. Robert Snoeck, Olga Mineeva-Sangwo, Hanna Schalkwijk, Fien Horsten, Martyna Pociupany, Sarah Gillemot, Brecht Dirix, Wim Werckx, Hien Do, Robbe Sinnesael – Rega Institute for Medical Research, Ku Leuven, Leuven, Belgium

(For evaluating the effect of Amenamevir combination therapy on HSV-1 resistance emergence, see chapter 5);

Prof. Anna Andolfi, Prof. Marina DellaGreca, Dr. Maria Michela Salvatore - Department of Chemical Sciences, University of Naples Federico II, Naples, Italy (For providing fungal secondary metabolites OMF, VER and PS, for scientific and technical collaboration, see chapters 3 and 4);

Prof. Giuseppe Iovane, Head of Infectious Disease Section, Prof. Luisa De Martino, Prof. Francesco Vinale, Dr. Francesca Paola Nocera, Dr. Luca Del Sorbo, Mr. Gaetano Vitagliano; Department of Veterinary Medicine and Animal Production, University of Naples Federico II, Naples, Italy (For providing fungal secondary metabolite 6PP, for scientific and technical collaboration, see chapters 1-4);

Prof. Rita Santamaria, Prof. Carlo Irace, Prof. Gian Carlo Tenore, Dr. Marialuisa Piccolo; Dr. Maria Grazia Ferraro – Department of Pharmacy, University of Naples Federico II, Naples, Italy (For providing Taurisolo, for scientific and technical collaboration, see chapter 4);

Prof. Valentina Iovane, Dr. Alessia Staropoli, Dr. Hiba Dakroub - Department of Agricultural Sciences, University of Naples Federico II, Portici, Italy (For providing fungal secondary metabolite 6PP, for scientific and technical collaboration, see chapter 3);

Prof. Ettore Novellino - Department of Medicine and Surgery, Catholic University of the Sacred Heart, Rome, Italy (For providing Taurisolo, for scientific and technical collaboration, see chapter 4);

Dr. Maria Grazia Amoroso, Dr. Francesco Serra, Dr. Alessia Pucciarelli - Istituto Zooprofilattico Sperimentale del Mezzogiorno, Unit of Virology, Department of Animal Health, Portici, Italy (For scientific and technical (real-time PCR) collaboration, see chapters 1-4);

Dr. Rosario Nicoletti - Institute for Sustainable Plant Protection, National Research Council, Portici, Italy; Council for Agricultural Research and Economics, Research Centre for Olive, Fruit and Citrus Crops, Caserta, Italy (For providing fungal secondary metabolites OMF, VER and PS, see chapters 3 and 4).

Some chapters presented in this thesis have been published on scientific journals. In the followed list, the papers embedded in this thesis are reported:

- **Cerracchio C**, Serra F, Amoroso MG, Fiorito F. Canine Coronavirus Activates Aryl Hydrocarbon Receptor during In Vitro Infection. Viruses 2022, 14, 2437. doi.org/10.3390/v14112437
- **Cerracchio C**, Iovane V, Salvatore MM, Amoroso MG, Dakroub H, DellaGreca M, Nicoletti R, Andolfi A, Fiorito F. Effectiveness of the Fungal Metabolite 3-O-Methylfunicone towards Canine Coronavirus in a Canine Fibrosarcoma Cell Line (A72). Antibiotics 2022, 11, 1594. doi.org/10.3390/antibiotics11111594
- **Cerracchio C**, Salvatore MM, Del Sorbo L, Serra F, Amoroso MG, DellaGreca M, Nicoletti R, Andolfi A, Fiorito F. In Vitro Evaluation of Antiviral Activities of Funicone-like Compounds Vermistatin and Penisimplicissin against Canine Coronavirus Infection. Antibiotics (Basel). 2023 Aug 15;12(8):1319. doi: 10.3390/antibiotics12081319.
- Fiorito F, **Cerracchio C**, Salvatore MM, Serra F, Pucciarelli A, Amoroso MG, Nicoletti R, Andolfi A. Antiviral Property of the Fungal Metabolite 3-O-Methylfunicone in Bovine Herpesvirus 1 Infection Microorganisms 2022, 10, 188; doi.org/10.3390/microorganisms10010188.
- **Cerracchio C**, Amoroso MG, Piccolo M, Ferraro MG, Nocera FP, De Martino L, Serra F, Irace C, Tenore GC, Novellino E, Santamaria R, Fiorito F. Antiviral activity of Taurisolo® during bovine alphaherpesvirus 1 infection. Virus Res. 2023 Sep 7;336:199217. doi: 10.1016/j.virusres.2023.199217.

CHAPTER 1 – STATE OF THE ART

CHAPTER 1 – STATE OF THE ART

Coronaviruses (CoVs) are enveloped RNA viruses which can infect several hosts like mammals and birds. Following transmission from their natural reservoirs, such as migratory birds or bats, CoVs accumulate some mutations in intermediate hosts, including domestic birds or unknown intermediate host, facilitating crossing species barriers and infect humans. The variant strains can transmit to other animal species including pets and wild animals (Kenney et al., 2021; Timurkan et al., 2021; Pratelli et al., 2021,2022; Kane et al., 2023). Therefore, novel strains emerge through molecular processes that affect their adaptation, transmissibility, host/tissue tropism, and pathogenicity. CoVs emerge or remerge and can mutate into new and more dangerous strains, such as SARS CoV-2, causing coronavirus disease 2019 (COVID-19), one of the most severe pandemics of the modern human history, as well as CCoV-HuPn-2018 (Vlasova et al., 2022) and HuCCoV-Z19Haiti (Lednicky et al.,2022), novel canine-feline recombinant alphacoronaviruses isolated from human patients.

Herpesviruses are another challenge both for humans and animals. Clinical symptoms in the peripheral and central nervous system and upper respiratory tract, and gastrointestinal tract are provoked by primary infection by herpes simplex virus type 1 (HSV-1), the most widely prevalent herpes virus worldwide (Jones, 2013, 2023; James et al., 2020). Recurrent ocular shedding leads to corneal scarring which can progress to vision loss. Similar properties to HSV-1 are provoked by Bovine herpesvirus 1 (BoHV-1), which causes health and economic losses to the cattle industry (Jones, 2013; Ostler and Jones, 2023). Both these viruses established latency in sensory neurons of trigeminal ganglia, but immunosuppression leads to a periodic reactivation of the infection, provoking a spread of virus and recurrent disease.

In the current scenario, to relieve the impact of both coronaviruses and herpesviruses, amazing research attempts focused on antiviral therapeutic development occur. The advance of useful strategies is based on the knowledge of molecular and cellular mechanisms of virus infections, which emphasizes the importance of investigating virus–host interactions to identify potential targets for antiviral action. To date, anti-viral natural compounds are scarce. Pharmaceutical research is strongly involved in the development of novel therapeutic strategies against viral diseases in order to minimize antivirals toxicity and fight antimicrobial-resistance phenomena, as well. In this context, natural compounds have been explored as nontoxic natural remedies. Fungi constitute an abundant resource of bioactive compounds with biological and antimicrobial activities

(Salvatore et al., 2022). Among these 3-O-methylfunicone (OMF), vermistatin (VER) and penisimplicissin (PEN) belonging to the funicones family, produced essentially by *Talaromyces species*, isolated from *Trichoderma atroviride*, showed antifungal, antiproliferative and antiviral activity (Salvatore et al., 2022). In addition, 6-Pentyl-α-Pyrone (6PP), having an important role in the defence against plant pathogens (Vinale et al. 2008; Comite et al., 2021), and in anti-biofilm-producing bacteria activity (Papaianni et al., 2020; Kotb et al., 2022), suggesting its promising application in agriculture and medicine. In this context, the pharmaceutical industry is constantly looking for new active drugs involving original mechanisms of action. The aryl hydrocarbon receptor (AhR), a ligand-activated transcription factor involving in several physiological functions, like embryonic and adult tissue developing, energy metabolism, chemical and microbial defence. It is activated by endogenous and exogenous substrates, including bilirubin, biliverdin, tryptophan metabolites, environmental pollutants (dioxin), and microbial metabolites (Yang et al., 2019; Torti et al., 2021). During infection, AhR regulates some aspects of the immunity, by interfering with natural protective immune responses to different microorganisms (Lawrence et al., 2013; Gutierrez-Vasquez et al., 2018; Rothammer and Quintana, 2019; Hu et al., 2023). In addition, it is also involved in the host response to different CoVs. AhR activation has been revealed during infection with murine coronavirus (MCoV), Middle East respiratory syndrome coronavirus (MERS-CoV), severe acute respiratory syndrome (SARS-CoV-1), SARS-CoV-2, and human coronavirus (HCoV) 229E (Tang et al., 2005; Grunewald et al., 2020; Giovannoni et al., 2021, Shi et al., 2023; Zhao et al., 2023; Yousefi et al., 2023). The AhR activation has been shown to also promote viral replication of several herpesviruses, such as CMV, HSV-2, and BoHV-1, affecting host resistance and survival (Veiga-Parga et al., 2011; Fiorito et al., 2017a; Torti et al., 2021; Bock 2021). Hence, AhR may be an interesting target to explore for developing new antivirals.

The viral DNA polymerase (DP) is the main target of antivirals that are currently approved for the treatment of HSV-1. However, several cases of HSV-1 drug-resistance have been found especially in immunocompromised subjects following therapy with acyclovir, the most commonly used drug for HSV-1 infections (Andrei et al., 2013; Sato et al., 2021, Schalkwijk et al., 2022). The increase of drug-resistant HSV-1 infections highlights the necessity for innovative therapeutic approaches. In this context, helicase primase complex has been investigated as target of new HSV-1 antivirals (Andrei et al., 2013; Sato et al., 2021, Schalkwijk et al., 2022).

Aims

Based on this evidence, within a One-Health approach to balance and optimize both human and animal health in the environment, this PhD research project focused on the study of both coronaviruses and herpesviruses infections in order to increase the knowledge about their mechanisms of action.

Two of the most studied animals CoVs are the canine coronavirus (CCoV) as well as feline infectious peritonitis virus (FIPV), a virulent pathotype of feline enteric coronavirus (FCoV). They are considered potential models for the study of antivirals against CoVs (Pratelli et al., 2021; Gao et al., 2023). Thus, to explore the mechanism of action of two alphacoronaviruses, CCoV and FCoV, AhR was investigated using the selective AhR antagonist CH223191, following *in vitro* replication of these CoVs, responsible for both enteric and respiratory diseases in dogs and cats, respectively.

The emerging pathogenic coronaviruses have also increased research activity focused on finding novel antivirals. Natural products offer a rich resource of potential substances for the identification and development of novel antivirals. Certainly, several compounds from various biological sources (i.e., medicinal plants, bacteria, fungi) are being studied with the aim to find and develop new nontoxic medicinal drugs. Fungi produce numerous bioactive secondary metabolites (SMs), some of which have been already used as antibiotics, plant growth regulators, fungicides and hormones. Funicones and related compounds are a homogeneous group of fungal polyketides possessing notable biological activities which have promoted their consideration as drug possibilities (Salvatore et al., 2022). Indeed, 3-O-methylfunicone (OMF), a benzo-γ-pyrone produced by *Talaromyces pinophilus*, has shown antifungal and antiproliferative activities (Salvatore et al., 2022), and potential antiviral properties, against hepatitis C virus (HCV) (Nakajima et al., 2013). In addition, the Trichoderma secondary metabolite 6-pentyl-α-pyrone (6PP) also plays an important role in the defence towards plant pathogens (Vinale et al. 2008; Comite et al., 2021), and in anti-biofilm-producing bacteria activity (Papaianni et al., 2020; Kotb et al., 2022), but the antiviral activity of 6PP has never been investigated so far.

Therefore, fungal secondary metabolites, like OMF, VER and PS, as well as 6PP, were investigated to explore their potential antiviral activity during *in vitro* CCoV infection.

BoHV-1 is a useful model for antiherpesvirus compounds testing (Akula et al., 2002; Boubaker-Elandalousi et al., 2014; Zhu et al., 2018; Fiorito et al., 2017b; Chang and Zhu 2020; Yesilbag et al., 2021). Hence, this project also aims to study the potential antiviral activity of some natural compounds, like OMF, and Taurisolo®, a grape pomace

polyphenolic extract obtained from the Aglianico cultivar grape. For this purpose, their action against BoHV-1 was investigated following *in vitro* infection in bovine cells (MDBK).

Finally, in order to determine if combination therapies may represent a valid alternative to well-known monotherapy of ACV or PFA, that have shown cases of HSV-1 drug resistance, the synergistic effects of AMV plus ACV or AMV plus PFA have been evaluated.

References

Andrei G, Snoeck R. Herpes simplex virus drug-resistance: new mutations and insights. Curr Opin Infect Dis. 2013 Dec;26(6):551-60.

Akula, S.M., Hurley, D.J., Wixon, R.L., Wang, C., Chase, C.C., 2002. Effect of genistein on replication of bovine herpesvirus type 1. Am. J. Vet. Res. 63, 1124–1128.

Bock, K.W., 2021. Aryl hydrocarbon receptor (AHR), integrating energy metabolism and microbial or obesity-mediated inflammation. Biochem. Pharmacol. 184, 114346.

Boubaker-Elandalousi, R., Mekni-Toujani, M., Kaabi, B., Larbi, I., Diouani, M.F., Gharbi, M., Akkari, H., B'chir, F., Ghram, A., 2014. Non-cytotoxic Thymus capitata extracts prevent Bovine herpesvirus-1 infection in cell cultures. BMC Vet. Res. 10, 231

Chang, L., Zhu, L., 2020. Dewormer drug fenbendazole has antiviral effects on BoHV-1 productive infection in cell cultures. J. Vet. Sci. 21, e72.

Comite, E., El-Nakhel, C., Rouphael, Y., Ventorino, V., Pepe, O., Borzacchiello, A., Vinale, F., Rigano, D., Staropoli, A., Lorito, M., Woo, S.L., 2021. Bioformulations with Beneficial Microbial Consortia, a Bioactive Compound and Plant Biopolymers Modulate Sweet Basil Productivity, Photosynthetic Activity and Metabolites. Pathogens 10, 870.

Fiorito, F., Santamaria, R., Irace, C., De Martino, L., Iovane, G., 2017a. 2,3,7,8-tetrachlorodibenzo-p-dioxin and the viral infection. Environ. Res. 153, 27-34.

Fiorito, F.; Iovane, V.; Cantiello, A.; Marullo, A.; De Martino, L.; Iovane, G. MG-132 reduces virus release in Bovine herpesvirus-1 infection. Sci. Rep. 2017b, 7, 13306.

Gao YY, Wang Q, Liang XY, Zhang S, Bao D, Zhao H, Li SB, Wang K, Hu GX, Gao FS. An updated review of feline coronavirus: mind the two biotypes. Virus Res. 2023 Mar;326:199059.

Giovannoni, F., Li, Z., Remes-Lenicov, F., Dávola, M.E., Elizalde, M., Paletta, A., Ashkar, A.A., Mossman, K.L., Dugour, A.V., Figueroa, J.M., Barquero, A.A., Ceballos, A., Garcia, C.C., Quintana, F.J., 2021. AHR signaling is induced by infection with coronaviruses. Nat. Commun. 12, 5148.

Grunewald, M.E., Shaban, M.G., Mackin, S.R., Fehr, A.R., Perlman, S., 2020. Murine coronavirus infection activates the aryl hydrocarbon receptor in an indoleamine 2,3-dioxygenase-independent manner, contributing to cytokine modulation and proviral TCDD-inducible-PARP expression. J. Virol. 94, 319–335. –

Gutierrez-Vazquez, C.; Quintana, F.J. Regulation of the immune response by the aryl hydrocarbon receptor. Immunity 2018, 48, 19–33.

Hu J, Ding Y, Liu W, Liu S. When AHR signaling pathways meet viral infections. Cell Commun Signal. 2023 Feb 24;21(1):42.

James, C., Harfouche, M., Welton, N. J., Turner, K. M., Abu-Raddad, L. J., Gottlieb, S. L., et al. (2020). Herpes simplex virus: global infection prevalence and incidence estimates, 2016. Bull. World. Health Organ. 98, 315–329.

Jones C. Bovine Herpes Virus 1 (BHV-1) and Herpes Simplex Virus Type 1 (HSV-1) Promote Survival of Latently Infected Sensory Neurons, in Part by Inhibiting Apoptosis. J Cell Death. 2013 Apr 9;6:1-16.

Jones C. Intimate Relationship Between Stress and Human Alpha-Herpes Virus 1 (HSV-1) Reactivation from Latency. Curr Clin Microbiol Rep. 2023 Dec;10(4):236-245.

Kane Y, Wong G, Gao GF. Animal Models, Zoonotic Reservoirs, and Cross-Species Transmission of Emerging Human-Infecting Coronaviruses. Annu Rev Anim Biosci. 2023 Feb 15;11:1-31.

Kenney SP, Wang Q, Vlasova A, Jung K, Saif L. Naturally Occurring Animal Coronaviruses as Models for Studying Highly Pathogenic Human Coronaviral Disease. Vet Pathol. 2021 May;58(3):438-452.

Kotb, A.M.E., Abd El-Aziz, N.K., Elariny, E.Y.T., Yahya, R., Alkhalifah, D.H.M., Ahmed, R.M., 2022. Synergistic Antibacterial Potential of 6-Pentyl-α-pyrone Lactone and Zinc Oxide Nanoparticles against Multidrug-Resistant Enterobacterales Isolated from Urinary Tract Infections in Humans. Antibiotics (Basel). 11, 440.

Lawrence, B.P., Vorderstrasse, B.A., 2013. New insights into the aryl hydrocarbon receptor as a modulator of host responses to infection. Semin. Immunopathol. 35, 615–626.

Lednicky JA, Tagliamonte MS, White SK, Blohm GM, Alam MM, Iovine NM, Salemi M, Mavian C, Morris JG. Isolation of a Novel Recombinant Canine Coronavirus From a Visitor to Haiti: Further Evidence

of Transmission of Coronaviruses of Zoonotic Origin to Humans. Clin Infect Dis. 2022 Aug 24;75(1):e1184-e1187.

Nakajima, S., Watashi, K., Kamisuki, S., Tsukuda, S., Takemoto, K., Matsuda, M., Suzuki, R., Aizaki, H., Sugawara, F., Wakita, T., 2013. Specific inhibition of hepatitis C virus entry into host hepatocytes by fungi-derived sulochrin and its derivatives. Biochem. Biophys. Res. Commun. 440, 515–520.

Ostler JB, Jones C. The Bovine Herpesvirus 1 Latency-Reactivation Cycle, a Chronic Problem in the Cattle Industry. Viruses. 2023 Feb 16;15(2):552.

Papaianni, M., Ricciardelli, A., Fulgione, A., d'Errico, G., Zoina, A., Lorito, M., Woo, S.L., Vinale, F., Capparelli, R., 2020. Antibiofilm Activity of a Trichoderma Metabolite against Xanthomonas campestris pv. campestris, Alone and in Association with a Phage. Microorganisms. 8, 620.

Pratelli, A., Buonavoglia, A., Lanave, G., Tempesta, M., Camero, M., Martella, V., Decaro, N., 2021. One world, one health, one virology of the mysterious labyrinth of coronaviruses: The canine coronavirus affair. Lancet Microbe 2, e646–e647.

Pratelli, A., Tempesta, M., Elia, G., Martella, V., Decaro, N., Buonavoglia, C., 2022. The knotty biology of canine coronavirus: A worrying model of coronaviruses' danger. Vet. Sci. 144, 190–195.

Rothhammer, V.; Quintana, F.J. The aryl hydrocarbon receptor: An environmental sensor integrating immune responses in health and disease. Nat. Rev. Immunol. 2019, 19, 184–197.

Salvatore, M.M., Dellagreca, M., Andolfi, A., 2022. New insights into chemical and biological properties of funicone-like compounds. Toxins. 14, 466.

Sato Y, Suenaga T, Kobayashi M, Miyazaki N, Suzuki T, Ishioka K, Suzutani T. Characteristics of Helicase-Primase Inhibitor Amenamevir-Resistant Herpes Simplex Virus. Antimicrob Agents Chemother. 2021 Sep 17;65(10):e0049421.

Schalkwijk HH, Snoeck R, Andrei G. Acyclovir resistance in herpes simplex viruses: Prevalence and therapeutic alternatives. Biochem Pharmacol. 2022 Dec;206:115322.

Shi, J., Du, T., Wang, J., Tang, C., Lei, M., Yu, W., Yang, Y., Ma, Y., Huang, P., Chen, H., Wang, X., Sun, J., Wang, H., Zhang, Y., Luo, F., Huang, Q., Li, B., Lu, S., Hu, Y., Peng, X., 2023. Aryl hydrocarbon receptor is a proviral host factor and a candidate pan-SARS-CoV-2 therapeutic target. Sci Adv. 9(22):eadf0211.

Tang, B.S.F., Chan, K.H., Cheng, V.C.C., Woo, P.C.Y., Lau, S.K.P., Lam, C.C.K., Chan, T.L., Wu, A.K.L., Hung, I.F.N., Leung, S.Y., Yuen, K.Y., 2005. Comparative Host Gene Transcription by Microarray Analysis Early after Infection of the Huh7 Cell Line by Severe Acute Respiratory Syndrome Coronavirus and Human coronavirus 229E. J. Virol. 79, 6180–6193.

Timurkan, M.O.; Aydin, K.; Dincer, E.; Coskun, N. Molecular characterization of canine coronaviruses: An enteric and pantropic approach. Arch. Virol. 2021, 166, 35–42.

Torti, M.F.; Giovannoni, F.; Quintana, F.J.; García, C.C. The aryl hydrocarbon receptor as a modulator of anti-viral immunity. Front. Immunol. 2021, 12, 624293.

Veiga-Parga, T.; Suryawanshi, A.; Rouse, B.T. Controlling viral immuno-inflammatory lesions by modulating aryl hydrocarbon receptor signaling. PLoS Pathog. 2011, 7, e1002427.

Vinale, F., Sivasithamparam, K., Ghisalberti, E. L., Marra, R., Barbetti, M. J., Li, H., Woo, S.L., Lorito, M., 2008. A novel role for Trichoderma secondary metabolites in the interactions with plants. Physiol. Mol. Plant Pathol. 72, 80-86.

Vlasova AN, Toh TH, Lee JS, Poovorawan Y, Davis P, Azevedo MSP, Lednicky JA, Saif LJ, Gray GC. Animal alphacoronaviruses found in human patients with acute respiratory illness in different countries. Emerg Microbes Infect. 2022 Dec;11(1):699-702.

Yang, T., Feng, Y.L., Chen, L., Vaziri, N.D., Zhao, Y.Y., 2019. Dietary natural flavonoids treating cancer by targeting aryl hydrocarbon receptor. Crit. Rev. Toxicol. 49, 445–460.

Yesilbag, K., Toker, E.B., Ates, O., 2021. Ivermectin also inhibits the replication of bovine respiratory viruses (BRSV, BPIV-3, BoHV-1, BCoV and BVDV) in vitro. Virus Res. 297, 198384

Yousefi M, Lee WS, Chan WOY, He W, Mah MG, Yong CL, Deerain JM, Wang L, Arcinas C, Yan B, Tan D, Sia WR, Gamage AM, Yang J, Hsu AC, Li S, Linster M, Yang X, Ghosh S, Anderson DE, Smith GJD, Tan CW, Wang LF, Ooi YS. Betacoronaviruses SARS-CoV-2 and HCoV-OC43 infections in IGROV-1 cell line require aryl hydrocarbon receptor. Emerg Microbes Infect. 2023 Dec;12(2):2256416.

Zhao, L., Yao, L., Chen, R., He, J., Lin, T., Qiu, S., Chen, G., Chen, H., Qiu, S.X., 2023. Pinostrobin from plants and propolis against human coronavirus HCoV-OC43 by modulating host AHR/CYP1A1 pathway and lipid metabolism. Antiviral Res. 212:105570.

Zhu, L., Wang, P., Yuan, W., Zhu, G., 2018. Kaempferol inhibited bovine herpesvirus 1 replication and LPS-induced inflammatory response. Acta Virol. 62, 220–225.

CHAPTER 2 - Mechanism of action of AhR during CCoV and FCoV infection

CHAPTER 2 - Mechanism of action of AhR during CCoV and FCoV infection

Brief summary

To explore the mechanism of action of two alphacoronaviruses, CCoV and FCoV, the role of aryl hydrocarbon receptor was investigated during infection.

The results showed that AhR, expressed in canine (A72) and feline (CRFK) cells, was considerably activated by CCoV (Cerracchio et al., 2022a) and FCoV infections, and that the selective AhR antagonist CH223191 reduces *in vitro* replication of these CoVs, coronaviruses responsible for both enteric and respiratory diseases in dogs and cats, respectively.

The following paper was embedded here:

- Cerracchio C, Serra F, Amoroso MG, Fiorito F. Canine Coronavirus Activates Aryl Hydrocarbon Receptor during In Vitro Infection. Viruses 2022, 14, 2437. https://doi.org/10.3390/v14112437 - Permission: https://www.mdpi.com/openaccess

Moreover, results of unpublished paper about the activation of AhR by FCoV following *in vitro* infection in CRFK cells were also showed.

1. Introduction

Coronaviruses (CoVs) are a large group of positive-stranded RNA viruses which can infect several hosts such as mammals and birds. They are able to mutate into new and more dangerous strains. Indeed, the propensity of CoV genomes to mutate and recombine allows them to overcome natural barriers preventing cross-species transmission, to adapt and proliferate in new species in a spillover phenomenon (Kenney et al., 2021; Timurkan et al., 2021; Pratelli et al., 2021,2022). Therefore, novel strains emerge through molecular processes that affect their adaptation, transmissibility, host/tissue tropism, and pathogenicity. Genotype II of canine coronavirus (CCoV-II), an alphacoronavirus, belongs to the subfamily of Orthocoronavirinae, family of Coronaviridae, order of Nidovirales. CCoV-II is generally responsible for self-limiting enteric infections, causing high morbidity and low mortality in dogs (Kenney et al., 2021; Timurkan et al., 2021; Pratelli et al., 2021, 2022). However, an extremely virulent CCoV-IIa strain (CB/05) has been detected from Italian outbreaks of fatal disease in puppies, due to multi-systemic infections with severe lesions in different organs (Buonavoglia et al., 2006). Genetic analysis highlighted a recombinant canine–feline–porcine origin of CB/05 due to a partial S-gene exchange with transmissible gastroenteritis virus of swine (TGEV) (Pratelli et al.,2021, 2022; Decaro et al., 2007, 2009, 2010). Recently, a new CCoV has been isolated in Malaysia from a child hospitalized for pneumonia between 2017 and 2018 (Vlasova et al., 2022). Genome sequencing has been identified it as a novel canine–feline recombinant alphacoronavirus (genotype II), called CCoV-HuPn-2018 (Vlasova et al., 2022). In addition, a novel CoV, named HuCCoV_Z19Haiti, has been isolated from the urine samples of a medical team member presenting mild fever and malaise after a travel to Haiti. The virus showed 99.4% similarity with the recombinant CCoV-HuPn-2018 identified in Malaysia (Lednicky et al., 2022).

Interestingly, as reviewed in the study by Vlasova et al. (2022), recombinant canine–feline–porcine alphacoronaviruses have been also found in humans in Thailand (Theamboonlers et al., 2007), as well as in USA (Silva et al., 2014), proposing that these viruses emerged in multiple geographic locations independently (Vlasova et al., 2022).

Feline coronavirus (FCoV), another Alphacoronavirus, is transmitted faeco-orally, generally causes infection in cat provoking moderate enteritis or chronic asymptomatic infection, but a small rate of FCoV-infected domestic felines can develop feline infectious peritonitis (FIP), a serious disease (Rottier et al., 2005; Kenney et al., 2021; Tasker et al., 2023). FCoV is closely correlated to both animals and human CoVs, such as the canine

coronavirus (CCoV) infecting dogs, the transmissible gastroenteritis virus (TGEV), which infects pigs, and human coronavirus CCoV-HuPn-2018 affecting humans (Vlasova et al., 2022). Based on serological responses, FCoV is divided into FCoV-I and FCoV-II, the last one due to a double recombination between FCoV-I and CCoV-II, developed by mutations between the S and M genes (Herrewegh et al., 1998; Capozza et al., 2021; Pratelli et al., 2021). Considering their pathobiology, FCoVs are classified into two biotypes, named feline enteric coronavirus (FECV), that typically induce mild or subclinical digestive symptoms, affects up to 90% of cats in multi-cat households (Addie et al., 2009), and feline infectious peritonitis virus (FIPV), a spontaneous mutation of FECV, responsible for FIP, a fatal viral disease, globally affecting wild and domestic felines. Indeed, mutations which happen in an individual cat may induce a change of cell tropism from enterocytes to monocytes subsequently developing high pathogenic FIP by FCoV (Kenney et al., 2021; Tasker et al., 2023). FIPV affects pedigree cats and those under two years old, especially animals from 4 to 16 months of age (Pedersen et al., 2009; Tasker et al., 2023). Infection, by severe systemic pyogranulomatous inflammatory damage, might target serosa membranes, may reach lungs, lymphoid tissues, hearth, eyes, liver, and brain, also causing fever, anorexia, and weight loss (Kenney et al., 2021; Tasker et al., 2023).

As previously described (Herrewegh et al., 1998; Terada et al., 2014), recombination between CCoV and FCoV occurs, but the development of a novel, highly pathogenic FCoV-CCoV recombinant has been recently detected, for a fast-spreading outbreak of FIP in cats of all ages from Cyprus (Attipa et al., 2023a; Warr et al., 2023). Interestingly, during the preparation of this thesis, it has been hypothesized that the recombination, due to a deletion together to amino acid changes in spike, may show a very high sequence identity (97%) to the pantropic CCoV CB/05, as reported in a preprint paper (Attipa et al., 2023b). These features mainly could modify the receptor binding domain, suggesting changes to receptor binding and cell tropism, when it was compared to other FCoV-2s (Attipa et al., 2023b).

AhR is a transcription factor activated by endogenous and exogenous substrates, including bilirubin, biliverdin, tryptophan metabolites, environmental pollutants (such as dioxin), and microbial metabolites (Yang et al., 2019; Bock, 2021; Torti et al., 2021). It is differently expressed in almost all mammalian cells (Torti et al., 2021). In the canonical pathway of AhR action, after ligand binding, the complex AhR-ligand is transferred inside the nucleus, in which the nuclear translocator the heterodimer of ARNT and AhR

is responsible for the interaction with specific sequences of DNA, for controlling the expression of target genes, such as those encoding the cytochrome P450 enzymes (e.g., CYP1A1, CYP1B1, and CYP2A1). As result, the release of cytokines and the control of immune response occur (Torti et al., 2021). During infection, AhR regulates some aspects of the immunity, by interfering with natural protective immune responses to different microorganisms (Lawrence et al., 2013; Gutierrez-Vasquez et al., 2018; Rothammer and Quintana, 2019; Hu et al., 2023). Indeed, AhR inhibits the production of type I interferons (IFN-I) (Yamada et al., 2016), specifically, during infection with Zika or dengue viruses (Giovannoni et al., 2020). In addition, it has been shown the involvement of AhR in the antiviral property of 3-O-methylfunicone, a secondary metabolite produced by fungus *Talaromyces pinophilus*, during bovine herpesvirus 1 infection (Fiorito et al., 2022). AhR is also involved in the host response to different CoVs. AhR activation has been revealed during infection with murine coronavirus (MCoV), Middle East respiratory syndrome coronavirus (MERS-CoV), severe acute respiratory syndrome (SARS-CoV-1), SARS-CoV-2, and human coronavirus (HCoV) 229E (Tang et al., 2005; Grunewald et al., 2020; Giovannoni et al., 2021). Specifically, during coronavirus-induced disease 2019 (COVID-19) SARS-CoV-2-induced, AhR modulates the expression of ACE-2 as well as its stabilizing partner, the broad neutral amino acid transporter 1 (B0AT1) (Giovannoni et al., 2021; Guarnieri et al., 2022), suggesting that AhR up-regulation is involved in promoting viral replication (Giovannoni et al., 2021). Furthermore, an AhR antagonist (CH223191) inhibits the replication in vitro of SARS-CoV-2 and HCoV-229E (Giovannoni et al., 2021).

Based on these findings, herein, it has been demonstrated that AhR, expressed in canine A72 cells as well as in feline CRFK cells, is activated by infection with CCoV and FCoV, respectively. Moreover, pharmacologic inhibition of AhR inhibits both CCoV and FCoV replication, recognizing AhR as a potential target for CCoV and FCoV antiviral therapy.

2. Materials and Methods

2.1. Cell Cultures and Virus Infection

A72 (canine fibrosarcoma cell line) cells were cultured in Dulbecco's modified Eagle's minimal essential medium (DMEM) supplemented with 10% fetal bovine serum (FBS) and incubated at 37 °C and 5% CO_2 (*De Martino et al., 2010; Marfè et al., 2011*). CCoV type II (strain S/378), kindly provided by Prof. C. Buonavoglia (University of Bari Aldo

Moro, Italy) was used throughout the study. A72 cells were used for virus stocks growth as well as for virus titration (*De Martino et al., 2010*).

CRFK (Crandell-Rees Feline Kidney cell line) cells were cultured in Dulbecco's modified Eagle's minimal essential medium (DMEM) supplemented with 10% fetal bovine serum (FBS) and incubated at 37 °C and 5% CO_2 (*Pratelli et al., 2008*). FCoV type I, biotype FECV (isolate "München"), kindly provided by the Friedrich-Loeffler-Institut (FLI, Insel Riems, Germany; viral registration number RVB-1259) was used throughout the study. CRFK cells were used for virus stocks growth as well as for virus titration.

2-methyl-2H-pyrazole-3-carboxylic acid (2-methyl-4-o-tolylazo-phenyl)-amide (CH223191) (Sigma-Aldrich, St. Louis, MI, USA), a synthetic and specific AhR competitive antagonist (*Kim et al., 2006; Torti et al., 2021*), was solubilized in DMSO (Sigma-Aldrich, St. Louis, MI, USA) and used at a concentration of 2, 5, 10 and 20 μM. Monolayers of both A72 and CRFK cells were pretreated for 1 h at 37 ◦C with DMEM 10% FBS containing different concentrations of CH223191 (2, 5, 10 and 20 μM). Then, A72 cells were infected or not with CCoV, and CRFK cells were infected or not with FCoV, at a multiplicity of infection (MOI) of 0.05 or 5) to obtain four groups/cell line: untreated uninfected cells; untreated infected cells; CH223191-treated uninfected cells; CH223191-treated infected cells. After 1 h of adsorption at 37 ◦C, cells were incubated and processed at different times post infection (p.i.). CCoV as well as FCoV were in culture medium throughout the course of the experiment.

2.2.Cell Viability

Cell viability was assessed by Trypan Blue (TB) (Sigma-Aldrich) exclusion test, as previously reported (*Fiorito et al., 2008; 2022*). In brief, monolayers of A72 cells and CRFK cells, pre-treated or not with CH223191 at different concentrations (2, 5, 10 and 20 μM), were infected or not infected with CCoV and FCoV respectively, at a MOI of 0.05. At different times p.i., cells were collected by trypsinization, mixed with TB, and scored through the TC20 automated cell counter (Bio-Rad Laboratories S.r.l., Segrate, Milan, Italy). Cell viability was calculated as the percentage of living cells over the total cell number. The results are reported as the mean ± S.D. of three independent experiments performed twice. In addition, cell viability was evaluated by the TB in cells attached to wells, as described (*Chowanadisai et al., 2013; Fiorito et al., 2020*).

2.3.Examination of Cell Morphology

Monolayers of cells, pretreated or not with CH223191, were infected or not, and incubated. After different times p.i., cells were washed twice with PBS, Giemsa staining and acridine orange/propidium iodide (AO/PI) were utilized to study cell morphology (*Bank et al., 1987; Fiorito et al., 2010; Ruggieri et al., 2007*). Cell death features were detected by using the criteria described (*Leite et al., 1999; Kroemer and Levine, 2008; Zakeri and Lockshin, 2008*).

For Giemsa staining, cells were fixed with 95% ethanol, drained, and dried. Afterward, cells were stained with a 5% Giemsa solution (Merck, Darmstadt, Germany). After 30 min, cells were rinsed with tap water and H_2O. Light microscopy examination was then performed using a ZOE Cell Imager (Bio-Rad Laboratories, Hercules, CA, USA).

For AO/PI, after treating with acridine orange/propidium iodide (AO/PI), fluorochromes used for the detection of both viable and dead cells, cells were observed by fluorescence microscopy. AO, which is membrane-permeable, binds to nucleic acids, provoking a green fluorescence. PI, impermeable to intact cell membrane, crosses the membrane of dead and dying cells and intercalates with nucleic acids, forming a bright red fluorescent complex. The combination of both fluorescent probes allows the simultaneous detection of cells with intact or compromised cell membranes (Bank, 1987). Fluorescence microscopy assessment was carried out by ZOE Cell Imager (Bio-Rad Laboratories, Hercules, CA, USA).

2.4.Immunofluorescence Staining

A72 and CRFK cells, pretreated or not with CH223191, were infected or not with CCoV and FCoV, respectively, at different MOI. At 24 h p.i., immunofluorescence staining was assessed (*Fiorito et al., 2022; Altamura et al., 2018*), by using the following antibodies, diluted in 5% bovine serum albumin-1x Tris-Buffered Saline, 0.1% Tween® 20 Detergent: rabbit polyclonal anti-AhR antibody (AhR) (Sigma-Aldrich, St. Louis, MI, USA) (1:250), mouse anti-CoV N protein monoclonal, MAB 938 (The Native Antigen Company) (1:250), mouse anti-FCoV N protein monoclonal (Bio-Rad, MCA2194) (1:400); Alexa Fluor 488 goat anti-mouse (Thermo Fisher Scientific) (1:1000), Texas Red goat anti-rabbit (Thermo Fisher Scientific, Waltham, MA, USA) (1:100). Microscopy and photography were evaluated by ZOE Fluorescent Cell Imager (Bio-Rad Laboratories).

Quantification of fluorescence signals from microscopy produced images, obtained by samples which were all run in the same experiment, were carried out by ImageJ (National Institutes of Health) software.

2.5.Virus Production

Monolayers of A72 and CRFK, pretreated or not with CH223191, were infected or not with CCoV and FCoV, respectively, at MOI of 0.05 and 5, incubated at 37 °C, and processed after 24 h of infection by real-time PCR for CCoV quantification. Furthermore, viral cytopathic effect (CPE) was evaluated, by examining cells under a light microscope at 24 h p.i. (*De Martino et al., 2010; Fiorito et al., 2022*).

2.6.CCoV Viral Nucleic Acids Extraction Procedures

Nucleic acid extraction was carried out from 200 µL of cell supernatant by using the King Fisher Flex System (Thermo Fisher Scientific, Waltham, MA, USA) with the Mag Max Viral Pathogen kit (Thermo Fisher Scientific, Waltham, MA, USA), according to the manufacturer's instructions. Nucleic acids were eluted in 60 µL of elution buffer. DMEM was utilized as a negative process control.

2.7. CCoV Viral Load Quantification by Real-Time Reverse Transcription PCR (RT-qPCR)

CCoV was quantified in all the samples by RT-qPCR. Detection was carried out on a QuantStudio 5 Real-Time PCR thermal cycler (Thermo Fisher Scientific, Waltham, MA, USA) in a total volume of 25 µL containing 5 µL of nucleic acid extract, 12.5 µL of AGPATH reaction kit with 1 µL of reverse transcriptase enzyme (Thermo Fisher Scientific, Waltham, MA, USA), 1 µL (10 µM) of primer forward CCoV-For (50 -TTGATCGTTTTTATAACGGTTCTACAA-30), 1 µL (10 µM) of primer reverse CCoV-Rev (50 -AATGGGCCATAATAGCCACATAAT-30) and 1 µL (6 µM) of probe CCoV-P (FAM-50 -ACCTCAATTTAGCTGGTTCGTGTATGGCATT-30 - TAMRA); for FCoV:

The thermal profile was the following: reverse transcription for 30 min. at 42 ◦C, initial denaturation for 15 min at 95 ◦C, 40 cycles of amplification for 15 s at 95 ◦C and for 60 s at 60 ◦C (Decaro et al., 2010). Quantification was carried out by a standard curve, developed by amplifying serial dilutions of the quantified extracted virus (from 3.5×10^9

to 3.5 × 10^4 $TCID_{50}$/mL) and plotting the Log $TCID_{50}$/mL versus the Ct number (Fiorito et al., 2022).

2.8. FCoV Viral Nucleic Acids Extraction Procedures

Nucleic acids eextraction was carried out on 200 µL of cell supernatant using QIAsymphony automated extraction system (Qiagen GmbH, Hilden, Germany) with the DSP Virus/Pathogen Mini kit (Qiagen GmbH, Hilden, Germany) according to the manufacturer's instructions. Nucleic acids were eluted in 60 µL of elution buffer.

2.9. FCoV Viral Load Quantification by RT-qPCR

Detection of FCoV was carried out by real-time RT-PCR. Reaction was performed on a QuantStudio 5 Real-Time PCR thermal cycler (Thermo Fisher Scientific, Waltham, Massachusetts, USA) in a total volume of 25 µl containing 5 µl of nucleic acids extract, 12.5 µl of AGPATH reaction kit with 1 µl of reverse transcriptase enzyme (Thermo Fisher Scientific, Waltham, Massachusetts, USA), 1 µl (6,25 µM) of primer forward FCoV-For (5'- AGCAACTACTGCCACRGGAT-3'), 1 µl (6,25 µM) of primer reverse FCoV-Rev (5'- GGAAGGTTCATCTCCCCAGT-3') and 1 µl (5 µM) of probe FCoV-P (5'-FAM-AATGGCCACACAGGGACAACGC-MGB-3'). The thermal profile was: reverse transcription for 30 min. at 48 ºC, initial denaturation for 15 min at 95 ºC, 45 cycles of amplification for 15 s at 95 ºC and for 60 s at 60 ºC (Dye et al., 2008). Quantification was carried out by a standard curve, developed by amplifying serial dilutions of the quantified extracted virus (from 1,0 x 10^{12} to 1,0 x 10^8 $TCID_{50}$/mL) and plotting the Log $TCID_{50}$/mL versus the Ct number (Fiorito et al., 2022).

2.10. Statistical Analysis

Results are described as mean ± S.D. One-way ANOVA with Tukey's post-test and by Student's t test was calculated by GraphPad InStat Version 3.00 for Windows 95 (GraphPad Software, San Diego, CA, USA). $p < 0.05$ was considered statistically significant.

3. Results

3.1. CH223191 Increases Cell Viability during both CCoV and FCoV Infection

The effects of four different concentrations of CH223191 (2, 5, 10 and 20 µM) on A72 and CRFK uninfected cells were tested. After 24 h of treatment, the cytotoxic concentration value required to reduce cell viability by 50% (CC_{50}) of CH223191 was identified and dose–response curve was developed in A72 cells (Figure 1a) and CRFK cells (Figure 2a). After 24 h of treatment, cell viability (% control) was detected in A72 cells with a CC_{50} of 9.6 µM CH223191, whereas, in CRFK with a CC_{50} of 5.9 µM CH223191 (Figures 1and 2). CH223191 at 2 µM in A72 (Figure 1a–c) and CRFK (Figure 1a–c) cells produced no significant differences in cell viability ($p > 0.5$)

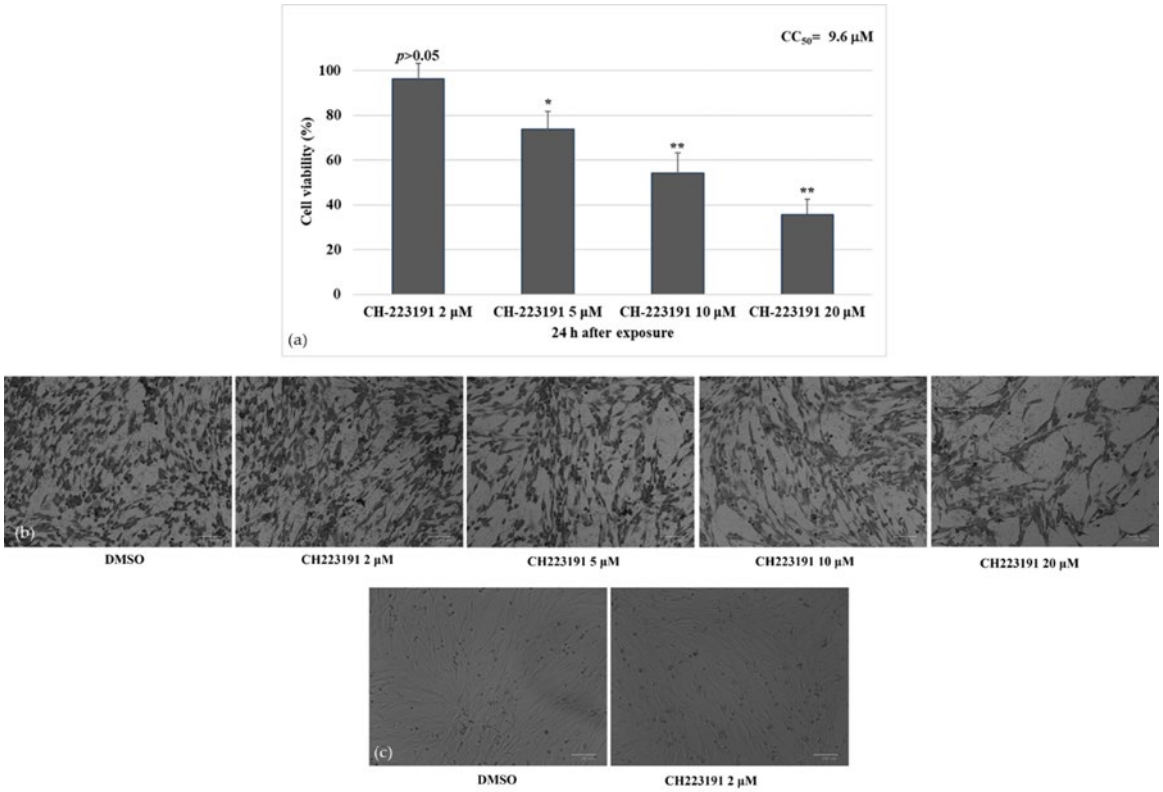

Figure 1. Identifying CC_{50} of CH223191 inhibitor at different doses and developing dose–response curve in A72 cells. (a) Dose–response curve of A72 cells treated with CH223191 at different concentrations (2, 5, 10 and 20 µM). After 24 h of treatment, cell viability was determined by TB staining while cells were attached to wells and counted under a light microscope. Significant differences between DMSO and CH223191-treated cells are indicated by probability p. * $p < 0.05$ and ** $p < 0.01$. (b) At 24 h after treatment, cells were stained with Giemsa and observed under a light microscope. (c) A72 cells treated with DMSO or with CH223191 (2 µM). Scale bar 100 µm.

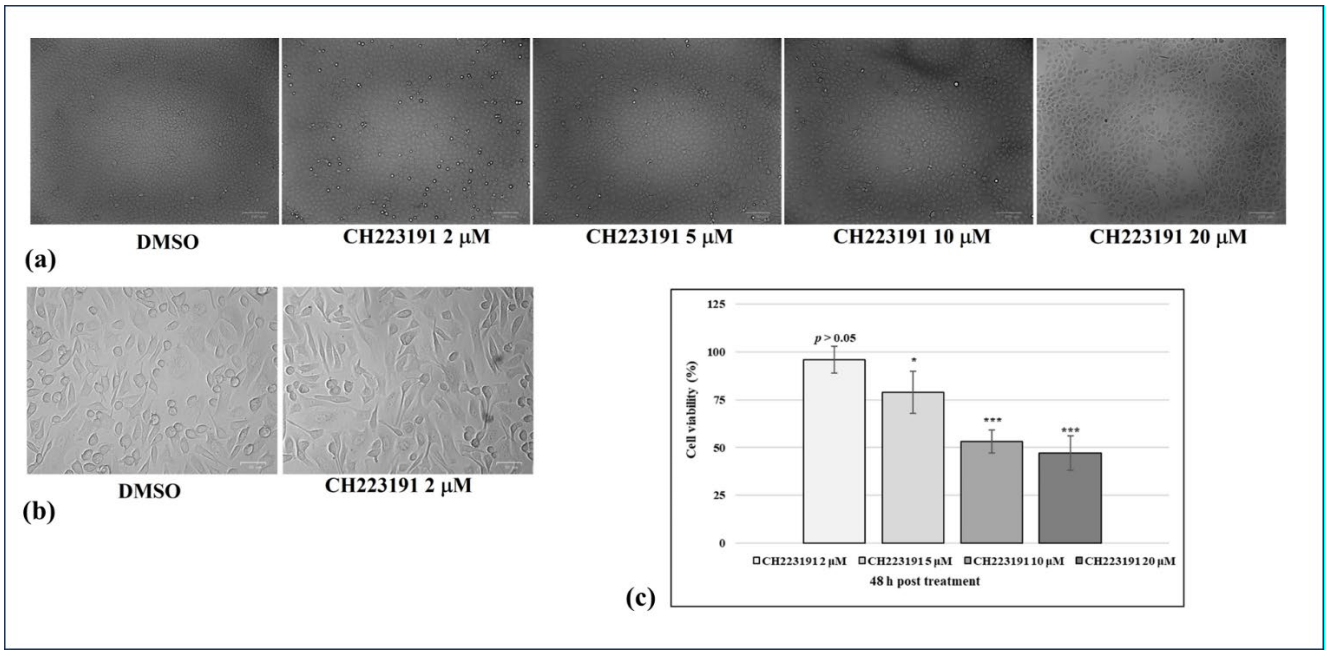

Figure 2. Identifying CC_{50} of CH223191 inhibitor at different doses and developing dose–response curve in CRFK cells. (a) Dose–response curve of CRFK cells treated with CH223191 at different concentrations (2, 5, 10 and 20 µM). After 24 h of treatment, cell viability was determined by TB staining while cells were attached to wells and counted under a light microscope. Significant differences between DMSO and CH223191-treated cells are indicated by probability p. * $p < 0.05$ and ** $p < 0.01$. (b) At 24 h after treatment, cells were stained with Giemsa and observed under a light microscope. (c) CRFK cells treated with DMSO or with CH223191 (2 µM). Scale bar 100 µm.

Then, monolayers of A72 and CRFK cells were infected with CCoV and FCoV, respectively, at MOI of 0.05 and were pretreated or not with CH223191 at different doses (2, 5, 10 and 20 µM). Following both CCoV and FCoV infection, a significant ($p < 0.05$) increase in cell viability in the presence of CH223191 at 2 µM in A72 (Figure 3) and CRFK cells (Figure 4) was observed.

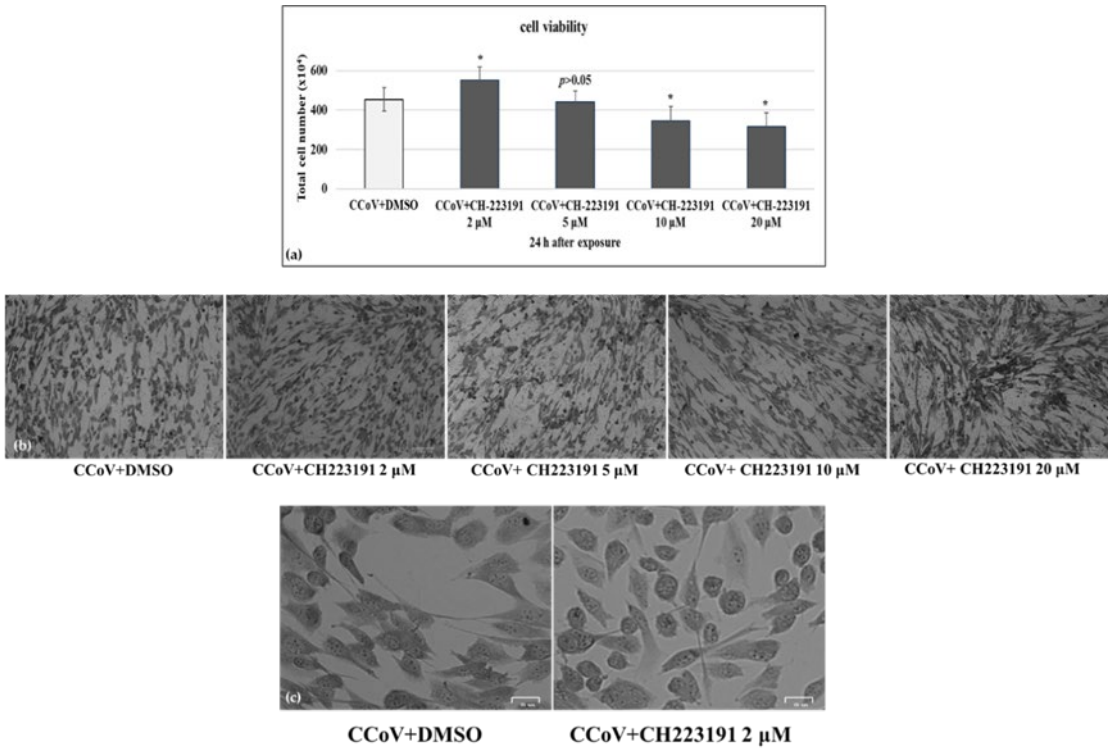

Figure 3. AhR inhibitor CH223191 increases cell viability during CCoV infection. (**a**) Dose–response curve of A72 cells treated with CH223191 at different concentrations (2, 5, 10 and 20 µM). After 24 h of treatment, cell viability was determined by TB staining while cells were attached to wells and counted under a light microscope. Significant differences between CCoV+DMSO and CCoV+CH223191-treated cells are indicated by probability *p*. * $p < 0.05$. (**b**) A72 cells infected with CCoV and treated or untreated with CH223191 at different concentrations (2, 5, 10 and 20 µM). At 24 h after treatment, cells were stained with Giemsa and observed under a light microscope. Scale bar 100 µm. (**c**) A72 cells infected with CCoV and treated or untreated with CH223191 (2 µM). At 24 h after treatment, cells were stained with Giemsa and observed under a light microscope. Scale bar 25 µm.

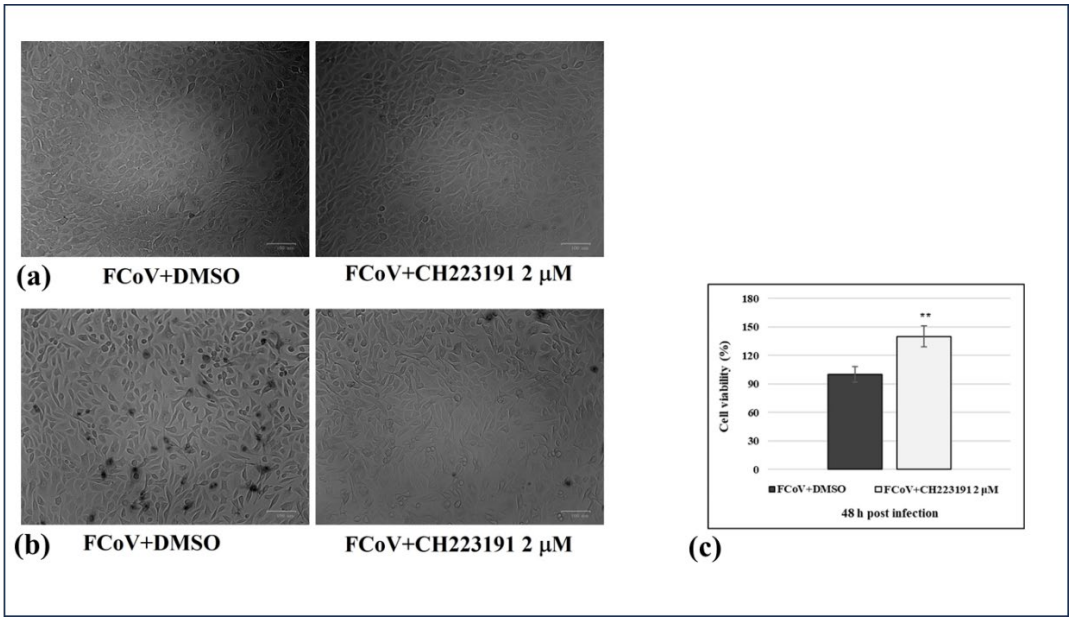

Figure 4. AhR inhibitor CH223191 increases cell viability during FCoV infection. (a) CRFK cells infected with FCoV and treated or untreated with CH223191 at 2 µM. At 24 h after treatment, cells were (b) unstained or (c) stained with TB and observed under a light microscope. Scale bar 100 µm. (b) Dose–response curve of CRFK cells treated with CH223191 at 2µM). After 24 h of treatment, cell viability was determined by TB staining while cells were attached to wells and counted under a light microscope. Significant differences between FCoV+DMSO and FCoV+CH223191-treated cells are indicated by probability *p*. ** $p < 0.01$.

Thus, the concentration of CH223191 at 2 μM was selected to be used throughout the study. These findings showed that in A72 and CRFK cells, at the non-toxic concentration of 2 μM, CH223191 significantly decreased cell death after 24 h of both CCoV and FCoV infection.

3.2. CH223191 Reduces Morphological Cell Death Features during CCoV and FCoV Infection in A72 and CRFK Cells

As displayed in Figure 5b, the lowest concentration of AhR inhibitor (2 μM) did not cause morphological changes on uninfected A72 cell groups compared to control, whereas in unexposed infected cells, an increase in intercellular spaces due to detachment from culture plate (Figure 5, arrow) was found. Changes in cell morphology suggesting signs of apoptosis, such as cell shrinkage (Figure 5, arrowhead; Figure 6, arrow), pyknosis and chromatin condensation (Figure 5, circle; Figure 6, arrowhead) were detected after Giemsa staining. All those cell death marks were markedly diminished when CCoV and FCoV-infected cells were treated with AhR inhibitor (Figures 5 and 6).

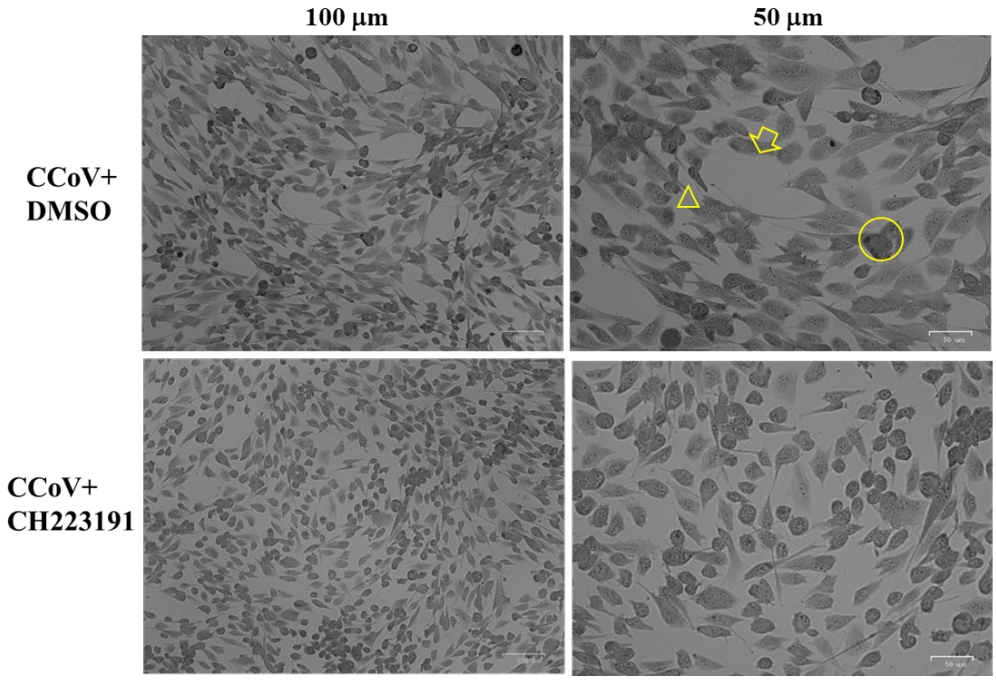

Figure 5. AhR inhibitor CH223191 reduces morphological cell death signs during CCoV infection in A72 cells. Cells were infected with CCoV, in the presence or absence of CH223191. At 24 h p.i., cells stained by Giemsa were analysed under a light microscope. Photomicrographs showing in unexposed infected groups, some cells with cell death features, such as an increase in intercellular spaces due to detachment from culture plate (arrow). In addition, morphological apoptotic marks, such as cell shrinkage (arrowhead), pyknosis and chromatin condensation (circle), were detected. In the presence of AhR inhibitor, all those cell death features were markedly diminished in CCoV-infected cells.

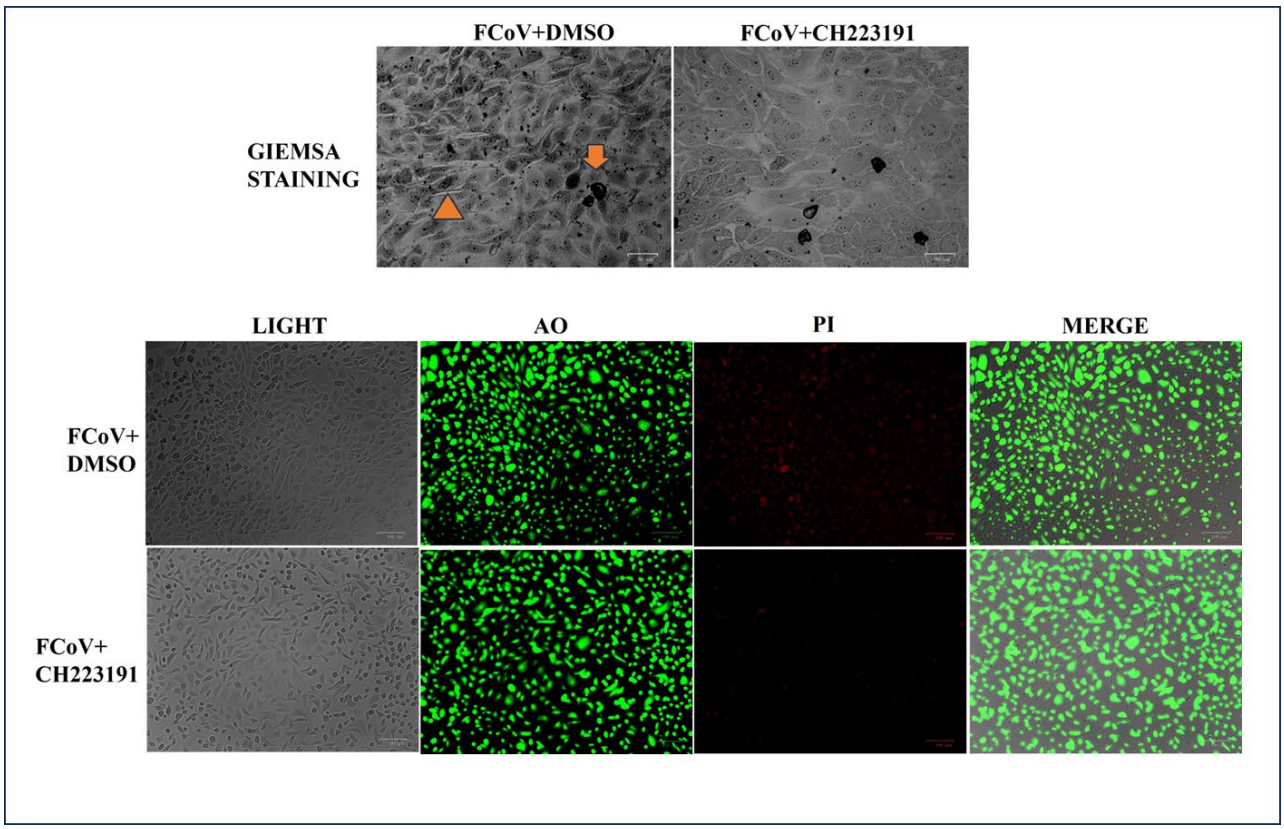

Figure 6. AhR inhibitor CH223191 reduces morphological cell death signs during FCoV infection in CRFK cells. Cells were infected with FCoV, in the presence or absence of CH223191. At 24 h p.i., cells stained by Giemsa were analysed under a light microscope. Signs of cell death, such as cellular shrinkage (A, arrowhead), pyknosis (A, arrow), were noticeably lessened in CH213191-treated groups. In AO/PI panels, PI fluorescent cells, indicating dead and dying cells, were mostly detected in FCoV-infected cells compared to cells treated with CH213191. Scale bar 100 µm.

After AO/PI staining, to detect both viable and dead cells, CRFK cells were observed by fluorescence microscopy. In the presence of CH223191, a decrease in PI fluorescent cells was observed in infected cells compared to CCoV untreated groups (Figure 6).

Overall, these findings demonstrated that CH223191 remarkably protected A72 and CRFK cells during CCoV and FCoV infection, respectively.

3.3. AhR was expressed in A72 and in CRFK cells

To investigate the expression of AhR in A72 as well as in CRFK cells, immunofluorescence staining was performed. As displayed in Figures 7 and 10, AhR was expressed by the canine fibrosarcoma cell line A72, and in feline CRFK. Interestingly, in A72 cells, AhR inhibitor CH223191 considerably decreased the expression of AhR

(Figure 7a), as confirmed by the measurement of integrated density fluorescence (Figure 7b).

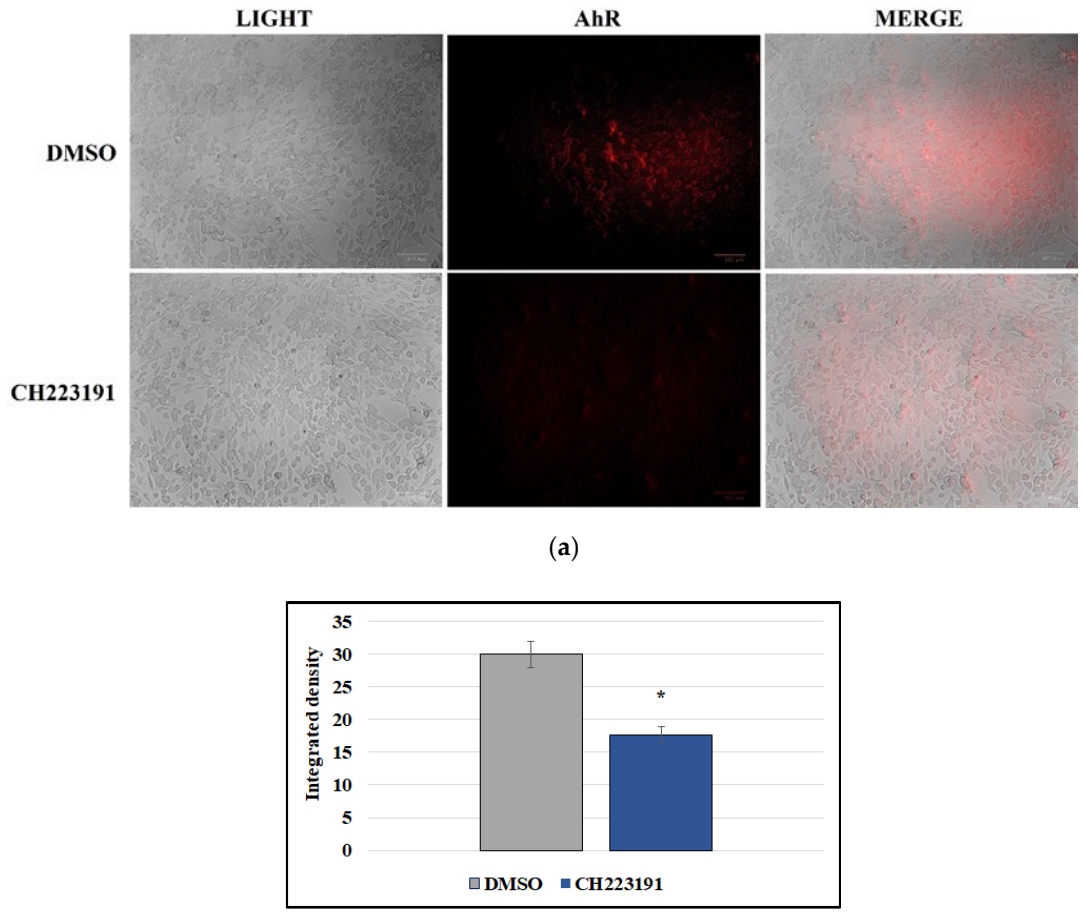

Figure 7. A72 cells express AhR. (**a**) Canine fibrosarcoma cell line A72 expressed AhR. AhR inhibitor CH223191 noticeably decreased the expression of AhR. Scale bar 100 µm. (**b**) Bars represent the mean ratio generated from the integrated density (product of the area and mean intensity of fluorescence) of the AhR expression evaluated by ImageJ. Error bars represent standard deviation measurement. Significant differences between CCoV-infected cells and AhR-inhibitor-treated infected cells are indicated by probability p. * $p < 0.05$.

3.4. CCoV and FCoV Infection Activate the Expression of AhR

In CCoV-infected cells, we detected a significant increase in AhR expression in A72 cells (Figure 8a). This finding was confirmed by integrated density measurement, indicating that up-regulation of AhR by CCoV was 1.7 times higher compared to uninfected cell group (Figure 8b).

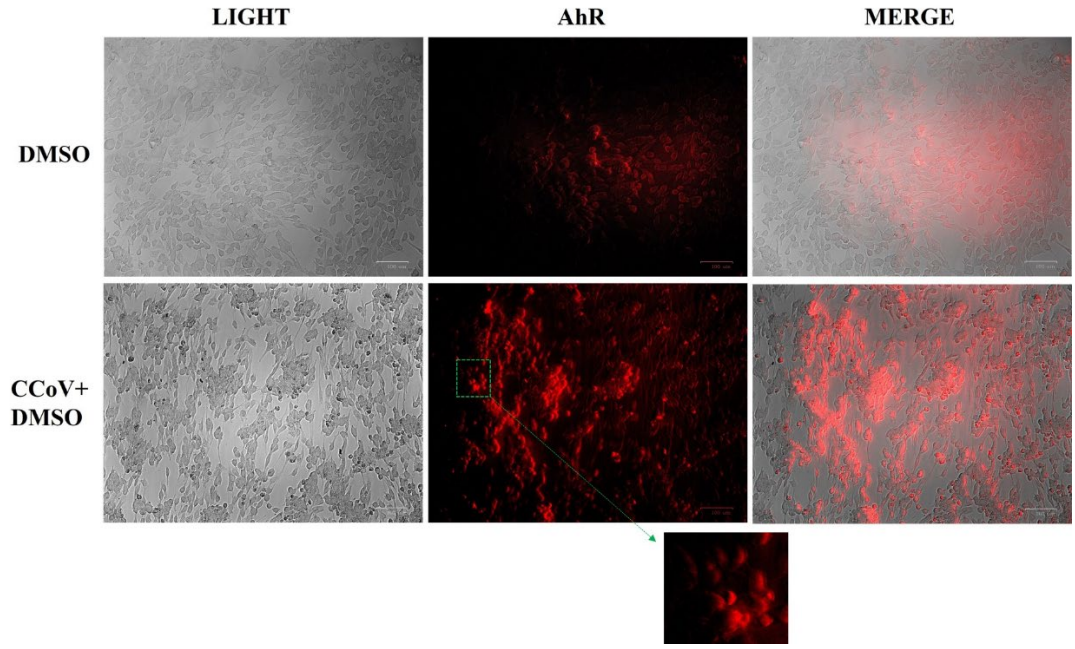

(**a**)

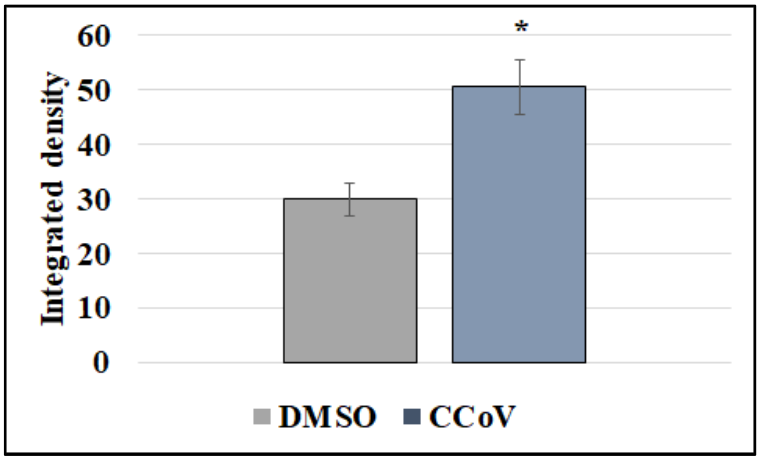

(**b**)

Figure 8. CCoV infection activates the expression of AhR in A72 cells. A72 cells were infected with CCoV at MOI of 0.05. At 24 h p.i., immunofluorescence staining for AhR was performed. (**a**) In CCoV-infected cells a significant increase in AhR expression was found. Scale bar 100 µm. (**b**) Bars represent the mean ratio generated from the integrated density (product of the area and mean intensity of fluorescence) of the AhR expression during CCoV infection evaluated by ImageJ. Error bars represent standard deviation measurement. Significant differences between CCoV-infected cells and AhR-inhibitor-treated infected cells are indicated by probability *p*. * $p < 0.05$.

3.5. Inhibitor CH223191 Inhibits both AhR and NP Expression during CCoV and FCoV Infection

The expression of AhR and NP during CCoV and FCoV infection in A72 and CRFK cells, respectively, were tested. NP was expressed during CCoV and FCoV infection, and a co-expression of NP and AhR in some merged images of both A72 and CRFK cells was found (Figures 9a and 10a - MERGE). Moreover, in both cell lines, using AhR inhibitor

CH223191, a down-regulation in the expression of AhR and NP was detected (Figures 9a and 10a). Those findings were confirmed by integrated density fluorescence measurement (Figures 9b,c and 10b,c).

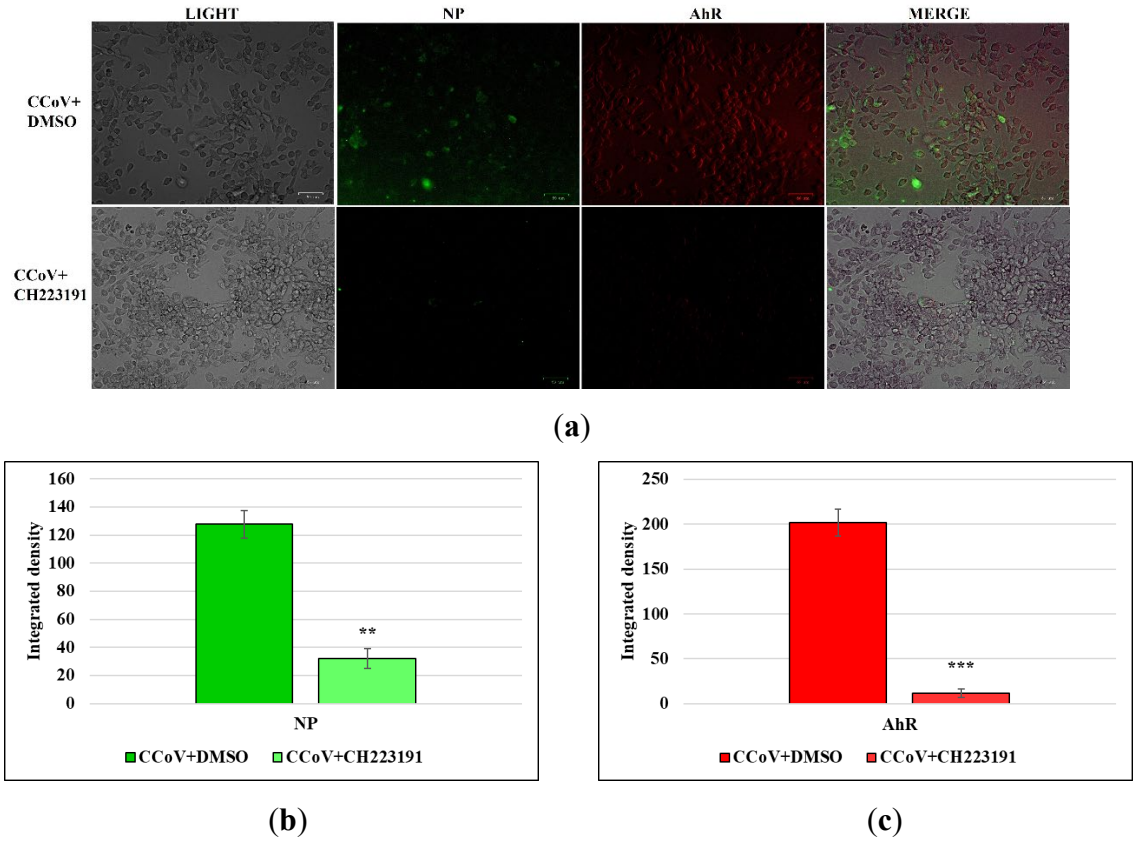

Figure 9. AhR inhibitor inhibits both AhR and NP expression during CCoV infection in A72 cells. A72 cells were infected with CCoV at MOI of 5. At 24 h p.i., immunofluorescence staining for AhR and NP was performed. (**a**) In CCoV-infected cells a significant up-regulation of AhR and NP expression was detected. In some merged images of A72 cells, co-expression of NP and AhR expression was found (MERGE). Following infection, in the presence of AhR inhibitor CH223191, both AhR and NP expression was down-regulated. Scale bar 59 µm. (**b**) Bars represent the mean ratio generated from the integrated density (product of the area and mean intensity of fluorescence) of the NP expression during CCoV infection evaluated by ImageJ. Error bars represent standard deviation measurement. Significant differences between CCoV-infected cells and AhR-inhibitor-treated infected cells are indicated by probability p. ** $p < 0.01$. (**c**) Bars represent the mean ratio generated from the integrated density (product of the area and mean intensity of fluorescence) of the AhR expression during CCoV infection evaluated by ImageJ. Error bars represent standard deviation measurement. Significant differences between CCoV-infected cells and AhR-inhibitor-treated infected cells are indicated by probability p. *** $p < 0.001$.

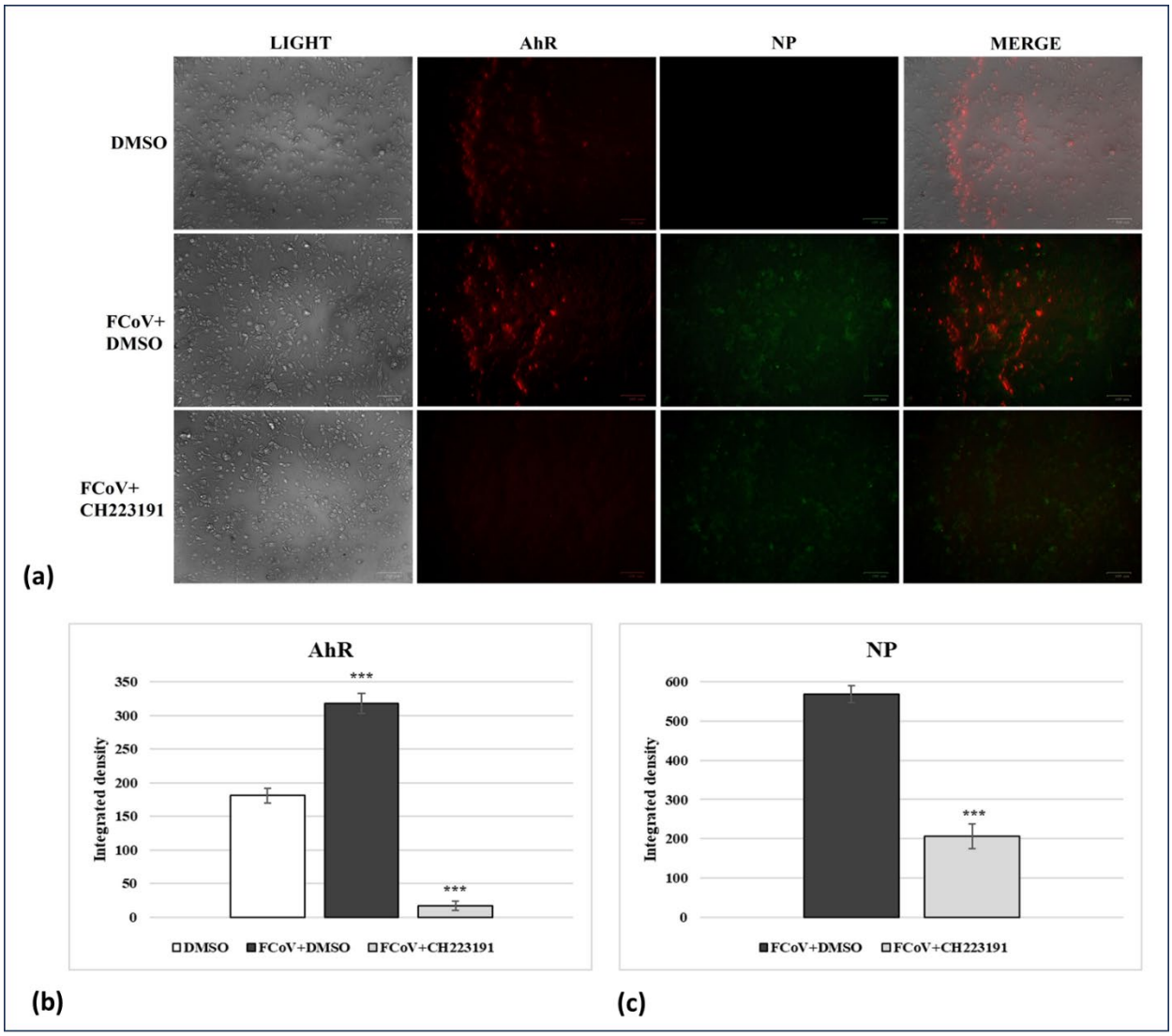

Figure 10. AhR inhibitor inhibits both AhR and NP expression during FCoV infection in CRFK cells. CRFK cells were infected with FCoV at MOI of 5. At 24 h p.i., immunofluorescence staining for AhR and NP was performed. (**a**) In FCoV-infected cells a significant up-regulation of AhR and NP expression was detected. Following infection, in the presence of AhR inhibitor CH223191, both AhR and NP expression was down-regulated. Scale bar 100 µm. (**b**) Bars represent the mean ratio generated from the integrated density (product of the area and mean intensity of fluorescence) of the NP expression during FCoV infection evaluated by ImageJ. Error bars represent standard deviation measurement. Significant differences between FCoV-infected cells and AhR-inhibitor-treated infected cells are indicated by probability p. *** $p < 0.001$. (**c**) Bars represent the mean ratio generated from the integrated density (product of the area and mean intensity of fluorescence) of the AhR expression during FCoV infection evaluated by ImageJ. Error bars represent standard deviation measurement. Significant differences between FCoV-infected cells and AhR-inhibitor-treated infected cells are indicated by probability p. *** $p < 0.001$.

Overall, these findings suggest that not only CCoV and FCoV infection activated AhR expression, but in some cells, co-expression of NP and AhR was detected. Interestingly, using AhR inhibitor, the down-regulation of both NP and AhR was found.

3.6. AhR Inhibitor Decreases Virus Yield during CCoV and FCoV Infection

CPE Evaluation

Following CCoV and FCoV infections in A72 cells (Figure 3) and in CRFK (Figure 12), respectively, at 24 h p.i. an increase in CPE was found. Indeed, morphological alterations, such as development in syncytia of giant cells and detachment from culture plate in CCoV-infected groups, were detected (Figures 3 and 12). These features were intensely reduced by the presence of AhR inhibitor (Figures 3 and 12).

Standard Curve and Virus Quantification

AhR ability to decrease virus yield was evaluated also by Rt-qPCR. Quantification was made by the mean of a standard curve. The standard curve was constructed based on the average Ct values of three replicates against the Log of known amount of each virus studied (expressed in $TCID_{50}$/mL). The standard curve was used in RT-qPCR assays (Fiorito et al., 2022) to estimate samples' virus titer starting from the Ct obtained in the amplification reaction. Our results showed that CCoV as well as FCoV virus yield were significantly reduced by AhR inhibitor in A72 and CRFK cells (Figures 11 and 12).

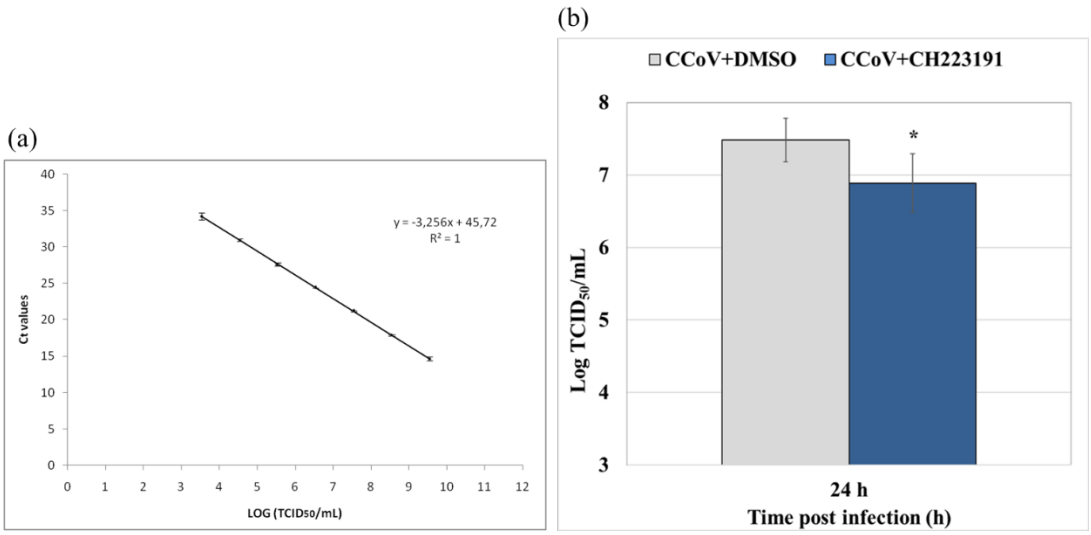

Figure 11. AhR inhibitor decreases virus yield during CCoV infection in A72 cells. Cells were infected with CCoV in the presence or absence of AhR inhibitor CH223191. At 24 h p.i., virus yield was evaluated by RT-qPCR by the mean of a standard curve (a) created plotting Log $TCID_{50}$/mL against the Ct number (b). Significant differences between CCoV-infected cells and AhR-inhibitor-treated infected cells are indicated by probability p. * $p < 0.05$.

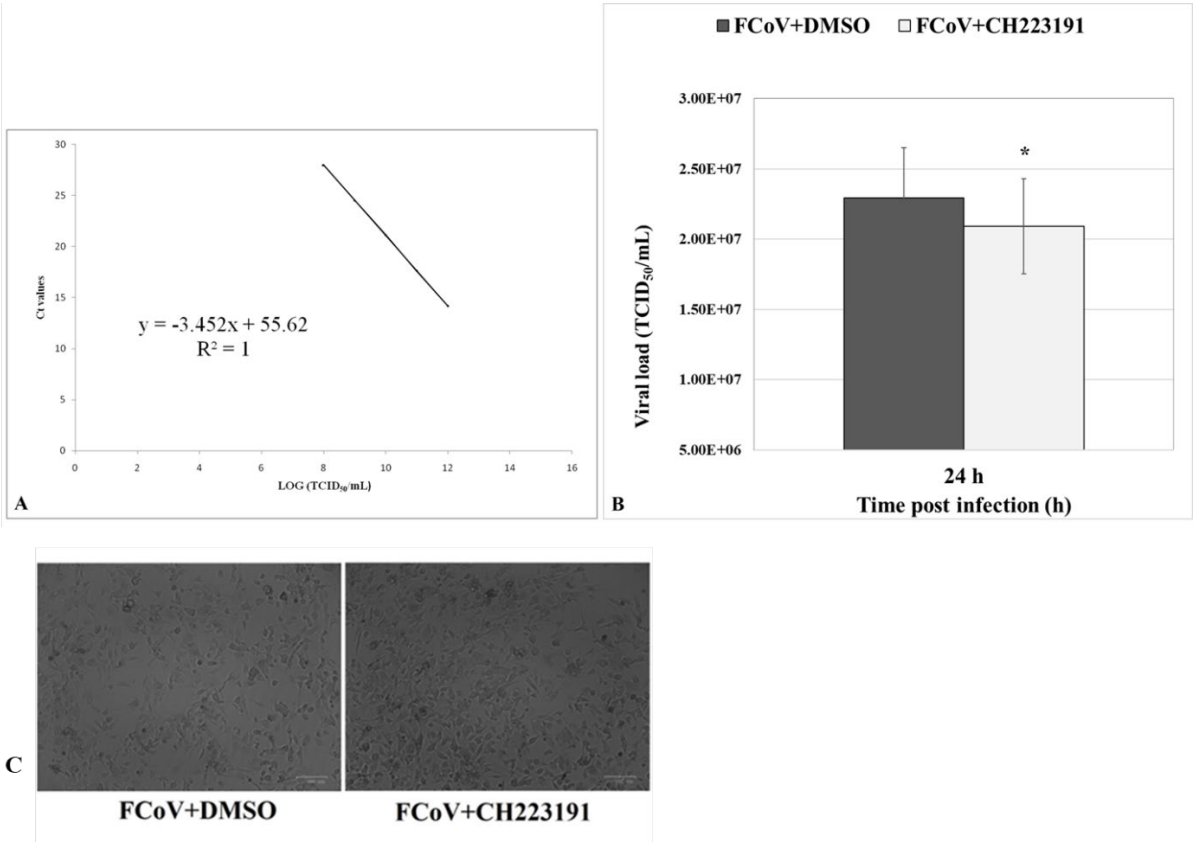

Figure 12. AhR inhibitor decreases virus yield during FCoV infection in CRFK cells. Cells were infected with FCoV in the presence or absence of AhR inhibitor CH223191. At 24 h p.i., virus yield was evaluated by RT-qPCR by the mean of a standard curve (a) created plotting Log $TCID_{50}$/mL against the Ct number (b). Significant differences between FCoV-infected cells and AhR-inhibitor-treated infected cells are indicated by probability p. * $p < 0.01$. (c) CPE was evaluated by ZOE Cell Imager.

Taken together, our results demonstrated that AhR inhibitor significantly reduced CCoV and FCoV virus yield during infection in A72 cells and in CRFK cells, respectively.

4. Discussion

The ability of CoVs to mutate and recombine their genome has been extensively proved. This feature allows them to cross interspecies barriers. Specifically, recent studies highlight the aptitude of CCoV, an alphacoronavirus, to mutate into new and more

dangerous variants (Kenney et al., 2021; Pratelli et al., 2021, 2022; Vlasova et al., 2022). In different countries of the world, and not simultaneously, extremely virulent recombinant canine–feline–porcine alphacoronaviruses have been identified in dogs as well as in humans (Kenney et al., 2021; Pratelli et al., 2021, 2022; Vlasova et al., 2022). These findings indicate the need for constant surveillance of CoVs, such as CCoV. To date, indomethacin, an anti-inflammatory drug, has been demonstrated to have effective antiviral properties against CCoV infection, acting on the virus replication cycle and blocking viral RNA synthesis (Amici et al., 2006; Xu et al., 2020; Gomeni et al., 2020). Although lethal FIP is very common in felines, therapeutic strategies are currently limited as well as highly toxic. Based on different mechanisms of action involved in FCoV life cycle, several attempts have been done (Delaplace et al., 2021; Tesker et al., 2023; Schmied et al., 2024). Compounds which act inhibiting fusion to cell and endocytosis, translation inhibition, translation inhibition, host protein inhibition and protease inhibitors have been tested. For example, hydroxychloroquine, a drug approved to treat malaria and immune-mediated diseases in humans, in association with interferon-ω is effective for FIPV in vitro (Takano et al., 2020). Itraconazole, an antifungal (Takano et al., 2019), sinefungin, a nucleoside antibiotic (Kuroda et al., 2019), 5-amino levulinic acid (Takano et al., 2021), doxycycline (Dunowska et Ghosh, 2021) inhibit FCoV infection. ERDRP-0519, a non-nucleoside inhibitor, which targets viral RNA polymerase, is suitable a highly effective against FIPV (Camero et al., 2022). In addition, natural products, like Thymus vulgaris essential oil (Catella et al., 2021), and napier grass (Pennisetum purpureum), which has high phenolic content (Chen et al., 2022), crude extracts of Talaromyces Strains (B18) (Vocadlova et al., 2023), the two flavonoids, isoginkgetin and luteolin (Triratapiban et al., 2023), rottlerin, a natural extract from Mallotus philippensis, loaded by liposomes (Choi et al., 2023) have antiviral activity against FIPV. But a recent alternative to euthanasia, making FIP often curable, is due to very effective result antiviral treatments based on nucleoside analogues remdesivir (Bohm, 2022) and GS-441524, a remdesivir derivate (Murphy et al., 2018; Dickinson et al., 2020; Izes et al., 2020; Paltrinieri et al., 2021; Jones et al., 2021; krentz et al., 2021; Delaplace et al., 2021; Cook et al., 2022; Doki et al., 2022; Meli et al., 2022; Addie et al., 2020a,b,2023; Taylor et al., 2023; Tasker et al., 2023; Cosaro et al., 2023; Coggins et al., 2023; Yan et al, 2023). Indeed, they are effective against FIP in both the short term as well as the long term (Zwicklbauer et al., 2023), but toxic effects could be induced by their use, such as acute progressive azotemia and multifocal urolithiasis (Allinder et al., 2024). Promising results

were found a new therapy based on unlicensed molnupiravir (Roy et al., 2022; Sase, 2023).

Recent advances reveal the involvement of AhR during CoVs infection (Tang et al., 2005; Grunewald et al., 2020; Giovannoni et al., 2021; Shi et al., 2023; Zhao et al., 2023; Yousefi et al., 2023). In particular, AhR antagonist, like CH223191, decreases the expression of the angiotensin-converting enzyme 2 (ACE2) receptor, via AhR activation, resulting in the suppression of SARS-CoV-2 infection in mammalian cells (Giovannoni et al., 2021). Herein, first, we found that AhR was expressed in canine A72 cells as well as in CRFK cells. Moreover, it was significantly activated during both CCoV and FCoV infection, as reported in other CoVs infections (Tang et al., 2005; Grunewald et al., 2020; Giovannoni et al., 2021). In fact, the measurement of integrated density fluorescence showed that the expression was significante higher in infected cell groups compared to uninfected cells. Using a well-known AhR inhibitor, CH223191, at dose of 2 M did not cause toxic effects both in A72 and in CRFK cells, and significantly reduced cell death after 24 h of CCoV and FCoV infection. In addition, CH223191 markedly diminished morphological cell death features, typical marks of CCoV infection in A72 cells (De Martino et al., 2010; Ruggieri et al., 2007), and of FCoV infection in CRFK cells Those findings were accompanied by a significant decline in both viruses yield, results supposing that AhR up-regulation may represent a common approach used by CoVs to stimulate viral replication (Tang et al., 2005; Grunewald et al., 2020; Giovannoni et al., 2021,) (see Table 1).

Following CCoV and FCoV infection, in the presence or in the absence of AhR inhibitor, the expression of both NP and AhR were simultaneously tested. Surprisingly, in some A72 and or in CRFK infected cells, a novel co-expression of NP and AhR expression was found, and the possible explanations for that finding need further investigation. Furthermore, the AhR inhibitor not only significantly down-regulated the expression of AhR, but also of NP in both infection studied. Evidence on structural knowledge as well as on the functional mechanism of viral nucleocapsid protein NP is considered a starting point for the development of potential inhibitors against CoV diseases. Indeed, NP is responsible of binding the viral RNA genome, packing viral genome RNA into ribonucleoproteins, and compressing it into a compact virion core (McBride et al., 2014). Moreover, it is generally more stable than the CoV spike protein, which has a higher mutation rate (Zhu et al., 2005; Dutta et al., 2020; Tseng et al., 2021).

Overall, based on our results, emphasizing the possible role of AhR as a target for antiviral therapy, we suppose that some AhR ligands may improve the host response to CoVs infection. Additionally, we identified NP antagonists for targeting not only CCoV but also FCoV. Future biochemical and structural studies may better delineate the current research. However, these results highlight the importance of screening hypothetical antivirals in in vitro animal models of CoVs to avoid the manipulation of extremely dangerous human CoVs (SARS-CoVs and MERS-CoV).

Conclusions

Our preliminary findings indicate that AhR up-regulation might be a common stratagem used by coronaviruses to stimulate viral replication. Pharmacologic inhibition of AhR by CH223191 repressed both CCoV and FCoV replication, recognizing AhR as a new target for identifying antiviral drugs to counteract CoVs. Importantly, animal coronaviruses, such as CCoV and FCoV, represent a valid alternative for carrying out preliminary studies on the efficacy of drugs, bypassing the risks of using a highly pathogenic and contagious virus for the first step of screening.

References

- Addie D, Belák S, Boucraut-Baralon C, Egberink H, Frymus T, Gruffydd-Jones T, Hartmann K, Hosie MJ, Lloret A, Lutz H, Marsilio F, Pennisi MG, Radford AD, Thiry E, Truyen U, Horzinek MC. Feline infectious peritonitis. ABCD guidelines on prevention and management. J Feline Med Surg. 2009 Jul;11(7):594-604. doi: 10.1016/j.jfms.2009.05.008.
- Addie DD, Bellini F, Covell-Ritchie J, Crowe B, Curran S, Fosbery M, Hills S, Johnson E, Johnson C, Lloyd S, Jarrett O. Stopping Feline Coronavirus Shedding Prevented Feline Infectious Peritonitis. Viruses. 2023 Mar 23;15(4):818. doi: 10.3390/v15040818.
- Addie DD, Covell-Ritchie J, Jarrett O, Fosbery M. Rapid Resolution of Non-Effusive Feline Infectious Peritonitis Uveitis with an Oral Adenosine Nucleoside Analogue and Feline Interferon Omega. Viruses. 2020a Oct 27;12(11):1216. doi: 10.3390/v12111216.
- Addie DD, Curran S, Bellini F, Crowe B, Sheehan E, Ukrainchuk L, Decaro N. Oral Mutian®X stopped faecal feline coronavirus shedding by naturally infected cats. Res Vet Sci. 2020 Jun;130:222-229
- Allinder M, Tynan B, Martin C, Furbish A, Austin G, Bartges J, Lourenço BN. Uroliths composed of antiviral compound GS-441524 in 2 cats undergoing treatment for feline infectious peritonitis. J Vet Intern Med. 2024 Jan-Feb;38(1):370-374.
- Altamura, G., Power, K., Martano, M., degli Uberti, B., Galiero, G., De Luca, G., Maiolino, P., Borzacchiello, G, 2018. *Felis catus* papillomavirus type-2 E6 binds to E6AP, promotes E6AP/p53 binding and enhances p53 proteasomal degradation. Sci. Rep. 8, 17529.
- Amici, C., Di Caro, A., Ciucci, A., Chiappa, L., Castilletti, C., Martella, V., Decaro, N., Buonavoglia, C., Capobianchi, M.R., Santoro, G.M., 2006. Indomethacin has a potent antiviral activity against SARS coronavirus. Antivir. Ther. 11, 1021–1030.
- Attipa C et al., 2023b Emergence and spread of feline infectious peritonitis due to a highly pathogenic canine/feline recombinant coronavirus | bioRxiv
- Attipa C, Gunn-Moore D, Mazeri S, Epaminondas D, Lyraki M, Hardas A, Loukaidou S, Gentil M. Concerning feline infectious peritonitis outbreak in Cyprus. Vet Rec. 2023a Jun 3;192(11):449-450.
- Bank HL. Assessment of islet cell viability using fluorescent dyes. Diabetologia. 1987 Oct;30(10):812-816.
- Bock, K.W., 2021. Aryl hydrocarbon receptor (AHR), integrating energy metabolism and microbial or obesity-mediated inflammation. Biochem. Pharmacol. 184, 114346.
- Bohm M. Successful treatment of a South African cat with effusive feline infectious peritonitis with remdesivir. J S Afr Vet Assoc. 2022 Nov;93(2):112-115.
- Buonavoglia C, Decaro N, Martella V, Elia G, Campolo M, Desario C, Castagnaro M, Tempesta M. Canine coronavirus highly pathogenic for dogs. Emerg Infect Dis. 2006 Mar;12(3):492-4.
- Camero M, Lanave G, Catella C, Lucente MS, Sposato A, Mari V, Tempesta M, Martella V, Buonavoglia A. ERDRP-0519 inhibits feline coronavirus in vitro. BMC Vet Res. 2022 Jan 25;18(1):55

- Capozza P, Pratelli A, Camero M, Lanave G, Greco G, Pellegrini F, Tempesta M. Feline Coronavirus and Alpha-Herpesvirus Infections: Innate Immune Response and Immune Escape Mechanisms. Animals (Basel). 2021 Dec 14;11(12):3548.
- Catella C, Camero M, Lucente MS, Fracchiolla G, Sblano S, Tempesta M, Martella V, Buonavoglia C, Lanave G. Virucidal and antiviral effects of Thymus vulgaris essential oil on feline coronavirus. Res Vet Sci. 2021 Jul;137:44-47.
- Chen YN, Kao WM, Lee SC, Wu JM, Ho YS, Hsieh MK. Antiviral Properties of Pennisetum purpureum Extract against Coronaviruses and Enteroviruses. Pathogens. 2022 Nov 17;11(11):1371.
- Choi JC, Jung SW, Choi IY, Kang YL, Lee DH, Lee SW, Park SY, Song CS, Choi IS, Lee JB, Oh C. Rottlerin-Liposome Inhibits the Endocytosis of Feline Coronavirus Infection. Vet Sci. 2023 May 30;10(6):380.
- Chowanadisai, W.; Graham, D.M.; Keen, C.L.; Rucker, R.B.; Messerli, M.A. Neurulation and neurite extension require the zinc transporter ZIP12 (slc39a12). Proc. Natl. Acad. Sci. USA 2013, 110, 9903–9908.
- Coggins SJ, Norris JM, Malik R, Govendir M, Hall EJ, Kimble B, Thompson MF. Outcomes of treatment of cats with feline infectious peritonitis using parenterally administered remdesivir, with or without transition to orally administered GS-441524. J Vet Intern Med. 2023 Sep-Oct;37(5):1772-1783.
- Cook SE, Vogel H, Castillo D, Olsen M, Pedersen N, Murphy BG. Investigation of monotherapy and combined anticoronaviral therapies against feline coronavirus serotype II in vitro. J Feline Med Surg. 2022 Oct;24(10):943-953.
- Cosaro E, Pires J, Castillo D, Murphy BG, Reagan KL. Efficacy of Oral Remdesivir Compared to GS-441524 for Treatment of Cats with Naturally Occurring Effusive Feline Infectious Peritonitis: A Blinded, Non-Inferiority Study. Viruses. 2023 Aug 1;15(8):1680.
- De Martino L, Marfé G, Longo M, Fiorito F, Montagnaro S, Iovane V, Decaro N, Pagnini U. Bid cleavage, cytochrome c release and caspase activation in canine coronavirus-induced apoptosis. Vet Microbiol. 2010 Feb 24;141(1-2):36-45.
- Decaro N, Mari V, Campolo M, Lorusso A, Camero M, Elia G, Martella V, Cordioli P, Enjuanes L, Buonavoglia C. Recombinant canine coronaviruses related to transmissible gastroenteritis virus of Swine are circulating in dogs. J Virol. 2009 Feb;83(3):1532-7.
- Decaro N, Martella V, Elia G, Campolo M, Desario C, Cirone F, Tempesta M, Buonavoglia C. Molecular characterisation of the virulent canine coronavirus CB/05 strain. Virus Res. 2007 Apr;125(1):54-60.
- Decaro, N.; Mari, V.; Elia, G.; Addie, D.D.; Camero, M.; Lucente, M.S.; Martella, V.; Buonavoglia, C. Recombinant canine coronaviruses in dogs, Europe. Emerg. Infect. Dis. 2010, 16, 41–47.
- Delaplace M, Huet H, Gambino A, Le Poder S. Feline Coronavirus Antivirals: A Review. Pathogens. 2021 Sep 7;10(9):1150.
- Dickinson PJ, Bannasch M, Thomasy SM, Murthy VD, Vernau KM, Liepnieks M, Montgomery E, Knickelbein KE, Murphy B, Pedersen NC. Antiviral treatment using the adenosine nucleoside analogue GS-

441524 in cats with clinically diagnosed neurological feline infectious peritonitis. J Vet Intern Med. 2020 Jul;34(4):1587-1593.

- Doki T, Takahashi K, Hasegawa N, Takano T. In vitro antiviral effects of GS-441524 and itraconazole combination against feline infectious peritonitis virus. Res Vet Sci. 2022 May;144:27-33.
- Dunowska M, Ghosh S. In Vitro Effects of Doxycycline on Replication of Feline Coronavirus. Pathogens. 2021 Mar 7;10(3):312.
- Dutta, N.K.; Mazumdar, K.; Gordy, J.T.; Dutch, R.E. The nucleocapsid protein of SARSCoV-2: A target for vaccine development. J. Virol. 2020, 94, e00647-20.
- Dye C, Helps CR, Siddell SG. 2008, Evaluation of real-time RT-PCR for the quantification of FCoV shedding in the faeces of domestic cats. J Feline Med Surg. 10, 167-174.
- Fiorito F, Cerracchio C, Salvatore MM, Serra F, Pucciarelli A, Amoroso MG, Nicoletti R, Andolfi A. Antiviral Property of the Fungal Metabolite 3-O-Methylfunicone in Bovine Herpesvirus 1 Infection Microorganisms 2022, 10, 188.
- Fiorito, F., Marf`e, G., Granato, G.E., Ciarcia, R., De Blasio, E., Tafani, M., Florio, S., De Martino, L., Muzi, G., Pagnini, U., Giordano, A., 2010. 2,3,7,8-Tetrachlorodibenzo-pdioxin modifies expression and nuclear/cytosolic localization of bovine herpesvirus 1 immediate-early protein (bICP0) during infection. J. Cell. Biochem. 111, 333–342. https://doi.org/10.1002/jcb.22700.
- Fiorito, F.; Marfè, G.; De Blasio, E.; Granato, G.E.; Tafani, M.; De Martino, L.; Montagnaro, S.; Florio, S.; Pagnini, U. 2,3,7,8- Tetrachlorodibenzo-p-dioxin regulates Bovine Herpesvirus type 1 induced apoptosis by modulating Bcl-2 family members. Apoptosis 2008, 13, 1243–1252.
- Fiorito, F.; Nocera, F.P.; Cantiello, A.; Iovane, V.; Lambiase, S.; Piccolo, M.; Ferraro, M.G.; Santamaria, R.; De Martino, L. Bovine herpesvirus-1 infection in mouse neuroblastoma (Neuro-2A) cells. Vet. Microbiol. 2020, 247, 108762.
- Giovannoni, F.; Bosch, I.; Polonio, C.M.; Torti, M.F.; Wheeler, M.A.; Li, Z.; Romorini, L.; Rodriguez Varela, M.S.; Rothhammer, V.; Barroso, A.; et al. AHR is a Zika virus host factor and a candidate target for antiviral therapy. Nat. Neurosci. 2020, 23, 939–951.
- Giovannoni, F.; Li, Z.; Remes-Lenicov, F.; Dávola, M.E.; Elizalde, M.; Paletta, A.; Ashkar, A.A.; Mossman, K.L.; Dugour, A.V.; Figueroa, J.M.; et al. AHR signaling is induced by infection with coronaviruses. Nat. Commun. 2021, 12, 5148.
- Gomeni, R., Xu, T., Gao, X., Bressolle-Gomeni, F., 2020. Model based approach for estimating the dosage regimen of indomethacin a potential antiviral treatment of patients infected with SARS CoV-2. J. Pharmacokinet. Pharmacodyn. 47, 189–198.
- Grunewald, M.E.; Shaban, M.G.; Mackin, S.R.; Fehr, A.R.; Perlman, S. Murine coronavirus infection activates the aryl hydrocarbon receptor in an indoleamine 2,3-dioxygenase-independent manner, contributing to cytokine modulation and proviral TCDD-inducible-PARP expression. J. Virol. 2020, 94, 319–335.

- Guarnieri, T. Hypothesis: Emerging Roles for Aryl Hydrocarbon Receptor in Orchestrating CoV-2-Related Inflammation. Cells 2022, 11, 648.
- Gutierrez-Vazquez, C.; Quintana, F.J. Regulation of the immune response by the aryl hydrocarbon receptor. Immunity 2018, 48, 19–33.
- Herrewegh AA, Smeenk I, Horzinek MC, Rottier PJ, de Groot RJ. Feline coronavirus type II strains 79-1683 and 79-1146 originate from a double recombination between feline coronavirus type I and canine coronavirus. J Virol. 1998 May;72(5):4508-14.
- Hu J, Ding Y, Liu W, Liu S. When AHR signaling pathways meet viral infections. Cell Commun Signal. 2023 Feb 24;21(1):42. doi: 10.1186/s12964-023-01058-8.
- Izes AM, Yu J, Norris JM, Govendir M. Current status on treatment options for feline infectious peritonitis and SARS-CoV-2 positive cats. Vet Q. 2020 Dec;40(1):322-330.
- Jones S, Novicoff W, Nadeau J, Evans S. Unlicensed GS-441524-Like Antiviral Therapy Can Be Effective for at-Home Treatment of Feline Infectious Peritonitis. Animals (Basel). 2021 Jul 30;11(8):2257.
- Kenney SP, Wang Q, Vlasova A, Jung K, Saif L. Naturally Occurring Animal Coronaviruses as Models for Studying Highly Pathogenic Human Coronaviral Disease. Vet Pathol. 2021 May;58(3):438-452
- Kim SH, Henry EC, Kim DK, Kim YH, Shin KJ, Han MS, Lee TG, Kang JK, Gasiewicz TA, Ryu SH, Suh PG. Novel compound 2-methyl-2H-pyrazole-3-carboxylic acid (2-methyl-4-o-tolylazo-phenyl)-amide (CH-223191) prevents 2,3,7,8-TCDD-induced toxicity by antagonizing the aryl hydrocarbon receptor. Mol Pharmacol. 2006 Jun;69(6):1871-1878.
- Krentz D, Zenger K, Alberer M, Felten S, Bergmann M, Dorsch R, Matiasek K, Kolberg L, Hofmann-Lehmann R, Meli ML, Spiri AM, Horak J, Weber S, Holicki CM, Groschup MH, Zablotski Y, Lescrinier E, Koletzko B, von Both U, Hartmann K. Curing Cats with Feline Infectious Peritonitis with an Oral Multi-Component Drug Containing GS-441524. Viruses. 2021 Nov 5;13(11):2228.
- Kroemer, G., Levine, B., 2008. Autophagic cell death: The story of a misnomer. Nat. Rev. Mol. Cell Biol. 9, 1004–1010.
- Kuroda Y, Yamagata H, Nemoto M, Inagaki K, Tamura T, Maeda K. Antiviral effect of sinefungin on in vitro growth of feline herpesvirus type 1. J Antibiot (Tokyo). 2019 Dec;72(12):981-985.
- Lawrence, B.P.; Vorderstrasse, B.A. New insights into the aryl hydrocarbon receptor as a modulator of host responses to infection. Semin. Immunopathol. 2013, 35, 615–626.
- Lednicky JA, Tagliamonte MS, White SK, Blohm GM, Alam MM, Iovine NM, Salemi M, Mavian C, Morris JG. Isolation of a Novel Recombinant Canine Coronavirus From a Visitor to Haiti: Further Evidence of Transmission of Coronaviruses of Zoonotic Origin to Humans. Clin Infect Dis. 2022 Aug 24;75(1):e1184-e1187.
- Leite, M., Quinta-Costa, M., Leite, P.S., Guimar˜aes, J.E., 1999. Critical evaluation of techniques to detect and measure cell death-study in a model of UV radiation of the leukaemic cell line HL60. Anal. Cell. Pathol. 19, 139–151. https://doi.org/10.1155/1999/176515, 1999.

- Marfè, G., Tafani, M., Fiorito, F., Pagnini, U., Iovane, G., De Martino, L., 2011. Involvement of FOXO transcription factors, TRAIL-FasL/Fas, and sirtuin proteins family in canine coronavirus type II-induced apoptosis. PLoS ONE 6, e27313.
- McBride, R.; van Zyl, M.; Fielding, B.C. The Coronavirus Nucleocapsid Is a Multifunctional Protein. Viruses 2014, 6, 2991–3018.
- Meli ML, Spiri AM, Zwicklbauer K, Krentz D, Felten S, Bergmann M, Dorsch R, Matiasek K, Alberer M, Kolberg L, von Both U, Hartmann K, Hofmann-Lehmann R. Fecal Feline Coronavirus RNA Shedding and Spike Gene Mutations in Cats with Feline Infectious Peritonitis Treated with GS-441524. Viruses. 2022 May 17;14(5):1069.
- Murphy BG, Perron M, Murakami E, Bauer K, Park Y, Eckstrand C, Liepnieks M, Pedersen NC. The nucleoside analog GS-441524 strongly inhibits feline infectious peritonitis (FIP) virus in tissue culture and experimental cat infection studies. Vet Microbiol. 2018 Jun;219:226-233.
- Paltrinieri S, Giordano A, Stranieri A, Lauzi S. Feline infectious peritonitis (FIP) and coronavirus disease 19 (COVID-19): Are they similar? Transbound Emerg Dis. 2021 Jul;68(4):1786-1799.
- Pedersen NC. A review of feline infectious peritonitis virus infection: 1963-2008. J Feline Med Surg. 2009 Apr;11(4):225-58. doi: 10.1016/j.jfms.2008.09.008.
- Pratelli A, Tempesta M, Elia G, Martella V, Decaro N, Buonavoglia C. The knotty biology of canine coronavirus: A worrying model of coronaviruses' danger. Res Vet Sci. 2022 May;144:190-195.
- Pratelli A. Comparison of serologic techniques for the detection of antibodies against feline coronaviruses. J Vet Diagn Invest. 2008 Jan;20(1):45-50.
- Pratelli, A., Buonavoglia, A., Lanave, G., Tempesta, M., Camero, M., Martella, V., Decaro, N., 2021. One world, one health, one virology of the mysterious labyrinth of coronaviruses: The canine coronavirus affair. Lancet Microbe 2, e646–e647.
- Rothhammer, V.; Quintana, F.J. The aryl hydrocarbon receptor: An environmental sensor integrating immune responses in health and disease. Nat. Rev. Immunol. 2019, 19, 184–197.
- Rottier PJ, Nakamura K, Schellen P, Volders H, Haijema BJ. Acquisition of macrophage tropism during the pathogenesis of feline infectious peritonitis is determined by mutations in the feline coronavirus spike protein. J Virol. 2005 Nov;79(22):14122-14130.
- Roy M, Jacque N, Novicoff W, Li E, Negash R, Evans SJM. Unlicensed Molnupiravir is an Effective Rescue Treatment Following Failure of Unlicensed GS-441524-like Therapy for Cats with Suspected Feline Infectious Peritonitis. Pathogens. 2022 Oct 20;11(10):1209.
- Ruggieri A, Di Trani L, Gatto I, Franco M, Vignolo E, Bedini B, Elia G, Buonavoglia C. Canine coronavirus induces apoptosis in cultured cells. Vet Microbiol. 2007 Mar 31;121(1-2):64-72.
- Sase O. Molnupiravir treatment of 18 cats with feline infectious peritonitis: A case series. J Vet Intern Med. 2023 Sep-Oct;37(5):1876-1880.

- Schmied K, Ehmann R, Kristen-Burmann C, Ebert N, Barut GT, Almeida L, Kelly JN, Thomann L, Stalder H, Lang R, Tekes G, Thiel V. An RNA replicon system to investigate promising inhibitors of feline coronavirus. J Virol. 2024 Jan 18:e0121623.
- Shi, J., Du, T., Wang, J., Tang, C., Lei, M., Yu, W., Yang, Y., Ma, Y., Huang, P., Chen, H., Wang, X., Sun, J., Wang, H., Zhang, Y., Luo, F., Huang, Q., Li, B., Lu, S., Hu, Y., Peng, X., 2023. Aryl hydrocarbon receptor is a proviral host factor and a candidate pan-SARS-CoV-2 therapeutic target. Sci Adv. 9(22):eadf0211.
- Silva, C.S.; Mullis, L.B.; Pereira, O., Jr.; Saif, L.J.; Vlasova, A.; Zhang, X.; Owens, R.J.; Paulson, D.; Yaylor, D.; Haynes, L.M.; et al. Human respiratory coronaviruses detected in patients with influenza-like illness in Arkansas, USA. Virol. Mycol. Infect. Dis. 2014, 2014 (Suppl. S2), 004.
- Takano T, Akiyama M, Doki T, Hohdatsu T. Antiviral activity of itraconazole against type I feline coronavirus infection. Vet Res. 2019 Jan 18;50(1):5.
- Takano T, Satoh K, Doki T, Tanabe T, Hohdatsu T. Antiviral Effects of Hydroxychloroquine and Type I Interferon on In Vitro Fatal Feline Coronavirus Infection. Viruses. 2020 May 24;12(5):576.
- Takano T, Satoh K, Doki T. Possible Antiviral Activity of 5-Aminolevulinic Acid in Feline Infectious Peritonitis Virus (Feline Coronavirus) Infection. Front Vet Sci. 2021 Feb 10;8:647189.
- Tang, B.S.F.; Chan, K.H.; Cheng, V.C.C.; Woo, P.C.Y.; Lau, S.K.P.; Lam, C.C.K.; Chan, T.L.; Wu, A.K.L.; Hung, I.F.N.; Leung, S.Y.; et al. Comparative Host Gene Transcription by Microarray Analysis Early after Infection of the Huh7 Cell Line by Severe Acute Respiratory Syndrome Coronavirus and Human coronavirus 229E. J. Virol. 2005, 79, 6180–6193
- Tasker S, Addie DD, Egberink H, Hofmann-Lehmann R, Hosie MJ, Truyen U, Belák S, Boucraut-Baralon C, Frymus T, Lloret A, Marsilio F, Pennisi MG, Thiry E, Möstl K, Hartmann K. Feline Infectious Peritonitis: European Advisory Board on Cat Diseases Guidelines. Viruses. 2023 Aug 31;15(9):1847.
- Taylor SS, Coggins S, Barker EN, Gunn-Moore D, Jeevaratnam K, Norris JM, Hughes D, Stacey E, MacFarlane L, O'Brien C, Korman R, McLauchlan G, Salord Torres X, Taylor A, Bongers J, Espada Castro L, Foreman M, McMurrough J, Thomas B, Royaux E, Calvo Saiz I, Bertoldi G, Harlos C, Work M, Prior C, Sorrell S, Malik R, Tasker S. Retrospective study and outcome of 307 cats with feline infectious peritonitis treated with legally sourced veterinary compounded preparations of remdesivir and GS-441524 (2020-2022). J Feline Med Surg. 2023 Sep;25(9):1098612X231194460.
- Terada Y, Matsui N, Noguchi K, Kuwata R, Shimoda H, Soma T, Mochizuki M, Maeda K. Emergence of pathogenic coronaviruses in cats by homologous recombination between feline and canine coronaviruses. PLoS One. 2014 Sep 2;9(9):e106534.
- Theamboonlers, A., Samransamruajkit, R., Thongme, C., Amonsin, A., Chongsrisawat, V., Poovorawan, Y., 2007. Human Coronavirus Infection among Children with Acute Lower Respiratory Tract Infection in Thailand. Intervirology 50, 71–77.
- Timurkan, M.O.; Aydin, K.; Dincer, E.; Coskun, N. Molecular characterization of canine coronaviruses: An enteric and pantropic approach. Arch. Virol. 2021, 166, 35–42.

- Torti, M.F.; Giovannoni, F.; Quintana, F.J.; Garcia, C.C. The Aryl Hydrocarbon Receptor as a Modulator of Anti-viral Immunity. Front. Immunol. 2021, 12, 624293.
- Triratapiban C, Lueangaramkul V, Phecharat N, Pantanam A, Lekcharoensuk P, Theerawatanasirikul S. First study on in vitro antiviral and virucidal effects of flavonoids against feline infectious peritonitis virus at the early stage of infection. Vet World. 2023 Mar;16(3):618-630.
- Tseng YY, Liao GR, Lien A, Hsu WL. Current concepts in the development of therapeutics against human and animal coronavirus diseases by targeting NP. Comput Struct Biotechnol J. 2021;19:1072-1080.
- Vlasova AN, Toh TH, Lee JS, Poovorawan Y, Davis P, Azevedo MSP, Lednicky JA, Saif LJ, Gray GC. Animal alphacoronaviruses found in human patients with acute respiratory illness in different countries. Emerg Microbes Infect. 2022 Dec;11(1):699-702.
- Vocadlova K, Lamp B, Benes K, Matha V, Lee KZ, Vilcinskas A. Crude Extracts of Talaromyces Strains (Ascomycota) Affect Honey Bee (Apis mellifera) Resistance to Chronic Bee Paralysis Virus. Viruses. 2023 Jan 25;15(2):343.
- Warr A, Attipa C, Gunn-Moore D, Tait-Burkard C. FCoV-23 causing FIP in a cat imported to the UK from Cyprus. Vet Rec. 2023 Nov 18;193(10):414-415.
- Xu, T.; Gao, X.; Wu, Z.; Selinger, D.W.; Zhou, Z. Indomethacin has a potent antiviral activity against SARS CoV-2 in vitro and canine coronavirus in vivo. bioRxiv 2020.
- Yamada, T.; Horimoto, H.; Kameyama, T.; Hayakawa, S.; Yamato, H.; Dazai, M.; Takada, A.; Kida, H.; Bott, D.; Zhou, A.C.; et al. Constitutive aryl hydrocarbon receptor signaling constrains type I interferon-mediated antiviral innate defense. Nat. Immunol. 2016, 17, 687–694.
- Yan Y, Li J, Jiao Z, Yang M, Li L, Wang G, Chen Y, Li M, Shen Z, Shi Y, Peng G. Better therapeutic effect of oral administration of GS441524 compared with GC376. Vet Microbiol. 2023 Aug;283:109781.
- Yang, T., Feng, Y.L., Chen, L., Vaziri, N.D., Zhao, Y.Y., 2019. Dietary natural flavonoids treating cancer by targeting aryl hydrocarbon receptor. Crit. Rev. Toxicol. 49, 445–460.
- Yousefi M, Lee WS, Chan WOY, He W, Mah MG, Yong CL, Deerain JM, Wang L, Arcinas C, Yan B, Tan D, Sia WR, Gamage AM, Yang J, Hsu AC, Li S, Linster M, Yang X, Ghosh S, Anderson DE, Smith GJD, Tan CW, Wang LF, Ooi YS. Betacoronaviruses SARS-CoV-2 and HCoV-OC43 infections in IGROV-1 cell line require aryl hydrocarbon receptor. Emerg Microbes Infect. 2023 Dec;12(2):2256416.
- Zakeri, Z.; Lockshin, R.A. Cell death: History and future. Adv. Exp. Med. Biol. 2008, 615, 1–11.
- Zhao, L., Yao, L., Chen, R., He, J., Lin, T., Qiu, S., Chen, G., Chen, H., Qiu, S.X., 2023. Pinostrobin from plants and propolis against human coronavirus HCoV-OC43 by modulating host AHR/CYP1A1 pathway and lipid metabolism. Antiviral Res. 212:105570.
- Zhu, Y.; Liu, M.; Zhao, W.; Zhang, J.; Zhang, X.; Wang, K.; Gu, C.; Wu, K.; Li, Y.; Zheng, C.; et al. Isolation of virus from a SARS patient and genome-wide analysis of genetic mutations related to pathogenesis and epidemiology from 47 SARS-CoV isolates. Virus Genes 2005, 30, 93–102.

- Zwicklbauer K, Krentz D, Bergmann M, Felten S, Dorsch R, Fischer A, Hofmann-Lehmann R, Meli ML, Spiri AM, Alberer M, Kolberg L, Matiasek K, Zablotski Y, von Both U, Hartmann K. Long-term follow-up of cats in complete remission after treatment of feline infectious peritonitis with oral GS-441524. J Feline Med Surg. 2023 Aug;25(8):1098612X231183250.

CHAPTER 3 – *In vitro* evaluation of natural compounds against CCoV infection

CHAPTER 3 - *In vitro* evaluation of natural compounds against CCoV infection

Brief summary

Herein, the potential antiviral properties of fungal secondary metabolites towards CCoV infection have been evaluated. Particularly, following infection in a canine fibrosarcoma (A72) cell line, OMF, PS and VER. obtained from *Talaromyces pinophilus,* were tested. Furthermore, 6PP, isolated from *Trichoderma atroviride,* against CCoV was evaluated on A72, and on Crandell-Rees Feline Kidney Cell (CRFK), a cell line derived from the feline kidney. The results showed that the fungal metabolites reduce the infectivity of CCoV. Moreover, all these compounds provoke a strong inhibition in the expression of AhR, a ligand-activated transcription factor that is activated during CCoV infection. In addition, in the presence of VER or PS, it has been found the alkalinization of lysosomes which may be involved in the observed antiviral activities.

The following papers were embedded here:

- Cerracchio C, Iovane V, Salvatore MM, Amoroso MG, Dakroub H, DellaGreca M, Nicoletti R, Andolfi A, Fiorito F. Effectiveness of the Fungal Metabolite 3-O-Methylfunicone towards Canine Coronavirus in a Canine Fibrosarcoma Cell Line (A72). Antibiotics 2022, 11, 1594. https://doi.org/10.3390/antibiotics11111594 - Permission: https://www.mdpi.com/openaccess
- Cerracchio C, Salvatore MM, Del Sorbo L, Serra F, Amoroso MG, DellaGreca M, Nicoletti R, Andolfi A, Fiorito F. In Vitro Evaluation of Antiviral Activities of Funicone-like Compounds Vermistatin and Penisimplicissin against Canine Coronavirus Infection. Antibiotics (Basel). Antibiotics 2023, 12, 1319. https://doi.org/10.3390/antibiotics12081319 - Permission: https://www.mdpi.com/openaccess

Moreover, the results of the following submitted manuscript have been included here:

Cerracchio C, Del Sorbo L, Serra F, Staropoli A, Amoroso MG, Vinale F, Fiorito F. Fungal metabolite 6-pentyl-α-pyrone reduces canine coronavirus infection.

1. Introduction

Fungal secondary metabolites

The recent pandemic of COVID-19 due to severe acute respiratory syndrome-coronavirus-2 (SARS-CoV-2) has turned the spotlight on CoVs that are able to mutate into new and more dangerous strains. Hence, in the current scenario of emerging pathogenic coronaviruses with pandemic potential similar to SARS-CoV2, there is intense investigational activity focused on finding novel antivirals. Natural products offer a rich source of potential materials for the identification and development of novel drugs. The potential of natural products in drug discovery should be investigated (Wright, 2019). Indeed, several compounds from various biological sources (i.e., medicinal plants, bacteria, fungi) are being studied with the aim to find and develop new nontoxic medicinal compounds. Fungi produce numerous bioactive secondary metabolites (SMs), some of which have been already used as antibiotics, fungicides, plant growth regulators and hormones. Funicones, as well as related compounds, constitute a homogeneous group of fungal polyketides possessing remarkable biological activities which have promoted their consideration as drug possibilities (Nicoletti et al., 2009; Salvatore et al., 2022). Among them, 3-*O*-methylfunicone (OMF), which is a benzo-γ-pyrone produced by *Talaromyces pinophilus* (Table 1), has shown significant antifungal, antiproliferative, and pro-apoptotic activities (Nicoletti et al., 2014), as well as potential antiviral properties, towards hepatitis C virus (HCV) (Nakajima et al., 2013) and bovine herpesvirus 1 (BoHV-1) (Fiorito et al., 2022).

The *Trichoderma* secondary metabolite 6-pentyl-α-pyrone (6PP) (Table 1) plays an important role in the defence against plant pathogens (Vinale et al. 2008; Comite et al., 2021), as well as in anti-biofilm-producing bacteria activity (Papaianni et al., 2020; Kotb et al., 2022), but the antiviral activity of 6PP has never been investigated so far.

Based on these observations, the potential antiviral effect of OMF against CCoV infection in canine fibrosarcoma cells (A72) was investigated after assessing the non-toxic in vitro dose of this compound.

Moreover, further research on CCoV antiviral properties of two additional funicone-like compounds named penisimplicissin (PS) and vermistatin (VER) was carried out. The latter represents the most common funicone-like compound, having been reported as a product of at least 15 fungal species (Nicoletti et al., 2023a,b; Salvatore et al., 2022). VER and PS have a very similar molecular structure (Table 1) which is characterized by a 4,6-dimethoxyphthalide moiety linked to a γ-pyridone (Salvatore et al., 2022).

In addition, the potential efficacy of 6PP. isolated from *Trichoderma atroviride*, against CCoV was evaluated on A72, a canine fibrosarcoma cell line, and on Crandell-Rees Feline Kidney Cell (CRFK), a cell line derived from the feline kidney, both are suitable for studying CCoV (Cerracchio et al., 2022; Crandell et al., 1973; Binn et al., 1980).

2. Materials and Methods

2.1.Production and Isolation of OMF, VER, PS and 6PP

Cultures of *T. pinophilus* (strain LT6) were prepared as previously reported (Salvatore et al., 2018). 6-Pentyl-α-pyrone was isolated from *Trichoderma atroviride*, strain P1 according to the method described by Vinale et al. (2008) (see Table 1).

Table 1. Fungal secondary metabolites assayed during CCoV infection.

Name	Chemical structure	Fungal species	References
3-O-Methylfunicone (OMF)	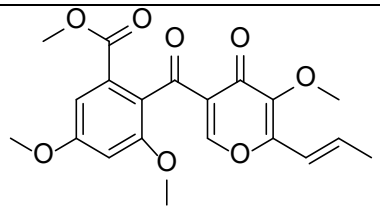	*Talaromyces pinophilus (strain LT6)*	Salvatore et al., 2018
Vermistatin (VER)	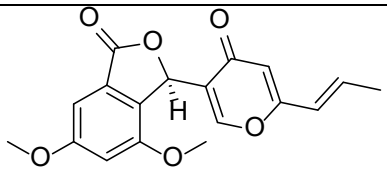	*Talaromyces pinophilus (strain LT6)*	Salvatore et al., 2018
Penisimplicissin (PEN)	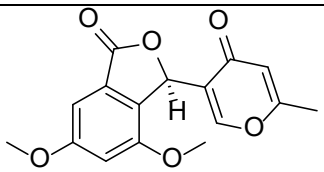	*Talaromyces pinophilus (strain LT6)*	Salvatore et al., 2018
6-Pentyl-α-Pyrone (6PP)	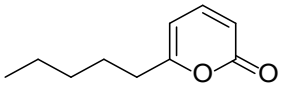	*Trichoderma atroviride (strain P1)*	Vinale et al., 2008

2.2.Cell Cultures and Virus Infection

A72 and CRFK cells were cultured in Dulbecco's modified Eagle's minimal essential medium (DMEM), 1% penicillin/streptomycin, plus 10% fetal bovine serum (FBS), and incubated at 37 °C and 5% CO_2 (Marfè et al., 2011; Drechsler et al., 2020). The following

Alphacoronavirus reference strain CCoV-IIa S378 (GenBank accession number KC175341) was used throughout the study. A72 cells were utilized for virus stocks growth. A72 and CRFK were used for virus titration (De Martino et al., 2010; Tian et al., 2021).

OMF was dissolved in DMSO, then added to the medium to obtain final concentrations of 0.5, 1, 2.5 and 5 μM.

VER and PS were dissolved in DMSO, then added to the medium to obtain final concentrations of 0.1, 0.5, 1, 2.5, and 5 μM.

6PP was solubilized in the vehicle DMSO, at 0.1 g/mL concentration (stock solution). The stock solution was then diluted in DMEM to obtain different concentrations. Vehicle control is indicated as DMSO diluted in DMEM (0.1% v/v) and used throughout the experiments.

A72 cells, in monolayers, were infected with CCoV, at different MOI, exposed to OMF, VER or PS, to produce four groups: CCoV uninfected or infected cells, OMF- VER- or PS-treated infected and uninfected cells. After adsorption at 37 °C (one hour), A72 cells were incubated, and processed at 24 and 48 h post infection. The virus remained in the medium.

A72 and CRFK cells, in monolayers, were infected or not with CCoV, at different MOI, and were treated or not with 6PP at different concentrations (0.001, 0.01, 0.1, 1 and 10 μg/mL) having four groups: CCoV uninfected or infected cells, 6PP treated infected and uninfected cells. One hour after adsorption at 37 °C, both cell lines were incubated, and processed at various times of infection. The virus remained in the medium.

2.3.Cell Viability

A72 cells were treated with OMF, infected with CCoV at MOI of 5 and incubated.

A72 cells were treated with VER or PS, infected with CCoV at MOI of 0.05 and incubated.

A72 and CRFK cells were exposed to 6PP, infected with CCoV, at MOI of 5 for A72, and at MOI of 1 for CRFK, and incubated.

After 48 h of treatment, cell viability was assessed by TB exclusion test, and it was obtained as a percentage of viable cells *vs.* control (Chowanadisai et al., 2013; Fiorito et al., 2020). Three independent experiments were performed in duplicate, and results are exhibited as the mean ± standard deviation (S.D.). The calculation of the IC_{50} in A72 as

well as CRFK cells was assessed by IC_{50} Calculator|AAT Bioquest (https://www.aatbio.com/tools/ic50-calculator, accessed on August 14, 2023).

2.4.Cell proliferation

3-(4,5-dimethyl-2-thiazolyl)-2,5-diphenyl-2H-tetrazolium bromide (MTT) assay was carried out to check cell proliferation (Fiorito et al. 2008; 2011; Santamaria et al. 2011). A72 cells cultured in 96-well plates were infected or not with CCoV at a MOI of 5, and exposed or not to OMF (0.5, 1, 2.5, and 5 μM) to obtain four groups: uninfected or infected cells, and OMF-exposed infected and uninfected cells, and then incubated. After 48 h of infection, MTT assays were performed. Briefly, cells cultured in 96-well plates were infected or not, exposed or not exposed, and incubated. Then, MTT assay was added to each well at different times, and then incubated for 3 h. At the end of the incubation, the medium was removed, and the converted dye was solubilized with acidic isopropanol (0.1N HCl in absolute isopropanol) and was measured at wavelength of 570 nm with background subtraction at 630 - 690 nm (*Mosmann, 1983*).

In a preliminary test of cell viability, five concentrations of 6PP (0.001, 0.01, 0.1, 1 and 10 μg/mL) were tested at 48 h p.i., and then we have chosen 0.1 μg/mL 6PP for MTT test. In brief, both A72 and CRFK cells were infected with CCoV (MOI 5 and MOI 1, respectively), in the presence or not of 6PP (0.1 μg/mL) were checked by MTT test after 48 h p.i..

Results were the mean ± S.D. of four independent experiments in duplicate.

2.5.Examination of Cell Morphology

Giemsa staining and acridine orange staining were performed to study cell morphology (Fiorito et al., 2008).

A72 cells were infected or not with CCoV at a MOI of 5, exposed or not to OMF (5 μM).

A72 cells were infected with CCoV, at MOI of 1, and treated or not with VER or PS.

Monolayers of A72 and CRFK, treated with 6PP, were infected with CCoV at MOI of 5 and at MOI of 1, respectively. After 24 h and 48 h of infection, acridine orange staining and Giemsa staining were carried out, then, light microscopy and fluorescence microscopy analysis were assessed by ZOE Cell Imager (Bio-Rad Laboratories, Segrate, Milan, Italy).

2.6.Immunofluorescence Staining

A72 cells were infected or not with CCoV at a MOI of 5, and exposed or not to OMF, VER or PS for 24 h.

A72 and CRFK cells, treated or not with 6PP were infected CCoV at MOI of 0.05 and 1, respectively.

At different times times p.i., IF staining was assessed cells (Fiorito et al., 2022; Altamura et al., 2018), using the following antibodies diluted in 5% bovine serum albumin-1x Tris-Buffered Saline, 0.1% Tween® 20 Detergent:, anti-nucleocapsid protein (NP), monoclonal mouse, MAB 938 (The Native Antigen Company, Kidlington, UK), anti-aryl hydrocarbon receptor (AhR) (Sigma-Aldrich, St. Louis, MI, USA) (1:250), Alexa Fluor 488 goat anti-mouse (Thermo Fisher Scientific, Waltham, MA, USA) (1:1000), and Texas Red goat anti-rabbit (Thermo Fisher Scientific, Waltham, MA, USA) (1:100). Microscopy and photography were assessed by ZOE Fluorescent Cell Imager. Fluorescence signals from micrographs were quantified by ImageJ software (National Institutes of Health, Bethesda, MD, USA).

2.7.LysoRed Staining

The cells were infected with CCoV, at MOI of 5, treated with VER or PS, and incubated for 24 and 48 h. In accordance with the user manual, cells were stained with CytoPainter LysoRed Indicator Reagent (Abcam) and incubated. The cells were then washed and observed under a fluorescence microscope (Alkharashi et al., 2019).

2.8.Virus Production

A72 cells were infected or not with CCoV at a MOI of 5, exposed or not to OMF, incubated at 37 °C, and processed after 0, 1, 12, 24, 48, and 72 h p.i. using RT-qPCR for CCoV quantification.

A72 cells were infected with CCoV at MOI 5, treated with VER or PS and incubated for 24 and 48 h. RT-qPCR was then used to quantify CCoV.

Monolayers of A72 and CRFK cells, treated or not with 6PP, were infected or not with CCoV, at MOI 5 for A72 and at MOI 10 for CRFK, and incubated at 37 °C. A72 cells were then processed by real-time PCR for CCoV quantification (Cerracchio et al., 2022). In CRFK cells, the virus titer was determined by 50% tissue culture infective dose ($TCID_{50}$) titration (Kojima et al., 1986; Tian et al., 2021). Moreover, at 48 h p.i., viral cytopathic effect (CPE) was assessed by light microscope.

2.9.Viral Nucleic Acids Extraction Procedure

Nucleic acid extraction was carried out from 200 µL of cell supernatant by using the King Fisher Flex System (Thermo Fisher Scientific, Waltham, MA, USA) with the Mag Max Viral Pathogen kit (Thermo Fisher Scientific, Waltham, MA, USA), according to the manufacturer's instructions. Nucleic acids were eluted in 80 µL of elution buffer and immediately analysed by Real-Time RT-PCR. DMEM was used as a negative process control (NCP). PCR inhibitors likely present in the samples were monitored by adding an external process control (EPC) as previously described (Amoroso et al. 2021).

2.10. CCoV Viral Load Quantification by Real-Time Reverse Transcription PCR (RT-qPCR)

Quantification of CCoV during infection in A72 cells was performed by RT-qPCR on a QuantStudio 1 Real-Time PCR thermal cycler (Thermo Fisher Scientific, Waltham, Massachusetts, USA) using AgPath-IDTM One-step RT-PCR kit (Applied biosystem by Thermo Fisher Scientific). The reaction was carried as described in Chapter 1.

2.11. Statistical Analysis

Statistical analysis was performed by using GraphPad InStat software Version 3.00 for Windows 95 (GraphPad Software, San Diego, CA, USA). One-way ANOVA with Tukey's post hoc test and Student's t-test at $p < 0.05$ were used to evaluate significant differences among samples.

3. Results

3.1.OMF, VER and PS Increased Cell Viability during CCoV Infection

To examine the effect of OMF in CCoV infection in A72 cells, cell proliferation by MTT and cell viability using a TB exclusion test were assessed. First, half-maximal inhibitory concentrations (IC_{50}) of OMF were identified and dose–response curves were developed after treatment of A72 cells with various concentrations of OMF (Figure 1a). Hence, A72 cells, in monolayer, were infected or not with CCoV at a multiplicity of infection (MOI) of 5, and were exposed or not to OMF at various doses (0.5, 1, 2.5 and 5 µM), yielding the following groups: uninfected or infected cells, and OMF-exposed infected and uninfected cells. Cell growth inhibition was detected in A72 cells with an IC_{50} of approximately 2.5 µM OMF after 48 h of treatment (Figure 1b). OMF at 1 and 0.5 µM in

A72 cells produced no significant differences in cell proliferation, as assessed using an MTT test ($p > 0.05$) (Figure 1b). Similar results were observed by analyzing cell viability using trypan blue (TB) staining (Figure 1c). Thus, these results demonstrated that OMF at a concentration of 0.5 µM did not significantly alter A72 cell viability or cell proliferation. Interestingly, the cell toxicity at 2.5 µM seemed to be high compared to 5 µM OMF in A72 cells (Figure 1a,b). This result was previously observed in bovine cells (MDBK) treated with OMF (Fiorito et al., 2022). This nonmonotonic dose–response has been observed for a variety of compounds, including micronutrients, endocrine disrupting chemicals, and endogenous hormones, which typically bind nuclear receptors (Vandenberg et al., 2012).

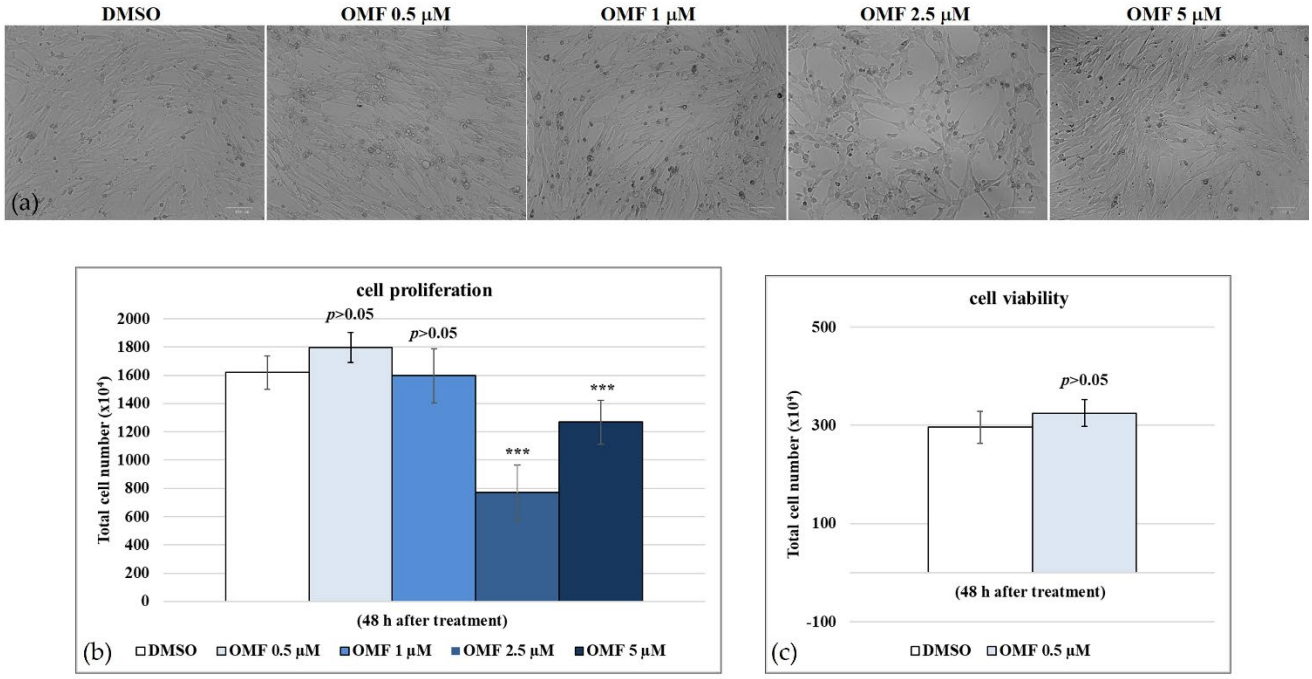

Figure 1. Determination of IC_{50} of OMF at various concentrations and development of dose–response curve for A72 cells. (a) A72 cells exposed to dimethyl sulfoxide (DMSO) (0.5 µM) or OMF at various doses (0.5, 1, 2.5, and 5 µM) at 48 h of treatment. (b) Dose–response curve of A72 cells exposed to DMSO (0.5 µM) or OMF at indicated doses (0.5, 1, 2.5, and 5 µM). At 48 h after treatment, A72 cells were tested using an MTT assay. (c) Cell viability was determined using TB staining and counted using a light microscope. Scale bar 100 µm. Significant differences between control and OMF-exposed cells were indicated by probability *p*. *** $p < 0.001$.

During CCoV infection in A72 cells in the presence of OMF at 0.5 µM, cell proliferation ($p < 0.01$) (Figure 2a,b) and cell viability ($p < 0.001$) (Figure 2c) significantly increased. Hence, the concentration of OMF at 0.5 µM was selected to be utilized throughout the

study. Our findings showed that during CCoV infection in A72 cells at the non-toxic dose of 0.5 µM, OMF significantly reduced cell death after 48 h of infection.

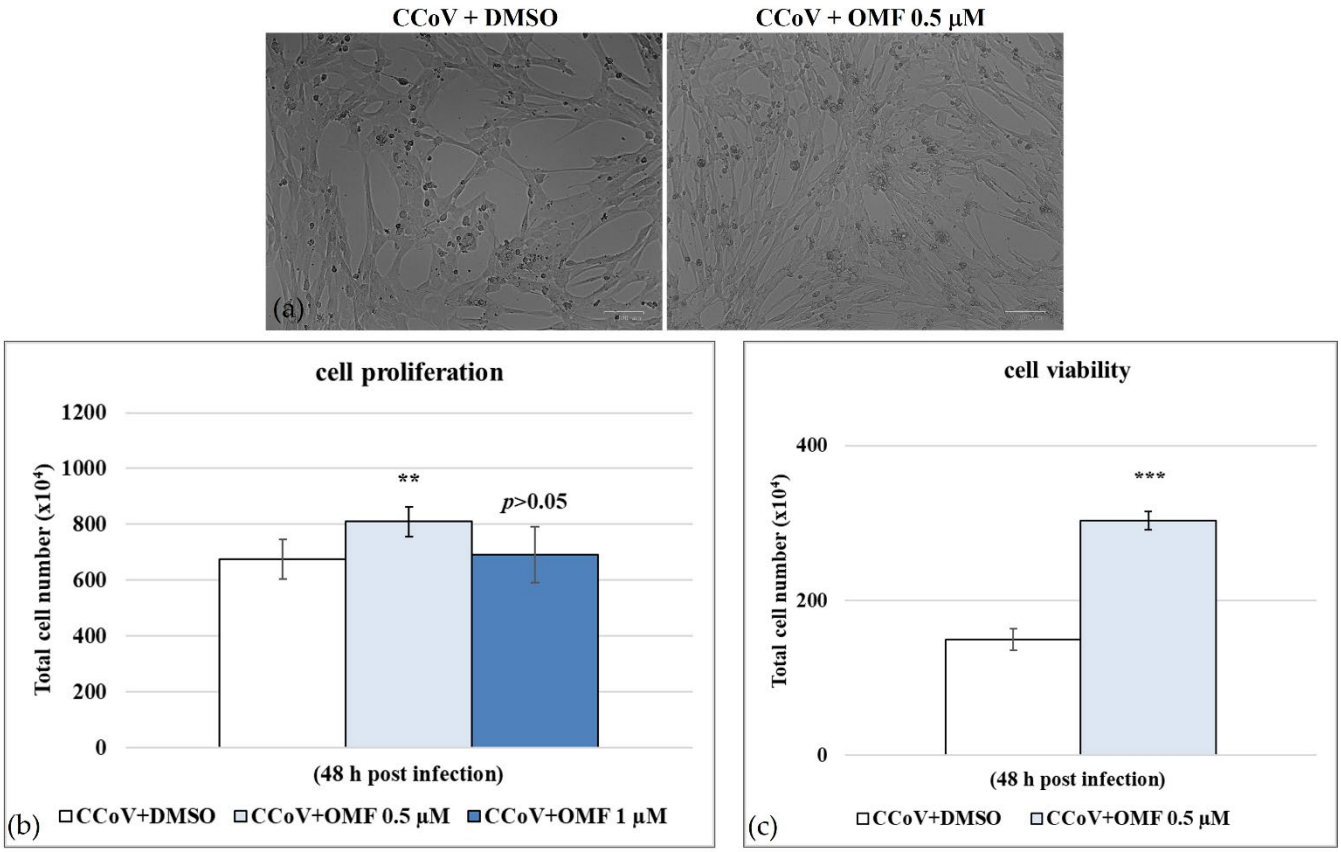

Figure 2. OMF reduced cell death during CCoV infection in A72 cells. (a) Cells infected with CCoV and exposed to OMF at various doses (0.5 and 1 µM) at 24 h after infection. (b) Dose–response curve of cells infected with CCoV, exposed to OMF (0.5 µM) for 48 h and tested using an MTT assay. (c) Dose–response curve of cells infected with CCoV, stained using TB and scored using a light microscope. Scale bar 100 µm. Significant differences between infected and OMF-exposed infected cells were indicated by probability *p*. ** $p < 0.01$ and *** $p < 0.001$.

To investigate the effect of VER and PS in CCoV infection, cell viability was assessed by TB exclusion test. We developed a dose-response curve after exposure of A72 cells to different doses of VER and PS (Figure 3A–D). VER at 0.1, 0.5 and 1 µM, as well as PS at 0.1, 0.5 and 2.5 µM, induced no differences in cell viability ($p > 0.05$) (Figure 3C,D). This non-monotonic dose-response was previously observed in bovine (MBDK) cells treated with OMF (Fiorito et al., 2022). In addition, in A72 cells, IC_{50} was obtained with 4.2556 µM VER and 4.9562 PS µM, respectively.

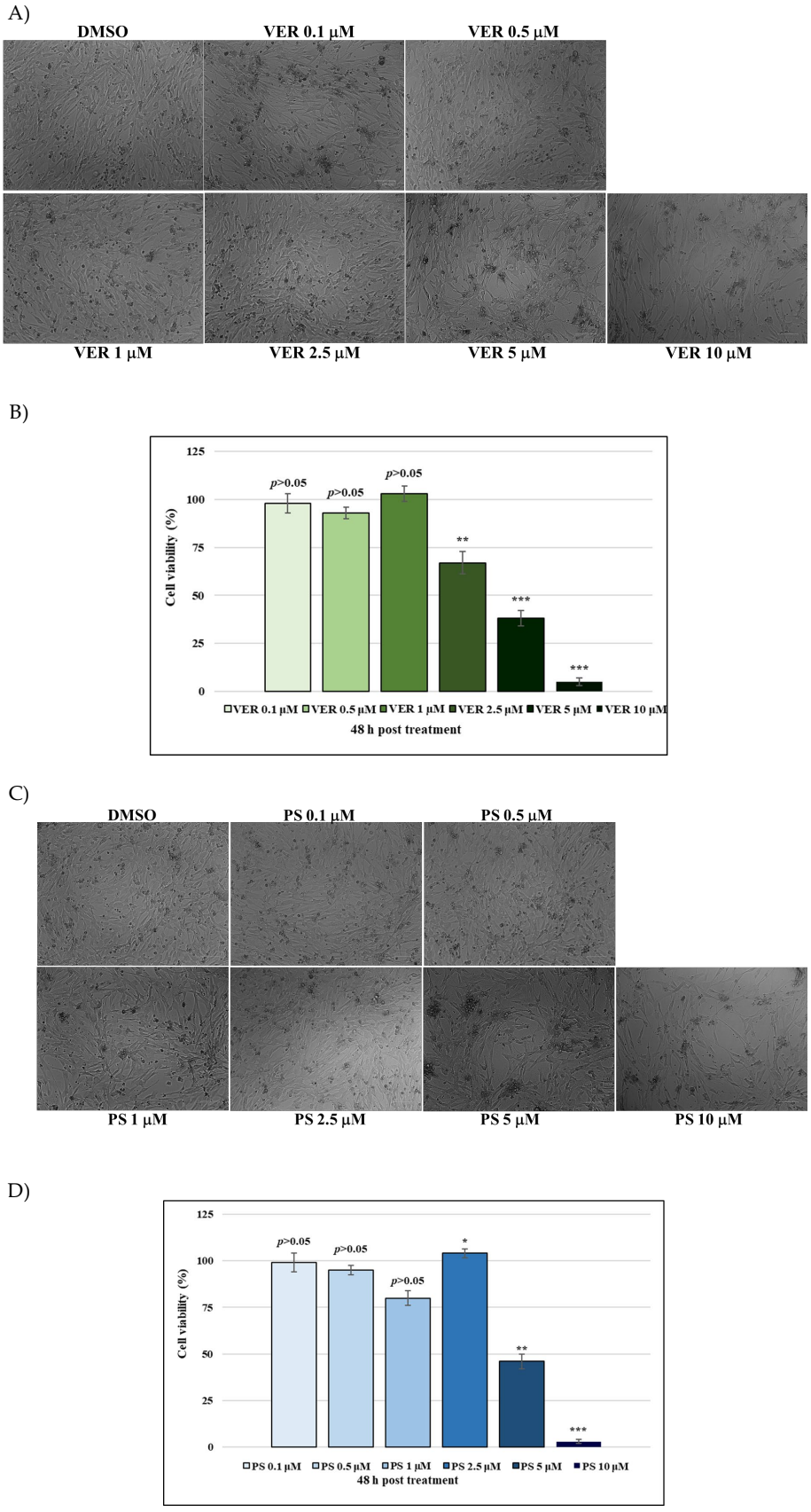

Figure 3. Identification of IC_{50} of VER and PS at various doses and development of dose-response curve. (A,B). Cells exposed to dimethyl sulfoxide (DMSO) or funicone-like compounds after 48 h of treatment. (C,D) Dose-response curve of A72 cells exposed to DMSO or both funicone-like compounds after 48 h of treatment. Scale bar 100 µm. Significant differences among DMSO and VER or PS groups were indicated by probability p. ** $p < 0.01$ and *** $p < 0.001$ for VER; * $p < 0.05$, ** $p < 0.01$ and *** $p < 0.001$ for PS.

Cell growth inhibition in CCoV infected cells treated with VER and PS was subsequently detected (Figure 4A–D). Following CCoV infection, both VER and PS significantly increased cell viability ($p < 0.01$ and $p < 0.05$) of A72 cells (Figure 4 B,C). Thus, VER at 1 µM and PS at 0.5 µM were chosen to be used throughout the study.

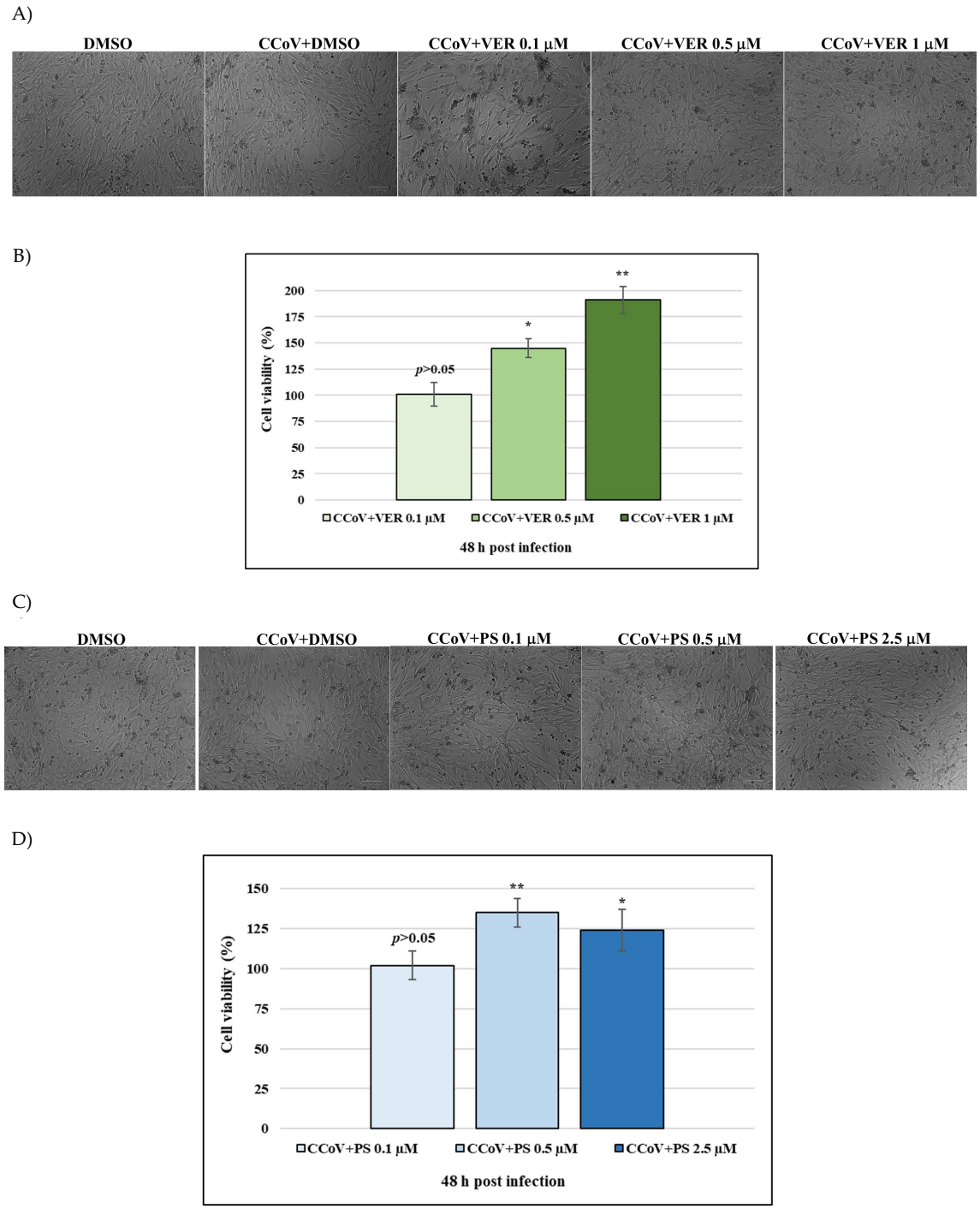

Figure 4. During CCoV infection VER and PS decrease cell death of A72 cells. (A, B) Cells infected with CCoV and treated with VER or PS at 48 h after infection (C, D) Dose-response curve of CCoV-infected cells treated with VER and PS for 48 h. Scale bar 100 µm. Significant differences among CCoV-infected and VER or PS-infected cells are pointed by probability *p*. ** $p < 0.01$ and * $p < 0.05$.

3.2.6PP Enhances Cell Viability and Cell Proliferation during CCoV Infection

To explore the effect of 6PP during CCoV infection in A72 and CRFK cells, cell viability (% control) was assessed by TB. Hence, the effects of five different concentrations of 6PP (0.01, 0.1, 1 and 10 μg/mL) on A72 and CRFK uninfected cells were examined, and a dose–response curve was developed (Figure 5a). In both cell lines, the 6PP response curve did not show a dose-dependency. After 48 h of treatment, IC50 was found with 0.9970 μg/mL 6PP in A72 cells, and with 0.7887μg/mL 6PP in CRFK cells (Figure 5a). No significant differences in A72 and CRFK cell viability ($p > 0.05$) were induced by 6PP at 0.001 and 0.1 μg/mL; whereas cell toxicity was observed using 6PP at 0.01, 1 and 10 μg/mL in both cell lines (Figure 5a,b). Interestingly, the cell toxicity at the lower concentration (0.01 μg/mL) of 6PP induced some cytotoxicity while the higher (0.1 μg/mL) did not. A similar trend was detected in bovine cells (MDBK) exposed to funicone-like compounds, other SMs (Fiorito et al., 2022). This kind of nonmonotonic dose–response has been noticed for different compounds, such as endocrine disrupting chemicals, endogenous hormones, and micronutrients, that generally bind nuclear receptors (Vandenberg et al., 2012).

To further check that 6PP at the concentration of 0.1 μg/mL was biocompatible as well as not cytotoxic, MTT assay was performed to examine the mitochondrial redox activity of A72 and CRFK cells. At 48 h of exposure, 6PP at 0.1 μg/mL did not induce significant ($p > 0.05$) changes in the mitochondrial dehydrogenase's activity compared to DMSO control groups (Fig. 5c).

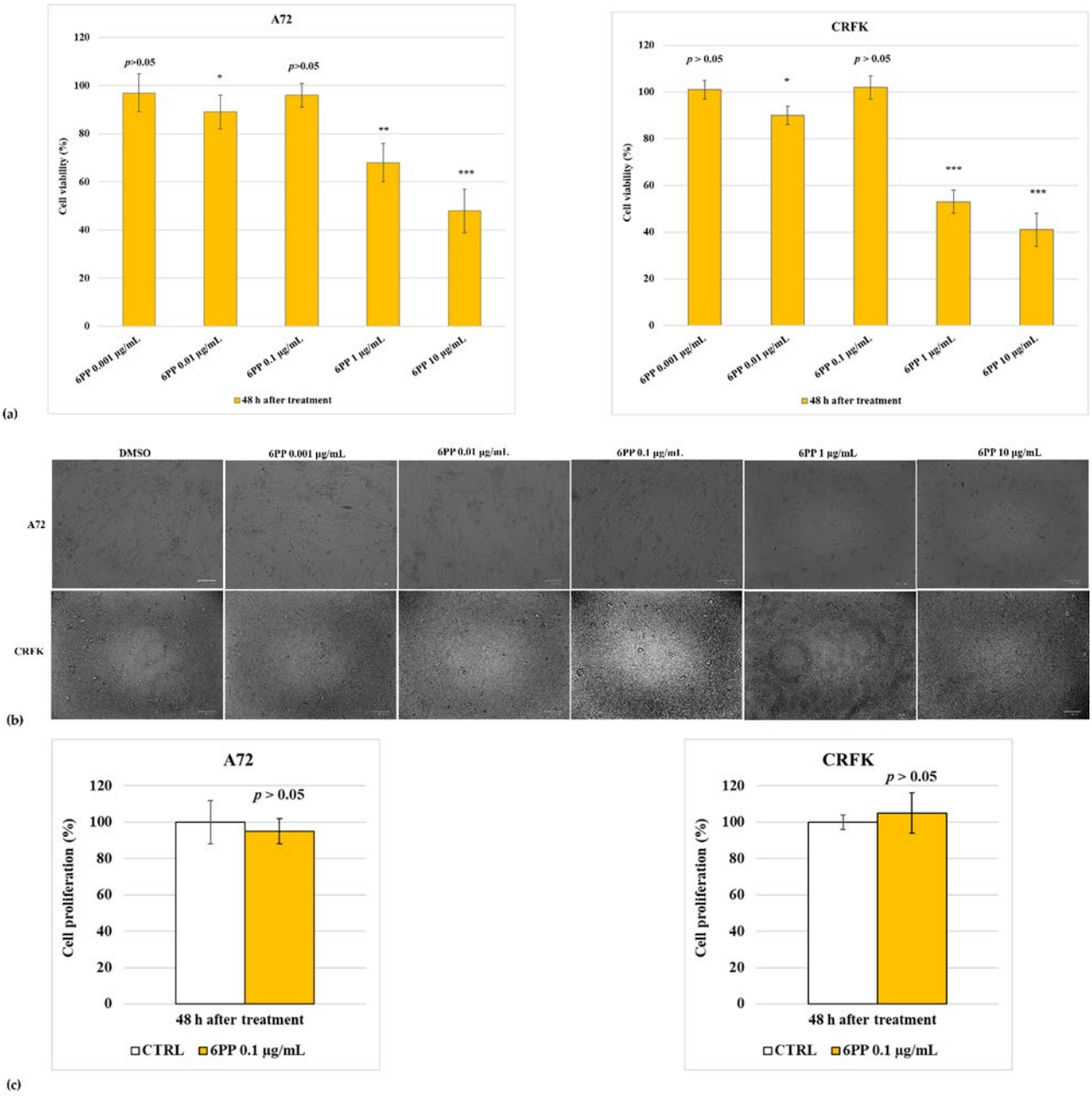

Figure 5. Identification of CC_{50} of 6PP at different concentrations and elaboration of dose–response curve in A72 and CRFK cells. (**a**) Dose–response curve of A72 and CRFK cells exposed to DMSO or 6PP at different concentrations (0.01, 0.1, 1 and 10 µg/mL). After 48 h from treatment, cell viability (% control) was assessed using TB staining. (**b**) A72 and CRFK cells treated with control (DMSO) or 6PP at different concentrations and observed by light microscope. Scale bar 100 µm. (c) Dose-response curve of A72 and CRFK cells treated with 6PP (0.1 µg/mL) for 48 h and analysed by MTT assay. Significant differences between control vehicle (DMSO) and 6PP-treated cells are indicated by probability *p*. ** $p < 0.01$ and *** $p < 0.001$ in A72 cells; * $p < 0.05$ and *** $p < 0.001$ in CRFK cells.

After that, A72 and CRFK cells were infected with CCoV at MOI of 5 and at MOI of 1, respectively, and exposed to no cytotoxic doses of 6PP (0.001 and 0.1 µg/mL). During infection, we found a significant reduction in both CCoV-infected cell lines, in the presence of the non-toxic dose of 0.1 µg/mL 6PP (Figure 6), which was chosen to be utilized for further experiments. At the concentration of 0.1 µg/mL, 6PP also enhanced cell proliferation ($p < 0.001$) in A72 cells as well as ($p < 0.01$) in CRFK cells (Fig. 36).

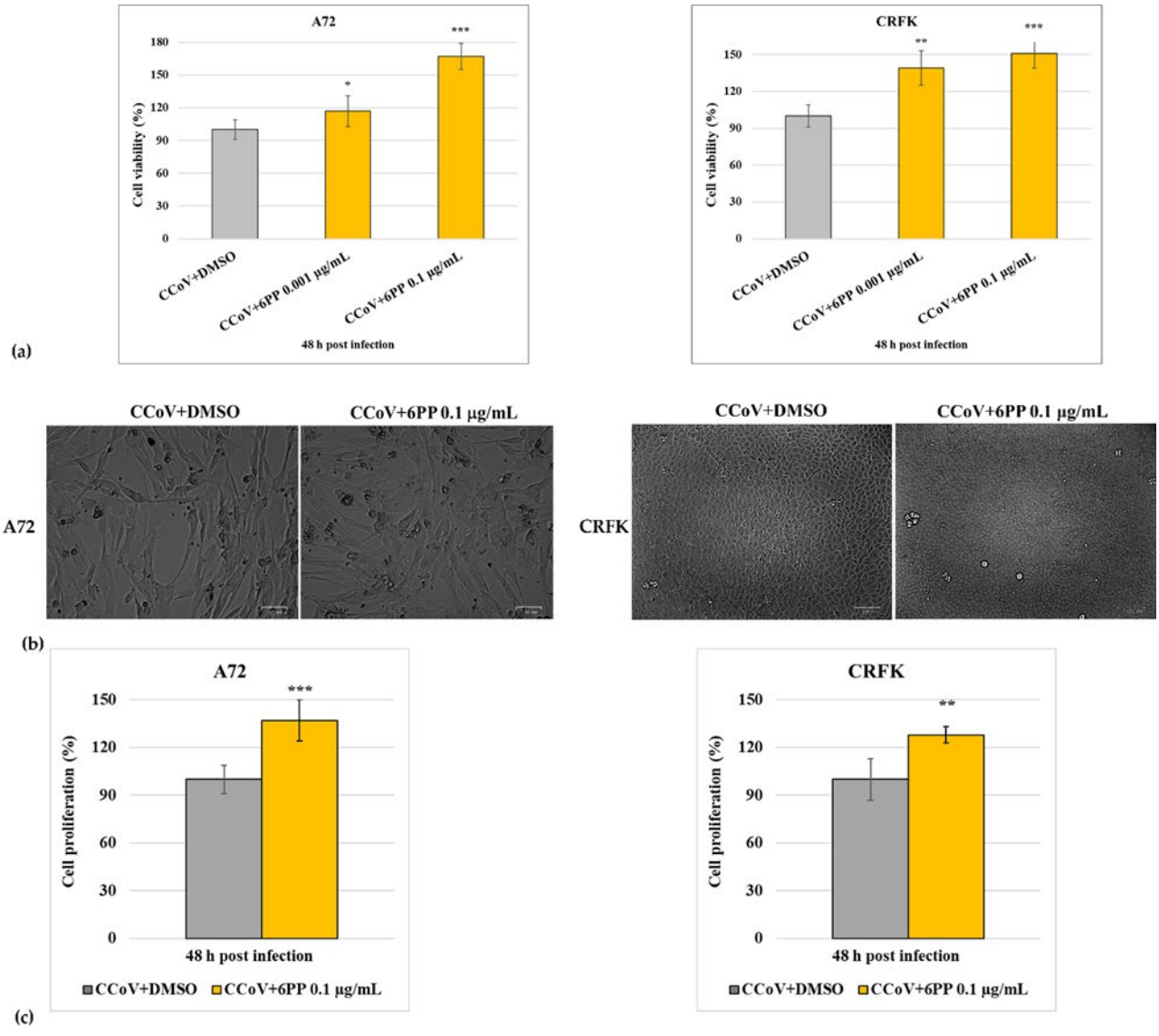

Figure 6. 6PP enhances cell viability during CCoV infection. (**a**) Dose–response curve of A72 and CRFK cells infected with CCoV and treated with 6PP (0.1 µg/mL). At 48 h of exposure, TB staining was used to determine cell viability, and cells were counted by light microscope. (**b**) Cells infected with CCoV, and treated or untreated with 6PP (0.1 µg/mL). At 48 h p.i., cells were observed by light microscope. Scale bar 50 µm. (c) Dose–response curve of A72 and CRFK cells infected with CCoV, exposed to 6PP (0.1 µg /mL) for 48 h and analyzed by MTT assay. Significant differences between CCoV and CCoV+6PP-treated cells are pointed by probability *p*. *** $p < 0.001$ and ** $p < 0.01$.

3.3. OMF, VER and PS Decrease Signs of Morphological Cell Death during CCoV Infection in A72 Cells

As displayed in Figure 7, the comparison between OMF-exposed uninfected cells and the control group showed no changes in morphology. An increase in intercellular spaces due to detachment from the culture plate were observed in unexposed infected cells. These features were accompanied by changes in morphology suggesting signs of apoptotic cell death, such as cellular shrinkage, pyknosis, and chromatin condensation (Figure 7, arrow). All cell death features were markedly diminished in CCoV-infected cells exposed to OMF (Figure 7, arrow). Overall, our findings demonstrated that OMF remarkably protected A72 cells during CCoV infection.

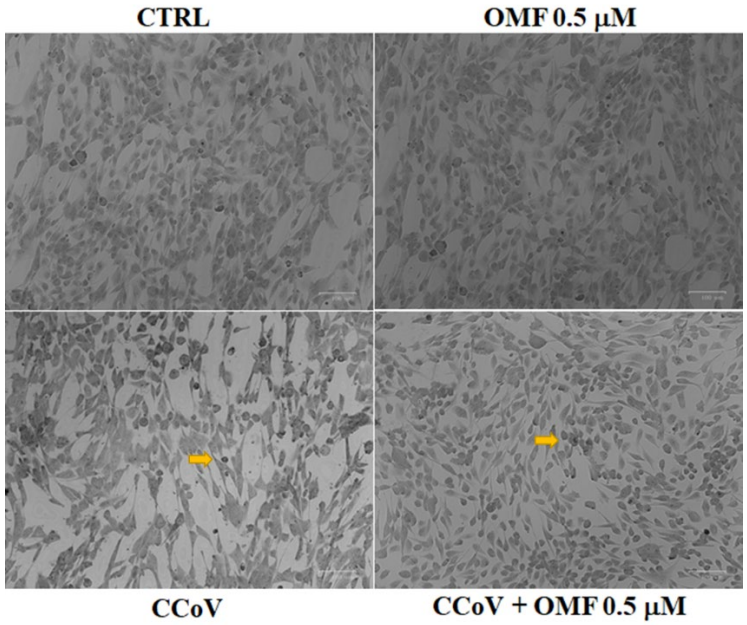

Figure 7. OMF diminished signs of morphological cell death during CCoV infection in A72 cells. Cells were infected with CCoV, exposed or not to OMF. After 48 h of infection, cells were observed under a light microscope after Giemsa staining. Comparing cells unexposed to OMF to control groups, photomicrographs revealed no morphological changes. In CCoV-infected groups, several cells showed signs attributable to apoptosis, such as pyknotic nuclei and nuclear fragmentation (arrow), whereas in OMF-treated infected cells, few signs of apoptotic cell death were noticed (arrow).
Scale bar 100 µm.

Analysis of cell morphology was carried out to assess the effect of both VER and PS during CCoV infection. After Giemsa staining, light microscopy analysis was performed.

In Figure 4A, the comparison between CCoV-infected cells treated or not with VER and PS displayed changes in cell morphology. Features of cell death, such as cellular shrinkage (Figure 8A, arrowhead), pyknosis (Figure 8A, arrow), were noticeably lessened by both funicone-like compounds (Figure 8A). Furthermore, an enhancement of intercellular spaces provoked by the detachment of cells from the culture plate was mostly detected in untreated CCoV-infected cells (Figure 8A, slim arrow). After treating with acridine orange/propidium iodide (AO/PI), fluorochromes used for the detection of both viable and dead cells, cells were observed by fluorescence microscopy. AO, which is membrane-permeable, binds to nucleic acids, provoking a green fluorescence. PI, impermeable to intact cell membrane, crosses the membrane of dead and dying cells and intercalates with nucleic acids, forming a bright red fluorescent complex. The combination of both fluorescent probes allows the simultaneous detection of cells with intact or compromised cell membranes (Bank, 1987). In the presence of VER and PS a decrease in PI fluorescent cells was observed in infected cells compared to CCoV untreated groups (Figure 8B). Overall, our results demonstrated that in A72 cells funicone-like compounds, like VER and PS, significantly reduced cell death, as well as morphological cell death signs during CCoV infection.

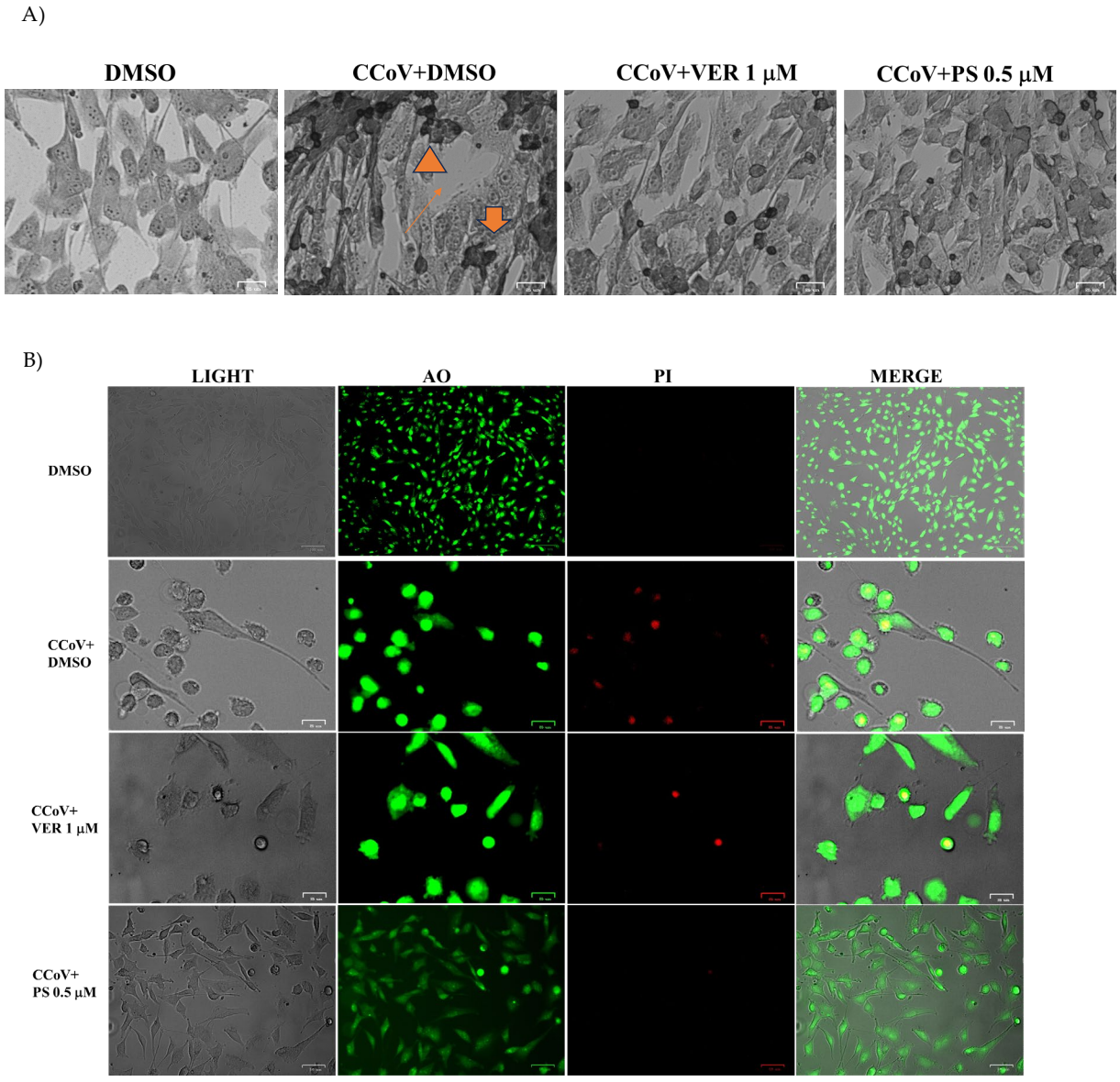

Figure 8. Funicone-like compounds reduce the typical morphological cell death features during CCoV infection. (A) Signs of cell death, such as cellular shrinkage (A, arrowhead), pyknosis (A, arrow), were noticeably lessened in VER- and PS-treated groups. Moreover, the enhancement of intercellular spaces produced by the detachment of cells from culture plate was mainly observed in untreated CCoV-infected cells (A, slim arrow). (B) In AO/PI panel, PI fluorescent cells, indicating dead and dying cells, were mostly detected in CCoV-infected cells compared to funicone-like compounds-infected groups. Scale bar 25 µm and 50 µm.

3.4. 6PP Decreases Signs of Morphological Cell Death during CCoV Infection in A72 and CRFK Cells

To investigate the effects of 6PP on cell morphology following CCoV infection, light microscopy examination of A72 and CRFK cells was achieved by using Giemsa staining and acridine orange staining, which are known methods to detect morphological features of cell death (Leite et al., 1999; Banfalvi et al., 2017). Herein, after Giemsa staining at 48 h p.i., in CCoV-infected cells, 6PP decreases signs of morphological cell death, while in

unexposed infected cells, an enhancement of intercellular spaces because of detachment from culture plate was detected in both cell lines (Figures 9a and 9b), in which pyknosis, chromatin condensation (Figure 9, circle), and cell shrinkage (Figure 9, arrowhead) were found. All these features of morphological cell death were remarkably reduced by 6PP in infected cells (Figure 9).

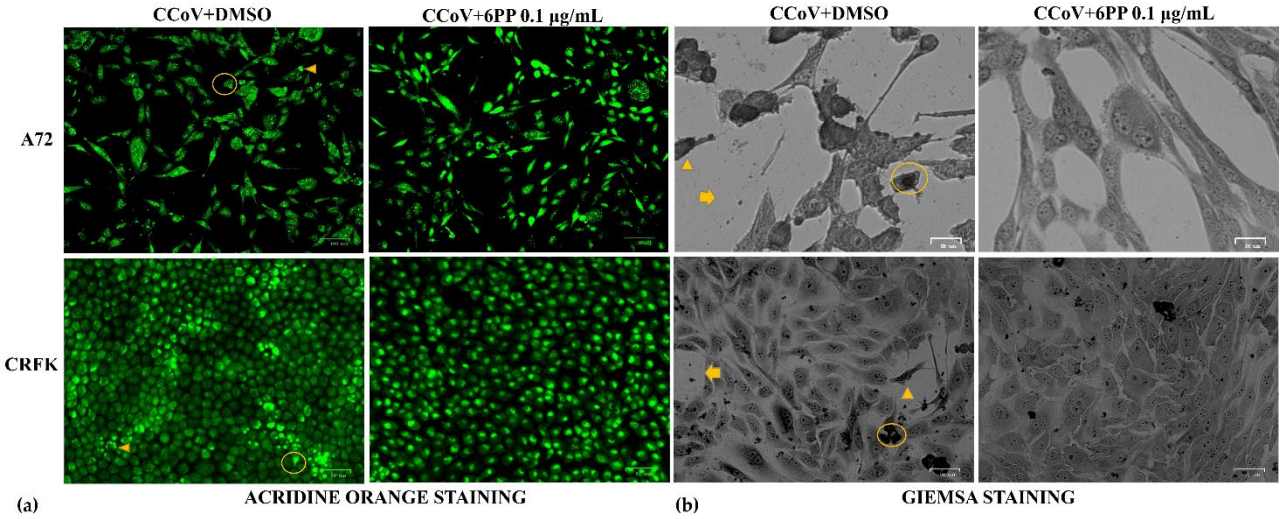

Figure 9. 6PP decreases features of morphological cell death during CCoV infection. A72 cells, infected with CCoV, in the presence or absence of 6PP, were stained by (a): acridine orange and observed by fluorescence microscope after 24 h of infection; (b): or by Giemsa and observed by light microscope after 48 h of infection. In unexposed infected cells, photomicrographs indicate an enhancement of intercellular spaces because of detachment from culture plate (arrow). Furthermore, morphological signs of cell death, like pyknosis and chromatin condensation (circle), as well as cell shrinkage (arrowhead), were identified in A72 as well as in CRFK cells. These signs of morphological cell death were noticeably reduced by the presence of 6PP in infected cells. Scale bar 100 µm and 25 µm.

3.5. OMF, VER and PS reduce CCoV during infection in A72 cells

To study the influence of OMF during CCoV infection in A72 cells, virus titer and viral cytopathic effects (CPE) were analysed for 72 h after infection. Remarkably, a statistically significant ($p < 0.001$ and $p < 0.05$) decline in virus titer was detected by Quantitative Real-time RT-PCR (RT-qPCR) after 48 h and 72 h of infection, respectively, in A72 cells treated with OMF during CCoV II infection (Figure 10). In addition, at 48 h after infection, CPE, featured by detachment from culture plate, was extensive in infected cells, whereas it noticeably lessened in OMF-treated infected cells (Figure 7). Therefore, our findings revealed that OMF noticeably decreases virus yield and CPE during CCoV II infection.

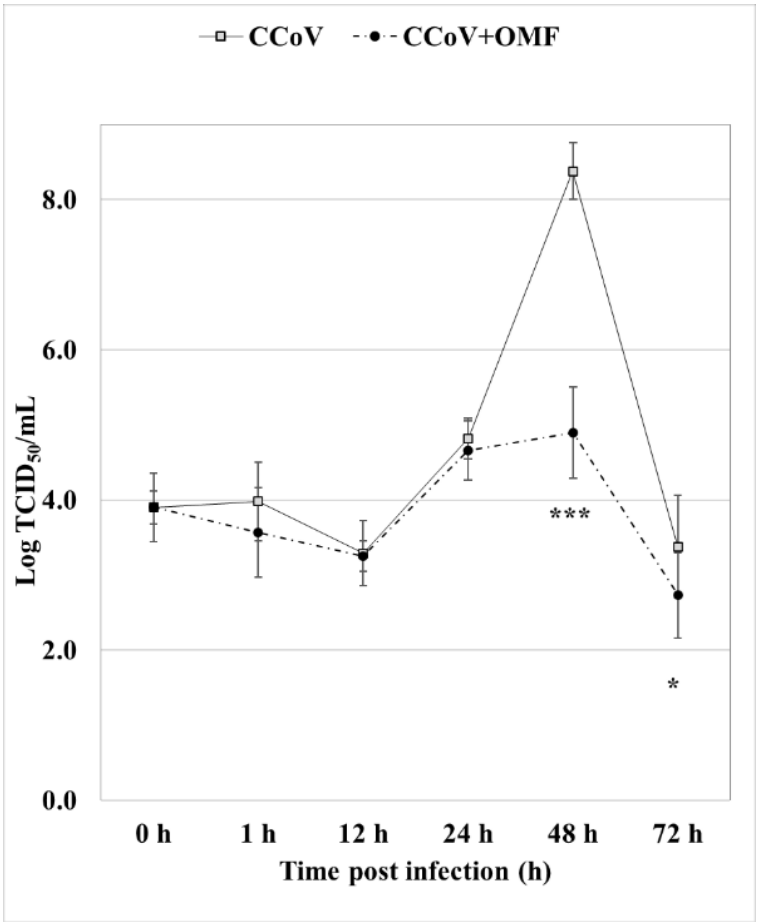

Figure 10. OMF reduces virus titer during CCoV II infection in A72 cells. For viral growth curves, A72 cells were infected with CCoV II at MOI of 5, in the presence or not of OMF. At indicated times post infection, virus titer was assessed by RT-qPCR. Significant differences between CCoV II infected cells and OMF treated infected cells were shown by probability *p*. ***$p < 0.001$ and *$p < 0.05$.

To explore the antiviral effect of VER and PS against CCoV infection, virus yield was evaluated after 48 h of infection in A72 cells. A significant ($p < 0.01$) decrease in virus titer was revealed by Quantitative Real-time RT-PCR (RT-qPCR) in VER- and PS-treated cells (Figure 11A). Additionally, a decreased cytopathic effect (CPE) was appreciable in both VER and PS-treated groups compared to untreated infected cells (Figure 11B). All those effects were accompanied by a significant decrease ($p < 0.001$ and $p < 0.01$) in the expression of the viral nucleocapsid protein (NP), as detected in VER- and PS-treated cells compared to CCoV-infected groups.

A)

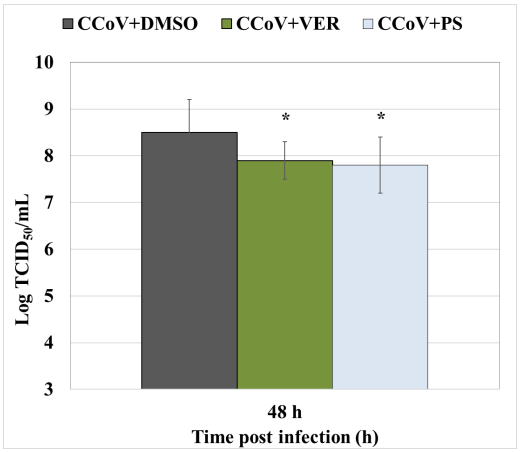

B)

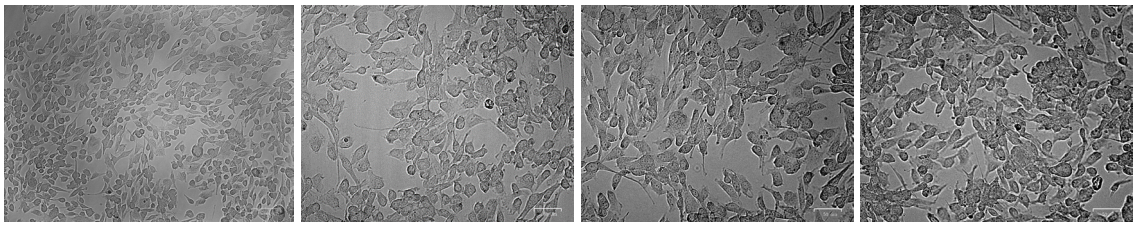

Figure 10. Funicone-like compounds reduce virus yield during CCoV infection. (A) For viral titer, cells were infected with CCoV and treated or not with VER and PS. After 48 h of infection, virus titer was evaluated by RT-qPCR. (B) Cytopathic effect (CPE), observed by light microscope (50 and 100 µm). Virus yield was evaluated by RT-qPCR using a standard curve created by amplifying serial known dilutions (three replicas/dilution) of the virus and plotting Log $TCID_{50}$/mL against average Ct number. The comparison between CCoV-infected cells treated with funicone-like compounds vs. untreated infected cells was significant (* $p < 0.05$).

Our observations showed that both OMF, VER and PS induce antiviral effects during CCoV infection.

3.6. 6PP Diminishes Virus Yield during CCoV infection

To investigate the effect of 6PP during CCoV infection, RT-qPCR as well as $TCID_{50}$ titration were performed, and CPE was examined.

To evaluate the effect of 6PP on CCoV yield during infection in A72 cells, RT-qPCR was carried out. Virus titer ($TCID_{50}$/mL) in the presence or not of 6PP was analysed at various times post infection (0, 1, 12, 24, 48, and 72 h) by running all the samples (in triplicate) with the standard curve protocol. Virus titer in each sample was then calculated using the standard curve equation starting from the Ct values obtained (Figure 11). In the presence of 6PP, our results showed a significant decrease in virus titer at 48 h and 72 h p.i. ($p < 0.001$ and $p < 0.05$, respectively) (Figure 12).

CCoV titration during infection in CRFK cells. Following infection in CRFK cells, in the presence of 6PP, a reduction of virus titer ($TCID_{50}$) was found at 24 h p.i. (Figure 12).

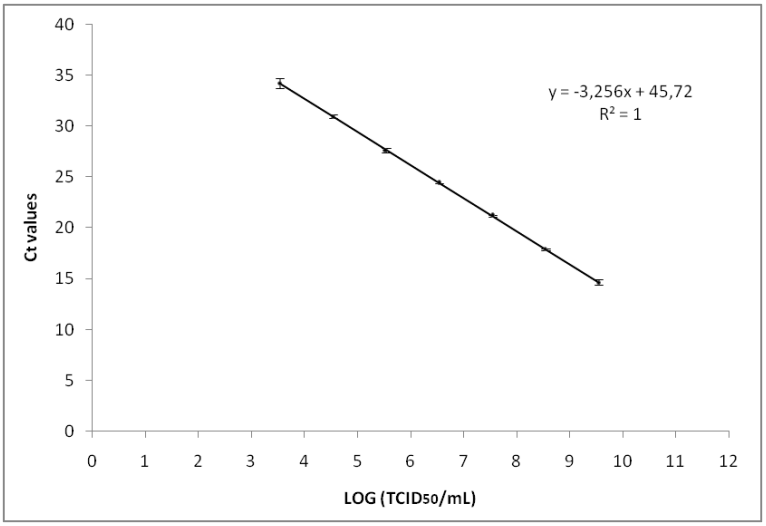

Figure 11. Standard curve obtained by qRT-PCR analyzing serial dilutions (from $3.5x10^9$ to $3.5x10^2$ $TCID_{50}$/mL) of canine coronavirus viral stock and plotting the C_t obtained against $TCID_{50}$/mL. C_t values are presented as the meaning of six replicates for each dilution ± SD.

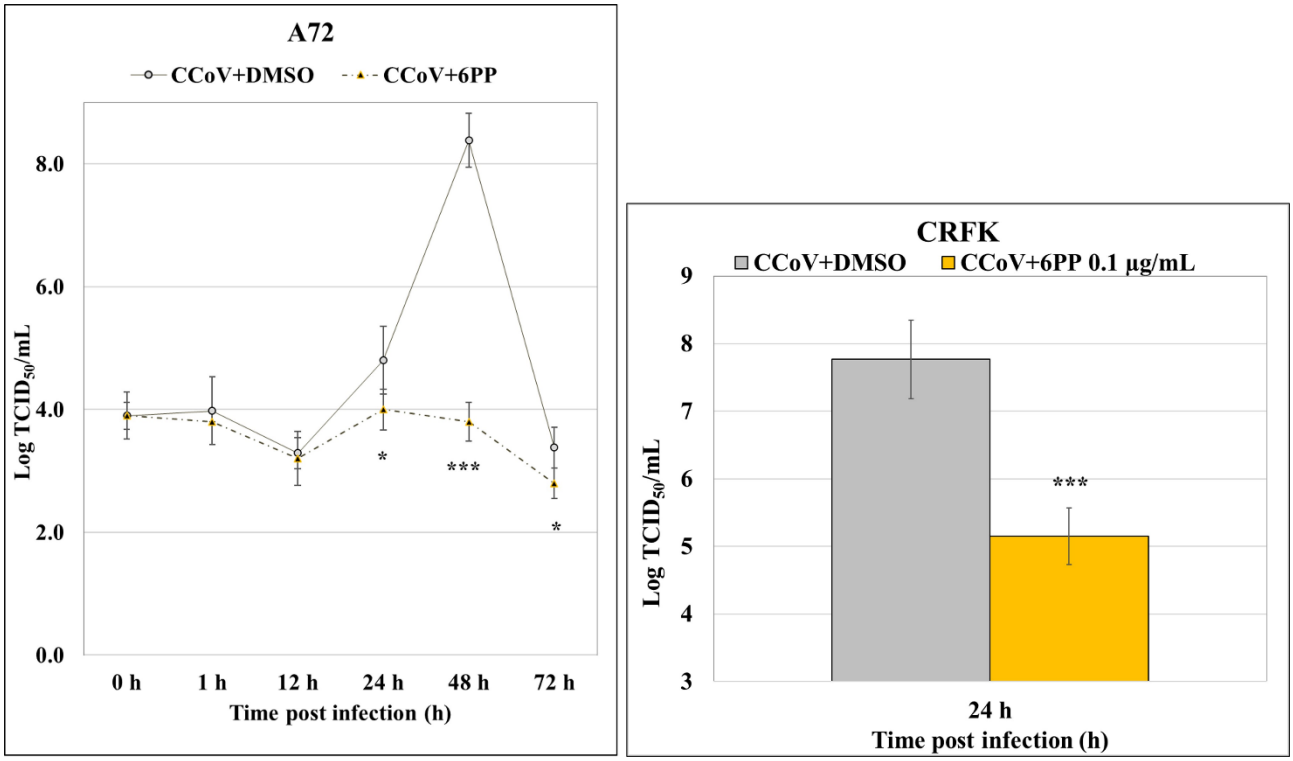

Figure 12. 6PP diminishes virus titer during CCoV infection. For viral growth curves, following CCoV infection in A72 cells, exposed or not to 6PP, virus titers were evaluated by RT-qPCR, at indicated times post infection. During CCoV infection in CRFK, virus titer was assessed by $TCID_{50}$. Comparing CCoV-infected cells to 6PP-treated infected cells, significant differences were indicated by probability *p*. ***$p <$ 0.001 and *$p < 0.05$ in A72 cells. ***$p < 0.001$ in CRFK cells.

Additionally, in A72 cells, at 48 h p.i., marks of CPE, detected through syncytia (Figure 4, arrowhead) and detachment of cells from culture plates (Figure 6 and Figure 9, arrow), were wide in infected groups. In CRFK cells, CCoV developed a typical CPE (Woods and Wesley, 1988), with granular (Figure 9, arrow) and small multinucleated cells (Figure 6 and Figure 9, arrowhead). In both cell lines, virus yield was markedly reduced by the presence of 6PP (Figures 6 and 9).

Overall, our results showed that 6PP strongly decreased virus yield as well as CPE during CCoV infection in both A72 and CRFK cells.

3.7. OMF Downregulated the Expression of AhR and NP during CCoV Infection

Based on findings in previous studies (Cerracchio et al., 2022; Fiorito et al., 2022), to investigate the influence of OMF on AhR protein expression during CCoV infection in A72 cells, immunofluorescence (IF) staining was carried out. In the control group, represented by uninfected cells, we found that AhR was expressed (Cerracchio et al., 2022); and, in OMF- VER- and PS- exposed cells, a downregulation of AhR protein expression was detected (Figures 13a-14a). These results were proven using integrated density fluorescence measurement (Figures 13b-14b).

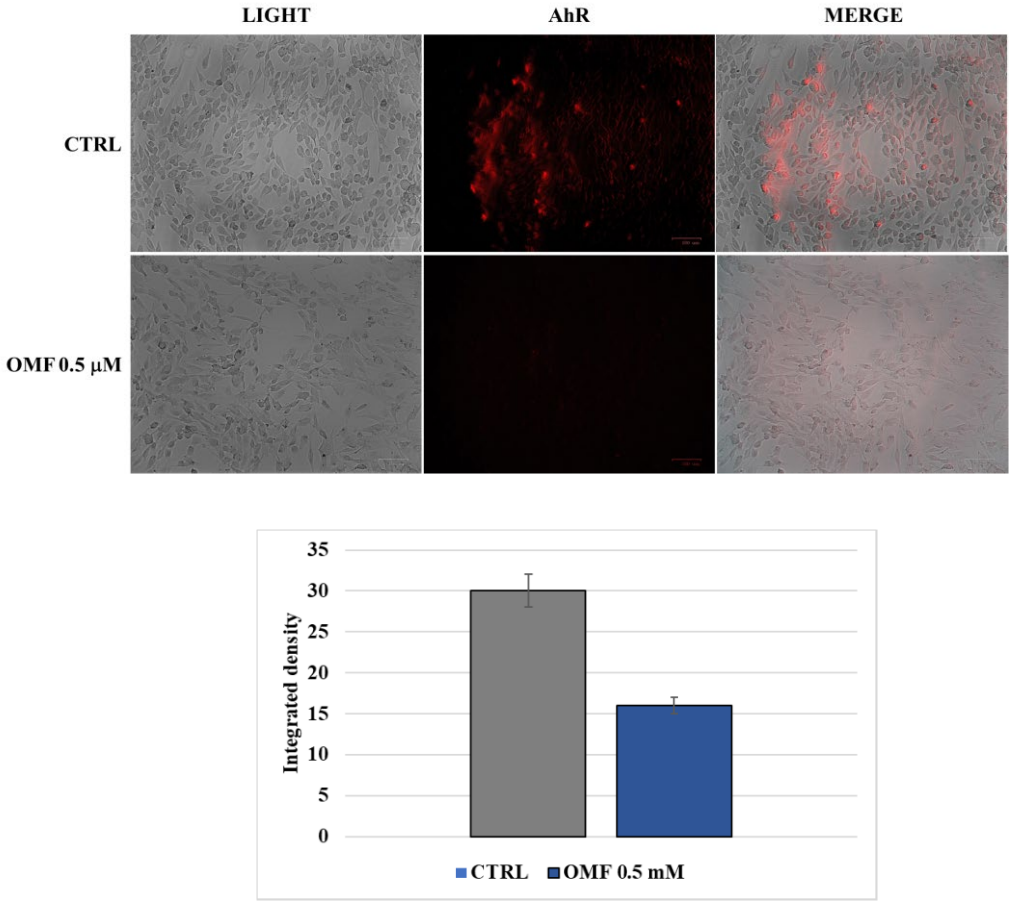

Figure 13. OMF downregulates the expression of AhR. (a) A72 uninfected control group expressed AhR. OMF at the concentration of 0.5 µM markedly reduced the expression of AhR. Scale bar 100 µm. (b) Bars represent the mean ratio generated from the integrated density (product of the area and mean intensity of fluorescence) of the AhR expression evaluated by ImageJ. Error bars represent standard error measurement.

A)

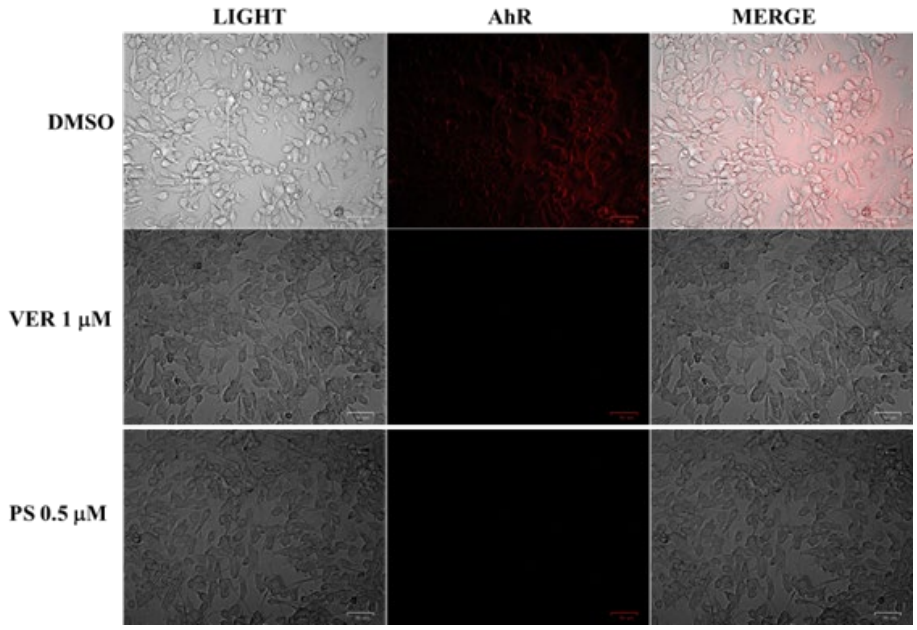

B)

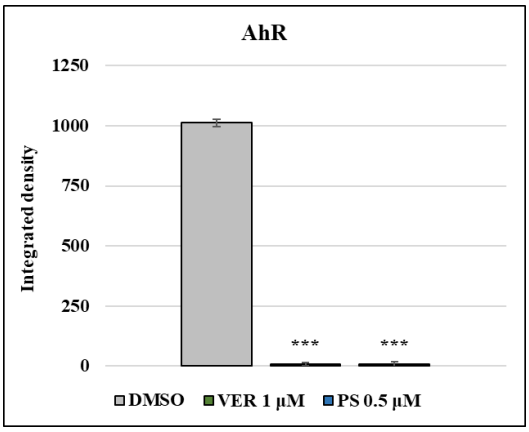

Figure 14. Funicone-like compounds reduce the expression of AhR. (A) DMSO control cells expressed AhR, which was significantly lessened by both VER and PS. Scale bar 50 µm. (B) Bars designate the mean ratio developed from the integrated density of AhR expression measured by ImageJ. Error bars correspond to standard deviation quantification and significant differences are indicated by probability p. *** $p < 0.001$.

Moreover, during CCoV II infection, in the presence or absence of OMF, as well as of both funicone-like compounds, VER and PS, the expression of AhR and NP was analysed by immunofluorescence staining. After 24 h of infection, a noticeable reduction of both AhR and NP was detected in the presence of OMF as well as of VER and PS (Figures 15 and 16).

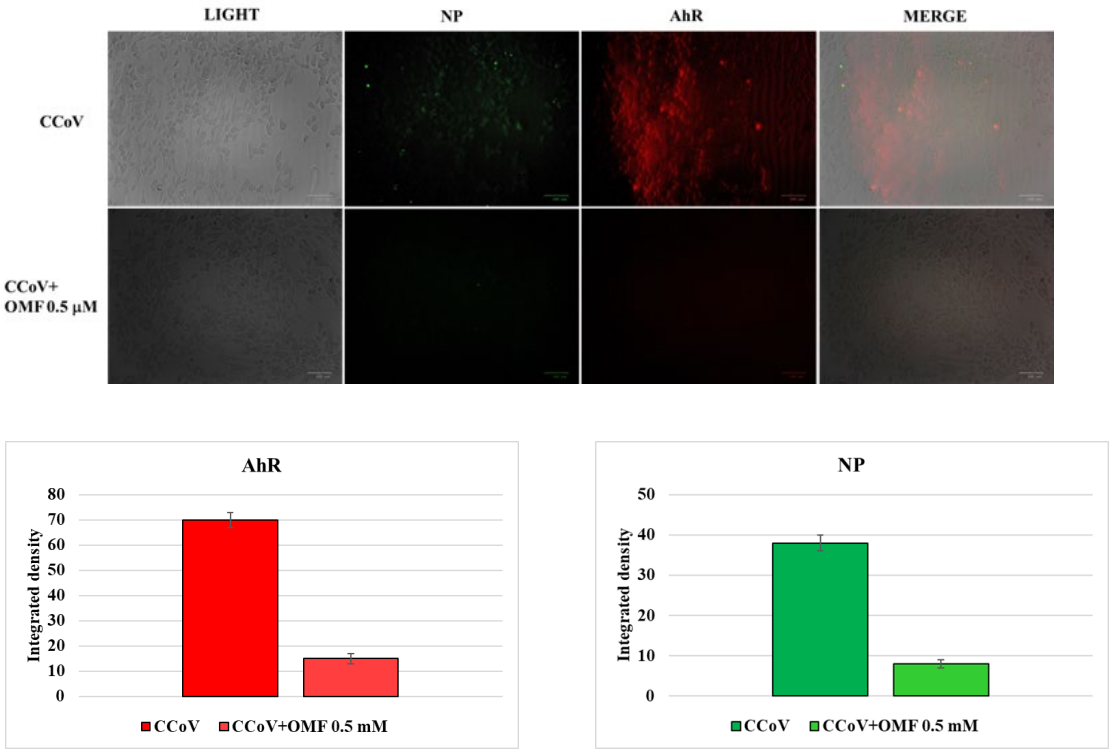

Figure 15. OMF decreases AhR and NP expression during CCoV II infection in A72 cells. Cells were infected with CCoV II at MOI of 5, in the presence or absence of OMF; at 24 h after infection, immunofluorescence staining for AhR (red fluorescence) and NP (green fluorescence) was performed. (a) In OMF-exposed group, the expression of AhR and NP was extremely decreased during CCoV II infection. Scale bar 100 µm. (b) Bars represent the mean ratio produced from the integrated density (product of the area and mean intensity of fluorescence) of the AhR expression calculated by ImageJ. Error bars are standard error measurement. (c) Bars represent the mean ratio produced from the integrated density (product of the area and mean intensity of fluorescence) of the NP expression calculated by ImageJ. Error bars are standard error measurement.

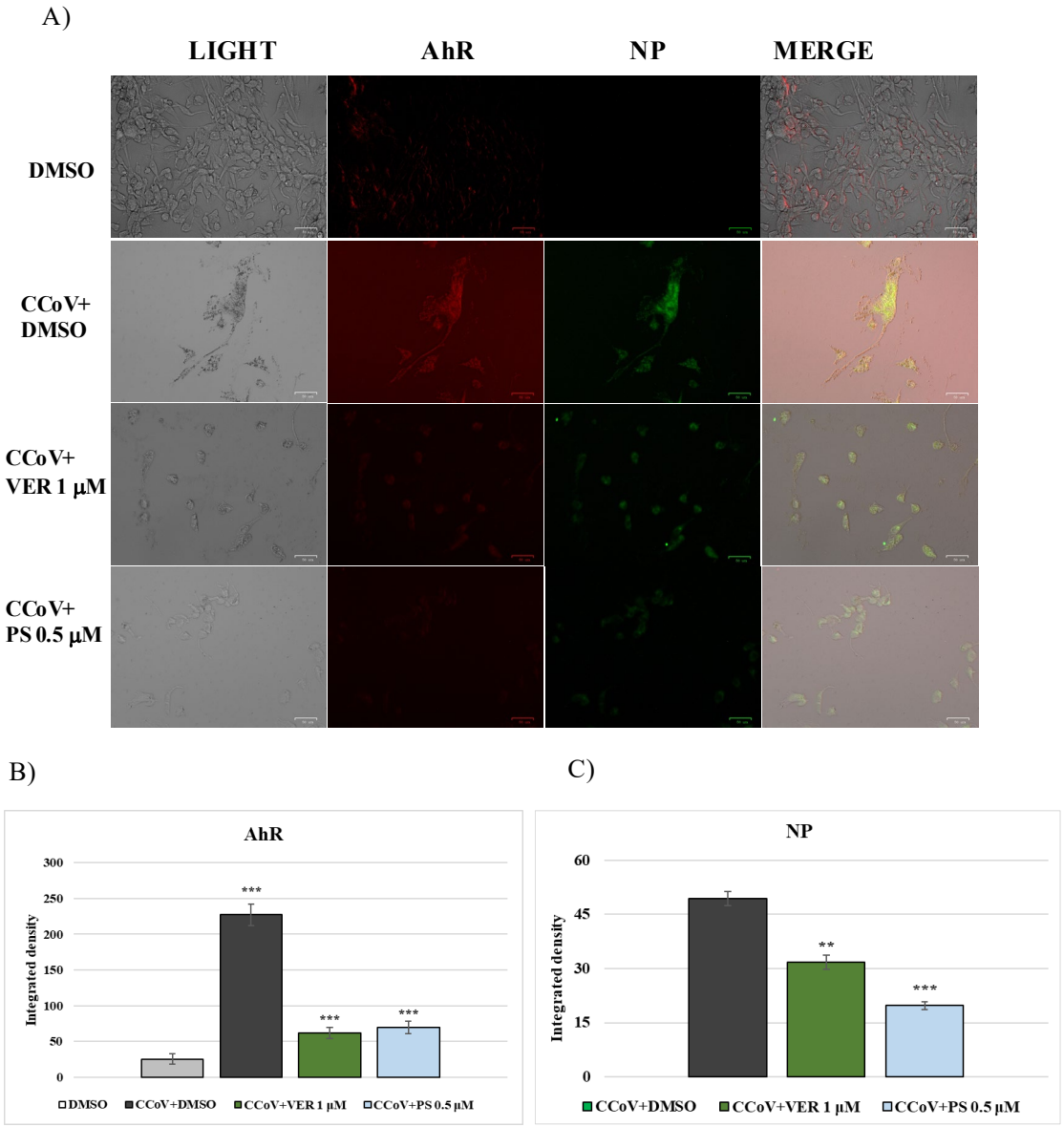

Figure 15. Funicone-like compounds reduce the expression of both AhR and viral nuclear protein (NP). CCoV-infected A72 cells were treated with VER and PS. After 24 h of infection, IF staining to detect AhR (red fluorescence) and NP (green fluorescence) was performed. (A) In both groups treated with funicone-like compounds, we observed a high reduction in the expression of AhR and NP. Scale bar 50 µm. Bars identify the mean ratio resulting from the integrated density of (B) AhR and (C) NP expression, analyzed by ImageJ. Error bars are the standard deviation quantification and significant differences are indicated by probability p. ** $p < 0.01$ and *** $p < 0.001$.

Taken together, these results showed that the expression of NP and AhR were decreased by OMF, VER and PS.

3.8. 6PP Decreased the Expression of AhR and NP during CCoV infection

To investigate whether 6PP affects AhR and NP expression during CCoV infection, immunofluorescence staining was made. Firstly, A72 and CRFK cells were treated with 6PP 0.1 µg/mL and, at 24 h post treatment a decrease of AhR expression, compared to DMSO, was noted in both cell lines used (Figure 16a, b).

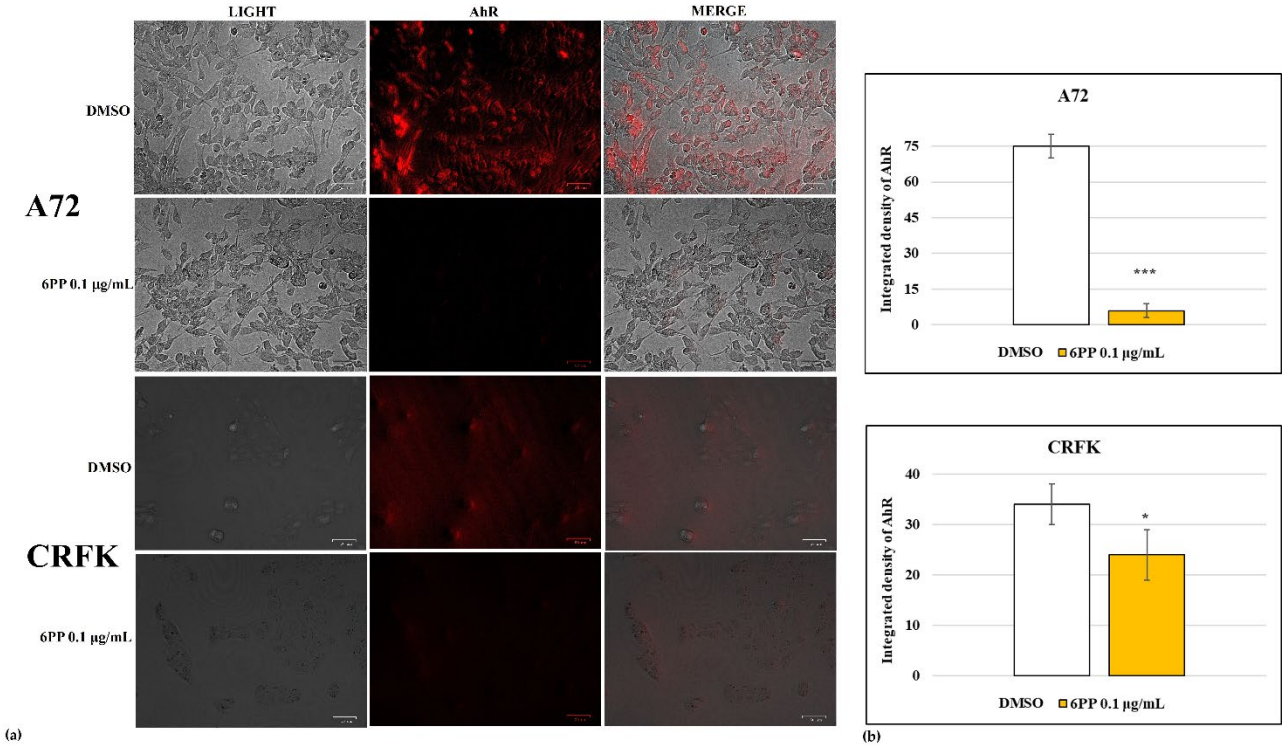

Figure 16. 6PP reduces the expression of AhR in A72 and in CRFK cells. A72 and CRFK cells were exposed to 6PP, and after 24 h of treatment, immunofluorescence staining for AhR was carried out. (**a**) In 6PP exposed cells a significant down-regulation of AhR expression was observed. Scale bar 50 µm. (**b**) Bars represent the mean ratio obtained from the integration of density (product of the area and mean intensity of fluorescence) of the expression of AhR in A72 and CRFK treated cells calculated by ImageJ. Error bars correspond to standard deviation measurement. Significant differences between 6PP-treated cells and DMSO are indicated by probability *p*. *** $p < 0.001$ in A72 cells; * $p < 0.05$ in CRFK cells.

Results shown in Figure 16 indicated that 6PP reduced the expression of NP and induced a markable down-regulation in the expression of AhR in both cell lines utilized.

Both A72 and CRFK cells were then subjected to CCoV infection and exposure to 6PP 0.1 µg/mL. At 24 h p.i. for CRFK, and at 48 h p.i. for A72, results of immunofluorescence staining showed a significant reduction of AhR in infected cells exposed to 6PP. Moreover, in both cell lines, a significant reduction of the viral protein NP in 6PP infected

groups was found (Figure 17a). Integrated measurement of density fluorescence confirmed these results obtained (Figure 17b).

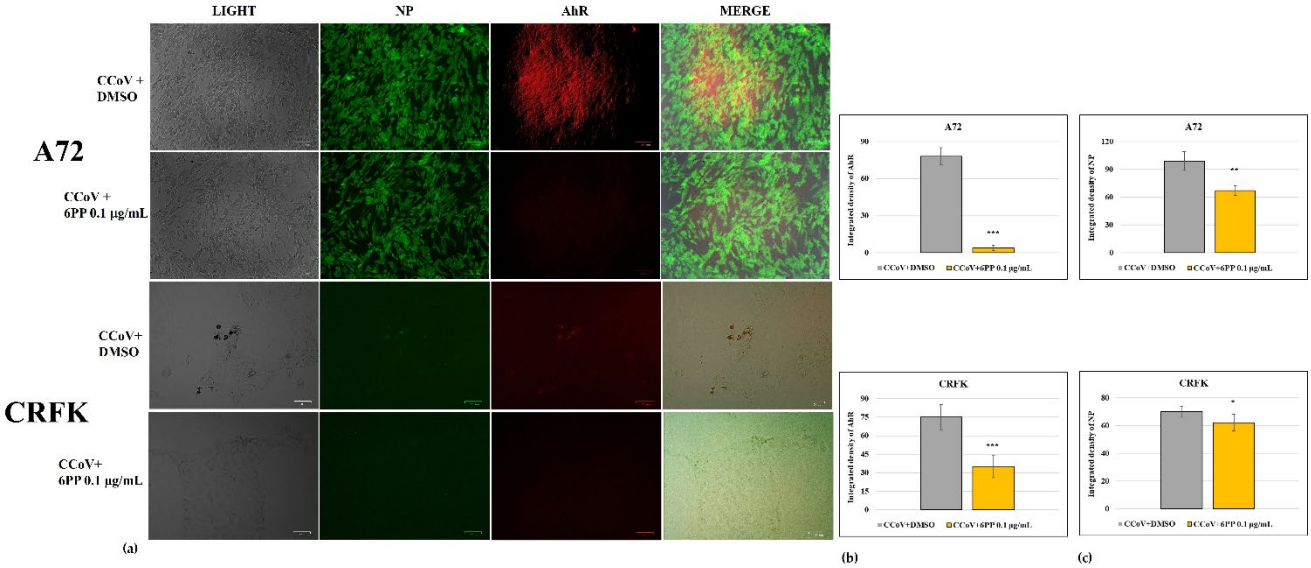

Figure 17. 6PP down-regulates the expression of AhR and NP following CCoV infection in A72 and in CRFK cells. A72 and CRFK cells, infected with CCoV, in the presence or not of 6PP, and at 48 h and 24 h p.i., respectively, immunofluorescence staining for AhR (red fluorescence) and NP (green fluorescence) was carried out. (a) 6PP induced a significant down-regulation of the expression of AhR and reduced the expression of NP during CCoV infection in both cell lines. Scale bar 50 µm. (b) Bars correspond to the mean ratio produced from the integrated density (product of the area and mean intensity of fluorescence) calculated by ImageJ of the AhR expression, and (c) of the NP expression. Error bars are standard deviation measurement. Significant differences between unexposed infected groups and 6PP-treated infected cells are indicated by probability *p*. *** $p < 0.001$ for AhR in both cell lines; and * $p < 0.05$ for NP in A72 and CRFK cells.

3.9. Funicone-like compounds VER and PS deacidify lysosome in A72 cells during CCoV infection

Lysosomes are cellular organelles, enclosing a variety of enzymes, which represent the digestive system of the cell. An acidic environment, developed by a proton pump, typifies lysosomes. The effect of VER and PS treatment on lysosomes was analyzed by LysoRed staining, a method used to label lysosomes in live cells. DMSO control cells showed an entirely acidified structure (Figure 8). In contrast, deacidification was observed in the presence of both funicone-like compounds in a significant number of cells (Figure 18). During CCoV infection in A72, we observed cellular deacidification (Figure 19), which were further alkalinized by both funicone-like compounds (Figure 20).

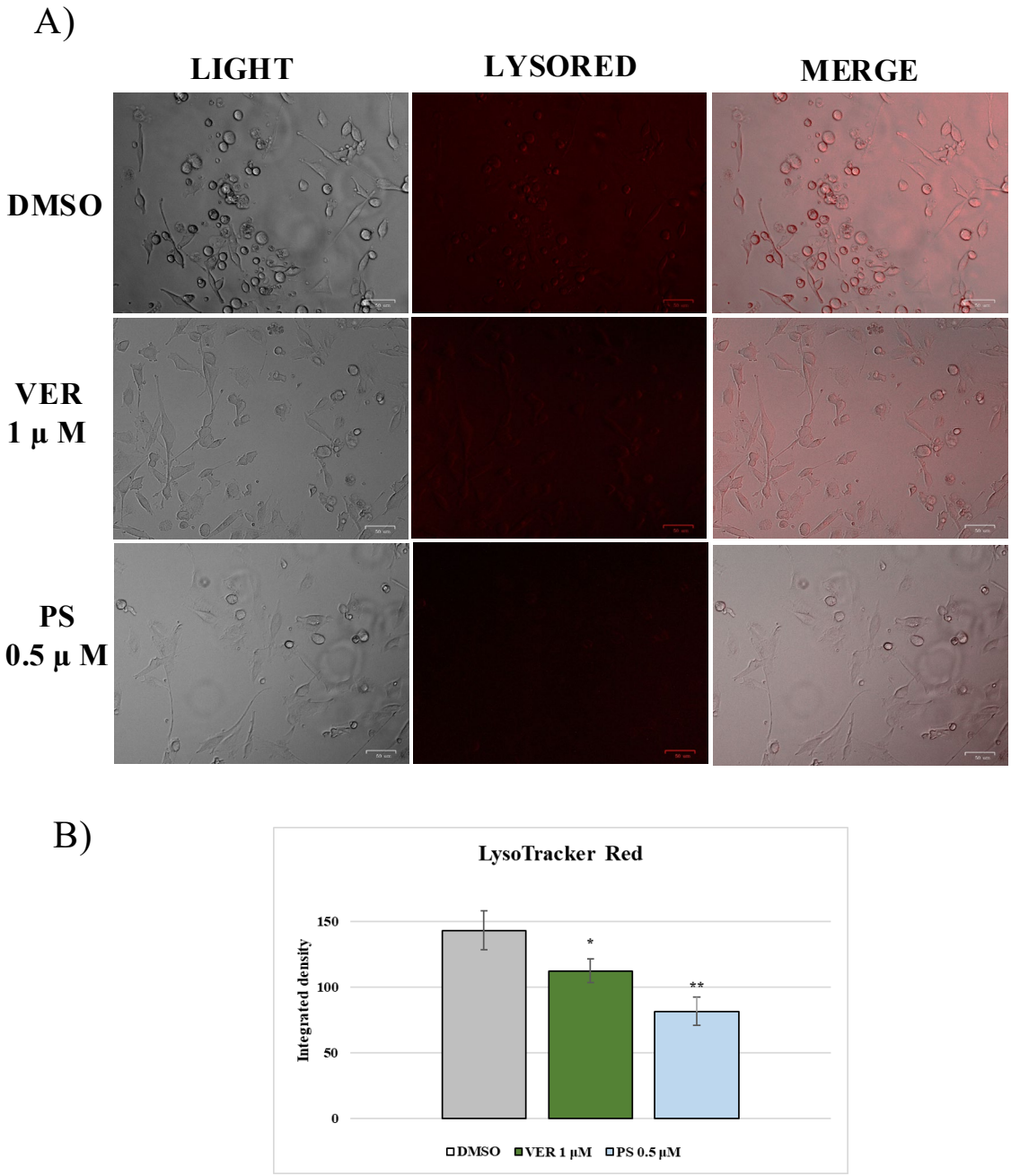

Figure 18. Funicone-like compounds deacidify lysosomes in A72 cells. (A) LysoRed staining of DMSO control group compared to cells treated with VER and PS. Scale bar 50 µm. (B) Bars designate the mean ratio obtained by the integrated density of LysoTracker calculated by ImageJ. Error bars represent standard deviation quantification and significant differences are indicated by probability p. * $p < 0.05$ and ** $p < 0.01$.

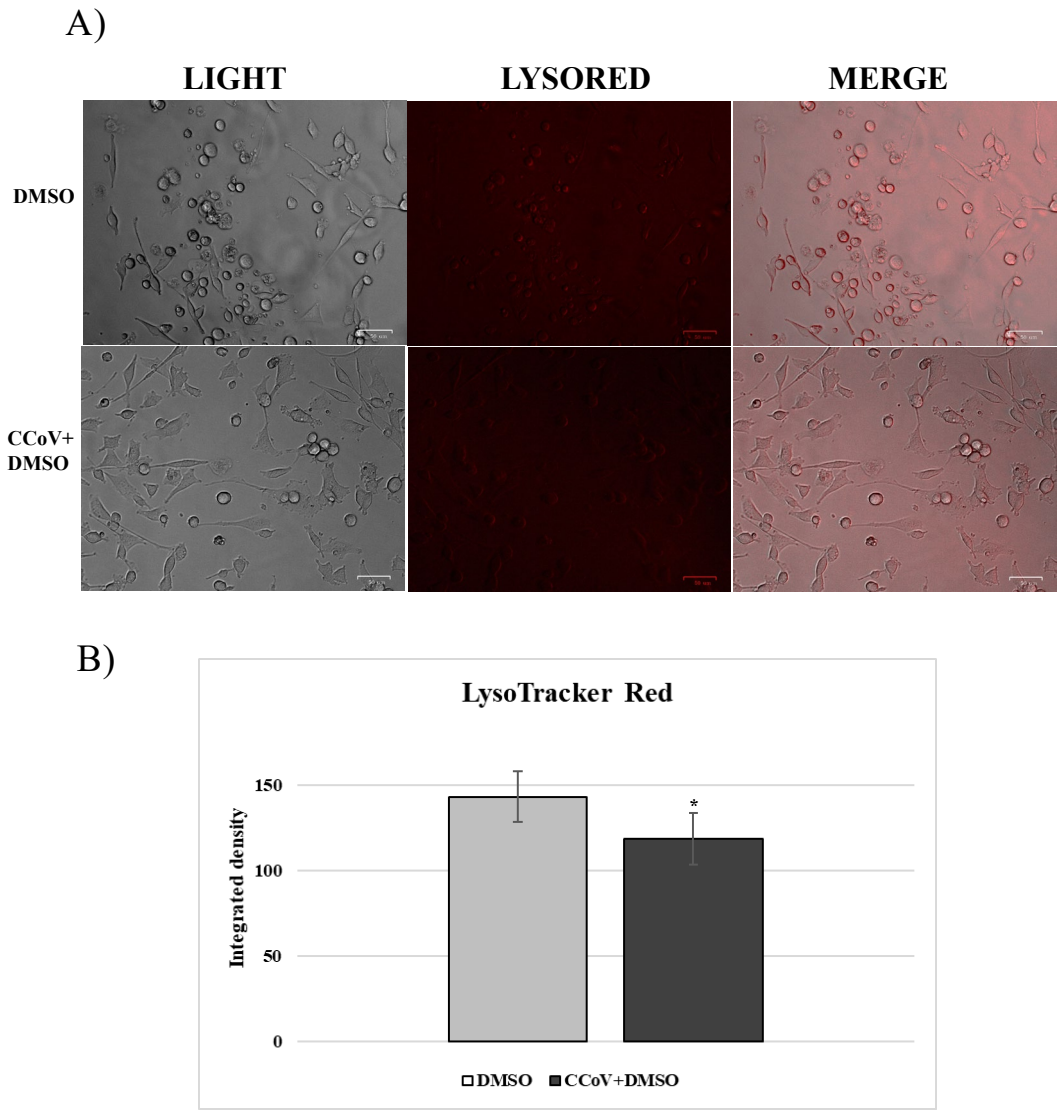

Figure 19. CCoV deacidifies lysosomes during infection. (A) LysoRed staining of CCoV-infected cells compared to Control group. Scale bar 50 μm. (B) Bars indicate the mean ratio obtained by the integrated density of LysoTracker measured by ImageJ. Error bars indicate standard deviation quantification and significant differences are indicated by probability p. * $p < 0.05$.

A)

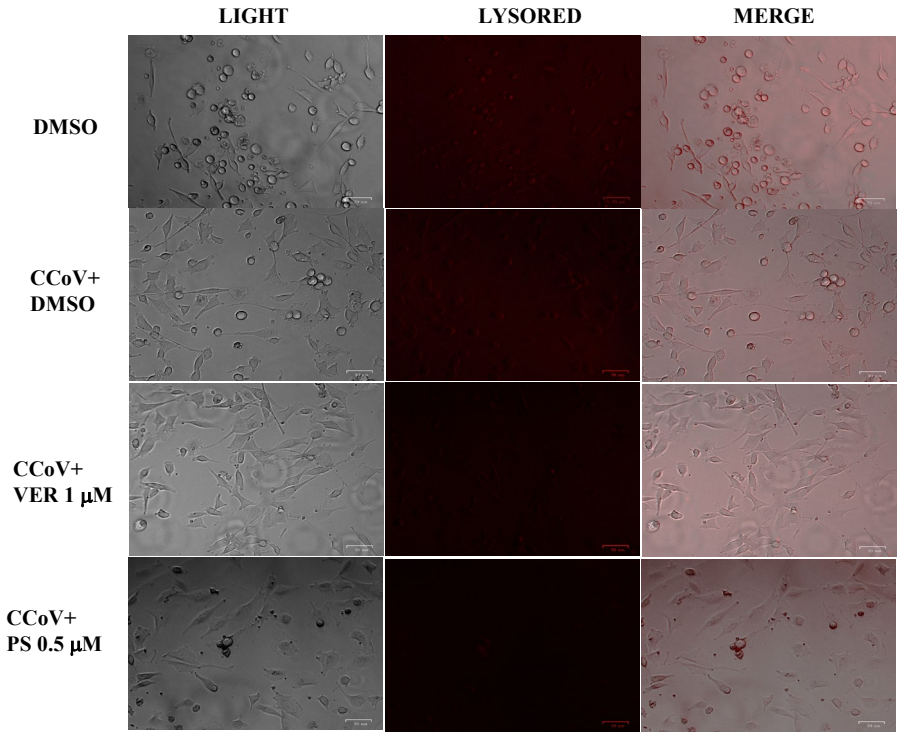

B)

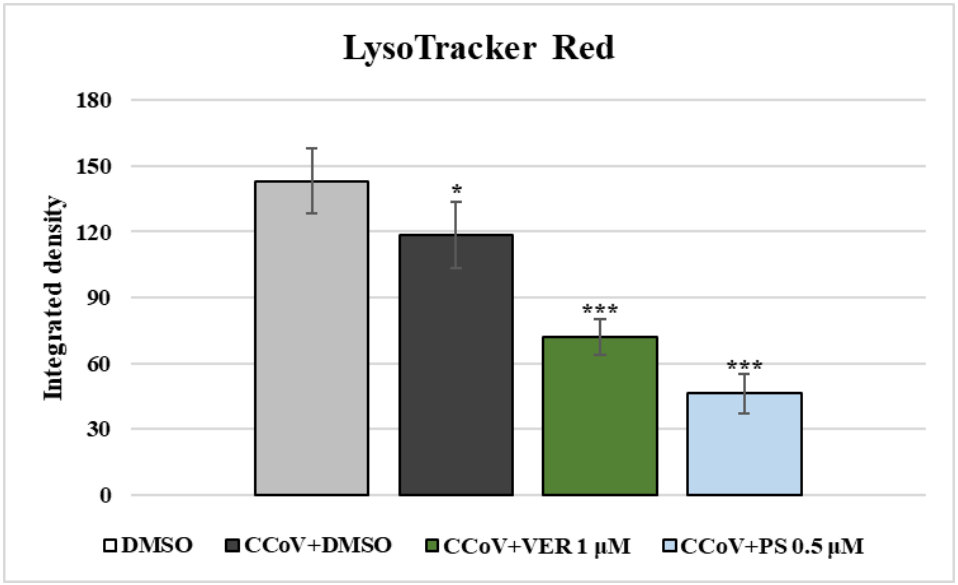

Figure 20. Funicone-like compounds deacidify lysosomes during CCoV infection (A) LysoRed staining of CCoV-infected cells compared to CCoV-infected cells treated with VER and PS. Scale bar 50 µm. (B) Bars indicate the mean ratio obtained by the integrated density of LysoTracker measured by ImageJ. Error bars indicate standard deviation quantification and significant differences are indicated by probability p. * $p < 0.05$ and *** $p < 0.001$.

4. Discussion

Coronaviruses, like CCoV, can rapidly mutate their genome, leading to the formation of new variants with increased infectivity and transmissibility, sometimes able to cross interspecies barriers. For example, recombinant canine–feline–porcine strains were isolated from dogs and humans in various countries of the world (Pratelli et al., 2022; Vlasova et al., 2022b). The emergence of remarkably virulent variants needs for continuous monitoring of CCoV, and also suggests the necessity for discovering novel antiviral agents. So far, it has been proved that the anti-inflammatory drug indomethacin has effective antiviral features to fight against CCoV infection, through action both on viral replication and block of viral RNA synthesis (Amici et al., 2006; Xu et al., 2020; Gomeni et al., 2020). Recent advances show as a recombinant adenovirus, which expresses canine interferon lambda 3, has an antiviral activity against CCoV (Kim et al., 2022). Due to high toxicity of the conventional antiviral drugs, numerous natural substances are being recently tested to conceive new therapeutics against viral infections. On this regard, natural products, such as bufotenine, an alkaloid obtained by skin secretions of amphibians and plant extracts, did not show potential antiviral activity against CCoV infection (Barboza et al., 2021).

The search for potential chemotherapeutics is supported by insights regarding the structural aspects of virus proteins (Takahashi et al., 2021). Indeed, computational approaches have confirmed that many fungal products could be effectively employed in therapy against SARS-CoV-2 by acting as protein inhibitors (Saied et al., 2021). Pyranonigrin A, produced by *Penicillium thymicola*, was identified as a possible inhibitor of the main protease (Mpro) of the virus using docking and molecular dynamics simulation (Belachew et al., 2021). Moreover, fonsecin, a naphthopyrone produced by *Aspergillus fonsecaeus*, displayed a high binding affinity for the papaine-like protease of SARS-CoV-2 through interaction with the Tyr268 amino acid residue of the enzyme cavity (Rao et al., 2020). Pyrrocidine A, a polyketide-amino acid-derivative from the endophytic fungus *Acremonium zeae*, and 18-methoxy-cytochalasin J were characterized as potent inhibitors of viral RNA-dependent RNA polymerase (Rao et al., 2022). Finally, cyclosporine A, a renowned immunosuppressant also proposed for the treatment of hepatitis C (Watashi et al., 2021) and MERS-CoV (Li et al., 2018), was shown to be able to suppress replication of CoVs (de Wilde et al., 2011; Sanders et al., 2020). Because of their attitude to live in extreme conditions for other organisms, fungi produce different secondary metabolites belonged to several chemical classes such as alkaloids, peptides,

quinones, terpenes, acyclic compounds, steroids, as well as pyrones. They have been investigated for different uses, from antibiotics to fungicides, plant growth regulators and hormones. In addition, previous studies on compounds derived from fungi have highlighted potential antiviral properties (Linnakosky et al., 2018; Roy, 2017; Deshmukh et al., 2022; Salvatore et al., 2022). In this respect, deoxyfunicone was reported to be effective as an HIV-1-integrase inhibitor (Sanders et al., 2020; Singh et al., 2003), and OMF was found to be able to reduce the infectivity of the hepatitis C virus (Nakajima et al., 2013). Concerning the latter compound, in our previous studies, OMF induced a significant reduction in virus yield, and deeply inhibited bICP0 expression, the main regulatory protein in the lytic cycle of BoHV-1 (Fiorito et al., 2022).

In this study, OMF, at the non-toxic concentration of 0.5 μM, did not significantly increase cell death during CCoV infection, and weakened morphological cell death marks, which typically developed during CCoV infection in A72 cells (Ruggeri et al., 2007; De Martino et al., 2010). Indeed, following *in vitro* infection, it has been shown that virus-induced apoptosis occurs in the presence of modulation in the levels of the sirtuin and FOXO family, which are proteins involved in cell damage due to apoptosis or oxidative stress (Marfè et al., 2011). Moreover, the funicone-like compounds vermistatin and penisimplicissin have shown antiviral properties against CCoV, and PS turned out to be more active than VER. In fact, our data show an increase in cell viability, with an improvement of morphological features in CCoV-infected cells, at the non-toxic doses of 1 μM for VER and at 0.5 μM for PS. In addition, a substantial decrease in virus yield was observed, accompanied by a reduction in the expression of viral protein NP. Herein, during CCoV infection, the non-toxic concentration of 0.1 μg/mL 6PP significantly increased cell viability, cell proliferation and reduced the typical signs of morphological cell death, both in A72 and in CRFK (Woods and Wesley,1988; Leite et al., 1999; Kroemer et al., 2008; Banfalvi et al., 2017). Furthermore, 6PP produced a considerable decline in virus yield, accompanied by a diminishment of NP expression and a strong reduction of AhR expression. Understanding the potential mechanism of action of funicones represents a fascinating challenge because of the involvement of a deeply mysterious actor, AhR. This receptor shows a regulatory activity of immune functions in response to endogenous metabolites (i.e., bilirubin, biliverdin and tryptophan) as well as exogenous ligands (i.e., dietary flavonoids, environmental contaminants, and microbial metabolites) (Fiorito et al., 2017; Torti et al., 2021; Yang et al., 2019).

Several studies highlighted the important role of AhR in the inflammatory response and in the modulation of immunity, emphasizing its involvement as a host factor for Zika and Dengue viruses, as well as for alpha and beta-CoVs. For example, the pharmacological block of AhR by chemicals (CH223191, FICZ) as well as by natural products (fungal SMs, bioflavonoids) that causes anti-CoVs activity *in vitro*, not only confirm the implication of AhR in CoVs infection, but also suggest targeting AhR for developing new antivirals (Tang et al., 2005; Lawrence et al., 2013; Yamada et al., 2016; Yang et al., 2019; Cerracchio et al., 2022; Giovannoni et al., 2020; 2021; Guarnieri, 2022; Grunewald et al., 2020; Shi et al., 2023; Zhao et al., 2023). Increasing evidence underlines the role of AhR in CoVs infection (Guarnieri, 2022). Indeed, both alphacoronavirus (H-CoV-229E and CCoV) and betacoronavirus (MCoV, MERS-CoV, SARS CoV-1 and SARSCoV- 2) up-regulate AhR during infection *in vitro* (Tang et al., 2005; Grunewald et al., 2020; Giovannoni et al., 2021; Cerracchio et al., 2022; Zhao et al., 2023; Shi et al., 2023), indicating AhR as a feasible target for antiviral therapy. Interestingly, the blocking of AhR, pharmacologically induced by CH223191, reduces the replication of CCoV *in vitro* (Cerracchio et al., 2022).

Herein, following *in vitro* CCoV infection, an antiviral activity, accompanied by a reduction in morphological apoptotic features, was likely due to SMs, as their aromatic nature (see, Table 1) probably inhibits AhR. Conversely, during BoHV-1 infection, OMF provokes an increase in the expression of AhR (Fiorito et al., 2022). This conflicting phenomenon emphasizes the timing of AhR induction for regulating the balance between immunopathology and antiviral defensive immunity (Torti et al., 2021). Indeed, it has been described that AhR activation promotes the replication of herpesviruses, including cytomegalovirus, herpes simplex I (HSV-1), HSV-II, and BoHV-1 (Fiorito et al., 2017; Veiga-Parga et al., 2011). In particular, several mice died due to herpes encephalitis following HSV-1 infection when AhR was up-regulated before infection, whereas, when stimulation of AhR occurred subsequent to HSV-1 infection, herpetic pathology was reduced.

An acidic environment characterizes lysosomes, due to a proton pump V-ATPase complex pumping H^+ from the cytoplasm into the endo-lysosome. The V-ATPase complex represents a key factor for viral entry into the host cell (Zhao et al., 2021; Pereira et al., 2021). In fact, the acidic lysosomal environment is required for lysosomal enzyme stability and activity, and even a small increase in pH is sufficient to inhibit these enzymes. Therefore, the pharmacological modulation of lysosomal pH can interfere with

the endosomal pathway and intracellular membrane trafficking crucial for viral infection. Hence, lysosomotropic agents (e.g., chloroquine, hydroxychloroquine or azithromycin) are able to prevent CoVs infection representing new therapeutic strategies. In fact, the basic amine property of chloroquine and similar molecules leads to their accumulation in cellular acidic compartments and raises their pH (Ghosh et al., 2020; Aslam and Ladilov, 2020; Gorsghkov et al., 2021; Liang et al., 2022). However, a significant deacidification of lysosomes during CoV infection was reported, along with a reduction in lysosomal enzyme activity. This deacidification mechanism is currently under investigation, but it was hypothesized that lysosomes become deacidified indirectly due to an excessive cargo (i.e., viruses) and/or perturbations in the proton pump or ion channel trafficking (Ghosh et al., 2020). In this work we observed that the acidic environment of A72 cells was deacidified by CCoV infection and this is in agreement with what is described above regarding CoV infection. In addition, at non-toxic doses both funicone-like compounds tested were active on cells, either CCoV-infected or not, inducing alkalinization of lysosomes. However, VER or PS could be not directly responsible for the observed increase in lysosome pH because, unlike the above-mentioned lysomotropic agents, these compounds do not have basic properties. For this reason, it can be deduced that the alkalinization of the acidic lysosomes is the result of a more complex interaction between funicone-like compounds and lysosomes. In fact, several molecular mechanisms could be implicated in the alteration.

Overall, the CCoV-induced activation of AhR was noticeably reduced by OMF, VER, PS and 6PP during infection. These findings highlight the importance to investigate the modulation of AhR signaling pathway to fight CoVs off infection. Herein, we identified valid *in vitro* models to select new potential therapeutics against CoVs, employing animal CoV, such as a reference strain of CCoV, not pathogen for humans.

Conclusions

In conclusion, due to the diversity of their chemical structures and biological properties, fungal SMs are able to inhibit the replication of CoVs, representing a large source for developing new potential antivirals. Thus. this study findings align with an important goal indicated in the 2030 Agenda of United Nations about good health and well-being.

References

- Alkharashi, N.A.O.; Periasamy, V.S.; Athinarayanan, J.; Alshatwi, A.A. Sulforaphane alleviates cadmium-induced toxicity in human mesenchymal stem cells through POR and TNFSF10 genes expression. Biomed. Pharmacother. 2019, 115, 108896.
- Altamura, G., Power, K., Martano, M., degli Uberti, B., Galiero, G., De Luca, G., Maiolino, P., Borzacchiello, G, 2018. *Felis catus* papillomavirus type-2 E6 binds to E6AP, promotes E6AP/p53 binding and enhances p53 proteasomal degradation. Sci. Rep. 8, 17529.
- Amici, C., Di Caro, A., Ciucci, A., Chiappa, L., Castilletti, C., Martella, V., Decaro, N., Buonavoglia, C., Capobianchi, M.R., Santoro, G.M., 2006. Indomethacin has a potent antiviral activity against SARS coronavirus. Antivir. Ther. 11, 1021–1030.
- Amoroso, M.G.; Di Concilio, D.; Langellotti, A.L.; Martello, A.; Cioffi, B.; Suffredini, E.; Cozzi, L.; Russo, V.; Mauriello, G.; Di Pasquale, S.; et al. Quantitative Real-Time PCR and digital PCR to evaluate residual quantity of HAV in experimentally depurated mussels. Food Environ. Virol. 2021, 13, 329–336.
- Aslam, M.; Ladilov, Y. Targeting the sAC-dependent cAMP pool to prevent SARS-Cov-2 infection. Cells 2020, 9, 1962.
- Baert, L.; Wobus, C.E.; Van Coillie, E.; Thackray, L.B.; Debevere, J.; Uyttendaele, M. Detection of murine norovirus 1 by using plaque assay, transfection assay, and real-time reverse transcription-PCR before and after heat exposure. Appl. Environ. Microbiol. 2008, 74, 543–546.
- Bai, M.; Zheng, C.J.; Tang, D.Q.; Zhang, F.;Wang, H.Y.; Chen, G.Y. Two new secondary metabolites from a mangrove-derived fungus Cladosporium sp. JS1-2. J. Antibiot. 2019, 72, 779–782.
- Bai, Y.; Jiang, L.P.; Liu, X.F.;Wang, D.; Yang, G.; Geng, C.Y.; Li, Q.; Zhong, L.F.; Sun, Q.; Chen, M. The role of oxidative stress in citreoviridin-induced DNA damage in human liver-derived HepG2 cells. Environ. Toxicol. 2015, 30, 530–537. [CrossRef] [PubMed]
- Banfalvi, G, 2017. Methods to detect apoptotic cell death. Apoptosis 22, 306–323.
- Bank, H.L. Assessment of islet cell viability using fluorescent dyes. Diabetologia 1987, 30, 812–816.
- Barboza, C.M., Pimenta, D.C., Vigerelli, H., de Cássia Rodrigues da Silva, A., Garcia, J.G., Zamudio, R.M., Castilho, J.G., Montanha, J.A., Roehe, P.M., de Carvalho Ruthner Batista, H.B., 2021. In vitro effects of bufotenine against RNA and DNA viruses. Braz J Microbiol. 52, 2475-2482.
- Belachew, A.M.; Feyisa, A.; Mohamed, S.B.; W/Mariam, J.F. Investigating fungi-derived bioactive molecules as inhibitor of the SARS coronavirus papain like protease: Computational based study. Front. Med. 2021, 8, 752095.
- Bills, G.F.; Gloer, J.B. Biologically active secondary metabolites from the fungi. Fungal Kingd. 2017, 4, 1087–1119.
- Binn, L.N., Marchwicki, R.H., Stephenson, E.H., 1980. Establishment of a canine cell line: Derivation, characterization, and viral spectrum. Am. J. Vet. Res. 41, 855–860.
- Blaess, M.; Kaiser, L.; Sommerfeld, O.; Csuk, R.; Deigner, H.P. Drugs, metabolites, and lung accumulating small lysosomotropic molecules: Multiple targeting impedes SARS-COV-2 infection and progress to COVID-19. Int. J. Mol. Sci. 2021, 22, 1797.
- Buonavoglia, C., Decaro, N., Martella, V., Elia, G., Campolo, M., Desario, C., Castagnaro, M., Tempesta, M., 2006. Canine Coronavirus Highly Pathogenic for Dogs. Emerg. Infect. Dis. 12, 492.
- Cerracchio, C., Serra, F., Amoroso, M.G., Fiorito, F., 2022. Canine coronavirus activates aryl hydrocarbon receptor during in vitro infection. Viruses 14, 2437.

- Chepkirui, C.; Stadler, M. The genus Diaporthe: A rich source of diverse and bioactive metabolites. Mycol. Prog. 2017, 16, 477–494.
- Chowanadisai, W., Graham, D.M., Keen, C.L., Rucker, R.B., Messerli, M.A., 2013. Neurulation and neurite extension require the zinc transporter ZIP12 (slc39a12). Proc. Natl. Acad. Sci. USA 110, 9903–9908.
- Clarke, R.; Connolly, L.; Frizzell, C.; Elliott, C.T. Cytotoxic assessment of the regulated, co-existing mycotoxins aflatoxin B1, fumonisin B1 and ochratoxin, in single, binary and tertiary mixtures. Toxicon 2014, 90, 70–81. [PubMed]
- Comite, E., El-Nakhel, C., Rouphael, Y., Ventorino, V., Pepe, O., Borzacchiello, A., Vinale, F., Rigano, D., Staropoli, A., Lorito, M., Woo, S.L., 2021. Bioformulations with Beneficial Microbial Consortia, a Bioactive Compound and Plant Biopolymers Modulate Sweet Basil Productivity, Photosynthetic Activity and Metabolites. Pathogens 10, 870.
- Crandell, R.A., Fabricant, C.G., Nelson-Rees, W.A., 1973. Development, characterization, and viral susceptibility of a feline (Felis catus) renal cell line (CRFK). Vitr. Cell. Dev. Biol.-Plant 9, 176–185.
- De Martino, L.; Marfé, G.; Longo, M.; Fiorito, F.; Montagnaro, S.; Iovane, V.; Decaro, N.; Pagnini, U. Bid cleavage, cytochrome c release and caspase activation in canine coronavirus-induced apoptosis. Vet. Microbiol. 2010, 141, 36–45.
- Decaro, N., Elia, G., Martella, V., Campolo, M., Mari, V., Desario, C., Lucente, M.S., Lorusso, E., Kanellos, T., Gibbons, R.H., Buonavoglia, C., 2010. Immunity after natural exposure to enteric canine coronavirus does not provide complete protection against infection with the new pantropic CB/05 strain. Vaccine 28, 724–729.
- Decaro, N., Mari, V., Campolo, M., Lorusso, A., Camero, M., Elia, G., Martella, V., Cordioli, P., Enjuanes, L., Buonavoglia, C., 2009. Recombinant canine coronaviruses related to transmissible gastroenteritis virus of swine are circulating in dogs. J. Virol. 83, 1532–1537. https://doi.org/10.1128/jvi.01937-08.
- Decaro, N., Martella, V., Elia, G., Campolo, M., Desario, C., Cirone, F., Tempesta, M., Buonavoglia, C., 2007. Molecular characterisation of the virulent canine coronavirus CB/05 strain. Virus Res. 125, 54–60.
- Decaro, N.; Cordonnier, N.; Demeter, Z.; Egberink, H.; Elia, G.; Grellet, A.; Le Poder, S.; Mari, V.; Martella, V.; Ntafis, V.; et al. European surveillance for pantropic canine coronavirus. J. Clin. Microbiol. 2013, 51, 83–88.
- Decaro, N.; Mari, V.; von Reitzenstein, M.; Lucente, M.S.; Cirone, F.; Elia, G.; Martella, V.; King, V.L.; Di Bello, A.; Varello, K.; et al. A pantropic canine coronavirus genetically related to the prototype isolate CB/05. Vet. Microbiol. 2012, 159, 239–244.
- Deshmukh, S.K., Agrawal, S., Gupta, M.K., Patidar, R.K., Ranjan, N., 2022. Recent Advances in the Discovery of Antiviral Metabolites from Fungi. Curr Pharm Biotechnol. 23, 495-537.
- deWilde, A.H.; Zevenhoven-Dobbe, J.C.; van der Meer, Y.; Thiel, V.; Narayanan, K.; Makino, S.; Snijder, E.J.; van Hemert, M.J. Cyclosporin A inhibits the replication of diverse coronaviruses. J. Gen. Virol. 2011, 92, 2542–2548.
- Drechsler, Y., Vasconcelos, E.J.R., Griggs, L.M., Diniz, P.P.P.V., Collisson, E., 2020. Host Gene Expression of Macrophages in Response to Feline Coronavirus Infection. Cells 9(6):1431. https://doi.org/10.3390/cells9061431.
- Fehr, A.R.; Perlman, S. Coronaviruses: An overview of their replication and pathogenesis. In Coronaviruses: Methods and Protocols; Humana: New York, NY, USA, 2015; pp. 1–23. ISBN 978-1-4939-2437-0.

- Fiorito, F., Cerracchio, C., Salvatore, M.M., Serra, F., Pucciarelli, A., Amoroso, M.G., Nicoletti, R., Andolfi, A., 2022. Antiviral Property of the Fungal Metabolite 3-O-Methylfunicone in Bovine Herpesvirus 1 Infection. Microorganisms 10, 188.
- Fiorito, F., Ciarcia, R., Granato, G.E., Marfè, G., Iovane, V., Florio, S., De Martino, L., Pagnini, U. 2011. 2,3,7,8-tetrachlorodibenzo-p-dioxin induced autophagy in a bovine kidney cell line. Toxicology 290, 258-270.
- Fiorito, F., Marfè, G., De Blasio, E., Granato, G.E., Tafani, M., De Martino, L., Montagnaro, S., Florio, S., Pagnini, U., 2008. 2,3,7,8-Tetrachlorodibenzo-p-dioxin regulates Bovine Herpesvirus type 1 induced apoptosis by modulating Bcl-2 family members. Apoptosis 13, 1243–1252.
- Fiorito, F., Nocera, F.P., Cantiello, A., Iovane, V., Lambiase, S., Piccolo, M., Ferraro, M.G., Santamaria, R., De Martino, L., 2020. Bovine herpesvirus-1 infection in mouse neuroblastoma (Neuro-2A) cells. Vet. Microbiol. 247, 108762.
- Fiorito, F., Santamaria, R., Irace, C., De Martino, L., Iovane, G., 2017. 2,3,7,8-tetrachlorodibenzo-p-dioxin and the viral infection. Environ. Res. 153, 27-34
- Fiorito, F.; Marfè, G.; Granato, G.E.; Ciarcia, R.; De Blasio, E.; Tafani, M.; Florio, S.; De Martino, L.; Muzi, G.; Pagnini, U.; et al. 2,3,7,8-Tetrachlorodibenzo-p-dioxin modifies expression and nuclear/cytosolic localization of bovine herpesvirus 1 immediateearly protein (bICP0) during infection. J. Cell. Biochem. 2010, 111, 333–342. [CrossRef]
- Fiorito, F.; Pagnini, U.; De Martino, L.; Montagnaro, S.; Ciarcia, R.; Florio, S.; Pacilio, M.; Fucito, A.; Rossi, A.; Iovane, G.; et al. 2,3,7,8-Tetrachlorodibenzo-p-dioxin increases bovine herpesvirus type-1 (BHV-1) replication in Madin-Darby Bovine Kidney (MDBK) cells in vitro. J. Cell. Biochem. 2008, 103, 221–233.
- Fiorito, F.; Santamaria, R.; Irace, C.; De Martino, L.; Iovane, G. 2,3,7,8-Tetrachlorodibenzo-p-dioxin and the viral infection. Environ. Res. 2017, 153, 27–34.
- Gao,W.; Jiang, L.; Ge, L.; Chen, M.; Geng, C.; Yang, G.; Li, Q.; Ji, F.; Yan, Q.; Zou, Y.; et al. Sterigmatocystin-induced oxidative DNA damage in human liver-derived cell line through lysosomal damage. Toxicol. Vitr. 2015, 29, 1–7.
- Ghosh, S.; Dellibovi-Ragheb, T.A.; Kerviel, A.; Pak, E.; Qiu, Q.; Fisher, M.; Takvorian, P.M.; Bleck, C.; Hsu, V.W.; Fehr, A.R.; et al. β-Coronaviruses use lysosomes for egress instead of the biosynthetic secretory pathway. Cell 2020, 183, 1520–1535.
- Giovannoni, F., Bosch, I., Polonio, C.M., Torti, M.F., Wheeler, M.A., Li, Z., Romorini, L., Rodriguez Varela, M.S., Rothhammer, V., Barroso, A. Tjon, E.C., Sanmarco, L.M., Takenaka, M.C., Modaresi, S.M.S., Gutiérrez-Vázquez, C., Zanluqui, N.G., Dos Santos, N.B., Munhoz, C.D., Wang, Z., Damonte, E.B., Sherr, D., Gehrke, L., Peron, J.P.S., Garcia, C.C., Quintana, F.J., 2020. AHR is a Zika virus host factor and a candidate target for antiviral therapy. Nat. Neurosci. 23, 939–951.
- Giovannoni, F., Li, Z., Remes-Lenicov, F., Dávola, M.E., Elizalde, M., Paletta, A., Ashkar, A.A., Mossman, K.L., Dugour, A.V., Figueroa, J.M., Barquero, A.A., Ceballos, A., Garcia, C.C., Quintana, F.J., 2021. AHR signaling is induced by infection with coronaviruses. Nat. Commun. 12, 5148.
- Gomeni, R., Xu, T., Gao, X., Bressolle-Gomeni, F., 2020. Model based approach for estimating the dosage regimen of indomethacin a potential antiviral treatment of patients infected with SARS CoV-2. J. Pharmacokinet. Pharmacodyn. 47, 189–198.
- Gorshkov, K.; Chen, C.Z.; Bostwick, R.; Rasmussen, L.; Tran, B.N.; Cheng, Y.S.; Xu, M.; Pradhan, M.; Henderson, M.; Zhu,W.; et al. The SARS-CoV-2 cytopathic effect is blocked by lysosome alkalizing small molecules. ACS Infect. Dis. 2021, 7, 1389–1408.
- Grunewald, M.E., Shaban, M.G., Mackin, S.R., Fehr, A.R., Perlman, S., 2020. Murine coronavirus infection activates the aryl hydrocarbon receptor in an indoleamine 2,3-dioxygenase-

independent manner, contributing to cytokine modulation and proviral TCDD-inducible-PARP expression. J. Virol. 94, 319–335.
- Guarnieri, T. Hypothesis: Emerging roles for aryl hydrocarbon receptor in orchestrating CoV-2-related inflammation. Cells 2022, 11, 648.
- Keller, N.P. Fungal secondary metabolism: Regulation, function and drug discovery. Nat. Rev. Microbiol. 2019, 17, 167–180.
- Keller, N.P.; Turner, G.; Bennett, J.W. Fungal secondary metabolism-from biochemistry to genomics. Nat. Rev. Microbiol. 2005, 3, 937–947.
- Kenney, S.P., Wang, Q., Vlasova, A., Jung, K., Saif, L., 2021. Naturally Occurring Animal Coronaviruses as Models for Studying Highly Pathogenic Human Coronaviral Disease. Vet. Pathol. 58, 438–452.
- Kenney, S.P.;Wang, Q.; Vlasova, A.; Jung, K.; Saif, L. Naturally occurring animal coronaviruses as models for studying highly pathogenic human coronaviral disease. Vet. Pathol. 2021, 58, 438–452.
- Kenney, S.P.;Wang, Q.; Vlasova, A.; Jung, K.; Saif, L. Naturally occurring animal coronaviruses as models for studying highly pathogenic human coronaviral disease. Vet. Pathol. 2021, 58, 438–452. [PubMed]
- Kim, D.H., Han, S.H., Go, H.J., Kim, D.Y., Kim, J.H., Lee, J.B., Park, S.Y., Song, C.S., Lee, S.W., Choi, I.S., 2022. Antiviral activity of canine interferon lambda 3 expressed using a recombinant adenovirus against canine coronavirus, canine parvovirus, and canine distemper virus. Vet Res Commun. 46, 1363-1368.
- Kojima, A., Takada, H., Okaniwa, A., 1986. Multiplication of canine coronavirus in CRFK cells. Nihon Juigaku Zasshi. 48, 1063-1070.
- Komai, S.I.; Hosoe, T.; Itabashi, T. New vermistatin derivatives isolated from Penicillium simplicissimum. Heterocycles 2005, 65, 2771–2776.
- Kotb, A.M.E., Abd El-Aziz, N.K., Elariny, E.Y.T., Yahya, R., Alkhalifah, D.H.M., Ahmed, R.M., 2022. Synergistic Antibacterial Potential of 6-Pentyl-α-pyrone Lactone and Zinc Oxide Nanoparticles against Multidrug-Resistant Enterobacterales Isolated from Urinary Tract Infections in Humans. Antibiotics (Basel). 11, 440.
- Kroemer, G., Levine, B., 2008. Autophagic cell death: The story of a misnomer. Nat. Rev. Mol. Cell Biol. 9, 1004–1010.
- Lawrence, B.P., Vorderstrasse, B.A., 2013. New insights into the aryl hydrocarbon receptor as a modulator of host responses to infection. Semin. Immunopathol. 35, 615–626
- Lednicky, J.A.; Tagliamonte, M.S.; White, S.K.; Blohm, G.M.; Alam, M.M.; Iovine, N.M.; Salemi, M.; Mavian, C.; Morris, J.G. Isolation of a novel recombinant canine coronavirus from a visitor to Haiti: Further evidence of transmission of coronaviruses of zoonotic origin to humans. Clin. Infect. Dis. 2022, 75, e1184–e1187.
- Lei, L.R.; Gong, L.Q.; Jin, M.Y.; Wang, R.; Liu, R.; Gao, J.; Liu, M.D.; Huang, L.; Wang, G.Z.; Wang, D.; et al. Research advances in the structures and biological activities of secondary metabolites from Talaromyces. Front. Microbiol. 2022, 13, 984801. [CrossRef] [PubMed]
- Leite, M., Quinta-Costa, M., Leite, P.S., Guimarães, J.E., 1999. Critical evaluation of techniques to detect and measure cell death-Study in a model of UV radiation of the leukaemic cell line HL60. Anal. Cell. Pathol. 19, 139–151.
- Li, H.S.; Kuok, D.I.T.; Cheung, M.C.; Ng, M.M.T.; Ng, K.C.; Hui, K.P.Y.; Peiris, J.S.M.; Chan, M.C.W.; Nicholls, J.M. Effect of interferon alpha and cyclosporine treatment separately and in combination on Middle East Respiratory Syndrome Coronavirus (MERS-CoV) replication in a human in-vitro and ex-vivo culture model. Antivir. Res. 2018, 155, 89–96.

- Liang, H.; Luo, D.; Liao, H.; Li, S. Coronavirus usurps the autophagy-lysosome pathway and induces membranes rearrangement for infection and pathogenesis. Front. Microbiol. 2022, 13, 846543.
- Linnakoski, R., Reshamwala, D., Veteli, P., Cortina-Escribano, M., Vanhanen, H., Marjomäki, V., 2018. Antiviral agents from fungi: Diversity, mechanisms and potential applications. Front. Microbiol. 9, 2325.
- Marfè, G.; Tafani, M.; Fiorito, F.; Pagnini, U.; Iovane, G.; de Martino, L. Involvement of FOXO transcription factors, TRAILFasL/Fas, and Sirtuin proteins family in canine coronavirus type II-induced apoptosis. PLoS ONE 2011, 6, e27313.
- Mosmann T. 1983. Rapid colorimetric assay for cellular growth and survival: Application to proliferation and cytotoxicity assays. J Immunol Meth 65:55–63.
- Nakajima, S., Watashi, K., Kamisuki, S., Tsukuda, S., Takemoto, K., Matsuda, M., Suzuki, R., Aizaki, H., Sugawara, F., Wakita, T., 2013. Specific inhibition of hepatitis C virus entry into host hepatocytes by fungi-derived sulochrin and its derivatives. Biochem. Biophys. Res. Commun. 440, 515–520.
- Nicoletti, R. Antitumor and Immunomodulatory Compounds from Fungi. Encyclopedia of Mycology 2021, 2, 683–709.
- Nicoletti, R.; Andolfi, A.; Salvatore, M.M. Endophytic fungi of the genus Talaromyces and plant health. In Microbial Endophytes and Plant Growth; Accademic Press: London, UK, 2023a; pp. 183–213. ISBN 978-0-323-90620-3.
- Nicoletti, R.; Bellavita, R.; Falanga, A. The outstanding chemodiversity of marine-derived Talaromyces. Biomol. 2023b, 13, 1021.
- Nicoletti, R.; Manzo, E.; Ciavatta, M.L. Occurrence and bioactivities of funicone-related compounds. Int. J. Mol. Sci. 2009, 10, 1430–1444.
- Nicoletti, R.; Scognamiglio, M.; Fiorentino, A. Structural and bioactive properties of 3-O-methylfunicone. Mini Rev. Med. Chem. 2014, 14, 1043–1047.
- Papaianni, M., Ricciardelli, A., Fulgione, A., d'Errico, G., Zoina, A., Lorito, M., Woo, S.L., Vinale, F., Capparelli, R., 2020. Antibiofilm Activity of a *Trichoderma* Metabolite against *Xanthomonas campestris* pv. campestris, Alone and in Association with a Phage. Microorganisms. 8, 620.
- Pereira, G.J.d.S.; Leão, A.H.F.F.; Erustes, A.G.; Morais, I.B.d.M.; Vrechi, T.A.d.M.; Zamarioli, L.D.S.; Pereira, C.A.S.; Marchioro, L.d.O.; Sperandio, L.P.; Lins, Í.V.F.; et al. Pharmacological modulators of autophagy as a potential strategy for the treatment of COVID-19. Int. J. Mol. Sci. 2021, 22, 4067.
- Pratelli, A. Genetic evolution of canine coronavirus and recent advances in prophylaxis. Vet. Res. 2006, 37, 191–200.
- Pratelli, A., Buonavoglia, A., Lanave, G., Tempesta, M., Camero, M., Martella, V., Decaro, N., 2021. One world, one health, one virology of the mysterious labyrinth of coronaviruses: The canine coronavirus affair. Lancet Microbe 2, e646–e647.
- Pratelli, A., Tempesta, M., Elia, G., Martella, V., Decaro, N., Buonavoglia, C., 2022. The knotty biology of canine coronavirus: A worrying model of coronaviruses' danger. Vet. Sci. 144, 190–195.
- Pratelli, A.; Tempesta, M.; Elia, G.; Martella, V.; Decaro, N.; Buonavoglia, C. The knotty biology of canine coronavirus: A worrying model of coronaviruses' danger. Res. Vet. Sci. 2022, 144, 190–195.
- Pratelli, A.; Tempesta, M.; Elia, G.; Martella, V.; Decaro, N.; Buonavoglia, C.; Buonavoglia, A.; Lanave, G.; Tempesta, M.; Camero, M.; et al. One world, one health, one virology of the

mysterious labyrinth of coronaviruses: The canine coronavirus affair. Res. Vet. Sci. 2021, 2, e646–e647.
- Pratelli, A.; Tempesta, M.; Elia, G.; Martella, V.; Decaro, N.; Buonavoglia, C.; Buonavoglia, A.; Lanave, G.; Tempesta, M.; Camero, M.; et al. One world, one health, one virology of the mysterious labyrinth of coronaviruses: The canine coronavirus affair. Res. Vet. Sci. 2021, 2, e646–e647.
- Rao, P.; Patel, R.; Shukla, A.; Parmar, P.; Rawal, R.M.; Saraf, M.; Goswami, D. Identifying structural–functional analogue of GRL0617, the only well-established inhibitor for papain-like protease (PLpro) of SARS-CoV2 from the pool of fungal metabolites using docking and molecular dynamics simulation. Mol. Divers. 2022, 26, 309–329.
- Rao, P.; Shukla, A.; Parmar, P.; Rawal, R.M.; Patel, B.; Saraf, M.; Goswami, D. Reckoning a fungal metabolite, pyranonigrin A as a potential Main protease (Mpro) inhibitor of novel SARS-CoV-2 virus identified using docking and molecular dynamics simulation. Biophys. Chem. 2020, 264, 106425.
- Rothhammer, V. and Quintana, F.J., 2019. The aryl hydrocarbon receptor: An environmental sensor integrating immune responses in health and disease. Nat. Rev. Immunol. 19, 184–197.
- Roy, B.G. Potential of small-molecule fungal metabolites in antiviral chemotherapy. Antivir. Chem. Chemother. 2017, 25, 20–52.
- Ruggieri, A.; Di Trani, L.; Gatto, I.; Franco, M.; Vignolo, E.; Bedini, B.; Elia, G.; Buonavoglia, C. Canine coronavirus induces apoptosis in cultured cells. Vet. Microbiol. 2007, 121, 64–72.
- Saied, E.M.; El-Maradny, Y.A.; Osman, A.A.; Darwish, A.M.G.; Nahas, H.H.A.; Niedbała, G.; Piekutowska, M.; Abdel-Rahman, M.A.; Balbool, B.A.; Abdel-Azeem, A.M. A comprehensive review about the molecular structure of severe acute respiratory syndrome coronavirus 2 (SARS-CoV-2): Insights into natural products against COVID-19. Pharmaceutics 2021, 13, 1759.
- Salvatore, M.M., Dellagreca, M., Andolfi, A., 2022. New insights into chemical and biological properties of funicone-like compounds. Toxins. 14, 466.
- Salvatore, M.M.; DellaGreca, M.; Nicoletti, R.; Salvatore, F.; Vinale, F.; Naviglio, D.; Andolfi, A. Talarodiolide, a new 12-membered macrodiolide, and GC/MS investigation of culture filtrate and mycelial extracts of Talaromyces pinophilus. Molecules 2018, 23, 950.
- Sanders, J.M.; Monogue, M.L.; Jodlowski, T.Z.; Cutrell, J.B. Pharmacologic treatments for coronavirus disease 2019 (COVID-19): A review. JAMA—J. Am. Med. Assoc. 2020, 323, 1824–1836.
- Santamaria, R., Fiorito, F., Irace, C., De Martino, L., Maffettone, C., Granato, G.E., Di Pascale, A., Iovane, V., Pagnini, U., Colonna, A. 2011. 2,3,7,8-Tetrachlorodibenzo-p-dioxin impairs iron homeostasis by modulating iron-related proteins expression and increasing the labile iron pool in mammalian cells. Biochim. Biophys. Acta-Mol. Cell Res. 1813, 704–712.
- Shankar, A.; Sharma, K.K. Fungal secondary metabolites in food and pharmaceuticals in the era of multi-omics. Appl. Microbiol. Biotechnol. 2022, 106, 3465–3488.
- Shi, J., Du, T., Wang, J., Tang, C., Lei, M., Yu, W., Yang, Y., Ma, Y., Huang, P., Chen, H., Wang, X., Sun, J., Wang, H., Zhang, Y., Luo, F., Huang, Q., Li, B., Lu, S., Hu, Y., Peng, X., 2023. Aryl hydrocarbon receptor is a proviral host factor and a candidate pan-SARS-CoV-2 therapeutic target. Sci Adv. 9(22):eadf0211.
- Silva, C.S., Mullis, L.B., Pereira, O., Jr., Saif, L.J., Vlasova, A., Zhang, X., Owens, R.J., Paulson, D., Yaylor, D., Haynes, L.M., Azevedo, M.P., 2014. Human respiratory coronaviruses detected in patients with influenza-like illness in Arkansas, USA. Virol. Mycol. Infect. Dis. 2014 (Suppl. S2), 004

- Singh, S.; Malik, B.K.; Sharma, D.K. Targeting HIV-1 through molecular modeling and docking studies of CXCR4: Leads for therapeutic development. Chem. Biol. Drug Des. 2007, 69, 191–203.
- Singh, S.B.; Jayasuriya, H.; Dewey, R.; Polishook, J.D.; Dombrowski, A.W.; Zink, D.L.; Guan, Z.; Collado, J.; Platas, G.; Pelaez,F.; et al. Isolation, structure, and HIV-1-integrase inhibitory activity of structurally diverse fungal metabolites. J. Ind. Microbiol. Biotechnol. 2003, 30, 721–731.
- Staropoli, A., Iacomino, G., De Cicco, P., Woo, S.L., DI Costanzo, G., Vinale, F., 2023. Induced secondary metabolites of the beneficial fungus *Trichoderma harzianum* M10 through OSMAC approach. Chem. Biol. Technol. Agric. 10, 28.
- Sun, M.H.; Li, X.H.; Xu, Y.; Xu, Y.; Pan, Z.N.; Sun, S.C. Citrinin exposure disrupts organelle distribution and functions in mouse oocytes. Environ. Res. 2020, 185, 109476.
- Takahashi, J.A.; Barbosa, B.V.R.; Lima, M.T.N.S.; Cardoso, P.G.; Contigli, C.; Pimenta, L.P.S. Antiviral fungal metabolites and some insights into their contribution to the current COVID-19 pandemic. Bioorganic Med. Chem. 2021, 46, 116366.
- Tang, B.S.F., Chan, K.H., Cheng, V.C.C., Woo, P.C.Y., Lau, S.K.P., Lam, C.C.K., Chan, T.L., Wu, A.K.L., Hung, I.F.N., Leung, S.Y., Yuen, K.Y., 2005. Comparative Host Gene Transcription by Microarray Analysis Early after Infection of the Huh7 Cell Line by Severe Acute Respiratory Syndrome Coronavirus and Human coronavirus 229E. J. Virol. 79, 6180–6193.
- Theamboonlers, A., Samransamruajkit, R., Thongme, C., Amonsin, A., Chongsrisawat, V., Poovorawan, Y., 2007. Human Coronavirus Infection among Children with Acute Lower Respiratory Tract Infection in Thailand. Intervirology 50, 71–77.
- Thiemann, S.; Smit, N.; Strowig, T. Antibiotic resistance: Problems and new opportunities. In How to Overcome the Antibiotic Crisis Facts, Challenges, Technologies and Future Perspectives; Springer: Berlin/Heidelberg, Germany, 2016; Volume 398, pp. 1–236. ISBN 978-3-642-54826-0 978-3-642-54827-7.
- Tian, Z., Pan, Q., Zheng, M., Deng, Y., Guo, P., Cong, F., Hu, X., 2021. Molecular characterization of the FCoV-like canine coronavirus HLJ-071 in China. BMC Vet Res. 17, 364.
- Timurkan, M.O.; Aydin, H.; Dincer, E.; Coskun, N. Molecular characterization of canine coronaviruses: An enteric and pantropic approach. Arch. Virol. 2021, 166, 35–42.
- Tofani, S.; Ianiro, G.; De Sabato, L.; Monini, M.; Angeloni, G.; Ponterio, E.; D'Agostino, C.; Di Bari, M.A.; Valeri, M.; Di Bartolo, I. Detection and whole genome sequencing of murine norovirus in animal facility in Italy. Anim. Biotechnol. 2021, 1–8.
- Toghueo, R.M.K. Bioprospecting endophytic fungi from Fusarium genus as sources of bioactive metabolites. Mycology 2020, 11, 1–21. [CrossRef]
- Torti, M.F., Giovannoni, F., Quintana, F.J., Garcia, C.C., 2021. The Aryl Hydrocarbon Receptor as a Modulator of Anti-viral Immunity. Front. Immunol. 12, 624293.
- Torun, S.; Yilmaz, Z.; Pratelli, A. A serological evidence of minute virus of canines (MVC; canine parvovirus type-1) in dogs in Turkey. Turk. J. Vet. Anim. Sci. 2005, 29, 923–925.
- Vandenberg, L.N.; Colborn, T.; Hayes, T.B.; Heindel, J.J.; Jacobs, D.R.; Lee, D.H.; Shioda, T.; Soto, A.M.; vom Saal, F.S.; Welshons, W.V.; et al. Hormones and endocrine-disrupting chemicals: Low-dose effects and nonmonotonic dose responses. Endocr. Rev. 2012, 33, 378–455.
- Veiga-Parga, T.; Suryawanshi, A.; Rouse, B.T. Controlling viral immuno-inflammatory lesions by modulating aryl hydrocarbon receptor signaling. PLoS Pathog. 2011, 7, e1002427.
- Vinale, F., Sivasithamparam, K., Ghisalberti, E. L., Marra, R., Barbetti, M. J., Li, H., Woo, S.L., Lorito, M., 2008. A novel role for *Trichoderma* secondary metabolites in the interactions with plants. Physiol. Mol. Plant Pathol. 72, 80-86.

- Vlasova, A.N., Diaz, A., Damtie, D., Xiu, L., Toh, T.H., Lee, J.S., Saif, L.J., Gray, G.C., 2022b. Novel canine coronavirus isolated from a hospitalized pneumonia patient, East Malaysia. Clin. Infect. Dis. 74, 446–454.
- Vlasova, A.N., Toh, T.H., Lee, J.S.Y., Poovorawan, Y., Davis, P., Azevedo, M.S.P., Lednicky, J.A., Saif, L.J., Gray, G.C., 2022a. Animal alphacoronaviruses found in human patients with acute respiratory illness in different countries. *Emerg.* Microbes Infect. 11, 699–702.
- Wang, Y.; Wang, L.; Zhuang, Y.; Kong, F.; Zhang, C.; Zhu, W. Phenolic polyketides from the co-cultivation of marine-derived Penicillium sp. WC-29-5 and Streptomyces fradiae 007. Mar. Drugs 2014, 12, 2079–2088.
- Wang, Y.; Xing, C.H.; Chen, S.; Sun, S.C. Zearalenone exposure impairs organelle function during porcine oocyte meiotic maturation. Theriogenology 2022, 177, 22–28.
- Watashi, K.; Hijikata, M.; Hosaka, M.; Yamaji, M.; Shimotohno, K. Cyclosporin A suppresses replication of hepatitis C virus genome in cultured hepatocytes. Hepatology 2003, 38, 1282–1288.
- Woods, R.D., Wesley, R.D., 1988. Cultivation techniques for animal coronaviruses: Emphasis on feline infectious peritonitis virus, canine coronavirus, transmissible gastroenteritis virus, and porcine hemagglutinating encephalomyelitis virus. J Tissue Cult Methods. 11(2):95-100.
- Wright, G.D. 2019. Unlocking the potential of natural products in drug discovery. Microb Biotechnol. 12, 55-57.
- Xia, X.K.; Huang, H.R.; She, Z.G.; Cai, J.W.; Lan, L.; Zhang, J.Y.; Fu, L.W.; Vrijmoed, L.L.P.; Lin, Y.C. Structural and biological properties of vermistatin and two new vermistatin derivatives isolated from the marine-mangrove endophytic Guignardia sp. No. 4382. Helv. Chim. Acta 2007, 90, 1925–1931.
- Xu, T., Gao, X., Wu, Z., Selinger, D.W., Zhou, Z., 2020. Indomethacin has a potent antiviral activity against SARS CoV-2 in vitro and canine coronavirus in vivo. Front. Med. J.
- Yamada, T., Horimoto, H., Kameyama, T., Hayakawa, S., Yamato, H., Dazai, M., Takada, A., Kida, H., Bott, D., Zhou, A.C., Hutin, D., Watts, T.H., Asaka, M., Matthews, J., Takaoka, A., 2016. Constitutive aryl hydrocarbon receptor signaling constrains type I interferon-mediated antiviral innate defense. Nat. Immunol. 17, 687–694.
- Yang, T., Feng, Y.L., Chen, L., Vaziri, N.D., Zhao, Y.Y., 2019. Dietary natural flavonoids treating cancer by targeting aryl hydrocarbon receptor. Crit. Rev. Toxicol. 49, 445–460.
- Zakeri, Z.; Lockshin, R.A. Cell death: History and future. Adv. Exp. Med. Biol. 2008, 615, 1–11.
- Zhai, M.M.; Li, J.; Jiang, C.X.; Shi, Y.P.; Di, D.L.; Crews, P.; Wu, Q.X. The bioactive secondary metabolites from Talaromyces species. Nat. Prod. Bioprospect. 2016, 6, 1–24.
- Zhao, L., Yao, L., Chen, R., He, J., Lin, T., Qiu, S., Chen, G., Chen, H., Qiu, S.X., 2023. Pinostrobin from plants and propolis against human coronavirus HCoV-OC43 by modulating host AHR/CYP1A1 pathway and lipid metabolism. Antiviral Res. 212:105570.
- Zhao, Z.; Qin, P.; Huang, Y.W. Lysosomal ion channels involved in cellular entry and uncoating of enveloped viruses: Implications for therapeutic strategies against SARS-CoV-2. Cell Calcium 2021, 94, 102360.

CHAPTER 4 - *In vitro* evaluation of natural compounds against BoHV-1 infection

CHAPTER 4 - *In vitro* evaluation of natural compounds against BoHV-1 infection

Brief summary

Hence, the potential antiviral activity of some natural compounds, like OMF, and Taurisolo®, a grape pomace polyphenolic extract obtained from the Aglianico cultivar grape, was assessed against BoHV-1 infection. Both these natural substances have shown an excellent defence reaction during BoHV-1 infection involving AhR.

The following papers were embedded here:

- Fiorito F, **Cerracchio C**, Salvatore MM, Serra F, Pucciarelli A, Amoroso MG, Nicoletti R, Andolfi A. Antiviral Property of the Fungal Metabolite 3-O-Methylfunicone in Bovine Herpesvirus 1 Infection Microorganisms 2022, 10, 188; doi.org/10.3390/microorganisms10010188. -Permission: https://www.mdpi.com/openaccess
- **Cerracchio C**, Amoroso MG, Piccolo M, Ferraro MG, Nocera FP, De Martino L, Serra F, Irace C, Tenore GC, Novellino E, Santamaria R, Fiorito F. Antiviral activity of Taurisolo® during bovine alphaherpesvirus 1 infection. Virus Res. 2023 Sep 7;336:199217. https://doi.org/10.1016/j.virusres.2023.199217 - Permission: Copyright Elsevier.

Antiviral Property of the Fungal Metabolite 3-O-Methylfunicone in Bovine Herpesvirus 1 Infection

1. Introduction

Bovine herpesvirus 1 (BoHV-1), a pathogen belonging to the alphaherpesvirus subfamily, is responsible for considerable economic losses to the cattle industry as well as trade restrictions (*Muylkens et al., 2007; Jones et al., 2019*). Because of its immunosuppressive features, it may cause infectious bovine rhinotracheitis, vulvovaginitis, abortions, or polymicrobial infections. Indeed, BoHV-1 is an important cofactor for the bovine respiratory disease complex, the most important inflammatory disease in cattle, causing pneumonia and sometimes death (*Muylkens et al., 2007; Jones et al., 2019*). BoHV-1 establishes latency in sensory neurons of the infected host, and reactivation from latency is induced by corticosteroids, developing virus shedding, and spread to susceptible hosts (*Muylkens et al., 2007; Jones et al., 2019*). Similar to other members of the alphaherpesvirus subfamily, gene expression of BoHV-1 occurs in three temporally different phases known as immediate-early, early, and late; tissuespecific elements are involved in pathogenesis and/or in latency by affecting viral gene expression (*Muylkens et al., 2007; Jones et al., 2019*). bICP0, the bovine homologue of the herpes simplex virus type 1 (HSV-1) ICP0, controls these three phases through a strong activation or repression of certain viral promoters. bICP0 is the major regulatory protein that stimulates productive infection; it is expressed during infection in permissive cells and inhibits interferon-dependent transcription (*Jones et al., 2019; Fraefel et al., 1994; Inman et al., 2001; Fiorito et al., 2011*). To date, non-toxic active drugs against BoHV-1 are not available, but plant and fungal extracts are of great interest for the development of new antiviral drugs (*Moghadamtousi et al., 2015; Linnakoski et al., 2018; Manganyi et al., 2020; Salvatore et al., 2019; Nicoletti et al., 2018 a,b*). More specifically, some of these products, such as peptides derived from a strain of Scytalidium sp. (*Rowley et al., 2003*), macrolides derived from an unidentified fungus belonging to the Pleosporales (*Shushni et al., 2009*), and lactones derived from a strain of Aspergillus terreus (*Nong et al., 2014*), have shown inhibitory activity against herpesviruses. In relation to their great adaptability to the most varied habitats and lifestyles, fungi in the genus Talaromyces (Eurotiales: Trichocomaceae) are characterized by high biosynthetic versatility and have been reported as a source of many bioactive products of pharmaceutical interest, including antiviral drugs (*Nicoletti et al., 2009, 2018; Zhai et al., 2016; Lan et al., 2020*). The

emphasis in current literature is, in particular, on Talaromyces pinophilus, previously known as Penicillium pinophilum. In fact, its antagonistic behavior has been reported in relation to the production of 3-O-methylfunicone (OMF), a benzo-g-pyrone compound first characterized for its in vitro inhibitory effects on some plant pathogenic fungi (Figure 1) (*De Stefano et al., 1999; Nicoletti et al., 2008*). Subsequently, several studies reported the antiproliferative and proapoptotic proprieties of this compound on tumor cells (*Nicoletti et al., 2014; Buommino et al., 2011; Baroni et al., 2009*), which shed light on its potential use as a cancer therapeutic. In a screening conducted on some analogues of the funicone series, it was observed that OMF reduced infectivity of hepatitis C virus (HCV) (*Nakajima et al., 2013*). Despite the relevance of its biological properties, pathways underlying the biosynthesis of OMF have not been explored in depth. However, the recent genome sequencing of T. pinophilus has paved the way for the elucidation of the biochemical processes leading to the production of this secondary metabolite (*Li et al., 2017*).

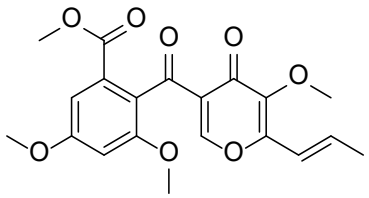

Figure 1. Chemical structure of 3-O-methylfunicone (OMF)

The aryl hydrocarbon receptor (AhR) is a ligand-activated transcription factor. It acts together with many endogenous and exogenous substances, involving bilirubin, biliverdin, tryptophan metabolites, environmental pollutants (dioxin), and microbial metabolites (*Yang et al., 2019*). After the activation, AhR translocases into the nucleus, where it controls the expression of target genes, such as the AhR repressor, detoxifying monooxygenases (CYP1A1 and CYP1B1), and cytokines. AhR is also involved in cellular mechanisms, such as proliferation and apoptosis, immune modulation, and other processes, which further affect cell growth, survival, migration, and invasion. In addition, recent evidence indicates that some agonists of AhR might improve the host response to a herpesvirus infection (*Torti et al., 2021*). Until now, no circumstantial study has been performed to assess the antiviral properties of OMF, and BoHV-1 represents a good model for anti-herpesvirus molecule screening, as previously described (*Fiorito et al., 2017; Chang et al., 2020; Yesilbag et al., 2021*). Based on these premises, this study aimed to evaluate the antiviral activity of OMF on BoHV-1.

2. Materials and Methods

2.1. *Production of OMF*

The OMF used in this study was extracted from an isolated LT6 of *T. pinophilus*, as previously reported (*Salvatore et al., 2018*).

2.2. *Cell Cultures and Virus Infection*

Madin Darby Bovine Kidney (MDBK), a bovine cell line (American Type Culture Collection, CCL22), was cultured in Dulbecco's modified Eagle's minimal essential medium (DMEM) and incubated at 37 C and 5% CO2, as previously described (*Fiorito et al., 2011*). BoHV-1 (Cooper strain) was utilized throughout the study. MDBK cells were used for virus stock growth and virus titration (*Fiorito et al., 2008, 2020, 2021*). OMF was dissolved in dimethyl sulfoxide (DMSO) and added to the medium at a final concentration of 1, 5, 10, 25, and 50 M. Monolayers of MDBK cells were either infected or not infected with BoHV-1, at a multiplicity of infection (MOI) of 0.1, 1, or 5, in the presence or absence of OMF, to obtain four groups: untreated uninfected cells; untreated infected cells; OMF-treated uninfected cells; OMF-treated infected cells. After 1 h of adsorption at 37 C, cells were incubated and processed at 1, 3, 6, 12, and 24 h post-infection (p.i.). The virus was in a culture medium through the course of the experiment.

2.3. *Cell Viability*

To assess cell viability, the trypan blue (TB) (Sigma-Aldrich, Milan, Italy) exclusion test was used, as previously described (*Fiorito et al., 2008*). Briefly, monolayers of MDBK cells were either infected or not infected with BoHV-1, at an MOI of 5, in the presence or absence of OMF at different concentrations (1, 5, 10, 25, and 50 μM) to obtain four groups: untreated uninfected cells; untreated infected cells; OMF-treated uninfected cells; OMF-treated infected cells. After 24 h of treatment, cells were collected by trypsinization, mixed with TB, and scored through the TC20 automated cell counter (Bio-Rad Laboratories S.r.l., Segrate, Milan, Italy). Cell viability was calculated as the percentage of living cells over the total cell number. The results are reported as the mean S.D. of three independent experiments performed twice. Furthermore, cell viability was evaluated by the TB in cells attached to wells, as described (*Fiorito et al., 2008, 2020, 2021*, *Chowanadisai et al., 2013*).

2.4. *Cell Proliferation*

To evaluate cell proliferation, a 3-(4,5-dimethyl-2-thiazolyl)-2,5-diphenyl-2H-tetrazolium bromide (MTT) assay was used, as previously described (*Fiorito et al., 2008, 2011; Santamaria et al., 2011).* Briefly, MDBK cultured in 96-well plates were infected with BoHV-1, at an MOI of 1, exposed or not exposed to OMF (5 μM), and incubated. At 24 h p.i., an MTT assay was carried out. The results were the mean S.D. of four independent experiments performed twice.

2.5. *Examination of Cell Morphology*

To examine cell morphology, light microscopy following Giemsa staining was used (*Fiorito et al., 2020*). Briefly, the monolayers of MDBK cells were either infected or not infected with BoHV-1, at an MOI of 1, in the presence or absence of OMF (5 μM), and incubated at 37 C. After 24 h p.i., Giemsa staining was performed, and a light microscopy examination was carried out under the ZOE Cell Imager (Bio-Rad Laboratories). The cell death features were identified by using the criteria previously described (*Leite et al., 1999; Kroemer et al., 2008; Zakeri et al., 2008*).

2.6. *Immunofluorescence Staining*

MDBK cells were either infected or not infected with BoHV-1, at an MOI of 0.1, and treated with OMF (5 μM). After 24 h p.i., immunofluorescence staining was performed as previously reported (*Altamura et al., 2018*), by using the following antibodies dissolved in 5% bovine serum albumin-TBST: anti-AhR (Sigma-Aldrich) (1:250); anti-bICP0 polyclonal rabbit (a.a. 663–676) serum (1:800), kindly provided by Prof. M. Schwyzer and Prof. Cornel Fraefel (University of Zurich, Zurich, Switzerland); and Texas Red goat anti-rabbit (Thermo Fisher Scientific,Waltham, MA, USA) (1:100). Nuclear counter-staining was evaluated by DAPI (1:1000). Microscopy and photography were assessed by the ZOE Fluorescent Cell Imager (Bio-Rad Laboratories, Hercules, CA, USA). Quantification of fluorescence signals from microscopy-generated images were performed using ImageJ (National Institutes of Health, Bethesda, MD, USA) software.

2.7. *Virus Production*

MDBK cells were infected with BoHV-1, at an MOI of 1, in the presence or absence of OMF, incubated at 37 C, and processed at 0, 1, 3, 6, 12, and 24 h p.i. by real-time PCR for BoHV-1 quantification. Furthermore, the virus titer was evaluated in MDBK cells by

the $TCID_{50}$ method, as previously described (*Fiorito et al., 2020, 2021*). In addition, viral cytopathic effects (CPE) were evaluated. To this purpose, cells were examined under a light microscope at indicated times of infection, as previously described (*Fiorito et al., 2021*).

2.8. *Viral Nucleic Acids Extraction Procedures*

Nucleic acids extraction was carried out from 200 µL of cell supernatant using the King Fisher Flex System (Thermo Fisher Scientific, Waltham, MA, USA) with the Mag Max Viral Pathogen kit (Thermo Fisher Scientific,Waltham, MA, USA), according to the instructions of the manufacturer. Nucleic acids were dissolved in 80 L of elution buffer. DMEM was used as negative process control.

2.9. *Real-Time PCR for Quantification of BoHV-1*

BoHV-1 was quantified in all the samples by quantitative real-time PCR. Detection was carried out on a Quant Studio 5 Real-Time PCR thermal cycler (Thermo Fisher Scientific, Waltham, MA, USA) in a total volume of 25 µL containing 5 µL of nucleic acids extract, 12.5 L of TaqMan Universal PCR Master Mix 2X (Thermo Fisher Scientific, Waltham, MA, USA), 1 µL (4.5 M) of primer forward gBF (50-TGTGGACCTAAACCTCACGGT-30), 1 µL (4.5 µM) of primer reverse gBR (50-GTAGTCGAGCAGACCCGTGTC-30), and 1 µL (3 µM) of probe gB-P (FAM-50-AGGACCGCGAGTTCTTGCCGC-30-TAMRA). The thermal profile was initial denaturation for 15 min at 95 C and 45 cycles of amplification for 15 s at 95 °C and for 45 s at 60 °C (OIE Manual of Terrestrial Animals Cap. 3.4.11. par B.1.3.1 2017). Quantification was carried out by a standard curve, analyzing serial dilutions of the quantified extracted virus (from 1×10^7 to 1×10^1 $TCID_{50}$/mL) and plotting the $TCID_{50}$/mL versus the threshold cycle (Ct).

2.10. *Statistical Analysis*

Data are presented as mean S.D. One-way ANOVA with Tukey's post-test was performed by GraphPad InStat Version 3.00 for Windows 95 (GraphPad Software, San Diego, CA, USA). $p < 0.05$ was considered statistically significant.

3. Results

3.1. *OMF Decreases Cell Death during BoHV-1 Infection*

To investigate the biological influence of OMF during BoHV-1 infection in MDBK cells, we first evaluated cell viability by TB exclusion test, and then we tested cell proliferation by MTT. As described above, identifying IC50 of OMF and developing a dose–response curve was carried out by treating MDBK cells with different doses of OMF. Thus, monolayers of MDBK cells were either infected or not infected with BoHV-1, at an MOI of 5, in the presence or absence of OMF at different concentrations (1, 5, 10, 25, and 50 μM) to obtain four groups: untreated uninfected cells; untreated infected cells; OMF-treated uninfected cells; OMF-treated infected cells. Dose-dependent inhibition of cell growth was detected in MDBK cells with an IC50 of about 10 μM OMF at 24 h (Figure 2a). OMF at 5 μM produced no significant differences in cell viability ($p > 0.05$) in MDBK cells (Figure 2a). Similar results were found on cell viability, analyzed using TB staining while cells were attached to wells and scored under a light microscope (Figure 2b).

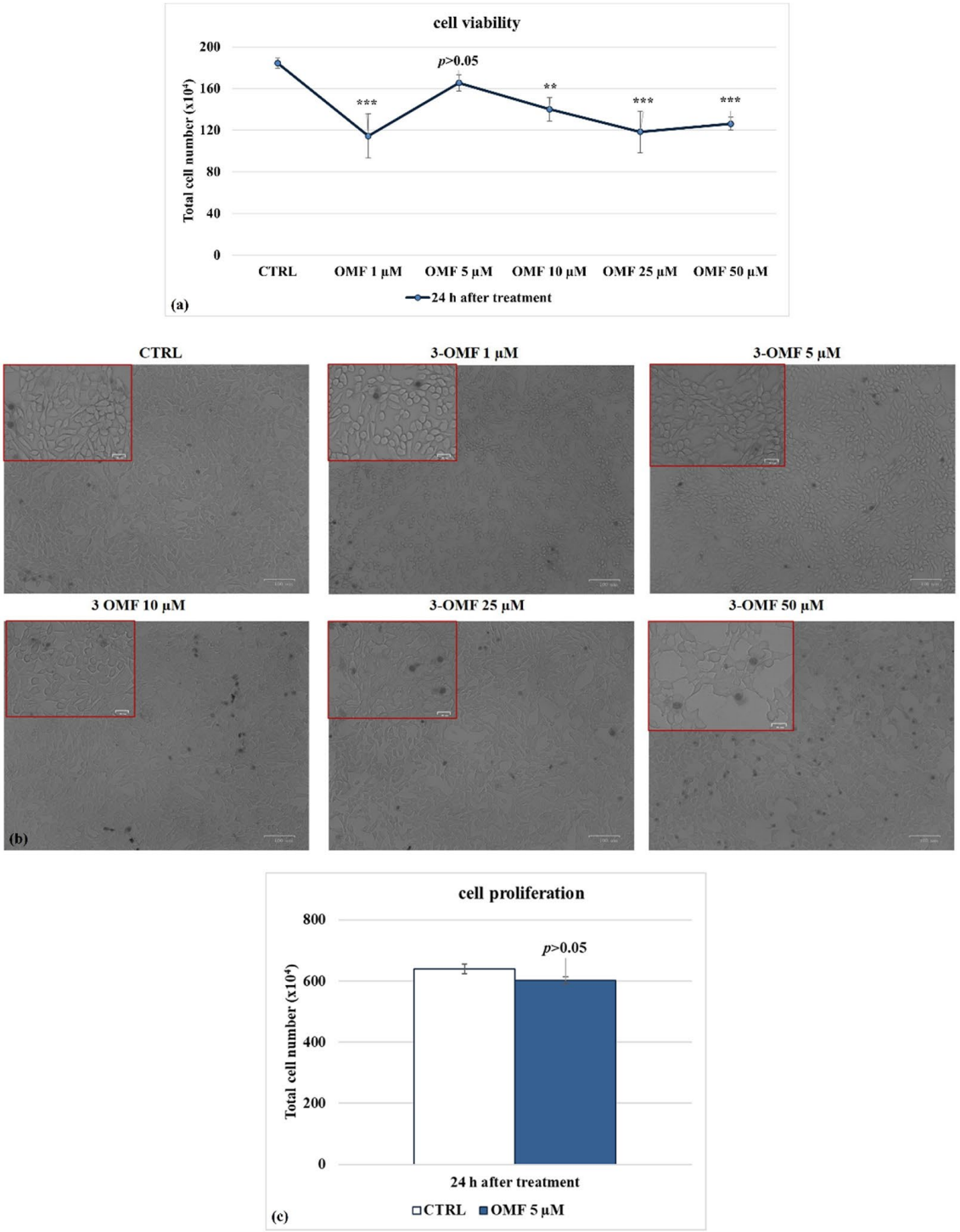

Figure 2. Identifying IC50 of OMF at different doses and developing dose–response curve in MDBK cells. (a) Dose–response curve of MDBK cells treated with OMF at different concentrations (1, 5, 10, 25, and 50 µM). At 24 h after treatment, cells were stained with TB and scored by automated cell counter, or (b) cell viability was determined by TB staining while cells were attached to wells and counted under a light microscope. (c) Dose–response curve of MDBK cells treated with OMF (5 µM) for 24 h and assessed by MTT assay. Significant differences between control and OMF-treated cells are indicated by probability p. ** $p < 0.01$ and *** $p < 0.001$. Scale bar 100 µm.

To explore the effect of OMF on MDBK cells' proliferation, the mitochondrial redox ability by MTT assay was analyzed. At 24 h p.i., OMF at 5 µM did not provoke significant

($p > 0.05$) time-dependent alteration in the amount of mitochondrial dehydrogenases activity compared to control cells (Figure 2c). In brief, these experiments showed that OMF at the concentration of 5 μM did not significantly modify MDBK cell viability and cell proliferation as compared to untreated cells.

Following BoHV-1 infection, in the presence of OMF at 5 μM, there was significantly ($p < 0.001$) decreased cytotoxicity (Figure 3 a,b) and increased cell proliferation ($p < 0.01$) during infection in MDBK cells (Figure 3c). Thus, the concentration of OMF at 5 μM for use throughout the study was selected. Overall, at the non-toxic concentration of 5 μM, OMF significantly decreased the MDBK cell death at 24 h p.i. during BoHV-1 infection.

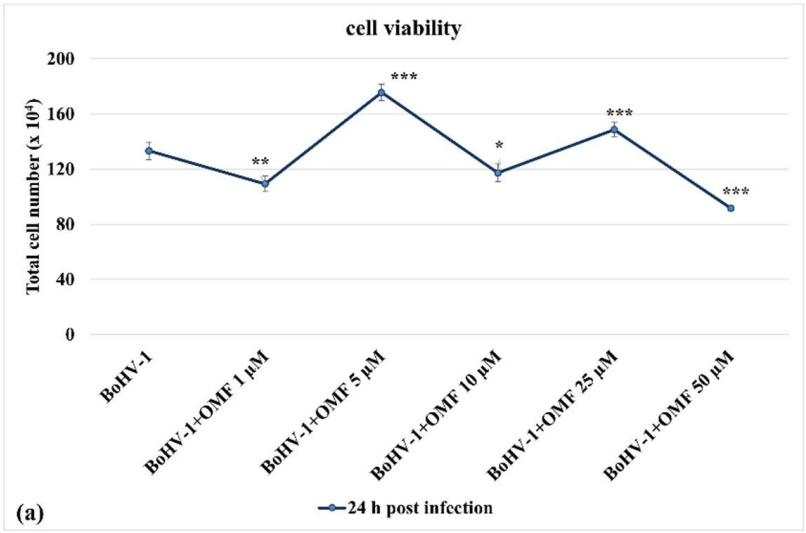

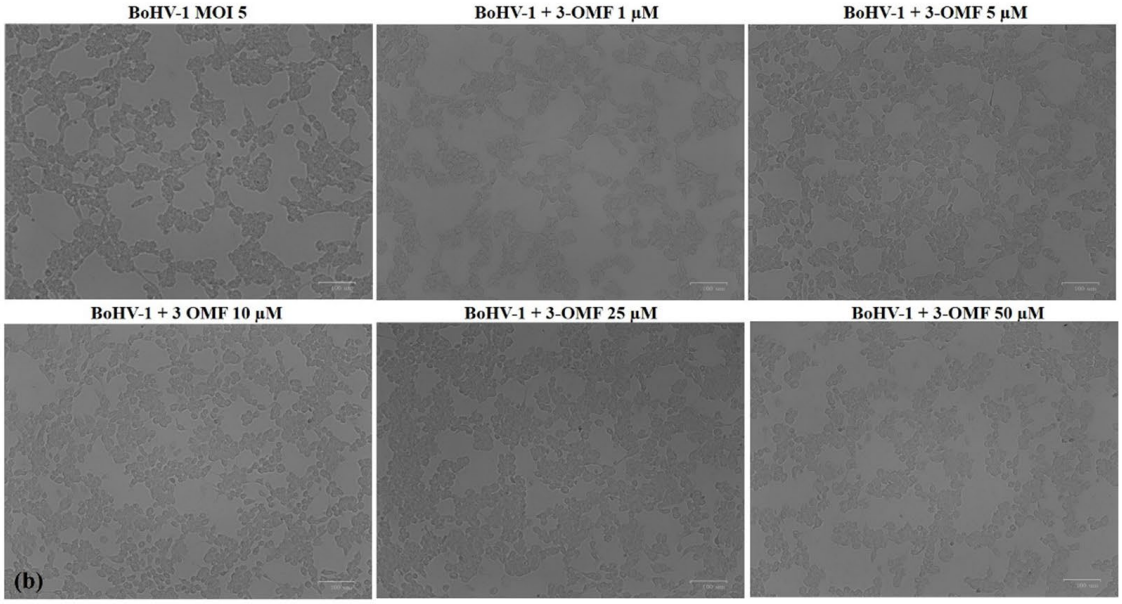

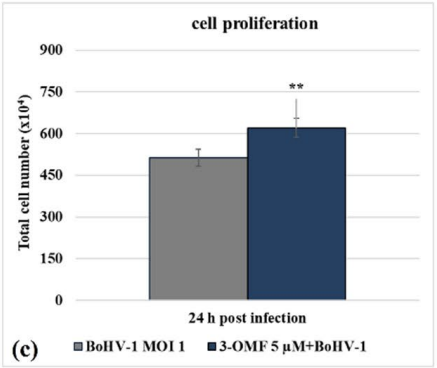

Figure 3. OMF decreases cell death during BoHV-1 infection. (a) Dose–response curve of MDBK cells infected with BoHV-1 and treated with OMF at different concentrations (1, 5, 10, 25, and 50 µM). At 24 h after treatment, cells were stained with TB and scored by an automated counter, or (b) cell viability was assayed by using TB staining while cells were attached to wells and counted under a light microscope. (c) Dose–response curve of MDBK cells infected with BoHV-1, treated with OMF (5 µM) for 24 h and analyzed by MTT assay. Significant differences between control and OMF-treated cells are indicated by probability p. * $p < 0.05$, ** $p < 0.01$, and *** $p < 0.001$. Scale bar 100 µm.

3.2. *OMF decreases cell membrane damage and morphological cell death features during BoHV-1 infection in MDBK cells*

To detect cell morphology, the effects of OMF in BoHV-1-infected cells were examined by light microscopy after Giemsa staining. After 24 h of infection, no morphological alterations were found in the OMF unexposed groups compared to the control, as shown in Figure 4. In unexposed infected cells, we observed a growth of intercellular spaces and alteration in morphology, indicating marks of apoptotic cell death due to cell shrinkage, pyknosis, chromatin condensation, and fragmentation of nuclei (Figure 4, arrow). These features were accompanied by necrosis because of nuclear and cytoplasmic swelling due to a break of the plasma membrane, provoking a decreased definition of cell shapes (Figure 4, arrowhead). While only a few signs of necrosis were observed in BoHV-1-infected cells treated with OMF (Figure 4, arrowhead), these results showed that MDBK cells infected with BoHV-1, in the presence of OMF, did not undergo either apoptotic or necrotic.

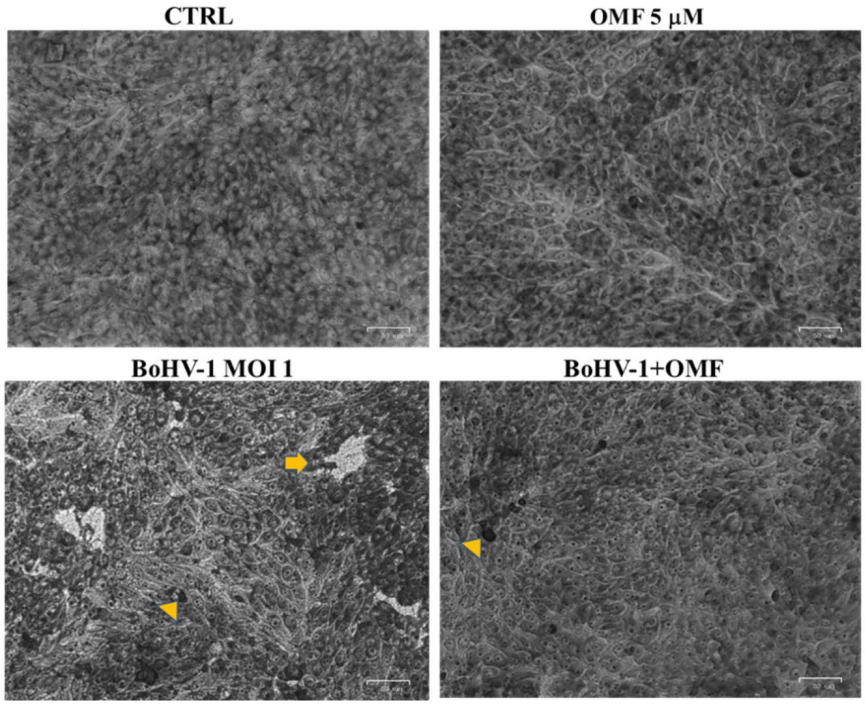

Figure 4. OMF decreases cell membrane damage and morphological cell death features during BoHV-1 infection in MDBK cells. Cells were infected with BoHV-1, in the presence or absence of OMF. At 24 h p.i., cells after Giemsa staining were examined under a light microscope. Photomicrographs showed no morphological alterations in OMF unexposed groups compared to control. By comparing BoHV-1-infected cells to the control, some cells displayed apoptotic features, attributable to pyknotic nuclei and nuclear fragmentation (arrow), or necrosis marks, such as nuclear and cytoplasmic swelling (arrowhead). In OMF-treated infected cells, only a few signs of necrosis were found (arrowhead). Scale bar 50 µm.

3.3. *OMF Decreases Virus Yield and Reduces the Expression of bICP0 during BoHV-1 Infection*

Following BoHV-1 infection for 24 h in MDBK cells, we analyzed virus titer and viral CPE to explore the effect of OMF on virus production. Thus, MDBK cells were infected with BoHV-1, at an MOI of 1, in the presence or absence of OMF at the non-toxic concentration of 5 μM and processed. Interestingly, a statistically significant ($p < 0.05$) decrease in the virus titer was seen at 24 h p.i. in cells treated with OMF during BoHV-1 infection (Figure 5). Similar results were found carrying out the virus titer by $TCID_{50}$ (data not shown). Moreover, at 24 h p.i., CPE, due to syncytia development as well as damaged cellular sheet, was considerable in Figure 4.

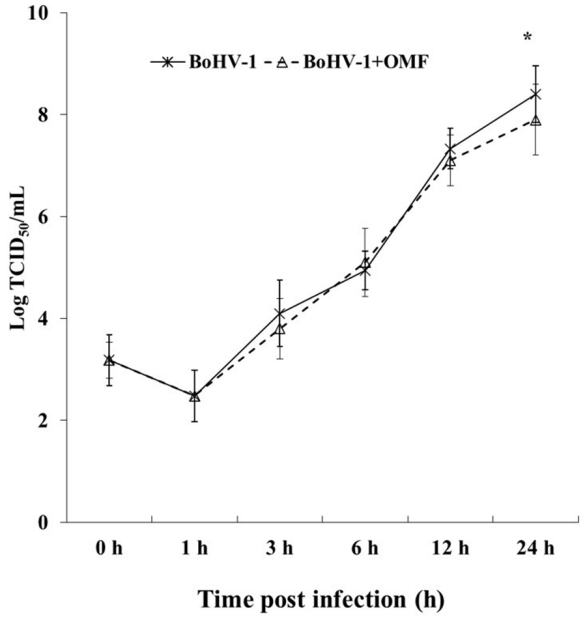

Figure 5. OMF decreases virus yield during BoHV-1 infection in MDBK cells. Cells were infected with BoHV-1 in the presence or absence of OMF. For viral growth curves, MDBK cells were infected with BoHV-1 in the presence or absence of OMF. At indicated times, p.i., virus titer was evaluated by real-time PCR. Significant differences between BoHV-1-infected cells and OMF-treated infected cells are indicated by probability p. * $p < 0.05$.

To further clarify the effects of OMF during BoHV-1 infection, we analyzed bICP0 protein expression, the main protein involved in the transcription of BoHV-1 (*Muylkens et al., 2007; Jones et al., 2019*). Indeed, bICP0 is expressed during infection in permissive cells, in which it promotes productive infection (*Fraefel et al., 1994; Inman et al., 2001; Wirth et al., 1992; Fiorito et al., 2014, 2017*). At 24 h p.i., bICP0 was found in BoHV-1-infected cells (Figure 6), whereas the protein was considerably decreased in the presence of OMF (5 M) (Figure 6). These results demonstrate that the bICP0 viral protein is

generally expressed in BoHV-1-infected cells, and its expression was reduced in infected cells treated with OMF.

3.4. *OMF Induces the Expression of AhR during BoHV-1 Infection in MDBK Cells*

To explore the potential involvement of OMF in the regulation of AhR, we carried out an immunofluorescence assay for AhR, a receptor expressed in MDBK cells (*Fiorito et al., 2014*). Herein, OMF induced the activation of AhR in MDBK cells, and, following infection with BoHV-1, a noteworthy activation of AhR in OMF-treated cells was detected (Figure 7). Our results showed that the AhR cellular receptor, generally expressed in MDBK cells, was activated in the presence of OMF. In addition, the expression of AhR strongly increased in infected cells treated with OMF.

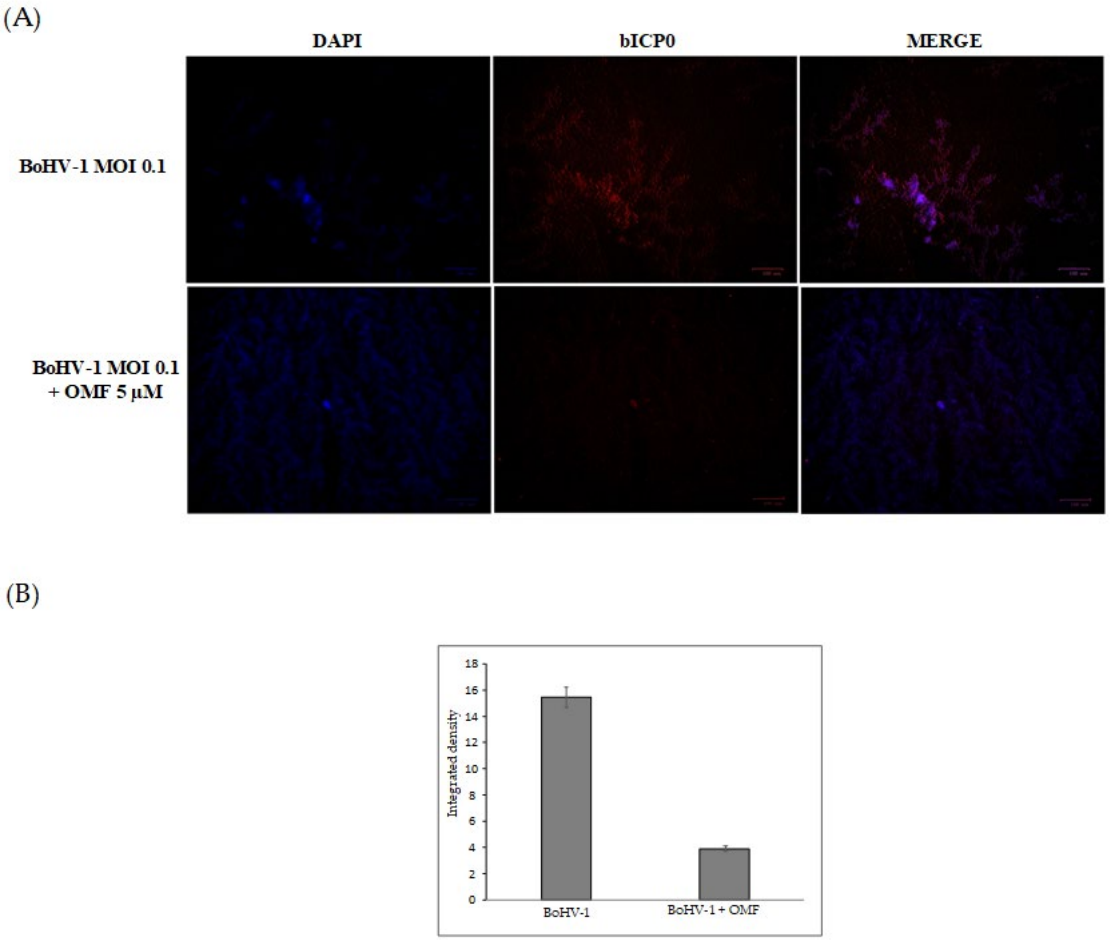

Figure 6. OMF reduces the expression of bICP0 during BoHV-1 infection in MDBK cells. (A) Cells were infected with BoHV-1, at an MOI of 0.1, in the presence or absence of OMF, and after 24 h p.i., immunofluorescence staining for bICP0 (red fluorescence) was performed as described in the Methods section. Nuclei were counterstained with DAPI. During infection, bICP0 was localized in both the nucleus and cytoplasm. In the presence of OMF, the expression of bICP0 was noticeably reduced during BoHV-1 infection. Scale bar 100 µm. (B) Bars represent the mean ratio generated from the integrated density (product of the area and mean intensity of fluorescence) of the bICP0 expression evaluated by ImageJ. Error bars represent standard error measurement.

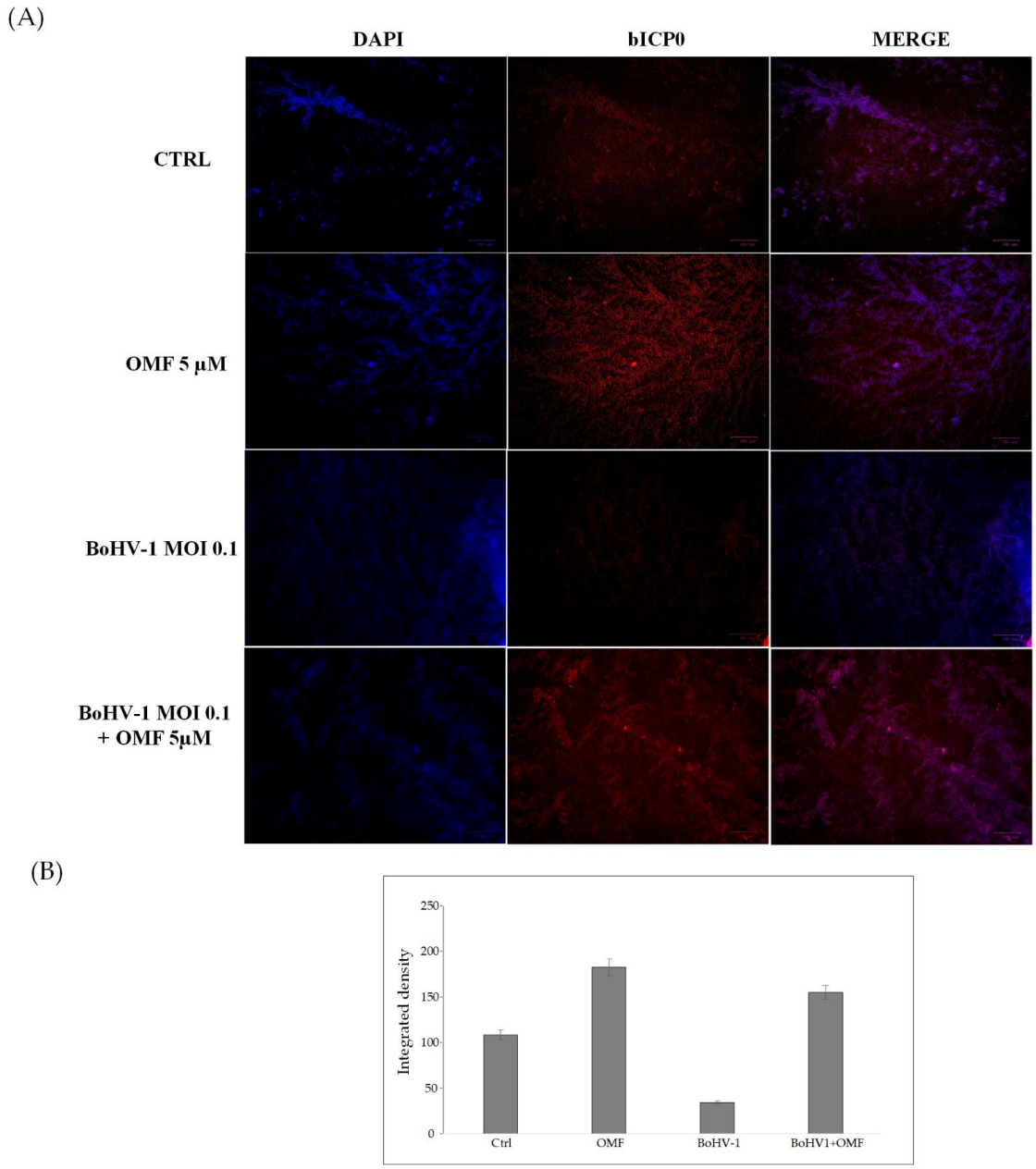

Figure 7. OMF induces the expression of AhR during BoHV-1 infection in MDBK cells. (A) Representative microphotographs of uninfected (control) or infected cells (BoHV-1), OMF-treated infected (BoHV-1+OMF), and uninfected cells (OMF), after 24 h of infection, stained with immunofluorescence for AhR (red fluorescence), as described in the Methods section. Nuclei were counterstained with DAPI. AhR was expressed in MDBK cells and localized in both the nucleus and cytoplasm. The expression of AhR was induced in the presence of OMF. During infection, the expression of AhR was drastically reduced. In the presence of OMF, the expression of AhR was remarkably enhanced during BoHV-1 infection. Scale bar 100 µm (B) Bars represent the mean ratio generated from the total integrated density (product of the area and mean intensity of fluorescence) of the AhR expression evaluated by ImageJ. Error bars represent standard error measurement.

4. Discussions

Many fungal metabolites have caught the attention of researchers involved in the development of novel therapeutic strategies against viral diseases. In fact, they might represent an attractive tool to be exploited with reference to their diverse structures and mechanisms of action. The available data concerning bioactivity of fungal products or extracts against herpes viruses are limited, but it is worth noting that some compounds, including butyrolactone derivatives, macrolides, naphthalenones, resorcylic acid lactones, sterols, and peptides, may act as anti-HSV agents (*Moghadamtousi et al., 2015; Linnakoski et al., 2018; Roy et al., 2017*). The structural variability of fungal metabolites with anti-HSV activity might be related to different mechanisms of action, but there is a lack of information on this aspect. It was hypothesized that the lipophilic linear peptides, halovirs, could destabilize the virus membrane (*Rowley et al., 2003*). Herein, we explored the effect of OMF during a BoHV-1 infection. In MDBK cells, OMF offered good protection against virus action by inducing a significant increase in cell viability as well as in cell proliferation. Typically, BoHV-1 stimulates cell death in a cell-type-dependent trend (*Fiorito et al., 2020; Geiser et al., 2008*), and the morphological evaluation of MDBK during infection revealed a decrease in cell membrane damage and cell death features, which are considerably reduced by OMF. Similar signs of MDBK cell protection during BoHV-1 infection were previously detected in the presence of the proteasome inhibitor MG-132 (*Fiorito et al., 2017*). Similarly, a decrease in virus replication in OMF-treated infected cells was found. Indeed, a reduction in CPE and a significant decrease in virus yield were detected. Interestingly, these results were accompanied by a marked reduction in bICP0 expression, indicating that the virus discharge was considerably reduced by OMF.

Concerning the BoHV-1, there are some reports of new potential agents with inhibitory effects against this virus, but they are often classical synthetic agents (acyclovir, famciclovir, fenbendazole, and ivermectin) used alone or in combination with natural products (*Chang et al., 2020; Yesilbag et al., 2021*). Inference of bioactivity of fungal products against this virus was derived from the evaluation of extracts of the mushrooms Agaricus blazei (*Bruggeman et al., 2006*) and Lentinula edodes (*Rincao et al., 2012*). Hence, the OMF inhibitory activity against BoHV-1 observed in the present investigation represents the first evidence concerning a purified metabolite. So far, anti-HCV properties of this compound were reported in a comparative study where the examination of two

funicone derivatives suggested that the 1,3-dihydroxy-5-methylbenzene moiety is important for antiviral activity (*Nakajima et al., 2013*). It is possible that the arylic nature of this part of the molecule interacts with AhR, a ligand-activated transcription factor that interacts with aromatic compounds, but this hypothetical interaction should be further investigated. AhR has been described as a multifunctional sensor, integrator system, and ligandactivated transcription factor of the bHLH/PAS family. In the complexity of signaling,

AhR regulates elements of the innate and adaptive immune response to various microorganisms. Moreover, AhR is involved in the modulation of the host response to viral infection. Furthermore, the well-known activation of AhR by 2,3,7,8-tetrachlorodibenzo-p-dioxin (TCDD or dioxin) may induce a generalized suppression of immune response and increase susceptibility to infectious agents, such as viruses, both in vivo and in vitro (*Fiorito et al., 2017; Bock et al., 2021*). Specifically, the AhR activation has been shown to promote viral replication of several herpesviruses, such as cytomegalovirus (CMV), herpes simplex II, and BoHV-1. In addition, dioxin may stimulate a worsening of latent infection caused by CMV or Epstein-Barr virus (*Fiorito et al., 2017*). Similar responses were detected during HSV-1 infection in mice (*Veiga-Parga et al., 2011*). In fact, dioxin-treated mice had higher virus titers, and many of them died due to herpes encephalitis if AhR was stimulated before to infection. Interestingly, if AhR activation occurred after HSV-1 infection, the pathogenic signs, such as herpes encephalitis, diminished, and eye tissue pathology improved (*Veiga-Parga et al., 2011*), highlighting the importance of timing in AhR stimulation to regulate the balance between reducing immunopathology and removing antiviral defensive immunity (*Torti et al., 2021*). Taken together, our results showed a potential antiviral role of OMF during BoHV-1 infection in MDBK cells by involving AhR. Consequently, AhR targeted therapy may become a new method for antiviral treatment.

References

Muylkens, B.; Thiry, J.; Kirten, P.; Schynts, F.; Thiry, E. Bovine herpesvirus 1 infection and infectious bovine rhinotracheitis. Vet.Res. 2007, 38, 181–209.

Jones, C. Bovine herpesvirus 1 counteracts immune responses and immune-surveillance to enhance pathogenesis and virus transmission. Front. Immunol. 2019, 10, 1008.

Fraefel, C.; Zeng, J.; Choffat, Y.; Engels, M.; Schwyzer, M.; Ackermann, M. Identification and zinc dependence of the bovine herpesvirus 1 transactivator protein BICP0. J. Virol. 1994, 68, 3154–3162.

Inman, M.; Zhang, Y.; Geiser, V.; Jones, C. The zinc ring finger in the bICPO protein encoded by bovine herpesvirus-1 mediates toxicity and activates productive infection. J. Gen. Virol. 2001, 82, 483–492.

Fiorito, F.; Ciarcia, R.; Granato, G.E.; Marfe, G.; Iovane, V.; Florio, S.; De Martino, L.; Pagnini, U. 2,3,7,8-Tetrachlorodibenzo-pdioxin induced autophagy in a bovine kidney cell line. Toxicology 2011, 290, 258–270.

Moghadamtousi, S.Z.; Nikzad, S.; Kadir, H.A.; Abubakar, S.; Zandi, K. Potential antiviral agents from marine fungi: An overview. Mar. Drugs 2015, 13, 4520–4538.

Linnakoski, R.; Reshamwala, D.; Veteli, P.; Cortina-Escribano, M.; Vanhanen, H.; Marjomäki, V. Antiviral agents from fungi: Diversity, mechanisms and potential applications. Front. Microbiol. 2018, 9, 2325.

Manganyi, M.C.; Ateba, C.N. Untapped potentials of endophytic fungi: A review of novel bioactive compounds with biological applications. Microorganisms 2020, 8, 1934.

Salvatore, M.M.; Nicoletti, R.; DellaGreca, M.; Andolfi, A. Occurrence and properties of thiosilvatins. Mar. Drugs 2019, 17, 664.

Nicoletti, R.; Salvatore, M.M.; Ferranti, P.; Andolfi, A. Structures and bioactive properties of myrtucommulones and related acylphloroglucinols from Myrtaceae. Molecules 2018, 23, 3370.

Nicoletti, R.; Vinale, F. Bioactive compounds from marine-derived Aspergillus, Penicillium, Talaromyces and Trichoderma Species. Mar. Drugs 2018, 16, 408.

Rowley, D.C.; Kelly, S.; Kauffman, C.A.; Jensen, P.R.; Fenical,W. Halovirs A-E, new antiviral agents from a marine-derived fungus of the genus Scytalidium. Bioorg. Med. Chem. 2003, 11, 4263–4274.

Shushni, M.A.M.; Mentel, R.; Lindequist, U.; Jansen, R. Balticols A-F, new naphthalenone derivatives with antiviral activity, from an ascomycetous fungus. Chem. Biodivers. 2009, 6, 127–137.

Nong, X.H.; Wang, Y.F.; Zhang, X.Y.; Zhou, M.P.; Xu, X.Y.; Qi, S.H. Territrem and butyrolactone derivatives from a marine-derived fungus Aspergillus Terreus. Mar. Drugs 2014, 12, 6113–6124.

Nicoletti, R.; Manzo, E.; Ciavatta, M.L. Occurence and bioactivities of funicone-related compounds. Int. J. Mol. Sci. 2009, 10, 1430–1444.

Zhai, M.M.; Li, J.; Jiang, C.X.; Shi, Y.P.; Di, D.L.; Crews, P.; Wu, Q.X. The bioactive secondary metabolites from Talaromyces species. Nat. Prod. Bioprospect. 2016, 6, 1–24.

Nicoletti, R.; Salvatore, M.M.; Andolfi, A. Secondary metabolites of mangrove-associated strains of Talaromyces. Mar. Drugs 2018, 16, 12.

Lan, D.; Wu, B. Chemistry and bioactivities of secondary metabolites from the genus Talaromyces. Chem. Biodivers. 2020, 17, e2000229.

De Stefano, S.; Nicoletti, R.; Milone, A.; Zambardino, S. 3-O-Methylfunicone, a fungitoxic metabolite produced by the fungus Penicillium pinophilum. Phytochemistry 1999, 52, 1399–1401.

Nicoletti, R.; Buommino, E.; De Filippis, A.; Lopez-Gresa, M.P.; Manzo, E.; Carella, A.; Petrazzuolo, M.; Tufano, M.A. Bioprospecting for antagonistic Penicillium strains as a resource of new antitumor compounds. World J. Microbiol. Biotechnol. 2008, 24, 189–195.

Nicoletti, R.; Scognamiglio, M.; Fiorentino, A. Structural and bioactive properties of 3-O-methylfunicone. Mini Rev. Med. Chem. 2014, 14, 1043–1047.

Buommino, E.; Tirino, V.; de Filippis, A.; Silvestri, F.; Nicoletti, R.; Ciavatta, M.L.; Pirozzi, G.; Tufano, M.A. 3-O-methylfunicone, from Penicillium pinophilum, is a selective inhibitor of breast cancer stem cells. Cell Prolif. 2011, 44, 401–409.

Baroni, A.; De Luca, A.; De Filippis, A.; Petrazzuolo, M.; Manente, L.; Nicoletti, R.; Tufano, M.A.; Buommino, E. 3-Omethylfunicone, a metabolite of Penicillium pinophilum, inhibits proliferation of human melanoma cells by causing G2 + M arrest and inducing apoptosis. Cell Prolif. 2009, 42, 541–553.

Nakajima, S.; Watashi, K.; Kamisuki, S.; Tsukuda, S.; Takemoto, K.; Matsuda, M.; Suzuki, R.; Aizaki, H.; Sugawara, F.; Wakita, T. Specific inhibition of hepatitis C virus entry into host hepatocytes by fungi-derived sulochrin and its derivatives. Biochem. Biophys. Res. Commun. 2013, 440, 515–520.

Li, C.X.; Zhao, S.; Zhang, T.; Xian, L.; Liao, L.S.; Liu, J.L.; Feng, J.X. Genome sequencing and analysis of Talaromyces pinophilus provide insights into biotechnological applications. Sci. Rep. 2017, 7, 490.

Yang, T.; Feng, Y.L.; Chen, L.; Vaziri, N.D.; Zhao, Y.Y. Dietary natural flavonoids treating cancer by targeting aryl hydrocarbon receptor. Crit. Rev. Toxicol. 2019, 49, 445–460.

Torti, M.F.; Giovannoni, F.; Quintana, F.J.; García, C.C. The aryl hydrocarbon receptor as a modulator of anti-viral immunity. Front. Immunol. 2021, 12, 624293.

Fiorito, F.; Iovane, V.; Cantiello, A.; Marullo, A.; De Martino, L.; Iovane, G. MG-132 reduces virus release in Bovine herpesvirus-1 infection. Sci. Rep. 2017, 7, 13306.

Chang, L.; Zhu, L. Dewormer drug fenbendazole has antiviral effects on BoHV-1 productive infection in cell cultures. J. Vet. Sci. 2020, 21, e72.

Yesilbag, K.; Toker, E.B.; Ates, O. Ivermectin also inhibits the replication of bovine respiratory viruses (BRSV, BPIV-3, BoHV-1, BCoV and BVDV) in vitro. Virus Res. 2021, 297, 198384.

Salvatore, M.M.; DellaGreca, M.; Nicoletti, R.; Salvatore, F.; Vinale, F.; Naviglio, D.; Andolfi, A. Talarodiolide, a new 12-membered macrodiolide, and GC/MS investigation of culture filtrate and mycelial extracts of Talaromyces pinophilus. Molecules 2018, 23, 950.

Fiorito, F.; Marfè, G.; De Blasio, E.; Granato, G.E.; Tafani, M.; De Martino, L.; Montagnaro, S.; Florio, S.; Pagnini, U. 2,3,7,8-Tetrachlorodibenzo-p-dioxin regulates bovine herpesvirus type 1 induced apoptosis by modulating Bcl-2 family members. Apoptosis 2008, 13, 1243–1252.

Fiorito, F.; Nocera, F.P.; Cantiello, A.; Iovane, V.; Lambiase, S.; Piccolo, M.; Ferraro, M.G.; Santamaria, R.; De Martino, L. Bovine herpesvirus-1 infection in mouse neuroblastoma (Neuro-2A) cells. Vet. Microbiol. 2020, 247, 108762.

Fiorito, F.; Irace, C.; Nocera, F.P.; Piccolo, M.; Ferraro, M.G.; Ciampaglia, R.; Tenore, G.C.; Santamaria, R.; De Martino, L. MG-132 interferes with iron cellular homeostasis and alters virulence of bovine herpesvirus 1. Res. Vet. Sci. 2021, 137, 1–8.

Fiorito, F.; Pagnini, U.; De Martino, L.; Montagnaro, S.; Ciarcia, R.; Florio, S.; Pacilio, M.; Fucito, A.; Rossi, A.; Iovane, G.; et al. 2,3,7,8-Tetrachlorodibenzo-p-dioxin increases bovine herpesvirus type-1 (BHV-1) replication in Madin-Darby Bovine Kidney (MDBK) cells in vitro. J. Cell. Biochem. 2008, 103, 221–233.

Chowanadisai,W.; Graham, D.M.; Keen, C.L.; Rucker, R.B.; Messerli, M.A. Neurulation and neurite extension require the zinc transporter ZIP12 (slc39a12). Proc. Natl. Acad. Sci. USA 2013, 110, 9903–9908.

Santamaria, R.; Fiorito, F.; Irace, C.; De Martino, L.; Maffettone, C.; Granato, G.E.; Di Pascale, A.; Iovane, V.; Pagnini, U.; Colonna, A. 2,3,7,8-Tetrachlorodibenzo-p-dioxin impairs iron homeostasis by modulating iron-related proteins expression and increasing the labile iron pool in mammalian cells. Biochim. Biophys. Acta-Mol. Cell Res. 2011, 1813, 704–712.

Leite, M.; Quinta-Costa, M.; Leite, P.S.; Guimarães, J.E. Critical evaluation of techniques to detect and measure cell death-Study in a model of UV radiation of the leukaemic cell line HL60. Anal. Cell. Pathol. 1999, 19, 139–151.

Kroemer, G.; Levine, B. Autophagic cell death: The story of a misnomer. Nat. Rev. Mol. Cell Biol. 2008, 9, 1004–1010.

Zakeri, Z.; Lockshin, R.A. Cell death: History and future. Adv. Exp. Med. Biol. 2008, 615, 1–11.

Altamura, G.; Power, K.; Martano, M.; degli Uberti, B.; Galiero, G.; De Luca, G.; Maiolino, P.; Borzacchiello, G. Felis catus papillomavirus type-2 E6 binds to E6AP, promotes E6AP/p53 binding and enhances p53 proteasomal degradation. Sci. Rep. 2018,8, 17529.

Wirth, U.V.; Fraefel, C.; Vogt, B.; Vlcek, C.; Paces, V.; Schwyzer, M. Immediate-early RNA 2.9 and early RNA 2.6 of bovine herpesvirus 1 are 3' coterminal and encode a putative zinc finger transactivator protein. J. Virol. 1992, 66, 2763–2772.

Fiorito, F.; Marfè, G.; Granato, G.E.; Ciarcia, R.; De Blasio, E.; Tafani, M.; Florio, S.; De Martino, L.; Muzi, G.; Pagnini, U.; et al. 2,3,7,8-Tetrachlorodibenzo-p-dioxin modifies expression and nuclear/cytosolic localization of bovine herpesvirus 1 immediateearly protein (bICP0) during infection. J. Cell. Biochem. 2010, 111, 333–342.

Fiorito, F.; Santamaria, R.; Irace, C.; De Martino, L.; Iovane, G. 2,3,7,8-Tetrachlorodibenzo-p-dioxin and the viral infection. Environ. Res. 2017, 153, 27–34.

Fiorito, F.; Cantiello, A.; Granato, G.E.; Marfè, G.; Ciarcia, R.; Florio, S.; Pagnini, U.; De Martino, L.; Iovane, G. Modulation of telomerase activity, bTERT and c-Myc induced by 2,3,7,8-tetrachlorodibenzo-p-dioxin during bovine herpesvirus 1 infection in MDBK cells. Toxicol. Vitr. 2014, 28, 24–30.

Roy, B.G. Potential of small-molecule fungal metabolites in antiviral chemotherapy. Antivir. Chem. Chemother. 2017, 25, 20–52.

Geiser, V.; Rose, S.; Jones, C. Bovine herpesvirus type 1 induces cell death by a cell-type-dependent fashion. Microb. Pathog. 2008, 44, 459–466.

Bruggemann, R.; Orlandi, J.M.; Benati, F.J.; Faccin, L.C.; Mantovani, M.S.; Nozawa, C.; Linhares, R.E.C. Antiviral activity of Agaricus blazei Murrill ss. Heinem extract against human and bovine herpesviruses in cell culture. Brazilian J. Microbiol. 2006, 37, 561–565.

Rincão, V.P.; Yamamoto, K.A.; Silva Ricardo, N.M.P.; Soares, S.A.; Paccola Meirelles, L.D.; Nozawa, C.; Carvalho Linhares, R.E. Polysaccharide and extracts from Lentinula edodes: Structural features and antiviral activity. Virol. J. 2012, 9, 37.

Bock, K.W. Aryl hydrocarbon receptor (AHR), integrating energy metabolism and microbial or obesity-mediated inflammation. Biochem. Pharmacol. 2021, 184, 114346.

Veiga-Parga, T.; Suryawanshi, A.; Rouse, B.T. Controlling viral immuno-inflammatory lesions by modulating aryl hydrocarbon receptor signaling. PLoS Pathog. 2011, 7, e1002427.

Antiviral activity of Taurisolo® during bovine alphaherpesvirus 1 infection

1. Introduction

Bovine alphaherpesvirus 1 (BoAHV-1), belonging to the Alphaherpesvirinae subfamily, causes an infection of the upper respiratory tract known as infectious bovine rhinotracheitis (IBR), conjunctivitis and genital disorders, which are often accompanied by lowered fertility, abortions, and reduced milk production. The virus, together with other pathogens, causes the bovine respiratory disease complex, leading to pneumonia and occasionally death in cattle (*Muylkens et al., 2007; Jones 2019*). BoAHV-1 establishes long-term latent infection in sensory neurons of the infected animals, and the reactivation from latency may prompt virus shedding and spread to susceptible animals (*Muylkens et al., 2007; Jones 2019*). Eradication programs are followed by several European countries, but IBR is still endemic in many regions, increasing the risk of virus transmission to free herds (*Iscaro et al., 2021*). IBR is currently listed in the Regulation 2016/429/EU and its Annexes (Animal Health Law), and outbreaks of IBR in IBR-free member states or in IBR-free zones of European countries should be subject to notification. Thus, IBR is responsible for large economic losses and trade restrictions (*Iscaro et al., al.,2021*). Vaccination is still the most efficient way to prevent the disease (*Righi et al., 2023*). To date, a potential antiviral effect against BoAHV-1 is due to conventional synthetic drugs (acyclovir, fenbendazole, famciclovir, ivermectin) administered alone or in combination with natural agents (*Yuan et al., 2016; Chang and Zhu 2020; Yesilbag et al., 2021*). Indeed, very few nontoxic medicinal compounds to fight BoAHV-1 infection are described, although plant extracts have been studied as potential new antiviral drugs. Polyphenols, for example, have been demonstrated to have noticeable anti-herpesvirus activity (*Vilhelmova-Ilieva et al., 2014; Boubaker-Elandalousi et al., 2014; Annunziata et al., 2018a, 2018b*). Furthermore, flavonoid derivatives have been shown to have antiviral activity against BoAHV-1 (*Akula et al., 2002; Boubaker-Elandalousi et al., 2014; Zhu et al., 2018*). Specifically, polyphenols and flavonoids derivatives have been shown to have antiviral activity in vitro in MDBK cells. For instance, genistein, a soy isoflavone, inhibits BoAHV-1 replication (*Akula et al., 2002*); Thymus capitata, reach in polyphenols and flavonoids, inhibits the viral replication by interfering with the early stages of viral adsorption and replication (*Boubaker-Elandalousi et al., 2014*); curcumin, a constituent of the spice turmeric inhibits BoAHV-1 entry into MDBK cells (*Zhu et al., 2015*); and kaempferol exhibits a robust antiviral

activity against virus replication (*Zhu et al., 2018*). Taurisolo®, a grape pomace polyphenolic extract obtained from the Aglianico cultivar grape, is a nutraceutical containing several substances such as catechin, resveratrol, procyanidins, epicatechin, flavonoids, and organic acids (gallic, syringic, caffeic, p-coumaric, ferulic) (*Annunziata et al., 2019a*). It has been shown that Taurisolo® reduces oxidative stress and oxidative damage in aged rats (*Annunziata et al., 2020, 2021a,b; Badolati et al., 2020*). Moreover, it decreases the levels of trimethylamine-N-oxide, a cardiovascular risk factor (*Annunziata et al., 2019a,b*) and preserves the vascular function against ox-inflamm-aging process and the consequent cardiovascular accidents (*Martelli et al., 2021*). In addition to antioxidant properties, it has recently demonstrated that Taurisolo® possesses antiviral activity against herpes simplex virus (HSV) type 1 and 2 (*Zannella et al., 2023*). Moreover, during a clinical trial, in patients affected by SARS-CoV-2 pneumonia, the administration of a Taurisolo® aerosol formulation reduced both the duration and the severity of symptoms (*Sanduzzi Zamparelli et al., 2022*). As previously reported, BoAHV-1 is a useful model for antiherpesvirus compounds testing (*Akula et al., 2002; Boubaker-Elandalousi et al., 2014; Zhu et al., 2018; Fiorito et al., 2017a, 2022; Chang and Zhu 2020; Yesilbag et al., 2021*). Thus, this study aimed to assess the potential antiviral activity of Taurisolo® against BoAHV-1.

2. Materials and methods

2.1. *Production of Taurisolo®*

Taurisolo® is a nutraceutical supplement containing a polyphenol extract from Vitis Vinifera cv 'Aglianico' grapes, collected in Montemarano (Avellino, Italy, Coordinates: 40◦54058″ N 14◦59054 optimized at the NutraPharmaLabs of the Department of Pharmacy, University of Naples Federico II (Naples, Italy). Then, the MB-Med Company (Turin, Italy) performed large-scale production (*Badolati et al., 2020; Annunziata et al., 2021a, b*). Taurisolo® consists of various molecules, such as organic acids (gallic, syringic, caffeic, p-coumaric, ferulic), catechin, procyanidins, quercetin, resveratrol and, rutin (*Badolati et al., 2020; Annunziata et al., 2021a,b*).

2.2. *Cell cultures and virus infection*

The bovine cell line Madin Darby Bovine Kidney (MDBK) (American Type Culture Collection, CCL22) was cultivated in Dulbecco's modified Eagle's minimal essential medium (DMEM) and incubated at 37 ◦C and 5% CO2 (*Longo et al., 2009; Fiorito et al., 2011*). BoAHV-1 (Cooper strain, accession number: KU198480) was used. Both for virus stocks growth and virus titration MDBK cells were utilized (*Fiorito et al., 2008a,b; 2020; 2021*). Taurisolo® was dissolved in DMEM to a final concentration of 0.1, 0.5, 1, 1.5 and 3 mg/mL. Monolayers of MDBK cells were infected or not with BoAHV-1, at a multiplicity of infection (MOI) of 0.1, 1, 5 or 10, in the presence or not of Taurisolo®, to obtain four groups: uninfected or infected cells, Taurisolo® treated infected and uninfected cells. After 1 hour of adsorption at 37 ◦C, cells were incubated and processed at 1, 3, 6, 12, 24, 48, 72 and 120 h post infection (p.i.). BoAHV-1 was in culture medium throughout the course of the experiment.

2.3. *Cell viability*

Trypan blue (TB) (Sigma-Aldrich) exclusion test was used to assess cell viability (Fiorito et al., 2008b). At 48 h post treatment, trypsin was added to the cells that were mixed with TB and counted by TC20 automated cell counter (Bio-Rad). Cell viability was obtained as the percentage of living cells over the total cell number. Results were reported as the mean ± S.D. of three independent experiments in duplicate.

2.4. *Cell proliferation*

3-(4,5-dimethyl-2-thiazolyl)-2,5-diphenyl-2H-tetrazolium bromide (MTT) assay was performed to examine cell proliferation (*Fiorito et al., 2008a; 2011; Santamaria et al., 2011*). Several concentrations of Taurisolo ® (0.1, 0.5, 1, 1.5 and 3 mg/mL) were evaluated after 48 h p.i. in a preliminary assay of cell viability and then we selected 0.5 mg/mL Taurisolo® for MTT experiments. Briefly, BoAHV-1 infected (MOI 0.1) cells, incubated or not with Taurisolo® (0.5 mg/mL) were tested by MTT assay after 48 h p.i.. Results were the mean ± S.D. of four independent experiments in duplicate.

2.5. *Examination of cell morphology*

Cell morphology was evaluated using Giemsa staining (*Fiorito et al., 2020; 2022*). Monolayers of MDBK were infected or not with BoAHV-1, at MOI of 5, in the presence or absence of Taurisolo® (0.5 mg/mL), and after 24 h of incubation, Giemsa staining and

light microscopy (ZOE Cell Imager, Bio-Rad Laboratories) were performed. The criteria described to explore cell death features were used (*Leite et al., 1999; Banfalvi et al. 2017*).

2.6. *Immunofluorescence staining*

In order to study the influence of Taurisolo® on both bICP0 and AhR expression in BoAHV-1-infected cells, immunofluorescence staining was carried out at 24 h p.i. (*Altamura et al., 2018; Fiorito et al., 2022*). The antibodies, dissolved in 5% bovine serum albumin-TBST, were: anti-AhR (Sigma-Aldrich) (1:250), anti-bICP0 polyclonal rabbit (a.a. 663–676) serum (1:800), kindly supplied by Prof. M. Schwyzer and Prof. Cornel Fraefel (University of Zurich, Switzerland), Texas Red goat anti-rabbit (Thermo Fisher Scientific) (1:100). DAPI (1:1000) was used as nuclear counter-staining. Microscopy and photography were valued by ZOE Fluorescent Cell Imager (Bio-Rad Laboratories). Fluorescence signals from microscopy-generated images were quantified by ImageJ (National Institutes of Health, Bethesda, MD, USA) software.

2.7. *BoAHV-1 infection*

Cells were infected with BoAHV-1 at MOI 1, in the presence or not of Taurisolo®, and processed at 0, 1, 3, 6, 12, 24, 48, and 72 h p.i. by realtime PCR for BoAHV-1 quantification. Furthermore, viral cytopathic effects (CPE) were evaluated at light microscope until 120 h p.i. (*De Martino et al. 2010; Fiorito et al., 2021*).

2.8. *Viral nucleic acids extraction*

Nucleic acids extraction was carried out from 200 µL of cell supernatant by using the King Fisher Flex System (Thermo Fisher Scientific, Waltham, Massachusetts, USA) with the Mag Max Viral Pathogen kit (Thermo Fisher Scientific, Waltham, Massachusetts, USA), according to the instructions of the manufacturer. Nucleic acids were dissolved in 80 µL of elution buffer. DMEM was utilized as a negative process control.

2.9. *Real-Time PCR for quantification of BoAHV-1*

BoAHV-1 was quantified in all the samples (cells infected with BoAHV-1 at MOI 1, in the presence or not of Taurisolo®, at 0, 1, 3, 6, 12, 24, 48, and 72 h p.i.) by quantitative real-time PCR, as described (Fiorito et al., 2022). Briefly, the detection was carried out on a Quant Studio 5 Real-Time PCR thermal cycler (Thermo Fisher Scientific, Waltham, Massachusetts, USA) in a total volume of 25 µL containing: 5 µL of nucleic acids extract, 12.5 µL of TaqMan Universal PCR Master Mix 2X (Thermo Fisher Scientific, Waltham,

Massachusetts, USA), 1 µL (4.5 µM) of primer forward gBF (5′- TGTGGAC-CTAAACCTCACGGT-3′), 1 µL (4.5 µM) of primer reverse gBR (5′-GTAGTCGAGCAGACCCGTGTC-3′) and 1 µL (3 µM) of probe gB-P (FAM-5′-AGGACCGCGAGTTCTTGCCGC-3′-TAMRA). The thermal profile consisted of initial denaturation for 15 min at 95 ◦C, 45 cycles of amplification for 15 s at 95 ◦C and, 45 s at 60 ◦C (OIE Manual of Terrestrial Animals Cap. 3.4.11. par B.1.3.1 2017). Then, quantification was performed by a standard curve, analysing serial dilutions of the quantified extracted virus (from 1×10^7 to 1×10^1 $TCID_{50}$/mL) and plotting the $TCID_{50}$/mL versus the threshold cycle (Ct) (*Fiorito et al., 2022; Cerracchio et al., 2022a,b, 2023*).

2.10. *Statistical analysis*

Data are presented as mean ± S.D. GraphPad InStat Version 3.00 for Windows 95 (GraphPad Software, San Diego, CA) was used to analyze one-way ANOVA with Tukey's post-test). $p < 0.05$ was judged statistically significant.

3. Results

3.1. *Taurisolo® reduces MDBK cell death during BoAHV-1 infection*

To examine the effect of Taurisolo® during BoAHV-1 infection, cell viability by TB was first assessed, then cell proliferation by MTT assay was analyzed. The assessment of IC50 values of Taurisolo® and the doseresponse curve were performed by treating cells with different doses of Taurisolo®, as above described. Inhibition of cell growth was detected in MDBK cell treated with Taurisolo® IC50 values ranging between 1.5 and 3 mg/mL, at 48 h, while there were no significant alterations after treatment with lower concentrations of this nutraceutical (Fig. 1a,b). So, we choose to select the concentrations of 0.1 and 0.5 mg/mL to continue the experimental design. To confirm that the 0.5 mg/mL concentration is biocompatible and not cytotoxic, the mitochondrial redox activity of MDBK cells was analysed by MTT assay. After 48 h of exposure, Taurisolo ® at 0.5 mg/mL did not produce significant ($p > 0.05$) timedependent changes in the mitochondrial dehydrogenase's activity compared to control cells (Fig. 1c). Finally, to evaluate the effect of Taurisolo® during BoAHV-1 infection, MDBK cells were infected with BoAHV-1 at MOI of 0.1 or 10 and treated or not with 0.1 mg/mL and 0.5 mg/mL of nutraceutical. After 48 h of treatment, cell viability and proliferation were evaluated. As

shown in Figs, 2a,b, Taurisolo® was able to increase – in a significant way ($p < 0.01$) - the cell viability during BoAHV-1 infection already at 0.1 mg/mL, and its effect resulted stronger at the concentration of 0.5 mg/mL. At this last concentration, the nutraceutical also increased cell proliferation ($p < 0.05$) in MDBK cells (Fig. 2c). Therefore, the concentration of Taurisolo® at 0.5 mg/mL was confirmed to be used throughout the study. Altogether, at the end of BoAHV-1 infection, in the presence of a nontoxic dose of 0.5 mg/mL, Taurisolo® significantly reduced the cytotoxicity induced by BoAHV-1 infection of MDBK cells.

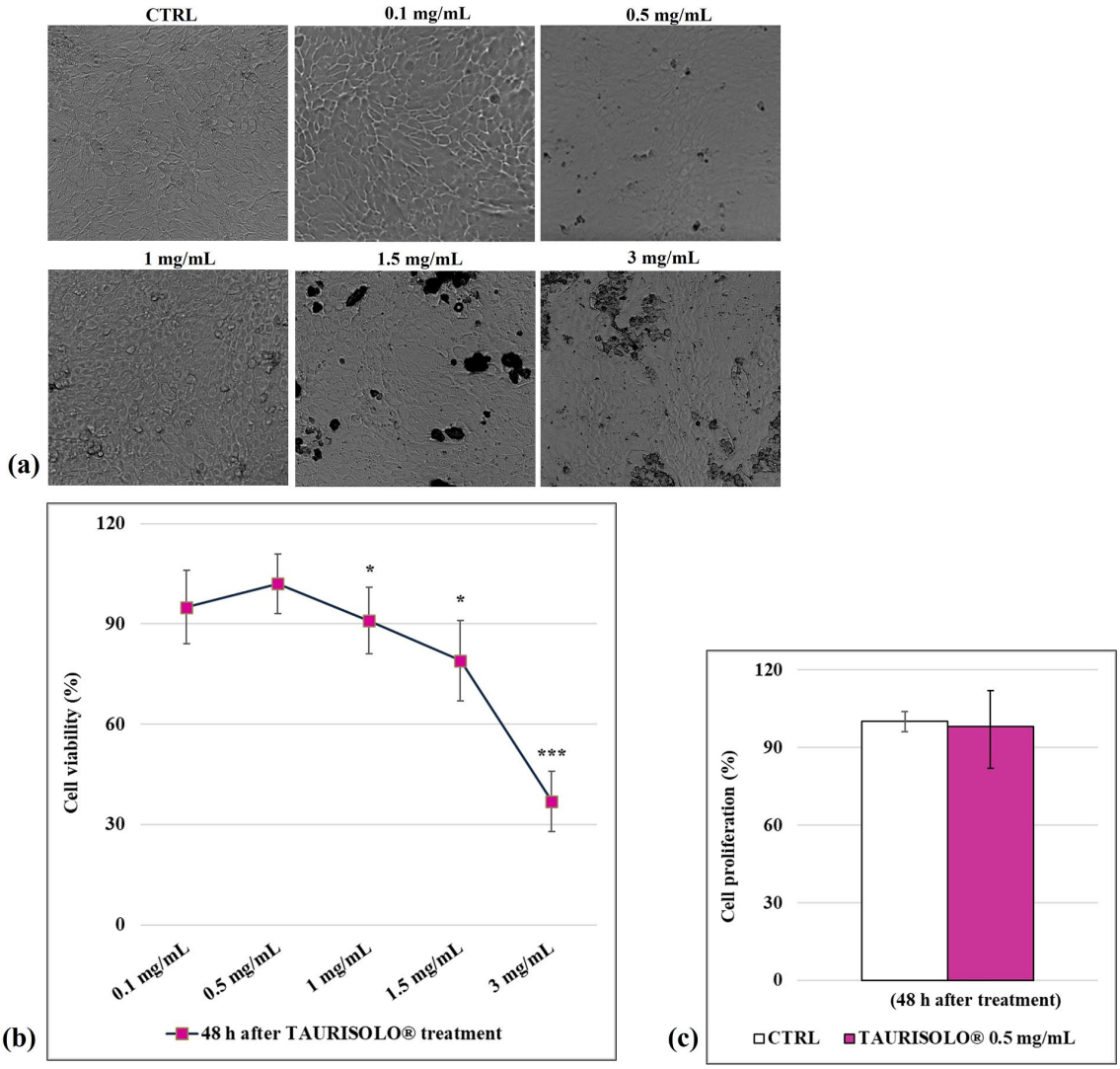

Fig. 1. Identification of Taurisolo® IC50 at different doses and doses-response curve in MDBK cells. (a) Microscope cells were stained with TB and scored by automated cell counter. (b) Dose-response curve of MDBK cells treated with Taurisolo® at different concentrations (0.1, 0.5, 1, 1.5, 3 mg/mL). At 48 h after treatment, cell viability was determined by TB staining while cells were attached to wells and counted under a light. (c) Dose-response curve of MDBK cells treated with Taurisolo® (0.5 mg/mL) for 48 h and assessed by MTT assay. Significant differences between control and Taurisolo®-treated cells are indicated by probability p. *** $p < 0.001$ and * $p < 0.05$. Scale bar 100 µm.

3.2. *Taurisolo® reduces distinctive features of morphological cell death during BoAHV-1 infection in MDBK cells*

To explore the effects of Taurisolo® in BoAHV-1-infected cells, we performed Giemsa staining, which allows to check the main differences between apoptosis and necrosis in cell morphology and evaluated it by light microscopy (*Banfalvi et al., 2017*). Taurisolo® exposed MDBK cells showed no cytomorphological changes when compared to controls (Fig. 3). Indeed, untreated infected cells, showed increased intercellular spaces and changes in cellular morphology such as chromatin condensation, fragmentation of nuclei, pyknosis and cell shrinkage, suggesting apoptosis activation) (*Leite et al., 1999; Banfalvi et al., 2017*) (Fig. 3, arrow). Furthermore, in infected cells, we observed typical signs of necrosis, due to nuclear and cytoplasmic swelling with chromatin appearing uniformly dense because of plasma membrane break (Fig. 3, arrowhead) (*Leite et al., 1999; Banfalvi et al., 2017*). On the other hand, only a few necrotic cell death features were detected in BoAHV-1 infected cells exposed to Taurisolo® (Fig. 3, arrowhead).

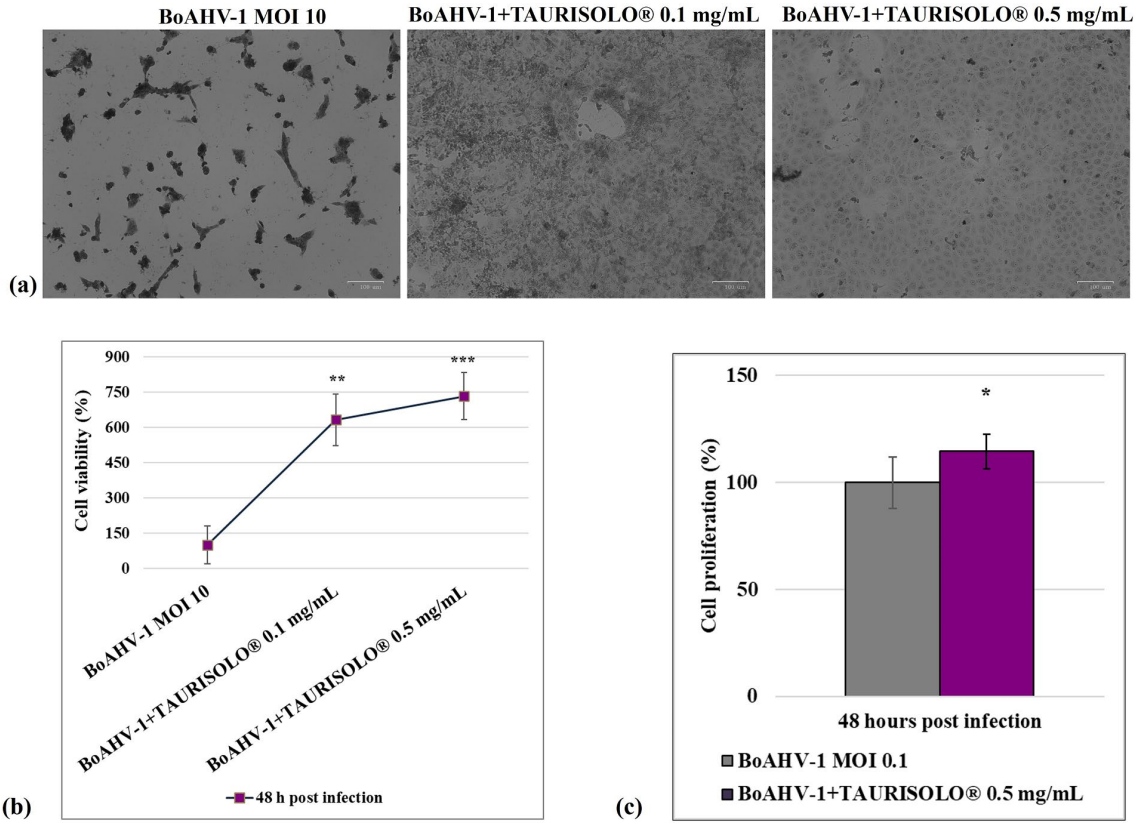

Fig. 2. Taurisolo® reduces cell death during BoAHV-1 infection. (a) Taurisolo® decreases cell death during BoAHV-1 infection in MDBK cells. Cells were infected with BoAHV-1, in the presence or absence of Taurisolo®. At 48 h p.i., cells were examined under a light microscope. In Taurisolo®-treated infected cells, only a few signs of cell death were

found. Scale bar 100 µm. (b) Dose–response curve of MDBK cells infected with BoAHV-1 and treated with Taurisolo® at different concentrations (0.1, 0.5 mg/mL). At 48 h after treatment, cell viability was assayed by using TB staining while cells were attached to wells and counted under a light microscope. (c) Dose–response curve of MDBK cells infected with BoAHV-1, treated with Taurisolo® (0.5 mg/mL) for 48 h and analyzed by MTT assay. Significant differences between analysed groups are indicated by probability p. *** $p < 0.001$, ** $p < 0.01$ and * $p < 0.05$.

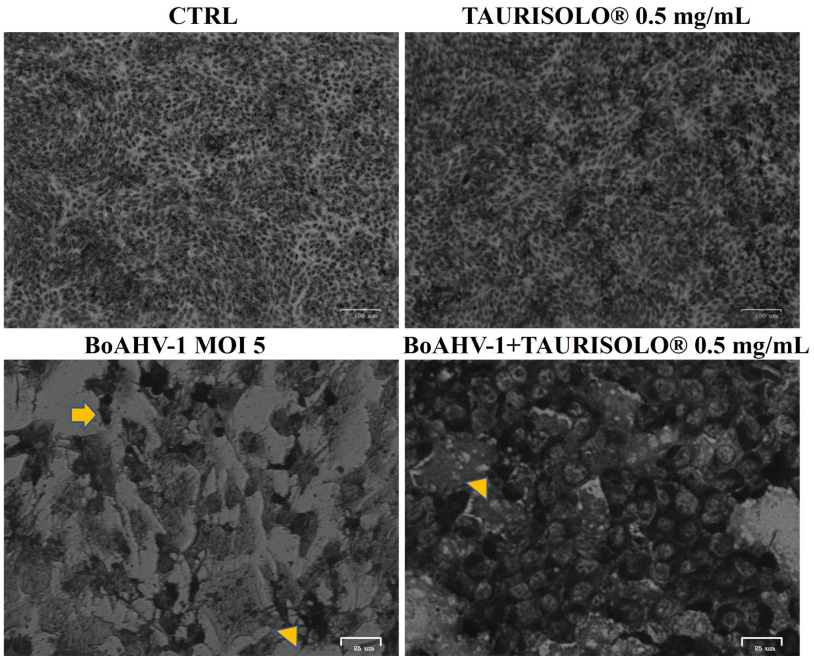

Fig. 3. Taurisolo® decreases morphological cell death features during BoAHV-1 infection. Taurisolo® reduces morphological cell death features during BoAHV-1 infection in MDBK cells. Cells were infected with BoAHV-1, in the presence or absence of Taurisolo®. At 24 h p.i., cells after Giemsa staining were examined under a light microscope. Photomicrographs showed no morphological alterations in Taurisolo® uninfected groups compared to control. By comparing BoAHV-1- infected cells to the control, some cells displayed apoptotic features, attributable to pyknotic nuclei and nuclear fragmentation (arrow), or necrosis marks, such as nuclear and cytoplasmic swelling (arrowhead). In Taurisolo®-treated infected cells, only a few signs of necrosis were found (arrowhead). Scale bar 100 and 25 µm.

Overall, these findings revealed that MDBK cells infected with BoAHV-1 and exposed to Taurisolo® were less subjected to apoptotic or necrotic cell death.

3.3. *Taurisolo® reduces virus yield and downregulates the expression of bICP0 during BoAHV-1 infection in MDBK cells*

To investigate Taurisolo® effects on virus production in MDBK BoAHV-1-infected cells, virus titer and viral CPE were analysed. Hence, MDBK cells were infected with BoAHV-1 at MOI of 1, in the presence or not of Taurisolo® at the nontoxic concentration of 0.5 mg/mL and processed. Following BoAHV-1 infection, a statistically significant ($p < 0.001$) decline in virus titer was found from 12 to 72 h post infection in cells treated with Taurisolo® (Fig. 4a). Furthermore, at 24 h p.i., a marked CPE was detected in

infected groups, caused by the development of syncytia and by destruction of cellular sheet, whereas these features were noticeably reduced in Taurisolo®-treated infected cells (Fig. 3). Interestingly, these characteristics were confirmed also in treated cells infected with BoAHV-1 at MOI 1 after 120 h p.i. (Fig. 4b). These results suggested that the nutraceutical significantly reduces virus yield and CPE during BoAHV-1 infection in MDBK cells. In addition, to further investigate Taurisolo® influence in BoAHV-1 infection, we explored the expression of bICP0, the key protein concerning the transcription of BoAHV-1 (Wirth et al., 1992; Muylkens et al., 2007; Fiorito et al., 2013; Jones, 2019). After 24 h p.i., the expression of bICP0 in BoAHV-1 infected cells (MOI 10) was considerably downregulated in the presence of Taurisolo® (Fig. 5a). This result was confirmed by integrated measurement of density fluorescence (Fig. 5b). These findings show that bICP0 viral protein, expressed in BoAHV-1- infected cells, was reduced in infected cells exposed to Taurisolo®.

(a)

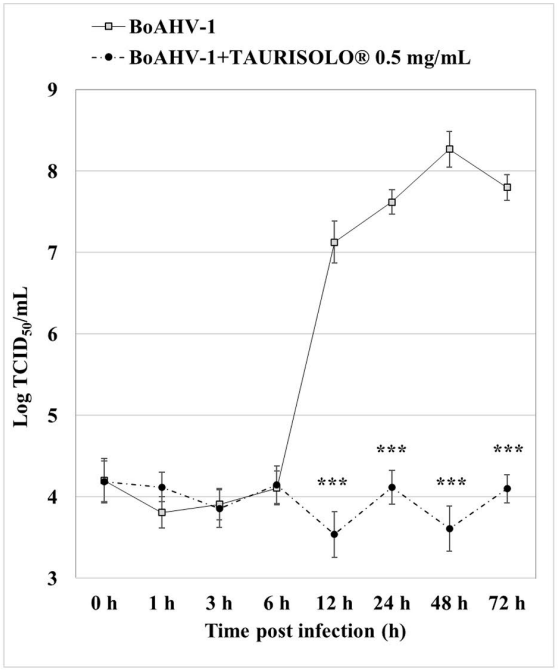

(b)

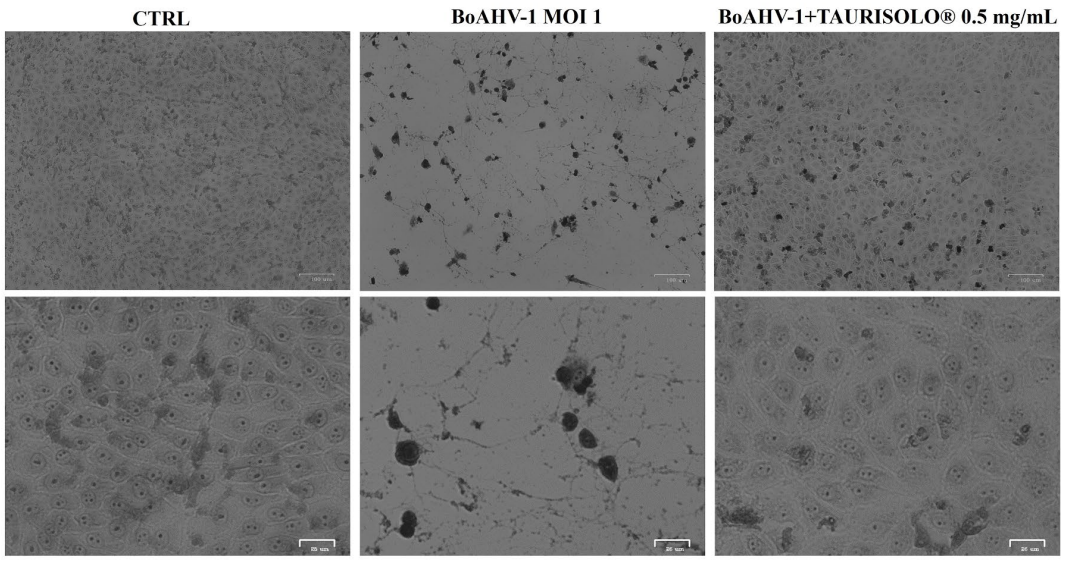

Fig. 4. Taurisolo® decreases virus yield during BoAHV-1 infection in MDBK cells. Cells were infected with BoAHV-1 in the presence or absence of Taurisolo®. (a) For viral growth curves, MDBK cells were infected with BoAHV-1 in the presence or absence of Taurisolo®. At indicated times, virus titer was evaluated by real-time PCR. Significant differences between BoAHV-1-infected cells and Taurisolo®-treated infected cells are indicated by probability p. *** $p < 0.001$. (b) For CPE evaluation, cells were infected with BoAHV-1 in the presence or absence of Taurisolo®. At 120 h p.i., CPE was observed. Scale bar 100 and 25 μm.

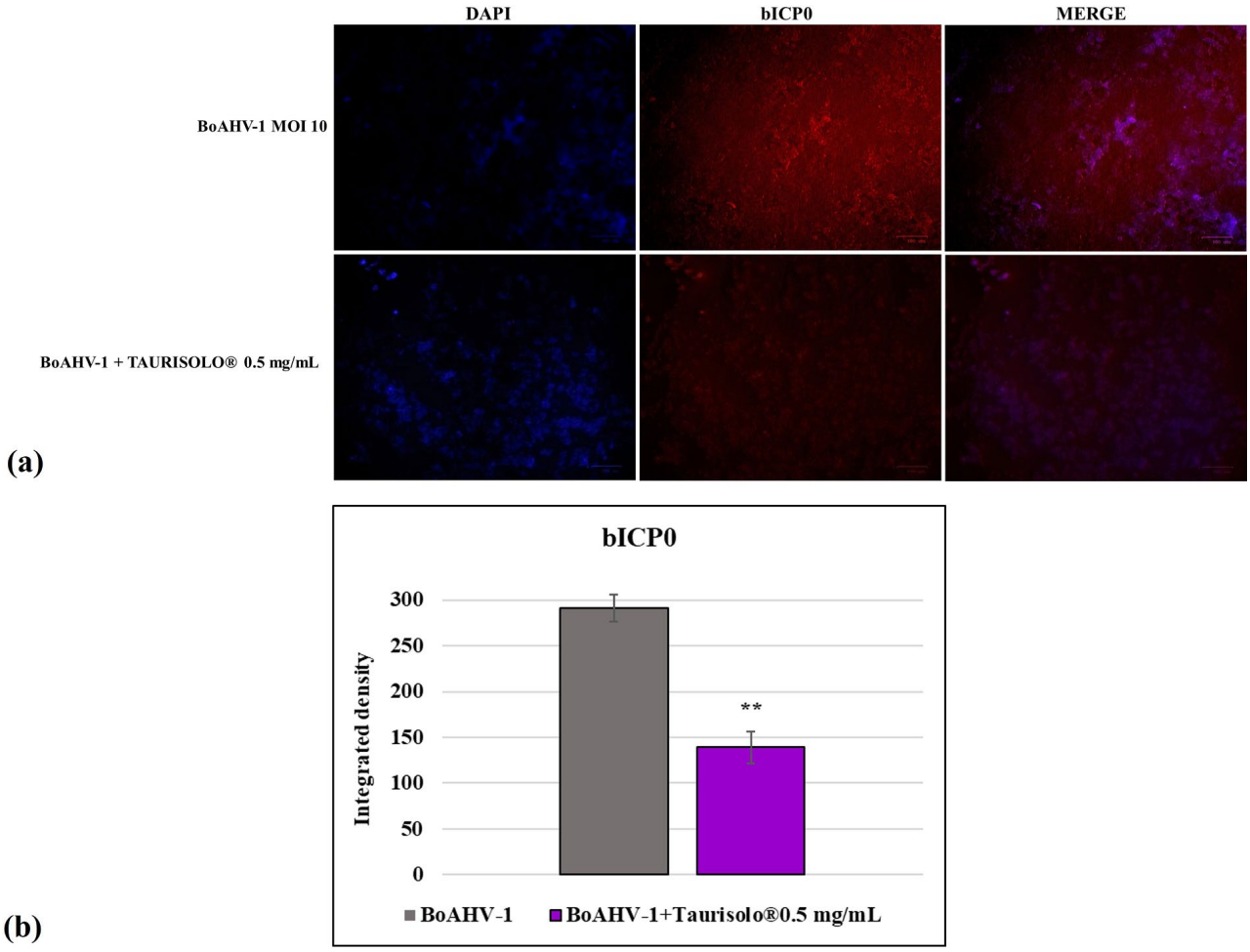

Fig. 5. Taurisolo® decreases the expression of bICP0 during BoAHV-1 infection in MDBK cells. Cells were infected with BoAHV-1, in the presence or absence of Taurisolo®, and after 24 h p.i, immunofluorescence staining for bICP0 (red fluorescence) was performed as described in the Method section. Nuclei were counterstained with DAPI. (a) During infection, bICP0 was localized both in nucleus and cytoplasm. In the presence of Taurisolo®, the expression of bICP0 was markedly reduced during BoAHV-1 infection. Scale bar 100 μm. (b) Bars correspond to the mean ratio produced from the integrated density (product of the area and mean intensity of fluorescence) calculated by ImageJ of the bICP0 expression. Error bars are standard deviation measurement. Significant differences between unexposed infected groups and Taurisolo®-treated infected cells are indicated by probability p. ** $p < 0.01$.

3.4. *Taurisolo® upregulates the expression of AhR during BoAHV-1 infection in MDBK cells*

To investigate the possible action of Taurisolo® in the regulation of AhR, we performed immunofluorescence analysis. Taurisolo® strongly stimulated AhR activation in MDBK cells until 120 h of treatment (Fig. 6a), and a remarkable stimulation of AhR in Taurisolo®-treated cells was detected during infection with BoAHV-1 after 24 h p.i. (Fig. 6b). These results were confirmed by integrated measurement of density fluorescence (Fig. 6c, d). These results showed the Taurisolo® capability to stimulate AhR cellular receptor in both BoAHV-1 infected and uninfected MDBK cells.

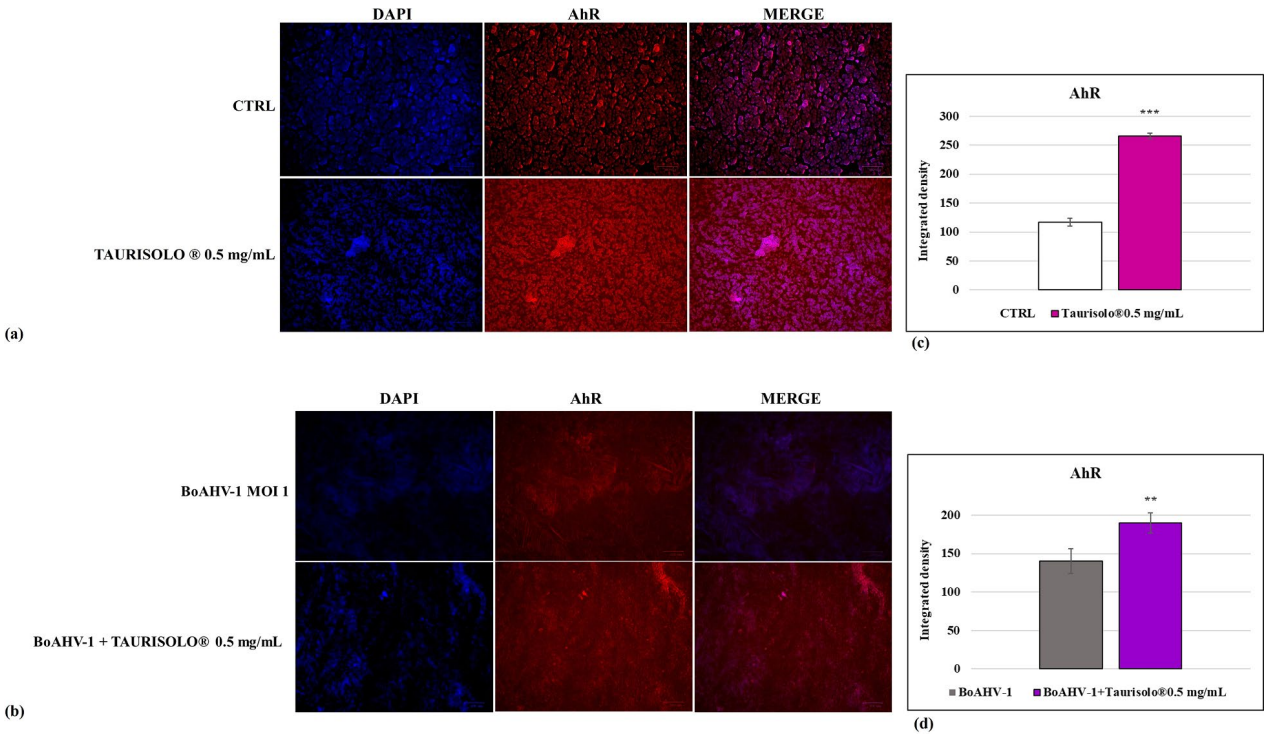

Fig. 6. Taurisolo® induces the expression of AhR during BoAHV-1 infection in MDBK cells. Representative microphotographs of uninfected (control) or infected cells (BoAHV-1), Taurisolo® -treated infected (BoAHV-1+Taurisolo®), and uninfected cells (Taurisolo®), stained with immunofluorescence for AhR (red fluorescence), as described in the Methods section. Nuclei were counterstained with DAPI. (a) AhR was expressed in MDBK cells and localized in both the nucleus and cytoplasm. The expression of AhR until 120 h after treatment was induced in the presence of Taurisolo®. (b) During infection, the expression of AhR was drastically reduced. In the presence of Taurisolo®, at 24 h p.i., the expression of AhR was remarkably enhanced during BoAHV-1 infection. Scale bar 100 µm. (c-d) Bars are the mean ratio produced from the integrated density (product of the area and mean intensity of fluorescence) calculated by ImageJ of the AhR expression. Error bars are standard deviation measurement. Significant differences between control cells and Taurisolo® exposed groups, as well as between unexposed infected groups and Taurisolo®- treated infected cells are indicated by probability p. *** $p < 0.001$ and ** $p < 0.05$.

4. Discussion

Pharmaceutical research is strongly involved in the development of novel therapeutic strategies against viral diseases in order to minimizeantiviral agents' toxicity and fight antibiotic-resistance phenomena, as well. In this context, plant extracts have been extensively explored as nontoxic natural remedies. To date, anti-herpesvirus natural compounds are scarce; for instance, anti-herpesvirus activity was detected in polyphenols (*Vilhelmova-Ilieva et al., 2014; Boubaker-Elandalousi et al., 2014; Annunziata et al., 2018a*), as well as in flavonoid derivatives (*Akula et al., 2002; Boubaker-Elandalousi et al., 2014; Zhu et al., 2015, 2018*). Taurisolo® is an extract which mainly contains polyphenols and flavonoids, and, in this study, we showed its capability to induce an

excellent defense reaction against BoAHV-1 activity, in infected MDBK cells, by stimulating a significant improvement in cell viability and proliferation. Generally, BoAHV-1 promotes cell death in a cell-type dependent manner (*Geiser et al., 2008; Fiorito et al., 2020*). Herein, during BoAHV-1 infection, morphological analysis of MDBK showed cell death hallmarks that were remarkably decreased by treatment with Taurisolo ®. Interestingly, BoAHV-1 infected MDBK cells treated with the proteasome inhibitor MG-132 (*Fiorito et al., 2017a,2021*) and the fungal metabolite 3-O-methylfunicone (OMF) (*Fiorito et al., 2022*) showed comparable morphological features of cell defense. Furthermore, a significant decrease in BoAHV-1 replication was detected in Taurisolo® treated infected cells, which showed a relevant decrease both in CPE and in virus yield. These findings suggest that polyphenols and flavonoids extract could act as anti-herpesvirus agents by influencing the early phases of infection (*Chattopadhyay et al., 2009; Boubaker-Elandalousi et al., 2014*). Indeed, Taurisolo® blocks HSV-1 and HSV-2 infection, in co-treatment as well as in pre-treatment, showing an inhibitory action in the early phases of both herpesviruses (*Zannella et al., 2023*). Indeed, gene expression of herpesviruses occurs in three phases named immediate-early, early, and late. The bovine homologue of HSV-1 ICP0, bICP0, regulates all three stages and promotes productive infection (*Fraefel et al., 1994; Inman et al., 2001; Fiorito et al., 2010; Jones 2019*). In our study, Taurisolo® remarkably reduced the expression of bICP0, in bovine cells and similar anti-BoAHV-1 activities were previously reported in the presence of chemical (MG-132) or natural (OMF) compounds (*Fiorito et al., 2017a,2021,2022*). Furthermore, Taurisolo® stimulated the activation of AhR in MDBK cells, also during BoAHV-1 infection. AhR can be activated by both endogenous and exogenous organic substrates, like tryptophan metabolites, bilirubin, biliverdin, environmental pollutants (dioxin), and microbial metabolites (*Bock, 2021*). After activation and translocation into the nucleus, AhR may stimulate target genes like AhR repressor, detoxifying monooxygenases (CYP1A1 and CYP1B1) and cytokines. Recent evidence suggests that diet products can activate and/or inhibit the AhR signaling pathway. Noteworthy, dietary flavonoids are the greatest class of natural AhR ligands, and some agonists/antagonists of AhR are used in clinical practice for cancer treatment (*Yang et al., 2019*). AhR is also implicated in the host response to viruses, such as coronaviruses (*Tang et al., 2005; Grunewald et al., 2020; Giovannoni et al., 2021; Cerracchio et al., 2022a,b*). Furthermore, targeting AhR may enhance the host response to herpesvirus infections (*Chen et al., 2021; Torti et al., 2021*). The first evidence of the involvement of AhR in

inhibitory activity against BoAHV-1 due to OMF, a secondary metabolite produced by Talaromyces pinophilus, was recently observed in MDBK (*Fiorito et al., 2022*), a cell line which expresses the AhR (*Fiorito et al., 2014, 2022*). Numerous AhR ligands with different properties have been identified: endobiotic, phytochemical, microbiota-generated ligands as well as xenobiotics/drugs (*Bock 2020*). Moreover, AhR signaling influences the immune response to different microorganisms (*Torti et al., 2021*). The replication of herpesviruses (cytomegalovirus, HSV-1, HSV-2, BoAHV-1) was stimulated by the activation of AhR. Dioxin (TCDD), a toxic environmental contaminant, through AhR, might provoke immune-suppression and enhances responsiveness to infectious agents (*Fiorito et al. 2017b, c; Bock 2021*). Veiga-Parga et al., showed that during HSV-1 infection in mice, dioxin-treated mice had the highest virus titers (*2011*). Particularly, if AhR was induced before infection, an increased number of mice died because of herpes encephalitis. Whereas, if AhR stimulation happened after HSV-1 infection, the disease features were ameliorated (*Veiga-Parga et al., 2011*). These findings also highlight the influence of timing in AhR activation in balancing pathology and antiviral defensive immunity (*Torti et al., 2021*). Taurisolo® is primarily composed of polyphenols and flavonoids, arylic nature molecules, which may interact with AhR. Flavonoids such as quercetin might be indirect AhR agonists (*Bock 2020*). The well-known polyphenol resveratrol has been recently recognized as a non-selective antagonist of AhR (*Coelho et al., 2022*). However, the hypothetical interaction between Taurisolo® and AhR in MDBK cells requests further investigations. Overall, our findings revealed a promising antiviral activity of Taurisolo® during BoAHV-1 infection in MDBK cells, by affecting AhR. Hence, AhR may be a new target to develop potential antiviral treatments.

References

Akula, S.M., Hurley, D.J., Wixon, R.L., Wang, C., Chase, C.C., 2002. Effect of genistein on replication of bovine herpesvirus type 1. Am. J. Vet. Res. 63, 1124–1128. https:// doi.org/10.2460/ajvr.2002.63.1124.

Altamura, G., Power, K., Martano, M., degli Uberti, B., Galiero, G., De Luca, G., Maiolino, P., Borzacchiello, G., 2018. Felis catus papillomavirus type-2 E6 binds to E6AP, promotes E6AP/p53 binding and enhances p53 proteasomal degradation. Sci. Rep. 8, 17529. https://doi.org/10.1038/s41598-018-35723-7.

Annunziata, G., Cap´o, X., Quetglas-Llabr´es, M.M., Monserrat-Mesquida, M., Tejada, S., Tur, J.A., Ciampaglia, R., Guerra, F., Maisto, M., Tenore, G.C., Novellino, E., Sureda, A., 2021a. Ex vivo study on the antioxidant activity of a winemaking byproduct polyphenolic extract (Taurisolo®) on human neutrophils. Antioxidants (Basel) 10 (7), 1009. https://doi.org/10.3390/antiox10071009.

Annunziata, G., Ciampaglia, R., Maisto, M., D'Avino, M., Caruso, D., Tenore, G.C., Novellino, E., 2021b. Taurisolo, a grape pomace polyphenol nutraceutical reducing the levels of serum biomarkers associated with atherosclerosis. Front. Cardiovasc. Med. 8, 697272 https://doi.org/10.3389/fcvm.2021.697272.

Annunziata, G., Maisto, M., Schisano, C., Ciampaglia, R., 2018a. Resveratrol as a novel anti-herpes simplex virus nutraceutical agent: an overview. Viruses 10 (9), 473. https://doi.org/10.3390/v10090473.

Annunziata, G., Jimenez-García, M., Tejada, S., Moranta, D., Arnone, A., Ciampaglia, R., Tenore, G.C., Sureda, A., Novellino, E., Cap´o, X., 2020. Grape polyphenols ameliorate muscle decline reducing oxidative stress and oxidative damage in aged rats. Nutrients 12, 1280. https://doi.org/10.3390/nu12051280.

Annunziata, G., Maisto, M., Schisano, C., Ciampaglia, R., Daliu, P., Narciso, V., Tenore, G.C., Novellino, E., 2018b. Colon bioaccessibility and antioxidant activity of white, green and black tea polyphenols extract after in vitro simulated gastrointestinal digestion. Nutrients 10, 1711. https://doi.org/10.3390/nu10111711.

Annunziata, G., Maisto, M., Schisano, C., Ciampaglia, R., Narciso, V., Tenore, G.C., Novellino, E., 2019a. Effects of grape pomace polyphenolic extract (Taurisolo ®) in reducing tmao serum levels in humans: preliminary results from a randomized, placebo-controlled, cross-over study. Nutrients 11, 139. https://doi.org/10.3390/nu11010139.

Annunziata, G., Maisto, M., Schisano, C., Ciampaglia, R., Narciso, V., Hassan, S.T.S., Tenore, G.C., Novellino, E., 2019b. Effect of grape pomace polyphenols with or without pectin on TMAO serum levels assessed by LC/MS-based assay: a preliminary clinical study on overweight/obese subjects. Front. Pharmacol. 10, 575. https://doi.org/10.3389/fphar.2019.00575.

Badolati, N., Masselli, R., Sommella, E., Sagliocchi, S., Di Minno, A., Salviati, E., Campiglia, P., Dentice, M., Tenore, G.C., Stornaiuolo, M., Novellino, E., 2020. The hepatoprotective effect of taurisolo, a nutraceutical enriched in resveratrol and polyphenols, involves activation of mitochondrial metabolism in mice liver. Antioxidants (Basel) 11 (5), 410. https://doi.org/10.3390/antiox9050410, 9.

Banfalvi, G., 2017. Methods to detect apoptotic cell death. Apoptosis 22, 306–323. https://doi.org/10.1007/s10495-016-1333-3.

Bock, K.W., 2021. Aryl hydrocarbon receptor (AHR), integrating energy metabolism and microbial or obesity-mediated inflammation. Biochem. Pharmacol. 184, 114346 https://doi.org/10.1016/j.bcp.2020.114346.

Bock, K.W., 2020. Aryl hydrocarbon receptor (AHR) functions: balancing opposing processes including inflammatory reactions. Biochem. Pharmacol. 178, 114093 https://doi.org/10.1016/j.bcp.2020.114093. Epub 2020 Jun 11.

Boubaker-Elandalousi, R., Mekni-Toujani, M., Kaabi, B., Larbi, I., Diouani, M.F., Gharbi, M., Akkari, H., B'chir, F., Ghram, A., 2014. Non-cytotoxic Thymus capitata extracts prevent Bovine herpesvirus-1 infection in cell cultures. BMC Vet. Res. 10, 231. https://doi.org/10.1186/s12917-014-0231-6.

Cerracchio, C., Iovane, V., Salvatore, M.M., Amoroso, M.G., Dakroub, H., DellaGreca, M., Nicoletti, R., Andolfi, A., Fiorito, F., 2022a. Effectiveness of the fungal metabolite 3- o-methylfunicone towards canine coronavirus in a canine fibrosarcoma cell line (A72). Antibiotics 11, 1594. https://doi.org/10.3390/antibiotics11111594.

Cerracchio, C., Salvatore, M.M., Del Sorbo, L., Serra, F., Amoroso, M.G., DellaGreca, M., Nicoletti, R., Andolfi, A., Fiorito, F., 2023. In vitro evaluation of antiviral activities of funicone-like compounds vermistatin and penisimplicissin against canine coronavirus infection. Antibiotics (Basel) 12 (8), 1319. https://doi.org/10.3390/antibiotics12081319. Aug 15.

Cerracchio, C., Serra, F., Amoroso, M.G., Fiorito, F., 2022b. Canine coronavirus activates aryl hydrocarbon receptor during in vitro infection. Viruses 14, 2437. https://doi.org/10.3390/v14112437.

Chang, L., Zhu, L., 2020. Dewormer drug fenbendazole has antiviral effects on BoHV-1 productive infection in cell cultures. J. Vet. Sci. 21, e72. https://doi.org/10.4142/jvs.2020.21.e72.

Chattopadhyay, D., Chawla Sarkar, M., Chatterjee, T., Dey, R., Bag, P., Chakrabarty, S., Khan, M.T.H., 2009. Recent advancements for the evaluation of antiviral activities of natural products. New Biotechnol. 25, 347–368. https://doi.org/10.1016/j.nbt.2009.03.007.

Chen, J., Liang, J., Xu, H., Liu, W., Liu, S., Duan, L., Li, F., Wang, Z., Liu, Y., McSharry, B., Feng, C.G., Zhang, G., 2021. Targeting aryl hydrocarbon receptor signaling enhances type i interferon-independent resistance to herpes simplex virus. Microbiol. Spectr. 9, e0047321 https://doi.org/10.1128/Spectrum.00473-21.

Coelho, N.R., Pimp˜ao, A.B., Correia, M.J., Rodrigues, T.C., Monteiro, E.C., Morello, J., Pereira, S.A., 2022. Pharmacological blockage of the AHR-CYP1A1 axis: a call for in vivo evidence. J. Mol. Med. (Berl.) 100 (2), 215–243. https://doi.org/10.1007/s00109-021-02163-2.

De Martino, L., Marf´e, G., Longo, M., Fiorito, F., Montagnaro, S., Iovane, V., Decaro, N., Pagnini, U., 2010. Bid cleavage, cytochrome c release and caspase activation in canine coronavirus-induced apoptosis. Vet. Microbiol. 141, 36–45. https://doi.org/10.1016/j.vetmic.2009.09.001.

Fiorito, F., Cantiello, A., Granato, G.E., Marf`e, G., Ciarcia, R., Florio, S., Pagnini, U., De Martino, L., Iovane, G., 2014. Modulation of telomerase activity, bTERT and c-Myc induced by 2,3,7,8-tetrachlorodibenzo-p-dioxin during Bovine Herpesvirus 1 infection in MDBK cells. Toxicol. In Vitro 28, 24–30. https://doi.org/10.1016/j.tiv.2013.06.020.

Fiorito, F., Ciarcia, R., Granato, G.E., Marf`e, G., Iovane, V., Florio, S., De Martino, L., Pagnini, U., 2011. 2,3,7,8-tetrachlorodibenzo-p-dioxin induced autophagy in a bovine kidney cell line. Toxicology 290, 258–270. https://doi.org/10.1016/j.tox.2011.10.004.

Fiorito, F., Iovane, V., Cantiello, A., Marullo, A., De Martino, L., Iovane, G., 2017a. MG-132 reduces virus release in Bovine herpesvirus-1 infection. Sci. Rep. 7, 13306. https://doi.org/10.1038/s41598-017-13717-1.

Fiorito, F., Iovane, V., Marullo, A., Costagliola, A., Granato, G.E., De Martino, L., 2017b. 2,3,7,8-Tetrachlorodibenzo-p-dioxin influences bovine herpesvirus 1 replication through upregulation of SIRT3 and cytoskeletal reorganization. Vet. Res. Commun. 41 (4), 299–306. https://doi.org/10.1007/s11259-017-9701-1.

Fiorito, F., Irace, C., Di Pascale, A., Colonna, A., Iovane, G., Pagnini, U., Santamaria, R., De Martino, L., 2013. 2,3,7,8-Tetrachlorodibenzo-p-dioxin promotes BHV-1 infection in mammalian cells by interfering with iron homeostasis regulation. PLoS ONE 8, e58845. https://doi.org/10.1371/journal.pone.0058845.

Fiorito, F., Marf`e, G., De Blasio, E., Granato, G.E., Tafani, M., De Martino, L., Montagnaro, S., Florio, S., Pagnini, U., 2008a. 2,3,7,8-tetrachlorodibenzo-p-dioxin regulates bovine herpesvirus type 1 induced apoptosis by modulating Bcl-2 family members. Apoptosis 13, 1243–1252. https://doi.org/10.1007/s10495-008-0249-y.

Fiorito, F., Marf`e, G., Granato, G.E., Ciarcia, R., De Blasio, E., Tafani, M., Florio, S., De Martino, L., Muzi, G., Pagnini, U., Giordano, A., 2010. 2,3,7,8-Tetrachlorodibenzo-pdioxin modifies expression and nuclear/cytosolic localization of bovine herpesvirus 1 immediate-early protein (bICP0) during infection. J. Cell. Biochem. 111, 333–342. https://doi.org/10.1002/jcb.22700.

Fiorito, F., Nocera, F.P., Cantiello, A., Iovane, V., Lambiase, S., Piccolo, M., Ferraro, M. G., Santamaria, R., De Martino, L., 2020. Bovine herpesvirus-1 infection in mouse neuroblastoma (Neuro-2A) cells. Vet. Microbiol. 247, 108762 https://doi.org/10.1016/j.vetmic.2020.108762.

Fiorito, F., Pagnini, U., De Martino, L., Montagnaro, S., Ciarcia, R., Florio, S., Pacillo, M., Fucito, A., Rossi, A., Iovane, G., Giordano, A., 2008b. 2,3,7,8-tetrachlorodibenzo-pdioxin increases bovine herpesvirus type-1 (BHV-1) replication in Madin-Darby Bovine Kidney (MDBK) cells in vitro. J. Cell. Biochem. 103, 221–233. https://doi.org/10.1002/jcb.21398.

Fiorito, F., Santamaria, R., Irace, C., De Martino, L., Iovane, G., 2017c. 2,3,7,8-tetrachlorodibenzo-p-dioxin and the viral infection. Environ. Res. 153, 27–34. https://doi.org/10.1016/j.envres.2016.11.004.

Fiorito, F., Cerracchio, C., Salvatore, M.M., Serra, F., Pucciarelli, A., Amoroso, M.G., Nicoletti, R., Andolfi, A., 2022. Antiviral property of the fungal metabolite 3-Omethylfunicone in bovine herpesvirus 1 Infection. Microorganisms 10, 188. https://doi.org/10.3390/microorganisms10010188.

Fiorito, F., Irace, C., Nocera, F.P., Piccolo, M., Ferraro, M.G., Ciampaglia, R., Tenore, G. C., Santamaria, R., De Martino, L., 2021. MG-132 interferes with iron cellular homeostasis and alters virulence of bovine herpesvirus 1. Res. Vet. Sci. 137, 1–8. https://doi.org/10.1016/j.rvsc.2021.04.023.

Fraefel, C., Zeng, J., Choffat, Y., Engels, M., Schwyzer, M., Ackermann, M., 1994. Identification and zinc dependence of the bovine herpesvirus 1 transactivator protein BICP0. J. Virol. 68, 3154–3162. https://doi.org/10.1128/JVI.68.5.3154-3162.1994, 1994.

Geiser, V., Rose, S., Jones, C., 2008. Bovine herpesvirus type 1 induces cell death by a cell-type-dependent fashion. Microb. Pathog. 44, 459–466. https://doi.org/10.1016/j.micpath.2007.10.014.

Giovannoni, F., Li, Z., Remes-Lenicov, F., D´avola, M.E., Elizalde, M., Paletta, A., Ashkar, A.A., Mossman, K.L., Dugour, A.V., Figueroa, J.M., Barquero, A.A., Ceballos, A., Garcia, A.C., Quintana, F.J., 2021. AHR signaling is induced by infection with coronaviruses. Nat. Comm. 12 https://doi.org/10.1038/s41467-021-25412-x.

Grunewald, M.E., Shaban, M.G., Mackin, S.R., Fehr, A.R., Perlman, S., 2020. Murine coronavirus infection activates the aryl hydrocarbon receptor in an indoleamine 2,3-dioxygenase-independent manner, contributing to cytokine modulation and proviral TCDD-inducible-PARP expression. J. Virol. 94, 319–335. https://doi.org/10.1128/JVI.01743-19.

Inman, M., Zhang, Y., Geiser, V., Jones, C., 2001. The zinc ring finger in the bICPO protein encoded by bovine herpesvirus-1 mediates toxicity and activates productive infection. J. Gen. Virol. 82, 483–492. https://doi.org/10.1099/0022-1317-82-3-483.

Iscaro, C., Cambiotti, V., Petrini, S., Feliziani, F., 2021. Control programs for infectious bovine rhinotracheitis (IBR) in European countries: an overview. Anim. Health Res.Rev. 22, 136–146. https://doi.org/10.1017/S1466252321000116.

Jones, C., 2019. Bovine herpesvirus 1 counteracts immune responses and immunesurveillance to enhance pathogenesis and virus transmission. Front. Immunol. 10, 1008. https://doi.org/10.3389/fimmu.2019.01008.

Leite, M., Quinta-Costa, M., Leite, P.S., Guimar˜aes, J.E., 1999. Critical evaluation of techniques to detect and measure cell death-study in a model of UV radiation of the leukaemic cell line HL60. Anal. Cell. Pathol. 19, 139–151. https://doi.org/10.1155/1999/176515, 1999.

Longo, M., Fiorito, F., Marf˙e, G., Montagnaro, S., Pisanelli, G., De Martino, L., Iovane, G., Pagnini, U., 2009. Analysis of apoptosis induced by Caprine Herpesvirus 1 in vitro. Virus Res. 145 (2), 227–235. https://doi.org/10.1016/j.virusres.2009.07.008.

Martelli, A., Flori, L., Gorica, E., Piragine, E., Saviano, A., Annunziata, G., Di Minno, M.N. D., Ciampaglia, R., Calcaterra, I., Maione, F., Tenore, G.C., Novellino, E., Calderone, V., 2021. Vascular

effects of the polyphenolic nutraceutical supplement Taurisolo®: focus on the protection of the endothelial function. Nutrients 13 (5), 1540. https://doi.org/10.3390/nu13051540.

Muylkens, B., Thiry, J., Kirten, P., Schynts, F., Thiry, E., 2007. Bovine herpesvirus 1 infection and infectious bovine rhinotracheitis. Vet. Res. 38, 181–209. https://doi.org/10.1051/vetres:2006059.

Righi, C., Franzoni, G., Feliziani, F., Jones, C., Petrini, S., 2023. The cell-mediated immune response against bovine alphaherpesvirus 1 (BoHV-1) infection and vaccination. Vaccines (Basel) 11, 785. https://doi.org/10.3390/vaccines11040785.

Sanduzzi Zamparelli, S., Capitelli, L., Coppola, N., Venditto, C., Santoro, C., Annunziata, G., Bruzzese, D., Cuomo, N., Gentile, I., Bocchino, M., Sanduzzi Zamparelli, A., 2022. A phase II study on the effect of Taurisolo® Administered via AEROsol in hospitalized patients with mild to moderate COVID-19 Pneumonia: the TAEROVID-19 study. Cells 11, 1499. https://doi.org/10.3390/cells11091499.

Santamaria, R., Fiorito, F., Irace, C., De Martino, L., Maffettone, C., Granato, G.E., Di Pascale, A., Iovane, V., Pagnini, U., Colonna, A., 2011. 2,3,7,8-Tetrachlorodibenzo-pdioxin impairs iron homeostasis by modulating iron-related proteins expression and increasing the labile iron pool in mammalian cells. Biochim. Biophys. Acta-Mol. Cell Res. 1813, 704–712. https://doi.org/10.1016/j.bbamcr.2011.02.003.

Tang, B.S.F., Chan, K.H., Cheng, V.C.C., Woo, P.C.Y., Lau, S.K.P., Lam, C.C.K., Chan, T.L., Wu, A.K.L., Hung, I.F.N., Leung, S.Y., Yuen, K.Y., 2005. Comparative host gene transcription by microarray analysis early after infection of the Huh7 cell line by severe acute respiratory syndrome coronavirus and human coronavirus 229E. J. Vir. 79 https://doi.org/10.1128/JVI.79.10.6180-6193.2005.

Torti, M.F., Giovannoni, F., Quintana, F.J., García, C.C., 2021. The aryl hydrocarbon receptor as a modulator of anti-viral immunity. Front. Immunol. 12, 624293 https://doi.org/10.1016/j.bcp.2008.10.031.

Veiga-Parga, T., Suryawanshi, A., Rouse, B.T., 2011. Controlling viral immunoinflammatory lesions by modulating aryl hydrocarbon receptor signaling. PLoS Pathog. 7, e1002427 https://doi.org/10.1371/journal.ppat.1002427.

Vilhelmova-Ilieva, N., Jacquet, R., Quideau, S., Galabov, A.S., 2014. Ellagitannins as synergists of ACV on the replication of ACV-resistant strains of HSV 1 and 2. Antiviral Res. 110, 104–114. https://doi.org/10.1016/j.antiviral.2014.07.017. Epub 2014 Aug 9.

Wirth, U.V., Fraefel, C., Vogt, B., Vlcek, C., Paces, V., Schwyzer, M., 1992. Immediateearly RNA 2.9 and early RNA 2.6 of bovine herpesvirus 1 are 3' coterminal and encode a putative zinc finger transactivator protein. J. Virol. 66, 2763–2772. https://doi.org/10.1128/JVI.66.5.2763-2772.

Yang, T., Feng, Y.L., Chen, L., Vaziri, N.D., Zhao, Y.Y., 2019. Dietary natural flavonoids treating cancer by targeting aryl hydrocarbon receptor. Crit. Rev. Toxicol. 49, 445–460. https://doi.org/10.1080/10408444.2019.1635987.

Yesilbag, K., Toker, E.B., Ates, O., 2021. Ivermectin also inhibits the replication of bovine respiratory viruses (BRSV, BPIV-3, BoHV-1, BCoV and BVDV) in vitro. Virus Res. 297, 198384 https://doi.org/10.1016/j.virusres.2021.198384.

Yuan, Ch, Fu, X., Huang, L., Ma, Y., Ding, X., Zhu, L., Zhu, G., 2016. The synergistic antiviral effects of GSH in combination with acyclovir against BoHV-1 infection in vitro. Acta Virol. 60, 328–332. https://doi.org/10.4149/av_2016_03_328.

Zannella, C., Chianese, A., Annunziata, G., Ambrosino, A., De Filippis, A., Tenore, G.C., Novellino, E., Stornaiuolo, M., Galdiero, M., 2023. Antiherpetic activity of Taurisolo®, a grape Pomace polyphenolic extract. Microorganisms 11, 1346. https://doi.org/10.3390/microorganisms11051346.

Zhu, L., Ding, X., Zhang, D., Yuan, Ch, Wang, J., Ndegwa, E., Zhu, G., 2015. Curcumin inhibits bovine herpesvirus type 1 entry into MDBK cells. Acta Virol. 59, 221–227. https://doi.org/10.4149/av_2015_03_221.

Zhu, L., Wang, P., Yuan, W., Zhu, G., 2018. Kaempferol inhibited bovine herpesvirus 1 replication and LPS-induced inflammatory response. Acta Virol. 62, 220–225. https://doi.org/10.4149/av_2018_206.

CHAPTER 5 - *Evaluating the effect of Amenamevir combination therapy on HSV-1 resistance emergence*

Chapter 5 - Evaluating the effect of Amenamevir combination therapy on HSV-1 resistance emergence

Brief summary

In this project the antiviral effects of the combination therapy of amenamevir (AMV) and acyclovir (ACV) or Foscarnet (PFA) against HSV-1 KOS strain on HEL fibroblast cell line were evaluated. In particular, the study focused on the detection of new mutations that could have given drug resistance to HSV-1.

The results showed that known and unknown mutations have been detected on AMV+ACV combination, while for AMV+PFA combination any new mutation has been found.

1. Introduction

Herpes simplex virus 1 (HSV-1) is an ubiquitous alphaherpesvirus that infects humans and it has been estimated to be one of the most common pathogens (*James et al., 2020*). It is generally associated with oral herpes, due to close contact transmission, but it can also cause genital herpes, through oral–genital contact, as well as keratitis, encephalitis, and neonatal herpes when the virus is passed to a baby through close contact with a person suffering from an active HJSV-1 infection (*James et al., 2020; Šudomová M, Hassan STS, 2023*). The infection is initiated by surface viral glycoproteins that interact with host cell receptors, resulting in viral entry. Once infected the host cells, HSV-1 replicates easily in the tissues of the epithelial mucosa. Specifically, the double-stranded DNA is released into the nucleus where transcription and replication take place and new viral particles are produced (*Šudomová M, Hassan STS, 2023*). The cellular RNA polymerase II (RNA pol II) is responsible for the transcription of the viral genome with temporal expression of the immediate early (IE or α), early (E or β), and late (L or γ) viral genes. The replication process is facilitated by several viral proteins, including the origin binding protein (UL9), single-stranded DNA binding protein (ICP8), helicase–primase complex (UL5, UL8, and UL52), DNA polymerase (UL30), and its processivity factor (UL42) (*Packard et al., 2021*). Then, the assembly and egress of the viral particles occurs, following a complex multistage process involving different cellular compartments and the activity of various viral and cellular proteins. (*Šudomová M, Hassan STS, 2023*). HSV-1, as well as other

Herpesviruses, is responsible for two types of infection: lytic infection, characterized by active replication resulting in the production and release of virions, and latent infection, in which the virus remains latent in sensory neurons and does not actively replicate. From its latent state, HSV-1 can reactivate periodically, due to physiological or environmental factors, especially as a result of immunosuppression. The ability of the virus to establish latency makes humans life-long infected (*Šudomová M, Hassan STS, 2023*). While for immunocompetent subjects HSV-1 infection may resolve without serious consequences, immunocompromised subjects often suffer from severe disease requiring long-term antiviral therapy and this can lead to the development of drug-resistant viruses (*Andrei et al., 2013*).

The different steps of the replicative cycle of the virus, including viral entry, replication, assembly, and release, can be used as targets of antiviral drugs (*Šudomová M, Hassan STS, 2023*). Most antivirals currently in use against HSV-1 inhibit the viral DNA polymerase (DP), including acyclovir (ACV), the first-line treatment for HSV-1 infections (*Schalkwijk et al., 2022*). Tri-phosphorylation is necessary for the guanosine analogue ACV to bind and inhibit the viral DP. The first phosphorylation is performed by the viral thymidine kinase (TK), encoded by the UL23 gene, while the second and third steps are carried out by cellular kinases (*Sadowski et al., 2021*). Long-term treatment with ACV may increase the emergence of HSV-1 resistant strains, mostly due to the acquisition of mutations in the TK. Thus, new antivirals, which do not require TK phosphorylation, have been under investigation (*Sadowski et al., 2021; Schalkwijk et al., 2022*). In this sense, foscarnet (PFA), a pyrophosphate analogue that can inhibit the DP without TK-mediated phosphorylation, has been used as an alternative option for the treatment of ACV-resistant HSV-1 infections bearing mutations in the viral TK (*Sadowski et al., 2021; Sato et al., 2021*). Nevertheless, DP mutations can confer ACV/PFA cross-resistance and these strains have been detected in immunocompromised patients treated with PFA alone or associated to ACV (*Sato et al., 2021*). Because mutations in the DP may induce resistance to multiple antivirals, drugs with a different viral target, such as inhibitors of the helicase-primase complex are being developed (*Sadowski et al., 2021; Sato et al., 2021*). The helicase-primase complex is essential for replication of the viral genome and is composed of three proteins: helicase (encoded by UL5 gene), primase (encoded by UL52 gene) and cofactor subunits (encoded by UL8 gene), necessary for the replication of DNA (*Sato et al., 2021*). Amenamevir (AMV), one of the inhibitors of helicase-primase complex that is undergoing clinical investigation,

likely acts by inhibiting the protein-protein interactions between UL52 and UL5 encoded proteins, necessary for the formation of helicase-primase complex (*Sadowski et al., 2021*). Although AMV-resistance mutations have been found in both the helicase and primase, they do not seem to be related to the use of the inhibitor, which has only been approved in Japan for the treatment of herpes zoster, caused by reactivation of varicella zoster virus (*Sadowski et al., 2021; Sato et al., 2021*).

A possible strategy to stop resistance mutations emergence is multidrug therapy, that has already been proven to be effective for other viral infections such as HIV and Hepatitis C (*Sun et al., 2016; Wyles et al., 2016*). Indeed, different mechanism of actions of the virus can be affected at the same time, limiting viral replication and consequently the occurrence of any resistant mutations. On the other hand, these drugs can have an antagonizing, additive or synergistic effect with each other and identifying these interactions can be difficult (*Greeley et al., 2020*). However, it has previously been demonstrated that combined therapy is a good substitute for monotherapy (*Greeley et al., 2020; Chono et al., 2013*). Hence, the aim of this study is to evaluate the acquisition of HSV-1 drug resistance in vitro when treated with AMV alone or combined with ACV or PFA.

2. Material and methods

2.1.Cell cultures and virus infection

Human embryonic lung (HEL) fibroblasts (ATCC CCL-137) were cultured in Dulbecco's modified Eagle's medium (DMEM) supplemented with 8% fetal bovine serum (FBS), 0.1 mM non-essential amino acids, 1 mM sodium pyruvate, 2 mM L-glutamine, and 10 mM HEPES and incubated at 37 °C and 5% CO2. The HSV-1 wild-type strain KOS (ATCC VR-1493) was used.

2.2.Compounds

The compound used are: Amenamevir (Cayman Chemical), Acyclovir (Merck), Foscarnet (Merck).

2.3.Synergistic activity

HEL cells monolayers were infected with 100-fold the 50% cell culture infective dose ($CCID_{50}$) of the KOS strain and treated with different concentrations of AMV, ACV and

PFA alone or in combination (AMV+ACV or AMV+PFA). After 72 hours of infection, cells were frozen. After thawing, supernatants were collected and titrated in 10-fold dilution steps on HEL cells. Virus titers were determined by the Reed and Muench method (*Reed LJ, Muench H., 1938*). Synergistic activity was examined with the Zero Interaction Potency (ZIP) model using SynergyFinder (https://tangsoftwarelab.shinyapps.io/synergyfinder) (*Ianevski A et al., 2020*).

2.4.Cytotoxicity assay

A density of 5x103 cells/well was used to seed HEL cells in 96-well plates, and the cells were left to grow for 24 h. Cells were then treated with different concentrations of AMV, or combinations of compound (ACV+AMV or PFA+AMV) for 72 hours, after which cell counts were determined with a Z1 Coulter Counter (Beckman Coulter). SyngeryFinder 3.0 software was used to determine potential synergistic effects (Schalkwijk et al., 2022).

2.5.Selection of drug resistance

Increasing concentrations of AMV either separately or in combination with ACV or PFA, were used to passage the KOS strain in HEL cells in a sequence manner. Resistance selection was initiated from two distinct drug concentrations for each condition. The virus cultures were frozen when complete cytopathic effect (CPE) was observed. After thawing and freezing, the viruses were collected and used to infect new cell cultures, increasing the concentrations with each successive passage. From passage 6 onwards, drug concentrations were not further increased. After ten days of infection, if full CPE was not seen, the medium was replaced every five days with fresh medium, without compounds, until full CPE was seen. In this case, the same drug concentrations were used for the subsequent passage. Deep sequencing was used to genotype the virus cultures that were obtained from each condition.

2.6.Deep sequencing

To determine the frequency of resistance mutations in the virus cultures after two, five and ten passages, amplicon-based next-generation sequencing (NGS) was used. The entire TK and UL52 genes were amplified by PCR (Platinum SuperFi, Thermo Fisher Scientific), while the DP and UL5 genes were only amplified partially, encompassing the regions known to carry drug-resistance mutations. After the purification [QIAquick PCR Purification Kit (Qiagen)] and quantification [Qubit dsDNA HS Assay Kit on the Qubit®2.0 fluorometer (Thermo Fischer Scientific)], PCR products were used to prepare

DNA libraries (one library per sample) with 1 ng of DNA with Nextera XT DNA Sample Preparation Kit and Nextera XT DNA Sample Preparation IndexKit (Illumina).

After purification with Agencourt® AMPure® XPbeads, the resulting barcoded libraries were normalized to a 2 nM concentration and pooled. 5% PhiX Control v3 library (12.5pM; Illumina) was added to the libraries after the normalization step. Paired-end (2 × 150bp) reads on the Miseq v.2 system (Illumina) was used to sequence the library pool. CLC bioGenomics Workbench version 12 (Qiagen) was used to analysed the obtained sequence reads (Andrei et al., 2019). The HSV-1 strain 17 genome (GenBank accession number NC_001806.2) was used to map the reads and the low-frequency variant detection tool was used to identify variants with a frequency >1%.

3. Results

3.1. Additive anti-HSV-1 activity of AMV in combination with ACV or PFA

To evaluate the antiviral effects of AMV in combination with ACV or PFA, serial dilutions of the antivirals alone or in combination were added to HEL cells infected with HSV-1 wild-type strain KOS. Taken together, these results showed that the AMV+ACV and AMV+PFA combinations had moderate additive effects, with an overall synergy score of -2.65 and 1.77, respectively (Figure 1). Interestingly, these effects were already detected at low concentrations of both compounds.

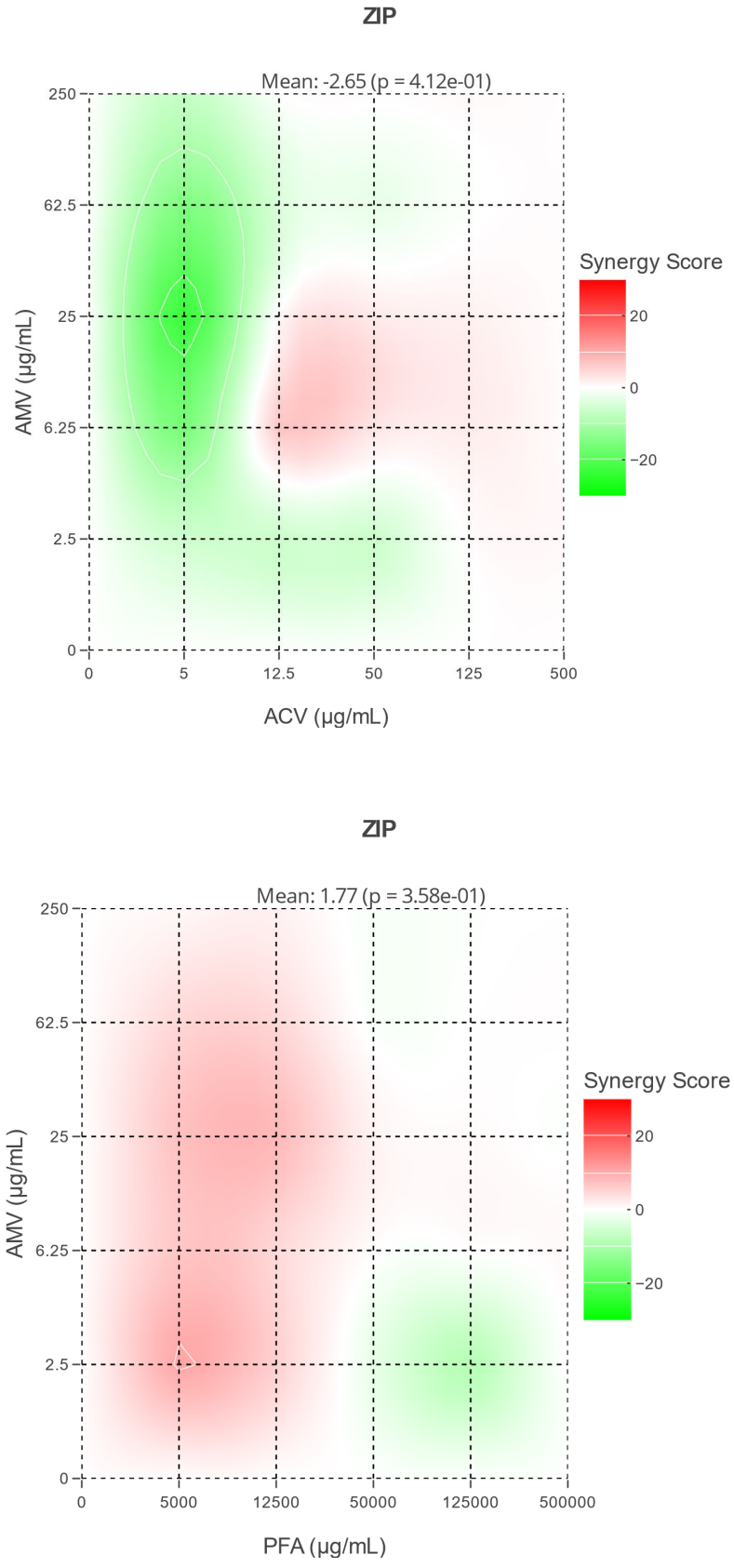

Figure 1. Amenamevir activity in combination with acyclovir or foscarnet against HSV-1. HEL cells infected with HSV-1 wild-type strain KOS were treated with various concentrations of one or two antivirals

(n=2). Inhibitory effects of the antivirals were evaluated by determining the reduction of HSV-1 virus titers. Interaction plots for (a) amenamevir (AMV) and acyclovir (ACV) and (b) amenamevir (AMV) and foscarnet (PFA) were generated with SynergyFinder 2.0 using the Zero Interaction Potency (ZIP) model. Overall synergy scores are shown above the plots. Synergy score < -10, antagonism; between -10 and 10, additive; >10 synergy.

3.2. Cytotoxic activity of AMV in combination with ACV and PFA

To exclude the possibility that the observed additive anti-HSV effects of the drug combinations were due to toxicity, the cytotoxic activity of AMV alone or in combination with ACV and PFA was evaluated (Figure 2). To this end, HEL cells were exposed to different concentrations of AMV+ACV or AMV+PFA. Taken together, these drug combinations did not display a higher cytotoxicity than treatment with the individual drugs.

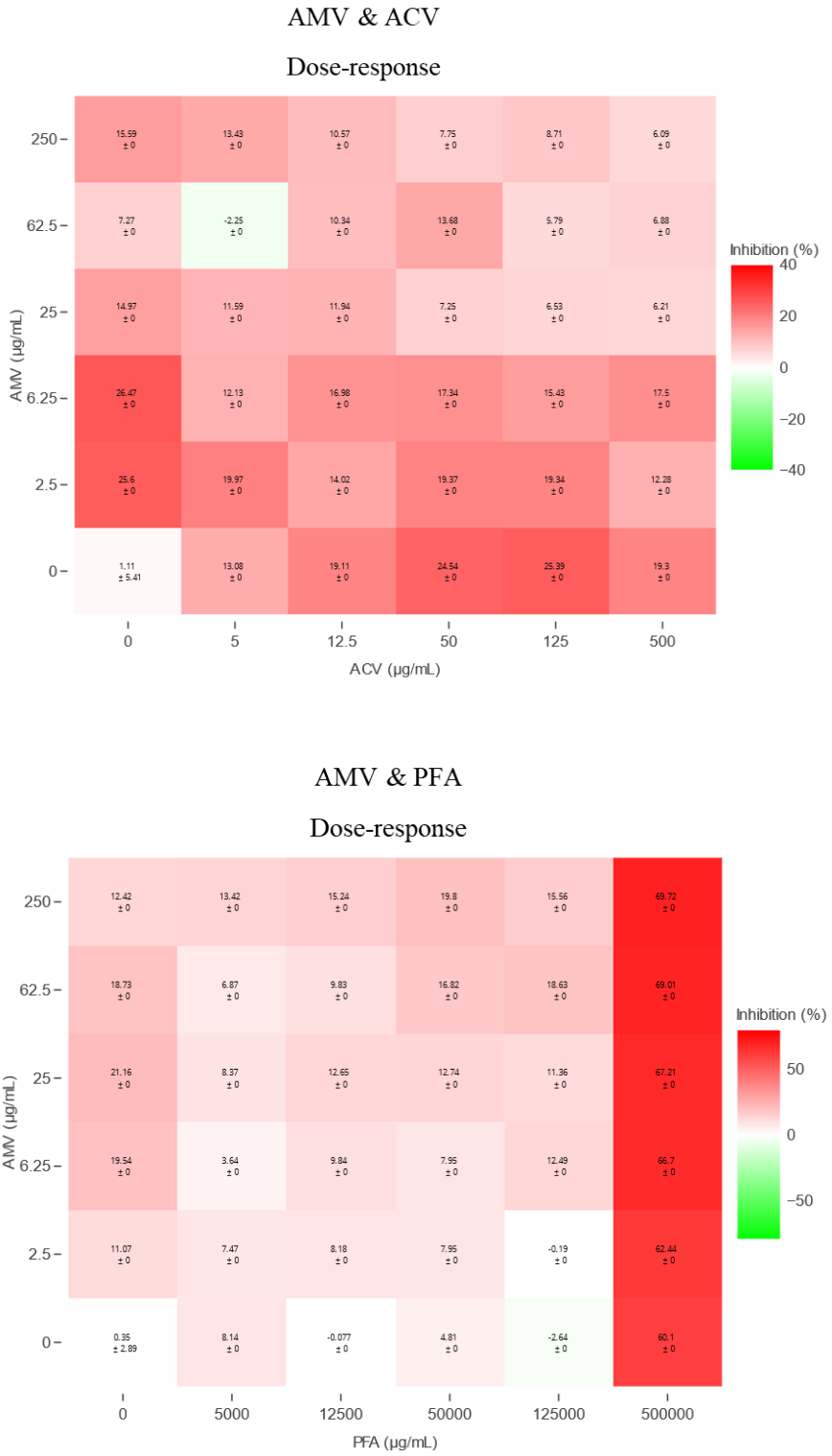

Figure 2. Cytotoxic activity of antiviral compounds in combination. HEL cells were exposed to different concentrations of one or two antiviral compounds. After three days of incubation (n=3), Z1 Coulter Counter was used to define cell counts. The presented dose-response matrices were generated with SynergyFinder 2.0. The % inhibition indicate the reduction of cell count relative to untreated cells.

3.3.*Deep sequencing of HSV-1 cultures following antiviral pressure*

Two different starting concentrations of AMV, AMV+ACV and AMV+PFA were evaluated in the resistance selection procedure, the lower concentration is indicated as 'L' and the higher as 'H'. Following five passages, virus cultures were genotyped by deep sequencing.

Frequency of mutations emerging under monotherapy pressure

Repetitive passaging under AMV pressure induced mutations in the UL5 gene of both AMV^{L} and AMV^{H} (Table 1). Following passage five, the novel R849H substitution was detected at a 4.5% frequency, but this change was replaced by the K356E change (99.95%) following passage 10. The K356E change had an unknown effect on drug susceptibility, though other changes at this locus, i.e., K356N/Q/T, have been linked to AMV resistance (*Collot et al., 2016*). In the AMVL virus culture, the known resistance mutation K356Q was found following passage number 5 (98.21%) and 10 (99.79%).

Frequency of mutations identified following AMV combination therapy

NGS showed that the HSV-1 cultures, treated with the AMV and ACV combination, acquired several mutations, which were located in the TK, UL5, and UL52 genes (Table 1). The virus culture selected under lower concentrations of ACV and AMV presented a nucleotide deletion in the TK at nucleotide 476, resulting in a frameshift mutation and therefore in the production of an inactive enzyme most likely associated with ACV resistance. The deletion was detected from passage 2 (2.11%) onwards and increased in to a frequency >99% in the subsequent passages. In addition, a novel amino acid change, N342H at the same position as the previously described AMV-resistance mutation N342K, was detected in the UL5 gene, after the passage number 5, with a frequency of 10.01 %, which tended to increase up to 36.46% in passage 10. Furthermore, a known AMV-resistance mutation, i.e., F360V in the UL52 gene, was found in the virus cultured under ACV and AMV pressure initiated from lower concentrations from passage 5 onwards, at a high frequency (>85%). In the ACV+AMVH virus culture, a C insertion at the 548-553 homopolymer stretch was found in the TK gene at a high frequency (>90%) from passage 2 onwards. Interestingly, the unknown mutation, N343T change was found in the UL5 gene of the ACV+AMVH virus culture. This new mutation was already detected at passage 5 with a high frequency (99.92%), confirming the same frequency at passage 10 (99.96%).

The NGS sequencing of virus cultures selected under AMV and PFA pressure have been performed up to passage 5. The virus culture selected under lower drug concentrations showed two substitutions in the DP gene: E597G, with a frequency of 15.55%, and L802F, with a frequency of 75.61%, both detected at passage 5, while no mutations, both resistance or not, were detected in the UL5 and UL52 genes. The virus culture PFA+AMVH remained free of mutations up to passage 5.

Table 1. Mutations detected following 2, 5 and 10 passages under AMV (combinatorial) pressure.

Condition	Gene	Mutation	Frequency (%) ± SD		
			Passage 2	Passage 5	Passage 10
AMV^{L} (0,025 → 0,2)	**UL5**	**K356E**	**-**	**-**	**99.95 ± 0.02**
		R849H	**-**	**4.55 ± 1.29**	**-**
	UL52	-	-	-	N.P.
AMV^{H} (0,05 → 0,4)	**UL5**	**K356Q**	**-**	**98.21 ± 0.11**	**99.79 ± 0.01**
	UL52	-	-	-	N.P.
ACV+AMV^{L} (0,025+0,0125→0,2+0,1)	**TK**	**del T nt 476**	**2.11 ± 0.09**	**99.13 ± 0.19**	**99.18 ± 0.14**
	DP	-	-	-	-
	UL5	**N342H**	**-**	**10.01 ± 0.11**	**36.46 ± 0.12**
	UL52	**F360V**	**-**	**85.63 ± 0.27**	**97.17 ± 0.07**
ACV+AMV^{H} (0,050+0,025→0,4+0,2)	**TK**	**Ins C nts 548-553**	**93.41 ± 0.56**	**94.21 ± 0.22**	**94.01 ± 0.55**
	DP	-	-	-	-
	UL5	**N343T**	**-**	**99.92 ± 0.02**	**99.96 ± 0.00**
	UL52	-	-	-	-
PFA+AMV^{L} (0,125+0,025→0,25+0,5)	**DP**	**E597G**	**-**	**15.55 ± 0.03**	N.P.
		L802F	**-**	**75.61 ± 0.90**	N.P.
	UL5	-	-	-	N.P.
	UL52	-	-	-	N.P.
PFA+AMV^{H} (0,1875+0,05)	DP	-	-	-	N.P.
	UL5	-	-	-	N.P.
	UL52	-	-	-	N.P.

The initial and final concentrations (in µg/mL) of the antivirals used during resistance selection are indicated in parenthesis, 'L': refers to the lower initial drug concentration and 'H' to the highest one. The same antiviral concentrations were used for passages 5 to 10. The resistance selection procedure of PFA+AMV has not been performed (N.P.) for passage 10. Known drug-resistance mutations have been highlighted in red (https://www.uniklinikum-jena.de/virologie/Links/HSV+Resistance+database.html) (*Collot et al., 2016*). New detected mutations with an unknown effect on drug susceptibility have been highlighted in blue.

4. Discussion

The development of drug-resistant HSV-1 strains in the clinic and the low number of antiviral drugs, warrants the study of new therapies and strategies (such as combination therapy) to manage HSV-1 infections., Furthermore, none of the current available therapies is curative (*Sadowski et al., 2021*). Indeed, drug-resistant viral strains have emerged as a result of the prolonged use of ACV and ongoing active replication of the viruses in immunocompromised patients. There has been evidence of a significant rate of TK mutations leading to resistance to antiviral drugs (*Sauerbrei et al., 2016*). Therefore, a direct DNA polymerase inhibitor, Foscarnet, has been used as alternative therapy, even though resistance mutations have been found also for this compound, often conferring cross-resistance to both ACV and PFA (*Andrei et al., 2013*).

The helicase-primase complex represents a new target for HSV-1 (*Sato et al., 2021*), and inhibitors of this complex can also be used in combination therapy with a DNA polymerase inhibitor to better inhibit viral replication and diminish emergence of drug-resistance (*Greeley et al., 2020*). In this context, several studies have demonstrated how combination therapy can effectively suppress HSV-1 replication (*Quenelle et al., 2018; Greeley et al., 2020*). Another advantage of combination therapy might be the reduction of toxic side-effects, since combination therapy would likely require lower drug concentrations than monotherapy.

In this project the effects of AMV, a helicase-primase inhibitor, in combination with two DNA polymerase inhibitors, ACV and PFA, on HSV-1 inhibition and drug resistance development, have been investigated.

We noticed a stronger additive effect during HSV-1 infection for the PFA and AMV combination compared to ACV and AMV combination (*Greeley et al., 2020; Chono et al., 2013).*

Mutations emerged in all the viruses cultures selected under drug pressure, except for the PFA+AMVH virus culture. Both AMV and ACV+AMV pressure induced mutations in the UL5 and UL52 genes within 10 passages. These UL5 and UL52 mutations included known AMV-resistance mutations (UL5 K356N and UL52 F360V) and novel mutations (UL5 N342H, N343T, K356E, and R849H). Though drug susceptibility testing of these novel mutations is necessary to confirm their effect on AMV susceptibility, it is likely that they will be associated to AMV-resistance since most emerged at high frequency

upon AMV pressure. The acquisition of mutations in both the TK and UL5/UL52 genes following ACV+AMV combination therapy, at rates similar to monotherapy suggests that AMV and ACV combination therapy was not be able to suppress drug-resistance evolution in these experiments. However, higher concentrations of AMV and ACV might be effective in preventing drug resistance. The resistance selection under PFA and AMV pressure was only continued for five passages and induced DP mutations but no UL5 or UL52 mutations in the PFA+AMVL culture. The lack of any mutations in PFA+AMVH after 5 passages shows promise that this combination might be successful in preventing drug resistance development, though further passaging is needed to confirm this.

Taken together these results confirm that the combination therapy of DNA polymerase inhibitor PFA with the helicase-primase complex inhibitor AMV may be a valid alternative to monotherapy, since less resistance mutations were detected. On the other hand, the inhibitory effects and the reduced number of mutations found for PFA and AMV combination, already at low concentrations, indicate a good starting point to carry out further studies on this combination drugs.

References

Andrei G, Snoeck R. Herpes simplex virus drug-resistance: new mutations and insights. Curr Opin Infect Dis. 2013 Dec;26(6):551-60.

Andrei G, Van Loon E, Lerut E, Victoor J, Meijers B, Bammens B, Sprangers B, Gillemot S, Fiten P, Opdenakker G, Lagrou K, Kuypers D, Snoeck R, Naesens M. Persistent primary cytomegalovirus infection in a kidney transplant recipient: Multi-drug resistant and compartmentalized infection leading to graft loss. Antiviral Res. 2019 Aug;168:203-209.

Chono K, Katsumata K, Suzuki H, Shiraki K. Synergistic activity of amenamevir (ASP2151) with nucleoside analogs against herpes simplex virus types 1 and 2 and varicella-zoster virus. Antiviral Res. 2013 Feb;97(2):154-60.

Collot M, Rouard C, Brunet C, Agut H, Boutolleau D, Burrel S. High conservation of herpes simplex virus UL5/UL52 helicase-primase complex in the era of new antiviral therapies. Antiviral Res. 2016 Apr;128:1-6.

Greeley ZW, Giannasca NJ, Porter MJ, Margulies BJ. Acyclovir, cidofovir, and amenamevir have additive antiviral effects on herpes simplex virus TYPE 1. Antiviral Res. 2020 Apr;176:104754.

Ianevski A, Giri AK, Aittokallio T. SynergyFinder 2.0: visual analytics of multi-drug combination synergies. Nucleic Acids Res. 2020 Jul 2;48(W1):W488-W493. Erratum in: Nucleic Acids Res. 2022 Jul 8;50(12):7198.

James C, Harfouche M, Welton NJ, Turner KM, Abu-Raddad LJ, Gottlieb SL, Looker KJ. Herpes simplex virus: global infection prevalence and incidence estimates, 2016. Bull World Health Organ. 2020 May 1;98(5):315-329.

L.j. reed, H. Muench. A simple method of estimating fifty per cent endpoints. American Journal of Epidemiology, Volume 27, Issue 3, May 1938, Pages 493–497,

Packard JE, Dembowski JA. HSV-1 DNA Replication-Coordinated Regulation by Viral and Cellular Factors. Viruses. 2021 Oct 7;13(10):2015.

Quenelle DC, Birkmann A, Goldner T, Pfaff T, Zimmermann H, Bonsmann S, Collins DJ, Rice TL, Prichard MN. Efficacy of pritelivir and acyclovir in the treatment of herpes simplex virus infections in a mouse model of herpes simplex encephalitis. Antiviral Res. 2018 Jan;149:1-6.

Sadowski LA, Upadhyay R, Greeley ZW, Margulies BJ. Current Drugs to Treat Infections with Herpes Simplex Viruses-1 and -2. Viruses. 2021 Jun 25;13(7):1228.

Sato Y, Suenaga T, Kobayashi M, Miyazaki N, Suzuki T, Ishioka K, Suzutani T. Characteristics of Helicase-Primase Inhibitor Amenamevir-Resistant Herpes Simplex Virus. Antimicrob Agents Chemother. 2021 Sep 17;65(10):e0049421.

Sauerbrei A, Bohn-Wippert K, Kaspar M, Krumbholz A, Karrasch M, Zell R. Database on natural polymorphisms and resistance-related non-synonymous mutations in thymidine kinase and DNA polymerase genes of herpes simplex virus types 1 and 2. J Antimicrob Chemother. 2016 Jan;71(1):6-16.

Schalkwijk HH, Snoeck R, Andrei G. Acyclovir resistance in herpes simplex viruses: Prevalence and therapeutic alternatives. Biochem Pharmacol. 2022 Dec;206:115322.

Šudomová M, Hassan STS. Flavonoids with Anti-Herpes Simplex Virus Properties: Deciphering Their Mechanisms in Disrupting the Viral Life Cycle. Viruses. 2023 Nov 29;15(12):2340.

Sun W, Sanderson PE, Zheng W. Drug combination therapy increases successful drug repositioning. Drug Discov Today. 2016 Jul;21(7):1189-95.

Wyles DL, Sulkowski MS, Dieterich D. Management of Hepatitis C/HIV Coinfection in the Era of Highly Effective Hepatitis C Virus Direct-Acting Antiviral Therapy. Clin Infect Dis. 2016 Jul 15;63 Suppl 1(Suppl 1):S3-S11.

CHAPTER 6 – *Final Remarks*

Chapter 6 - Final Remarks

Evidence on structural knowledge as well as on functional mechanism of new potential antivirals are considered starting points for the development of drugs against viral diseases.

Herein, in order to increase the knowledge on mechanism of action involved in virus-host interaction, following *in vitro* infection, the implication of AhR was found in both CCoV (Cerracchio et al., 2022a) and FCoV infection. Pharmacologic inhibition of AhR by CH223191 repressed both CCoV (Cerracchio et al., 2022a) and FCoV replication, recognizing AhR as a new target for identifying antiviral drugs to counteract CoVs. Hence, our findings support the idea that AhR up-regulation might be a common strategy used by coronaviruses to stimulate viral replication.

The potential antiviral properties of fungal secondary metabolites, such as OMF (Cerracchio et al., 2022b), PS and VER (Cerracchio et al., 2023a), obtained from *Talaromyces pinophilus* as well as of 6PP, isolated from *Trichoderma atroviride*, have been shown in the suppression of CCoV infection. Moreover, in the presence of these compounds, a strong inhibition in the expression of AhR was found during infection.

Interestingly, in the presence of VER or PS, the alkalinization of lysosomes in CCoV-infected cells was detected (Cerracchio et al., 2023a). This original mechanism of action may be involved in the observed antiviral activities.

About herpesviruses, during in vitro infection, by using natural compounds, such as OMF (Fiorito et al., 2022) and Taurisolo® (Cerracchio et al., 2023b), a grape pomace polyphenolic extract obtained from the Aglianico cultivar grape, a promising antiviral action towards BoHV-1 infection was detected. This activity showed the involvement of AhR.

Moreover, the combination therapy against HSV-1 of AMV, a helicase primase inhibitor, and ACV or PFA, two DNA polymerase inhibitors, represent a valid alternative to monotherapy, since less resistance mutations have been found.

Our preliminary results highlight the importance of using *in vitro* system to improve the knowledge about viral mechanism of action. Herein, specifically, were provided new findings about original mechanisms of action involved in virus-host cell interaction, identifying both *in vitro* models to investigate antiviral activity against CoVs and

herpesviruses. These models have avoided using Biological Safety Level 3 (BSL3) laboratory and the manipulation of a highly pathogenic and contagious viruses, through the application of "do no significant harm", in compliance with article n. 17, EU Regulation 852/2020. In addition, these results allow to improve the knowledge of CoVs infectious diseases, as well as to introduce new tools in pharmaceutical industry using of non-toxic and more effective natural compounds to fight CCoV and FCoV, involving different scientific areas, in a transversal manner, since it embraces animals infectious disease, molecular biology, organic chemistry, and medical fields, well meeting the needs of One Health, so important in this historical moment in which the need for integration in scientific research. The One Health concept recognizes that human health is tightly connected to the health of animals and the environment. Thus, implementation and operationalization of the One Health concept often remains a challenge.

The findings here described may be useful for generating biological platforms suitable for potential compounds selection against CoVs and herpesviruses, as well as for studying *in silico* models, thus some compounds could be selected to test them in *in vivo* models. Furthermore, these results might be suitable also for creating stable collaborative networks of human resources across the international academic world, assembling skills and expertise of researchers working in the field of animal infectious diseases, with long-term experience in diagnostics, epidemiology and virus therapy and discovery.

Importantly, as above, animal coronaviruses (CCoV and FCoV) and herpesviruses (BoHV-1) represent a valid alternative for carrying out preliminary studies on the efficacy of potential compounds, bypassing the risks of using highly pathogenic and contagious viruses for the first step of screening.

Another meaningful goal of this study is confirming the identification of canine (A72), feline (CRFK) and bovine (MDBK) cell lines as effective *in vitro* models to investigate antiviral activity.

The elucidation of these mechanisms may support approaches to fight coronavirus and herpesviruses infections, and to prevent zoonotic introduction of highly pathogenic CoVs into the humans. In this perspective, studying antiviral compounds is needed to find new compounds for the treatment of viral infections. Developing antiviral compounds certainly may have potential applications in the treatment of coronaviruses as well as herpesviruses infections.

Overall, these results are in harmony with one of the sustainable development goals included in the agenda 2030 of United Nations: ensure healthy lives and promote well-being.

Clearly, despite the contribution of the present work, the current scenario reminds us that a lot of work remains to be done.